Peterhead CCS Project

Doc Title: Dynamic Reservoir Modelling Report

Doc No.	PCCS-05-PT-ZR-3323-00002
Date of issue:	12/09/14
Revision:	K01
DECC Ref No:	11.122
Knowledge Cat:	KKD Subsurface

KEYWORDS

Goldeneye, CO_2, Dynamic Modelling, Simulation, CCS, Peterhead.

Produced by Shell U.K. Limited

ECCN: EAR 99 Deminimus

IMPORTANT NOTICE

Information provided further to UK CCS Commercialisation Programme (the "**Competition**")

The information set out herein (the "**Information**") has been prepared by Shell U.K. Limited and its sub-contractors (the "**Consortium**") solely for the Department of Energy & Climate Change in connection with the Competition. The Information does not amount to advice on CCS technology or any CCS engineering, commercial, financial, regulatory, legal or other solutions on which any reliance should be placed. Accordingly, no member of the Consortium makes (and the UK Government does not make) any representation, warranty or undertaking, express or implied, as to the accuracy, adequacy or completeness of any of the Information and no reliance may be placed on the Information. Insofar as permitted by law, no member of the Consortium or any company in the same group as any member of the Consortium or their respective officers, employees or agents accepts (and the UK Government does not accept) any responsibility or liability of any kind, whether for negligence or any other reason, for any damage or loss arising from any use of or any reliance placed on the Information or any subsequent communication of the Information. Each person to whom the Information is made available must make their own independent assessment of the Information after making such investigation and taking professional technical, engineering, commercial, regulatory, financial, legal or other advice, as they deem necessary.

Table of Contents

TABLE OF CONTENTS 1
FIGURES 3
TABLES 9
1. EXECUTIVE SUMMARY 11
2. SUMMARY 13
2.1. Capacity 13
2.2. Well selection 14
2.3. Reservoir pressures 16
3. INTRODUCTION 19
4. RESERVOIR ENGINEERING WORKFLOW AND PHILOSOPHY 20
4.1. Objectives 20
4.2. Underpinning philosophy 20
4.3. Multiple scale modelling strategy 20
4.3.1. Full field dynamic modelling workflow 21
4.3.2. Fairway/Aquifer dynamic modelling workflow 22
4.3.3. Physics workflow 22
5. INPUT FOR FULL FIELD SIMULATION MODELS 24
5.1. Geological Model 24
5.1.1. Structural Model 24
5.1.2. Full Field Model Grid 27
5.1.3. Static Properties 28
5.1.4. Net to Gross, porosity & permeability modelling 29
5.1.5. Permeability reconciliation with dynamic data 30
5.2. Fluid description (PVT) 32
5.3. Saturation Functions 35
5.4. Relative Permeability 37
5.5. Initialisation 38
5.6. Production Data 39
5.7. In-place volumes from up-scaled static reservoir models 39
6. UNCERTAINTY FRAMEWORK 42
6.1. Static Uncertainties 43
6.2. Dynamic Uncertainties 45
6.2.1. Unstable displacement 51
6.2.2. Secondary Drainage Relative Permeability 53
6.2.3. CO_2/water relative permeability end points 56
7. ANALYTICAL ESTIMATE OF GEOLOGICAL STORAGE CAPACITY 59
7.1. Factors influencing the storage capacity of a depleted hydrocarbon reservoir 59
7.1.1. Total pore volume available: voidage from production 60
7.1.2. Possible increases in the sequestration capacity 60
7.1.2.1. Efficiency of refilling 64
8. GOLDENEYE FULL FIELD REFERENCE CASE MODEL 67
8.1. Model Behaviour 69
8.2. History Match 70
8.2.1. Vertical connectivity of main reservoir units (E,D,C) 70

8.2.2. GIIP volume and distribution among main reservoir units (E,D,C) *72*
8.2.3. Aquifers characterization both east and west of the Field *76*
8.2.4. Residual gas saturation (S_{gr}) and k_{rw}@S_{gr} *78*
8.3. History Match Results 79
9. GOLDENEYE FULL FIELD ALTERNATIVE REALISATIONS 80
9.1. Behaviour of alternative realisations 81
9.2. History Match 81
10. GOLDENEYE FULL FIELD FORECAST 84
10.1. Final production phase 84
10.2. Injection wells 85
10.3. Injection scenarios 85
10.3.1. Base case injection pattern – 10 Mt. *89*
10.3.2. Base case injection pattern – 20 Mt of CO_2 *94*
10.3.3. Sensitivity to rate of injection *96*
10.3.4. Maximum storage capacity *98*
10.3.5. Well injection pattern *102*
10.3.5.1. Injecting into GYA01 and GYA05 102
10.3.5.2. Injecting into GYA02S1 and GYA04 103
10.3.5.3. Injecting into one well only 104
10.4. Well completions 105
10.5. Implications of delayed start-up of injection 105
10.6. CO_2 Dissolution 107
10.7. Reservoir Compartmentalization 109
10.7.1. Pressure Transient Analysis *110*
10.7.2. Fault interpretation *110*
10.7.3. Permanent Downhole Gauges Bottom Hole Pressure data *111*
10.7.4. Sealing faults sensitivity scenario *113*
10.7.5. Thief zone *115*
10.8. Vertical Grid Refinement 117
11. FAIRWAY REGIONAL AQUIFER MODEL 120
11.1. Scope and Objectives 120
11.2. Static Model 121
11.3. Up-scaling and Inclusion of FFM 121
11.4. Aquifer extent 124
11.5. Relative Permeability Data 124
11.6. Capillary Pressure Data 125
11.7. PVT Data 125
11.7.1. Black Oil *125*
11.7.2. Compositional *125*
11.7.3. Water properties and CO_2 Dissolution *125*
11.8. Pressure Data 126
11.9. Well and Production Data 128
11.10. Initialisation 128
11.11. History Match 131
11.11.1. History Match Philosophy *131*
11.11.2. Initial Goldeneye Pressure Decline *131*
11.11.3. Match to Field Pressures *134*
11.12. Comparison of history match with FFM 139
11.13. Pressure Rise Following Shut in 140

11.14. CO_2 Injection 142
11.15. Pressure Change Post Injection 145
11.16. Effect of CO_2 Dissolution 149
11.17. Migration of CO_2 beyond the Spill Point 151
11.18. Effect of CO_2 Injection on Neighbouring Field Pressure 157
11.19. Summary of Results 160
12. SECONDARY CONTAINMENT/MIGRATION MODELLING 160
12.1. Geology of the secondary storage 161
12.2. Static modelling 162
12.3. Features of overburden dynamic models 168
12.4. Volume at risk 169
12.5. Well constraints and rates 170
12.6. Overburden Model Forecast (Box Model) 172
12.7. Overburden Model Forecast (3D Homogeneous Model) 178
12.7.1. Uncertainty Analysis 185
12.7.2. Alternative source points 190
12.7.3. Combined leak scenarios 192
12.8. Overburden Model Forecast (3D Heterogeneous Model) 196
12.9. Seismic detection of CO_2 198
12.10. Key results from the secondary containment study 198
13. CONCLUSIONS 199
14. BIBLIOGRAPHY 201
15. GLOSSARY OF TERMS 203

Figures

Figure 2-1: Estimated Storage capacity for pure CO_2 14
Figure 2-2: Extent of CO_2 at end injection of 10 Mt in 2029 15
Figure 2-3: Extent of CO_2 plume at end of injection of 20Mt in 2039. 16
Figure 2-4: Predicted Goldeneye pressure before injection 17
Figure 2-5: Predicted Goldeneye pressure after injection for different aquifer realisations – 1000 years 18
Figure 4-1. Multiple scale models approach. 23
Figure 5-1. Goldeneye location map. The Captain Sandstone in the outer Moray Firth: Captain Fairway highlighted in yellow, basinal areas in pale green 24
Figure 5-2. Goldeneye field top structure map. 25
Figure 5-3. Representative structural cross-sections through Goldeneye field. 26
Figure 5-4. Cross-section of Goldeneye FFM Zones. 27
Figure 5-5. Goldeneye Type Log. 29
Figure 5-6 Alternative porosity-permeability relationships 31
Figure 5-7 Goldeneye field top structure map showing well locations 32
Figure 5-8. Representative Goldeneye recombined gas composition and phase envelopes. 33

Figure 5-9. (a) Retrograde condensate %VDp match; (b) Cumulative % volume of the initial wellstream produced; (c) Gas viscosity (calculated); (d) Gas compressibility Z-factor. CVD data with full characterisation. 34
Figure 5-10. CO_2 Density error function versus pressure (psia) for a range of Cpen values 35
Figure 5-11. Comparison of different volumes calculated from SRM3.1 in static reservoir model (Petrel), during initial import into dynamic simulator (Reduce Voxel) and after upscaling (Reduce up-scaled/MoReS). 41
Figure 5-12. SRM3.1 : Comparison of FGIIP calculated from Petrel hydrocarbon pore volume and two values for formation volume factor (B_g). 41
Figure 6-1. Key static uncertainties - cross section along Captain fairway, east to west (left to right) 44
Figure 6-2. Static uncertainty matrix 45
Figure 6-3. Displacement process in Goldeneye lifecycle 46
Figure 6-4. CO_2 and Water viscosity and density vs. pressure and temperature. 47
Figure 6-5. Viscosity (left) and Density (right) ratio as a function of pressure and temp. 47
Figure 6-6. Trapped gas saturation to liquid. Land correlation. 49
Figure 6-7. Endpoint relative permeability at trapped gas saturation. 50
Figure 6-8. Cross section in ternary diagram. Sensitivity with k_{rw} = 0.6 @ S_{gr} = 0.30 51
Figure 6-9. Cross section in ternary diagram. Sensitivity with k_{rw} = 0.25 @ S_{gr} = 0.30 52
Figure 6-10. Cross section in ternary diagram. Sensitivity with k_{rw} = 0.10 @ S_{gr} = 0.30 52
Figure 6-11. Displacement processes in Goldeneye lifecycle. Zoom in to S_w in the plume. 54
Figure 6-12. Cross section vs. fractional flow curve with B-L solution. N_w = 5.0 55
Figure 6-13. Cross section vs. fractional flow curve with B-L solution. N_w = 3.0 55
Figure 6-14. Cross section vs. fractional flow curve with B-L solution. N_w = 2.0 56
Figure 6-15. Cross section in ternary diagram. Sensitivity with k_{rg} = 0.8 58
Figure 6-16. Cross section in ternary diagram. Sensitivity with k_{rg} = 0.50 58
Figure 6-17. Cross section in ternary diagram. Sensitivity with k_{rg} = 0.25 58
Figure 7-1: Factors impacting CO_2 storage capacity 60
Figure 7-2: Storage security depends on a combination of different trapping mechanisms. 61
Figure 7-3: Calculated CO_2 solubility in NaCl brine at 3800 psi. 62
Figure 7-4. Goldeneye GIIP distribution and average permeability per geological unit. 64
Figure 7-5. Post-injection effective storage capacity of Goldeneye 66
Figure 8-1: FFM diagnostics – reservoir pressure and wells rate. 69
Figure 8-2: FFM cross section showing pressure depletion level 71
Figure 8-3. 14/29-a3 FMT pressure data with log curves. 71
Figure 8-4. Formation pressure data. 72
Figure 8-5. Goldeneye Material Balance P/Z plot. Zoom at early shut-in pressure period. 73

Figure 8-6. Goldeneye Material Balance P/Z plot. GIIP extrapolation. 73
Figure 8-7. Havlena-Odeh material balance plot. 74
Figure 8-8. Havlena-Odeh material balance plot. Zoom in. 75
Figure 8-9. GIIP probability distribution based on 381 runs of the geologic model. 76
Figure 8-10. Distribution of Captain sandstones across the outer Moray Firth. 77
Figure 8-11. FFM 3.1 diagnostics – reservoir pressure and wells rate. History matched. 79
Figure 9-1. FFM 3.05 diagnostics – reservoir pressure and wells rate. History matched. 82
Figure 9-2: FFM 3.15 diagnostics – reservoir pressure and wells rate. History matched. 83
Figure 10-1. FFM3.1: Extent of CO_2 plume at top Captain D, at end of injection (2029). 90
Figure 10-2: FFM 3.1 - CO_2 plume, (A) after 5 years of injection and (B) after 10 years of injection. 91
Figure 10-3: FFM 3.1 - CO_2 plume, 5 (A) and 10 (B) years after end injection 92
Figure 10-4: FFM 3.1 – recovery of average reservoir pressure (Unit D) after injection 93
Figure 10-5. FFM 3.15, northern pinch-out sensitivity (A) and FFM 3.05, shallower flank (B) - Extent of CO_2 plume at top Captain D at end of injection (2029). 94
Figure 10-6: FFM 3.1 - Base case injection pattern - 20 Mt of CO_2 95
Figure 10-7: FFM 3.1: CO_2 plume, 5 (A) and 10 (B) years after end injection 96
Figure 10-8: FFM 3.05 – Cross section illustrating the Dietz effect. 97
Figure 10-9: FFM 3.1 (reference case): CO_2 plume at top D, when maximum storage capacity is reached for injection in GYA01 - Year 2050. 99
Figure 10-10: FFM 3.1, CO_2 plume extent five years after ceasing injection in GYA01 when maximum storage capacity was reached - Year 2055 100
Figure 10-11: FFM 3.15 - redistribution of CO_2 with time after cessation of injection assuming injection in western flank well GYA01. 101
Figure 10-12: FFM3.1, injecting in GYA01 and GYA05 only 103
Figure 10-13: FFM305, injecting in GY01 only and GYA05 only 103
Figure 10-14: FFM 315, (northern pinch-out sensitivity), injecting in GYA01 and GYA05 only 103
Figure 10-15. FFM 3.15 - injecting equally in wells GYA02S1 and GYA04 only. CO_2 plume after 10 years and 20 years injection (top Unit D), 104
Figure 10-16: FFM 3.15 (northern pinch-out sensitivity) – injection in well GYA01 only. CO_2 plume after 10 years and 20 years injection (top Unit D) 105
Figure 10-17. Difference in pre-injection pressure for delayed start dates. 106
Figure 10-18. Difference in post-injection pressure for delayed injection. 106
Figure 10-19. FFM 3.1: Extent of CO_2 plume at top Captain D at end of injection with dissolution (20 Mt CO_2 injected) 107
Figure 10-20. FFM 3.1: Mass of CO_2 dissolved in water during 10 year injection period (20 Mt case). 108

Figure 10-21. FFM 3.1: mass of CO_2 dissolved in water during 1000 years, after 20 Mt CO_2 injected.. 109
Figure 10-22. Seismic fault pattern Top Goldeneye Reservoir. 111
Figure 10-23. Downhole pressure for GE wells @ datum from PDHG. 112
Figure 10-24. Field pressure Build-up from Sep-2010 until October 2010. 113
Figure 10-25. FFM SRM3.1: 20 Mt CO_2 injection at end of injection, no seismic faults.114
Figure 10-26. FFM SRM3.1 : 20 Mt CO_2 injection at end of injection, with seismic faults included. 114
Figure 10-27. CO_2 Injection rate and field average reservoir pressure. 115
Figure 10-28: Permeability map of top unit D for FFM 3.1 model without thief zone (A) and for model with thief zone (B). 116
Figure 10-29: CO_2 plume after injection 20 Mt for FFM 3.1 model without thief zone (A) and for model with thief zone (B). 116
Figure 10-30. XY and YZ view of FFM SRM 3.15 with different vertical grid refinement levels. 118
Figure 10-31. Vertical grid refinement impact on CO_2 modelling. 119
Figure 11-1. Goldeneye aquifer model grid (Goldeneye and other regions highlighted). 123
Figure 11-2. Goldeneye RFT data. 126
Figure 11-3. Initial decline in Goldeneye Pressure from downhole gauges. 127
Figure 11-4. Change in Goldeneye pressure from 1996 to 2004. 127
Figure 11-5. Goldeneye model with initial fluid distribution. 130
Figure 11-6. Pre-production Goldeneye pressure decline for history match case 22 with additional eastern and western aquifers compared to PDG data. 132
Figure 11-7. History match to pre-production Goldeneye pressure decline for history match cases (see Table 11-5 for details). 132
Figure 11-8. Hannay pressure match. 134
Figure 11-9. Goldeneye pressure match. 135
Figure 11-10: Predicted Goldeneye Pressure with and without Hoylake and Buffalo Prospect included in Regional Aquifer model 136
Figure 11-11: Rochelle West Pressure Match 137
Figure 11-12. Cromarty pressure match. 138
Figure 11-13. Atlantic pressure match. 138
Figure 11-14. Comparison of flows from western aquifer for FFM and aquifer model. 139
Figure 11-15. Comparison of flows from eastern aquifer for FFM and aquifer model. 140
Figure 11-16. Predictions of Goldeneye pressure from field shut in at end 2010 to 2015. 141
Figure 11-17. CO_2 distribution at top D in 2029 for FFM 3.1. 143
Figure 11-18. CO_2 distribution at top D in 2029 for aquifer model 34 with no LGR. 143
Figure 11-19. CO_2 distribution at top D in 2029 for aquifer model 34 with LGR. 144
Figure 11-20. Comparison of western aquifer fluxes between FFM and aquifer model. 144

Figure 11-21. Comparison of eastern aquifer fluxes between FFM and aquifer model. 145
Figure 11-22. Pressure change over 75 year period after end of CO_2 injection. 146
Figure 11-23. Pressure change over 1000 year period after end of CO_2 injection. Again, dotted line represents case without Rochelle production. 147
Figure 11-24: Traverse Pressure Plot for Aquifer Model 34. 148
Figure 11-25: The pressure at end of injection in 2039 – 20 million tonnes of CO_2 149
Figure 11-26. Mass of CO_2 dissolved in water for case 27 with 10 years injection followed by 1000 years shut in. 150
Figure 11-27. East west cross-section showing distribution of CO_2 in water 1000 years after end of injection (logarithmic scale). This CO_2 is dissolution trapped. 151
Figure 11-28. Distribution of CO_2 28 years after injection of 1 million tonnes at spill point in Case 22 model (top E) 152
Figure 11-29. Distribution of CO_2 28 years after injection of 1 million tonnes at spill point in Case 22 model (west – east cross-section at Y=70). 153
Figure 11-30. Distribution of CO_2 100 years after injection of 1 million tonnes at spill point in Case 22 model (west – east cross-section at Y=70). 153
Figure 11-31. Distribution of CO_2 28 years after injection of 5 million tonnes at spill point in Case 22 model (west – east cross-section at Y=70). 154
Figure 11-32. Distribution of CO_2 100 years after injection of 5 million tonnes at spill point in Case 22 model (top D, showing abandoned wells to west). 154
Figure 11-33. Distribution of CO_2 1000 years after injection of 5 million tonnes at spill point in Case 22 model (top D, showing abandoned wells to west). 155
Figure 11-34. Distribution of CO_2 1000 years after injection of 5 million tonnes at spill point in Case 22 model (top E, showing abandoned wells to west). 155
Figure 11-35. Distribution of CO_2 in water (dissolution trapping) 1000 years after injection of 5 million tonnes at spill point in Case 22 model (Y=70, logarithmic scale). 156
Figure 11-36. Distribution of CO_2 in water 1000 years after injection of 5 million tonnes at spill point in Case 22 model (top D, showing abandoned wells to west, logarithmic scale). 156
Figure 11-37. Distribution of CO_2 in water 1000 years after injection of 5 million tonnes at spill point in Case 22 model (top E, showing abandoned wells to west, logarithmic scale). 157
Figure 11-38. Rise in Hannay pressure after end of Goldeneye production. 158
Figure 11-39. Rise in Atlantic pressure after end of Goldeneye production. 158
Figure 11-40. Rise in Cromarty pressure after end of Goldeneye production. 159
Figure 11-41: Rise in Rochelle West pressure after end of Goldeneye production. 159
Figure 12-1. Seismic Cross section showing the field, storage site, storage seal, storage complex and secondary storage i.e. Lista, Mey, Upper Balmorals Sandstone and Lower Balmoral sandstone and Tuffite Unit. 161
Figure 12-2. Figure shows the difficulty in picking a Top Lista on seismic, pick in wells does not conform to an easily identifiable, consistent seismic horizon. Foreset geometries can be seen. 164

Figure 12-3. Figure shows the difficulty in picking a Top Lista on seismic, pick in wells does not conform to an easily identifiable, consistent seismic horizon. 164
Figure 12-4. 2D data coverage (Millennium Atlas palaeogeography as backdrop) field highlighted by green oval. 165
Figure 12-5. 3D view of 2D line data set with the 14 seismic lines and all wells. Field area shown by solid surface. 165
Figure 12-6. New Top Lista map which ties to wells and available seismic lines. 166
Figure 12-7. New Top Chalk map which ties to wells and available seismic lines. 166
Figure 12-8. Clockwise from top 168
Figure 12-9. CO_2 below the top Captain penetrations of wells within Goldeneye, 25 years after cessation of injection (20 Mt), FFM3.15. 170
Figure 12-10. Estimated micro-annulus leak rates from Goldeneye reservoir into Mey 171
Figure 12-11. Distribution of CO_2 in top layer of model after 45 years for reference case. 172
Figure 12-12. Distribution of CO_2 in top layer of model after 1,000 years for reference case. 173
Figure 12-13. Distribution of CO_2 in cross section through well after 1,000 years for reference case. 173
Figure 12-14. Cross section through well showing concentration of CO_2 dissolved in water for reference case after 1,000 years (logarithmic scale). 174
Figure 12-15. Mass of CO_2 dissolved in water for reference case. 175
Figure 12-16. Distance of edge of CO_2 plume from well vs time. 176
Figure 12-17. Mass of CO_2 per unit area after 1000 years for reference case (10 million tonnes leaked). Lines indicate mass of CO_2 migrated beyond that point. 176
Figure 12-18. Mass of CO_2 migrating greater than given distance against time for reference case with 10 million tonnes leaked. 177
Figure 12-19. Distribution of CO_2 after 20 years in top layer of model for homogeneous case. 179
Figure 12-20. Distribution of CO_2 after 100 years in top layer of model for homogeneous case. 179
Figure 12-21. Distribution of CO_2 after 1000 years in top layer of model for homogeneous case. 180
Figure 12-22. Distribution of CO_2 in cross section through well after 1,000 years for homogeneous case. 181
Figure 12-23. CO_2 dissolved in brine @ 1000 years homogeneous model. 182
Figure 12-24. CO_2 Mass inventory as a function of time (left). CO_2 percentage inventory as a function of time (right) – homogenous model. 183
Figure 12-25. Distance of edge of CO_2 plume from well vs time, homogeneous model. 183
Figure 12-26. Mass of CO_2 after 1000 years for reference case, homogeneous model (10 million tonnes leaked). Lines indicate mass of CO_2 migrated beyond that point. 184

Figure 12-27. Mass of CO_2 migrating greater than given distance against time for reference case with 10 million tonnes leaked, homogeneous model. 185
Figure 12-28. Tornado diagram for migration sensitivities. 186
Figure 12-29. Distribution of CO_2 in XY and XZ sections through well after 1,000 years for 1500 tonnes/d (left) and 100 tonnes/day (right) leak rate case – homogeneous model. 187
Figure 12-30. Distribution of CO_2 in XZ sections through well after 1,000 years for k_v/k_h = 0.01 (left); 0.1 (middle:- Base Case); 1.0 (right) – homogeneous model. 188
Figure 12-31. Residual gas saturation sensitivity, homogenous model. Sgr = 0.20, 0.25, 0.30, 0.35. 188
Figure 12-32. Impact of Sgr on CO_2 dissolution in brine. 189
Figure 12-33. Well Risk map of the complex seal. 190
Figure 12-35. Residual gas saturation sensitivity, homogenous model. Sgr = 0.20, 0.25, 0.30, 0.35. 191
Figure 12-35. Impact of Sgr on CO_2 dissolution in brine. 191
Figure 12-36. Distribution of CO_2 in XY sections through well 14/29-a3 (left) and 14/29-a5 (right) after 1,000 years. Each concentric line represent 1 km. Both homogeneous models. 191
Figure 12-37: Distribution of CO_2 in XY section of well 20/4b-6 after 100 years. homogenous model 191
Figure 12-38. Distribution of CO_2 in XY and XZ sections through wells 14/29-a3 and 14/29-a5 after 20 years. 193
Figure 12-39. Distribution of CO_2 in XY and XZ sections through wells 14/29-a3 and 14/29-a5 after 40 years (top) and 1000 years (bottom). 193
Figure 12-40. CO_2 mass inventory as a function of time (top). CO_2 percentage inventory as a function of time (bottom). Combined leak scenario, homogeneous model. 194
Figure 12-41. Different residual gas saturation correlations (left). Lands correlation sensitivity (right) 195
Figure 12-42. Heterogeneous version of Mey Geological Model. Porosity distribution (top); Permeability distribution (middle); Net to Gross distribution (bottom). 196
Figure 12-43. Distribution of CO_2 in a 3D cross section at well 14/29-a3 after 1000 years. Heterogeneous model. 197
Figure 12-44. CO_2 distribution in 3D panel view at 100, 500 and 1000 years. Heterogeneous model. 197

Tables

Table 5-1. Sub-Division of the Captain reservoir, Goldeneye area. 28
Table 5-2: Well test/static permeability comparisons, Goldeneye flank wells 31
Table 5-3. Gas reservoir parameter input 36
Table 5-4. Oil reservoir parameter input 36

Table 5-5. Core data coverage 37
Table 5-6. MoReS relative permeability data input 38
Table 5-7. Equivalent quantities in Static Reservoir Model (SRM) and Full Field Model (FFM) used for simulation. 40
Table 5-8: Net volume, net pore volume, hydrocarbon pore volume for gas and free GIIP in three geological models. 42
Table 6-1. Uncertainty elements identified. 43
Table 8-1. Regional aquifer static characterization 78
Table 10-1. End of production life in different models 85
Table 10-2. Storage capacity results. Summary table for FFM 3.1 (reference case) 87
Table 10-3. Storage capacity results. Summary table for FFM 3.05 (west flank sensitivity) 88
Table 10-4. Storage capacity results. Summary table for FFM 3.15 (northern pinch-out sensitivity) 89
Table 10-5: Estimate of maximum storage capacity for FFM3.1 and variances for FFM3.05 (-) and FFM 3.15(+). 102
Table 10-6. Injection in wells GY01 and GYA05 only 102
Table 10-7. Injection in wells GY02S1 and GYA04 only 104
Table 10-8. Injection with one well only (GYA01) 105
Table 10-9. Vertical grid sensitivities. 117
Table 11-1. Details of neighbouring fields to Goldeneye. (28) 120
Table 11-2. Vertical layering of dynamic model. 122
Table 11-3. Aquifer model relative permeability parameters. 124
Table 11-4. Initialisation data used in model. 129
Table 11-5. Pressure decline in GYA01, GYA03 and GYA04 from April 2004 to August 2004 before start of Goldeneye production. 133
Table 11-6. Predicted Goldeneye pressure at 1 January 2019. 141
Table 11-7. Pressure in 2029 at end of CO_2 injection – 10 million tonnes 147
Table 11-8: Pressure in 2039 at end of CO_2 injection after injecting 20 Mt of CO_2 149
Table 12-1. Relative permeability parameters. 169
Table 12-2. Initial parameter sensitivities (high/low values represent distance CO_2 migrates, not size of parameter value). 177
Table 12-3. Parameter sensitivities (high/low values represent distance CO_2 migrates, not size of parameter value). 185
Table 12-4. Residual gas saturation sensitivity results 188
Table 12-5. Impact of Sgr on CO_2 dissolution in brine. 189
Table 12-6. Combined leak scenarios. 192
Table 12-7. Traffic light combined leak scenarios. 195
Table 15-1. Name abbreviations 204
Table 15-2. Unit Conversion Table 205

1. Executive Summary

Dynamic modelling is a key component in the assessment of the ability to store CO_2 in the subsurface. The dynamic modelling work brings together:

- the geological understanding of the storage formation
- the flow behaviour of fluids within the storage formation
- the ability of the surface facilities and wells to deliver CO_2 to the reservoir
- the influence of other activities with the hydraulically connected volume on the ability to store CO_2 and the impact of the storage of CO_2 on other activities.

The dynamic simulator (MoReS), which uses the static model created using Petrel software (up-scaled in Reduce++), describes the physics of the injection process and the interaction of the physical processes in the reservoir with the geological structure.

It is only by bringing all the above elements together in a 3D finite difference compositional reservoir simulator that the project can answer the questions: how fast can CO_2 be injected, how large will the CO_2 injection plume be, how will the pressure evolve in the system?

The results of the dynamic simulation form the input to other modelling work: geomechanical modelling looking at effect of the stresses of injection on the rock integrity, geochemical modelling exploring the rock chemistry interactions, monitoring feasibility assessments - especially for time-lapse seismic. The results of the geomechanical and geochemical modelling can also influence the dynamic modelling and sometimes iterations are important.

Storage in the Goldeneye field was studied in UK CCS Demonstration Competition for an injection volume of 20 million tonnes at 2Mtpa. This work has been extended and updated in the current report to take account of two years of additional pressure data collected from the Goldeneye field and data received from other operators in the hydraulically connected volume. This data has given more information on the properties of the Captain Aquifer system allowing further definition of the long term pressure effects during and after injection. The results have also been updated to reflect the delay in start-up when compared to UK CCS Demonstration Competition (leading to a greater pressure recovery in the field) and the altered injection rate of 1Mtpa.

Dynamic modelling of the injection of dense phase CO_2 into the Goldeneye depleted hydrocarbon reservoir has been performed with the following four aims:

- Showing that the system has sufficient capacity to store the required 10 million tonnes of CO_2, and demonstrating additional capacity for another 10 million tonnes.
- Predicting the reservoir pressures to use in injection well design and geomechanical risk assessment
- Assessing the impact of the injection of CO_2 in Goldeneye on other users of the subsurface and their impact on Goldeneye
- Determining the effect of injection well selection on the plume development within the CO_2 store and on the risk of lateral migration
- Explore the potential and consequences of egressions from the primary storage formation.

The modelling results demonstrated that Goldeneye has sufficient storage capacity to hold 10 million tonnes of CO_2 and possible extension to 20 million tonnes. All of the uncertainty scenarios currently evaluated showed that the field can safely sequester the intended volume.

None of the injected CO_2 would move outside the original oil water contact (OWC) when 10 million tonnes are injected for the Peterhead CCS Project. Cases in which 20 million tonnes were injected were also studied. In the 20 million tonne cases, the model indicated that only 3 % of the total injected CO_2 was located outside the original OWC at the end of injection. However, after cessation of injection all of the CO_2 is either recovered back into the geological store or is otherwise sequestered (by means of dissolution or capillary trapping).

A range of models has been used to predict future pressures in Goldeneye. These give a range of pressures before start of CO_2 injection in 2019 of 2703 psia to 2973 psia [186.4 bar to 206.7 bar].

After injecting 10 or 20 million tonnes, CO_2 is not expected to egress from the reservoir. For completeness, this scenario was tested by modelling injection of CO_2 directly at the spill point, thereby allowing the CO_2 to leave the store and migrate updip. This is a slow process due to the varying dip of the formation. After 1000 years, 5 million tonnes of CO_2 has migrated 6-7 km to the west and is dissolving in the aquifer water. It does not reach the Atlantic and Cromarty fields or any of the nearby abandoned exploration wells to the west. Injection directly at the spill point will not be done in reality.

The impact of the injection activities in Goldeneye on neighbouring fields was checked using the simulation models. The reservoir pressure in the neighbouring Hannay field is expected to rise by between 300 and 500 psi [20.7 – 34.5 bar] to over the period to 2029. The rise in pressure will be affected by not only Goldeneye, but also further activities in the West Rochelle field which started production in October 2013 and East Rochelle which started in January 2014. Atlantic and Cromarty pressures will rise by 200 - 500 psi [13.8 – 34.5 bar] over the period to 2029 but this is uncertain as they are more sensitive to the actual size and strength of the western aquifer and the impact of continuing production and injection at Blake. After cessation of production in Rochelle West and East, around 2020, the pressure rises rapidly by about 400 psi over the period to 2029.

The Goldeneye field is in fact the gateway to a much larger aquifer store. The larger aquifer store can be accessed by injecting more CO_2 into the Goldeneye facilities and moving from structural storage in a depleted field to aquifer storage. For the purposes of the Peterhead project, it was demonstrated that over 29 million tonnes of CO_2 can be stored in the depleted Goldeneye field. If a large storage volume is required, the CO_2 could be allowed to migrate out of the Goldeneye structural store and flow into the Captain aquifer, where it would ultimately be trapped by dissolution in the water or by reacting with minerals in the rock.

2. Summary

3D dynamic modelling of the injection of dense phase CO_2 into the Goldeneye depleted hydrocarbon reservoir has been performed with the following four aims:

- Showing that the system has sufficient capacity to store the required 10 Mt of CO_2, and demonstrating additional capacity for another 10 Mt.
- Predicting the reservoir pressures to use in injection well design and geomechanical risk assessment
- Assessing the impact of the injection of CO_2 in Goldeneye on other users of the subsurface and their impact on Goldeneye
- Determining the effect of injection well selection on the plume development within the CO_2 store and on the risk of lateral migration
- Explore the potential and consequences of egressions from the primary storage formation.

In order to address the above a multiple scale modelling approach was adopted. This facilitated the assessment of the interaction of the complex static and dynamic factors which may coincide during CO_2 injection into the Goldeneye reservoir. Results from a three-dimensional, three-phase, full field Goldeneye numerical simulation model, corroborated the initial storage capacity estimations. Different injection scenarios were evaluated to map out the range of capacity available for CO_2 storage.

The effects of geochemical reactivity were tested in the models – by running coupled fluid flow and chemical reactive transport simulations. This is documented in this report on geo-mechanical investigations (1). The results from the dynamic models were input into geo-mechanical models. These specialist models are discussed in separate reports and the effects were found to be small enough to separate from the fluid flow models (2).

2.1. Capacity

The Goldeneye field is an anticline in the large regional Captain aquifer; as such the ultimate storage capacity is defined by the capacity of the depleted hydrocarbon bearing structure added to the aquifer storage capacity. As only up to 20 Mt storage is required by the project at this time, this report concentrates on depleted field storage and does not explore the significant expansion capacity available in the Captain aquifer (3).

The CO_2 storage capacity was initially estimated based on the pore space available for CO_2 injection from a standard volumetric assumption. The method used to estimate the CO_2 storage volume in Goldeneye, a depleted gas reservoir, was hydrocarbon production-based, corrected for CO_2 density. This resulted in a theoretical maximum voidage replacement storage volume of 47 million tonnes of CO_2 equivalent available in Goldeneye.

This theoretical maximum initial estimate was modified by storage efficiency factors which account for the fact that CO_2 will not be able to completely refill this volume. The conjunction of static and dynamic uncertainty parameters dictates the framework necessary for understanding the storage efficiency factors that discount the total theoretical capacity.

In addition to the storage capacity defined by the structural trap of Goldeneye, numerical simulation results suggest that the water leg beneath the reservoir (that lies within the storage site) could also account for extra capacity. The build-up of capacity is shown in Figure 2-1:

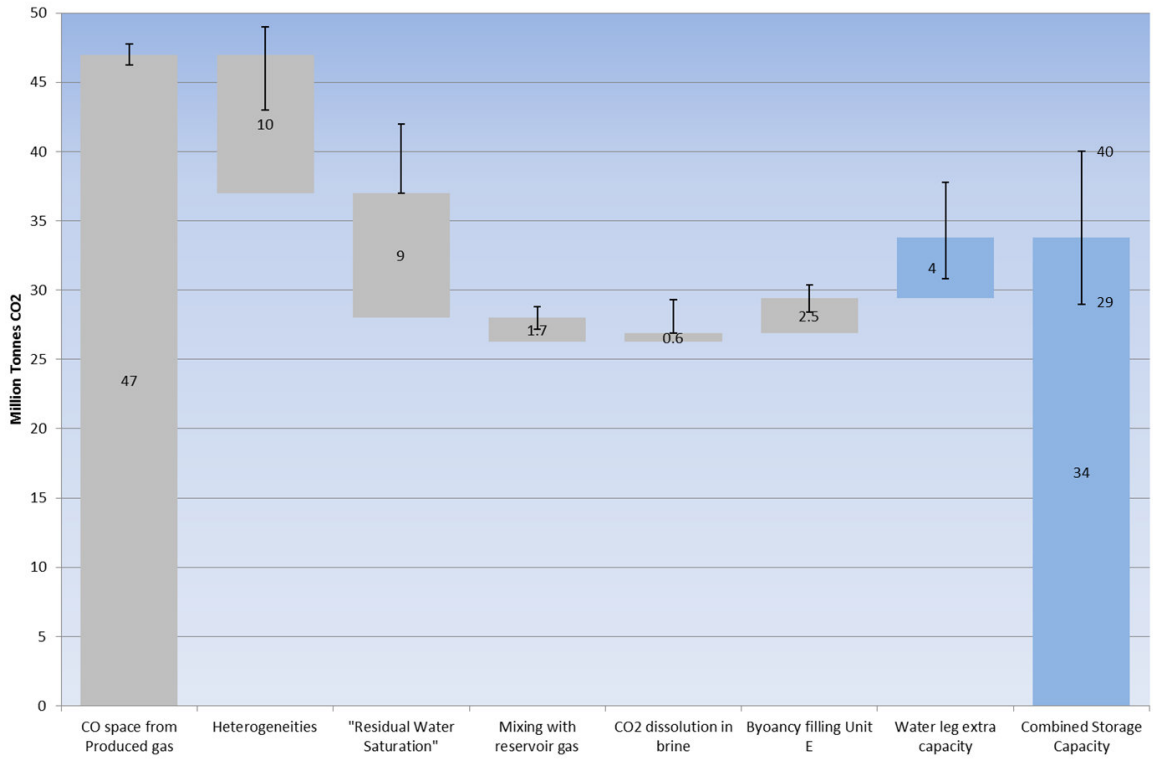

Figure 2-1: Estimated Storage capacity for pure CO_2

In order to determine an indicative maximum geologic carbon storage capacity for Goldeneye, a set of CO_2 injection scenarios was modelled. These revealed that over 29 million tonnes of CO_2 had to be injected to reach the structural spill point and create an egression. This capacity is shared between the original Goldeneye hydrocarbon reservoir and the water leg (saline aquifer) beneath the field. This gives confidence that Goldeneye has more than enough capacity to store 10 million tonnes of CO_2 plus well over 10 million tonnes potential additional storage.

CO_2 is not expected to egress from the reservoir. However, this scenario was tested by injecting CO_2 directly at the spill point which allows the CO_2 to migrate updip. This is a slow process due to the varying dip of the formation. After 1000 years 5 million tonnes of CO_2 has migrated 6-7 km to the west and is dissolving in the aquifer water. It does not reach the Atlantic and Cromarty fields or any of the nearby abandoned exploration wells to the west.

2.2. Well selection

The CO_2 will be injected into the Goldeneye Captain Sandstone using the existing hydrocarbon production wells, at a maximum rate of just over 1 million tonnes p.a. starting in 2019 for 10 years, with provision for expansion to up to 20 million tonnes CO_2 in total.

The complete suite of static reservoir models created to investigate CO_2 injection performance in the Goldeneye reservoir was tested in dynamic simulation. Injection scenarios ranged from:

- A reference case injecting in two out of the five injectors in a staged manner, one injector in the western part of the field for the first 5 years and a second injector in the eastern part of the field for next 5 years with an even injection rate for a total of 10 years.
- Balanced injection in two wells.
- Extreme cases where all the available CO_2 was injected in a single well.

- Extending the injection period for a total of 20 years to cater for 20 million tonnes of injected CO_2.
- Double the predicted injection rate.

In the reference case, using as injector wells GYA02S1 and GYA05, the injection target was achieved with no backing out of either of the two injectors and the model indicated that none of the injected CO_2 would move outside the original OWC when injecting 10 million tonnes as mandated by the Peterhead CCS Project. With provision for expansion up to 20 million tonnes the injection period was extended until 2039. In this case the model indicated that only 3% of the total injected CO_2 was lying outside the original OWC (water leg beneath the reservoir but still within the storage site) at the end of injection.

After cessation of injection all the CO_2 is either recovered back into the geological store or is otherwise sequestered (via dissolution or capillary trapping).

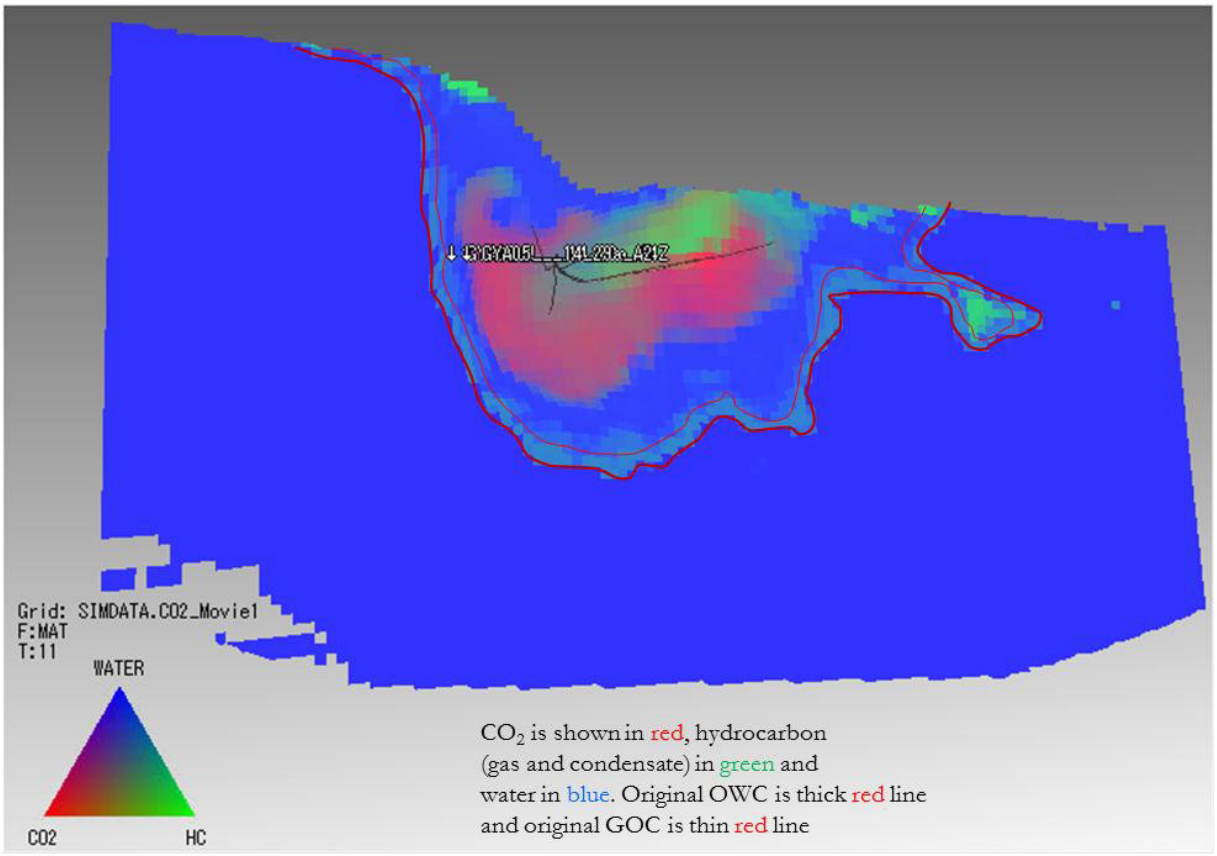

Figure 2-2: Extent of CO_2 at end injection of 10 Mt in 2029

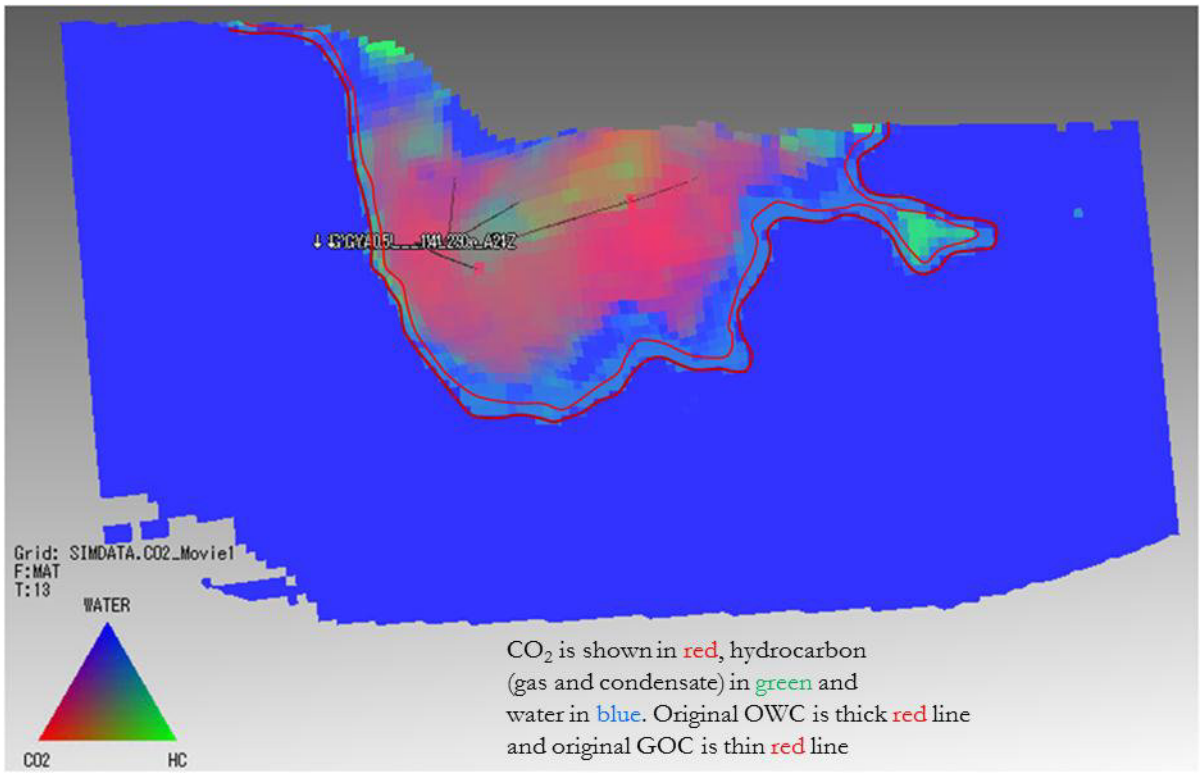

Figure 2-3: Extent of CO_2 plume at end of injection of 20Mt in 2039.

The injection is moderately independent on well choice (because of the storage margin) however, the use of down dip wells (GYA02S1 and GYA04) does reduce the risk of up dip migration for large injection volumes.

2.3. Reservoir pressures

The performance of the Goldeneye reservoir has been significantly influenced by the surrounding aquifer and neighbouring fields which were found to be in communication with Goldeneye and which might potentially influence its pressure, if not at present then in the future.

A dynamic model (termed the Regional Aquifer Model) of approximately 100 km of the Captain sandstone was created which contains Goldeneye and four other fields (Hannay, Atlantic, Cromarty, Blake and West and East Rochelle).

A range of scenarios were used to predict future pressures in Goldeneye before CO_2 injection begins. These give a range of pressures in year 2019 from 2703 to 2987 psia [186.4 bar to 206.0 bar] when accounting for Rochelle West and East production. Pressure may rise as high as 3074 psia [212 bar] if Rochelle East and West production is not accounted for (red dotted line in Figure 2-4 below). The original pressure in Goldeneye was 3800 psi [262 bar].

The match to historical data for a number of the aquifer scenarios in Figure 2-4 is good for the late production period and the pressure build period up until April 2014, while the main production period shows a small difference with pressures being predicted slightly too high. The history matching results gives confidence that the dynamic models are suitable to take forward into CO_2 injection.

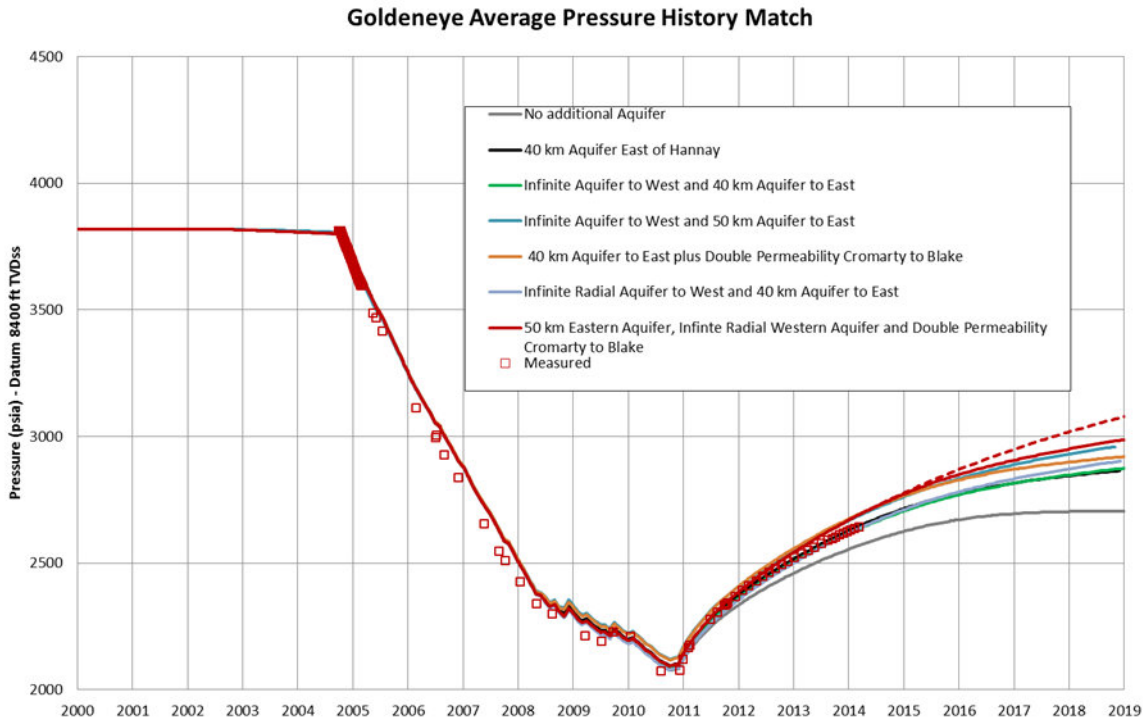

Figure 2-4: Predicted Goldeneye pressure before injection

Figure 2-5 shows the pressure changes during and after injection. Again, the red dotted line represents the case where Rochelle production has not been accounted for. Immediately after the end of CO_2 injection in 2029, the pressure starts to decline as pressure starts to equalise across the fairway. This is then followed by a slow rise in pressure which is due to the regional aquifer encroachment. Even with an infinite radial aquifer in the west this rise in pressure is slow and after 1000 years it may just reach initial conditions of the Goldeneye field.

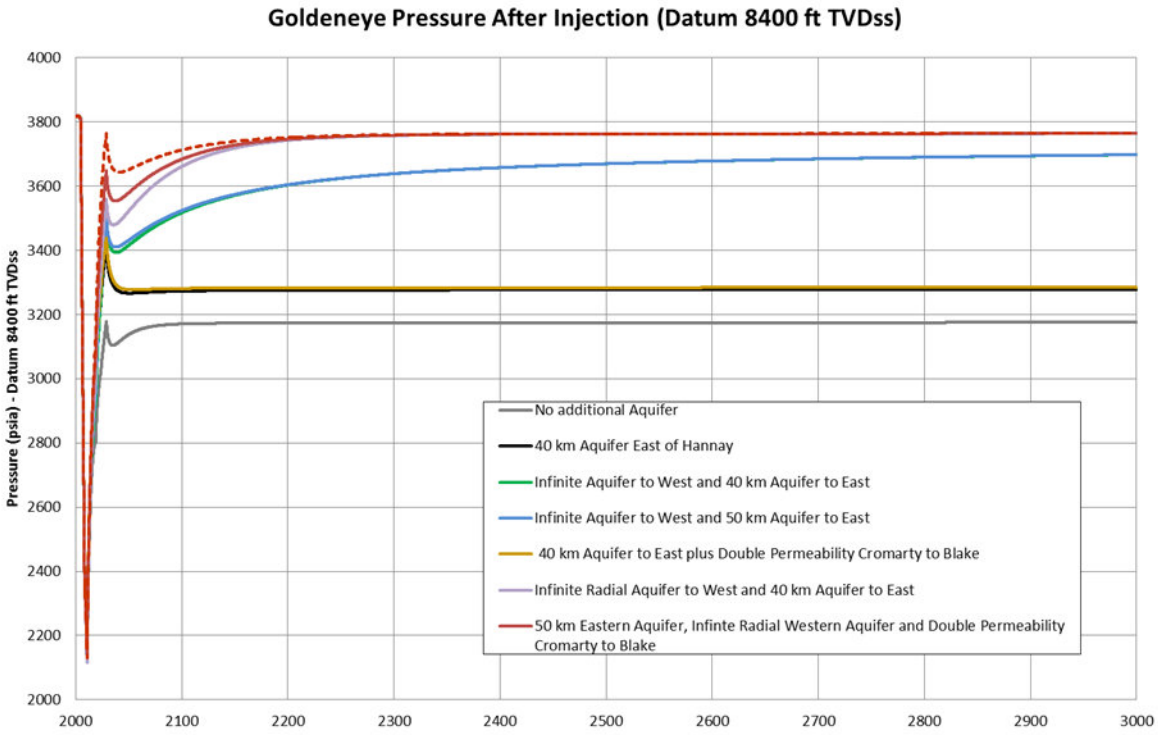

Figure 2-5: Predicted Goldeneye pressure after injection for different aquifer realisations – 1000 years

In all cases of 10 million tonnes of injected CO_2, the CO_2 plume does not reach the spill point. CO_2 dissolution traps approximately 5% of the injected CO_2 but this is thought to be optimistic due to factors such as the large grid size. A more detailed discussion of dissolution trapping and geochemical trapping is given in the report on geochemical reactivity (4).

The effect of CO_2 injection in Goldeneye on neighbouring field pressures has been investigated. The rise in pressure in the neighbouring Hannay field to 2029 is expected to fall in the range 300 - 500 psi [20.7 – 34.5 bar]. The rise in pressure will be affected by production from the West Rochelle field which started production in October 2013 and East Rochelle which started in January 2014. (Atlantic and Cromarty pressures will also rise by 200 - 500 psi [13.8 – 34.5 bar] over the period to 2029 but this is also uncertain as they are more sensitive to the size of the western aquifer and the impact of continuing production and injection at Blake.

3. Introduction

Goldeneye is a gas condensate field located in the UK part of the North Sea, approximately 100 km off the North-East coast of Scotland. The original gas column is about 300ft [91m], with a thin oil rim of 24ft. Permeabilities are high and varying between 700 and 1500 mDarcy in the productive sands with porosities of 22-24%. Depth of the field is about 8500ft [2591m] TVDSS and initial pressure was 3800 psia (at datum depth 8400ft [2560m] TVDSS).

The field was discovered in 1996 by the Captain Sandstone discovery well, 14/29-a3. Three further appraisal wells were drilled in Goldeneye. It was developed in 2003/04 with five subsea wells through a multiphase tie-back over a normally unattended installation to the St Fergus gas processing plant.

The reservoir rock, the Captain Sandstone Unit, comprises Early Cretaceous-aged sandstones deposited in a submarine environment. The trap is formed by a combination of structure and stratigraphic trapping. Hydrocarbon Initially In Place volume is over 800 Bscf [$22.65 \times 10^9 m^3$] of which some 568 Bscf were produced from October 2004 until December 2010, when cessation of production occurred. Depleted oil and gas reservoirs are prime candidates for CO_2 storage for several reasons:

- First, the oil and gas that originally accumulated in (structural and stratigraphic) traps was contained (in some cases for many millions of years), demonstrating the long term integrity of such reservoirs.
- The geological structure and physical properties of most oil and gas fields have been extensively studied and characterised.
- Some of the infrastructure and wells already in place may be used for handling CO_2 storage operations.

Goldeneye has all of these elements, making it an excellent candidate for CO_2 storage.

The geological carbon storage capacity of Goldeneye was estimated with conventional analytical volumetric assessment, based on total hydrocarbon production from the field. The analytical storage estimation was compared with results from three-dimensional, three-phase, full field Goldeneye numerical simulation model, with the objective of evaluating different injection scenarios to map out the range of capacity available for CO_2 storage.

The Goldeneye field is located in part of the Captain/Kopervik fairway. The performance of the Goldeneye reservoir has been significantly influenced by the surrounding aquifer. Additionally, nearby fields in the Captain sandstone: Hannay, Atlantic, Cromarty, Blake, East and West Rochelle, have been assessed to be in communication with Goldeneye and may potentially influence its pressure, if not at present then in the future. The neighbouring Hoylake field, not developed, also influencing the pressure in the Goldeneye reservoir. These interactions were investigated with a regional multi field, three-dimensional, three-phase, numerical simulation model of the Captain Fairway. This model is also documented in this report.

The objective of this report is to document all the dynamic modelling carried out in order to estimate the likelihood of injecting 10 million tonnes of carbon dioxide (CO_2) into the Goldeneye reservoir, as required by the UK CCS Commercialisation Competition. Goldeneye was also studied for the earlier UK CCS Demonstration Competition, for which a storage capacity of 20Mt CO_2 was required.

Analysis was carried out considering an uncertainty range based upon a collection of parameters, both static and dynamic, that affect the capability of Goldeneye to sequester carbon dioxide.

Assessment of the maximum capacity of the depleted Goldeneye field and the adjacent Captain/Kopervik fairway is outside the scope of this report and the UK CCS Commercialisation Competition.

4. Reservoir engineering workflow and philosophy

4.1. Objectives

- Establish the feasibility of sequestration (storage margins) – capacity, lateral containment.
- Determine the 3D pore volume that will constitute the primary storage
- Develop expectation injection/bottom hole and average reservoir pressure forecast; plus determine the ranges of injection pressure and deliver a number of reservoir pressure profiles
- Determine the optimum injection strategy – for injectivity and containment

4.2. Underpinning philosophy

In order to gain a CO_2 sequestration licence it is necessary to demonstrate that the required volume of CO_2 can be securely stored in Goldeneye. For practical simulation and study purposes this is interpreted to mean that the injected CO_2 is extremely unlikely to leak to the surface or move outside the licensed storage complex within 1000 years.

To show that the CO_2 is extremely unlikely to migrate, the concept of a storage margin was used. The demonstration is built up in two steps (i) show that significant egressions are unlikely (an egression is movement out of primary storage), and then (ii) show that leaks to surface are even less likely. The necessary steps to demonstrate this are:

- Determine the conditions that are required for a significant egression event (e.g. CO_2 reaching a neighbouring hydrocarbon field in the same formation), then show that the operating conditions of the CO_2 store are sufficiently removed from the conditions required to create the significant egression event
- Show that a number of significant egression events are necessary in series in order to create a leak to the surface. Show that this is extremely unlikely either because of multiple natural obstacles; or because of project controls; or a combination of both

In the ideal case, there will be a large safety margin between the operating conditions for the store and the conditions required for even a single significant egression event.

This first point is addressed in detail by the dynamic modelling while the second point is examined in detail in the subsurface risk assessment.

4.3. Multiple scale modelling strategy

The whole modelling strategy requires different levels of detail in order to address project decisions and to handle the uncertainties. The modelling was divided into three components as follows:

- Detailed modelling of the behaviour of CO_2 in the primary storage constrained by the boundary conditions set by the connected aquifer [Full Field Model, FFM]
- Modelling of the interaction of the primary storage and the connected aquifer in the Captain Fairway – this includes the potential size and extent of any lateral egression plumes [Fairway/aquifer model]

- Support by a physics work stream based on a simplified structure model (dipping box model) where specific elements were tested to ensure that the correct physics are implemented. Relevant results are taken into the FFM and other dynamic models.

In addition, a geomechanical model and a chemical reactive transport model complement the modelling phase of the Goldeneye Project. These two elements are reported separately.

4.3.1. Full field dynamic modelling workflow

A modified version of the full field model which had been used for the hydrocarbon producing period of the field's life was built in order to make it suitable for CO_2 modelling. The following workflow elements were employed:

- Check that the model has an acceptable bottomhole pressure (built up) history match, and a reasonable water breakthrough match.
- Check the validity of the model:
    - Start with the existing base case model. Add extensions to East and West (these extensions are the inclusion of more lateral aquifer grid blocks in order to better model CO_2 injection)
    - Work with black oil PVT during the history matching phase. Then convert it to compositional PVT (Peng Robinson 1978) (5)
    - Initialise as per the producing asset (i.e. at depleted state)
    - Run history match
    - Forecast final production in order to check well properties
- Examine uncertainty and create alternative realisations – as per uncertainty analysis.
    - Re-history match using similar approach as reference case.
- Check CO_2 sensitivity assumptions – do they harm the history match?
    - Increase layering in reservoir sands (grid sensitivities to CO_2 modelling)
    - Incorporate relative permeability hysteresis
    - Move to Equation of State (EOS) PR (6) representation
    - Turn on dissolution in water
    - Check history match for each of the above and then all of them together
    - This creates a set of three starter models that should incorporate the CO_2 injection static and dynamic model uncertainty realisations.
- Forecasting
    - For the purposes of the full field model, neighbouring fields are not explicitly included. Any impact they may have on Goldeneye will be handled as part of the analytical aquifers which are attached in MoReS. The larger Captain Fairway model includes several other fields with their production history.
    - For selected geological & aquifer strength realisations which satisfy the history match constraint), create a set of CO_2 realisations which will reflect the following elements:
        - Relative permeability hysteresis effects (trapped saturations)
        - Mixing effects (only if found to be significant)
        - CO_2 dissolution
        - Geochemical reactions (documented separately)
    - Develop effective injection strategies which are robust when tested against the realisations. Elements to test are:

- Injection patterns (including injection in the well most likely to give rise to an egression, or the well with the poorest injectivity)
- Injection of larger volumes, , at higher rates, for longer, at higher pressures

- Deliverables:
  - Injection pressure profiles – (in most of these study cases the injection rates are fixed) – bottom hole pressure and reservoir pressure – deliverable for wells, Production Technology, facilities
  - Storage capacity estimation and capacity margin.
  - Pressure/saturation fields for geo-mechanics and 4D synthetic seismic..
- Long term elements:
  - Aquifer strength (pressure build-up – increases force to push CO_2 through cap rock or abandoned wells)
  - Migration in E-sand (increases contact with cap rock)
  - Final pressures at cap rock
- What does it take to create a significant egression?

4.3.2. Fairway/Aquifer dynamic modelling workflow

- This model:
  - Provides boundary condition inputs to the FFM (for initialisation, injection and recovery)
  - Provides better understanding of material balance within the fairway (interaction with neighbouring fields) and pressure behaviour (aquifer characterization) in Goldeneye post depletion (field recharge pre and post CO_2 injection).
  - Allows modelling of potential plume extents (using volumes from FFM)
  - Allows modelling of pressure impact on neighbouring fields
  - Allows estimation of dissolution trapping, capillary trapping and chemical trapping (when linked to PHREEQC)
- The model is based on a new geological top map, petrophysical properties, and limited dynamic data from other operators.
- Includes only a single full 3D dynamic fairway realisation (reference case)

4.3.3. Physics workflow

This element includes the detailed analysis to create the inputs to the FFM and other dynamic models. It includes:

- Understanding the impact of SCAL uncertainties on CO_2 injection (especially hysteresis – trapped saturations)
- Support for SCAL programme definition
- Validation of the PVT modelling for the FFM and understanding and documenting the uncertainties and limitations
- Modelling of the chemical reactivity in the cap rock, reservoir and overburden
- Modelling of the geomechanical stress and potential effects of injection
  Modelling of the fracturing potential in the reservoir (thermal and pressure and from CO_2 weakening)[8]

- Modelling of thermal effects resulting from the injection of cold CO_2 in the reservoir (potential for hydrates and fracturing) [7,8]

Much of this work was performed in a simplified structure model (dipping box model). Relevant results were taken into the FFM and other dynamic models.

The list of models used and their purpose (in relation to project decisions and uncertainties) can be summarized in Figure 4-1.

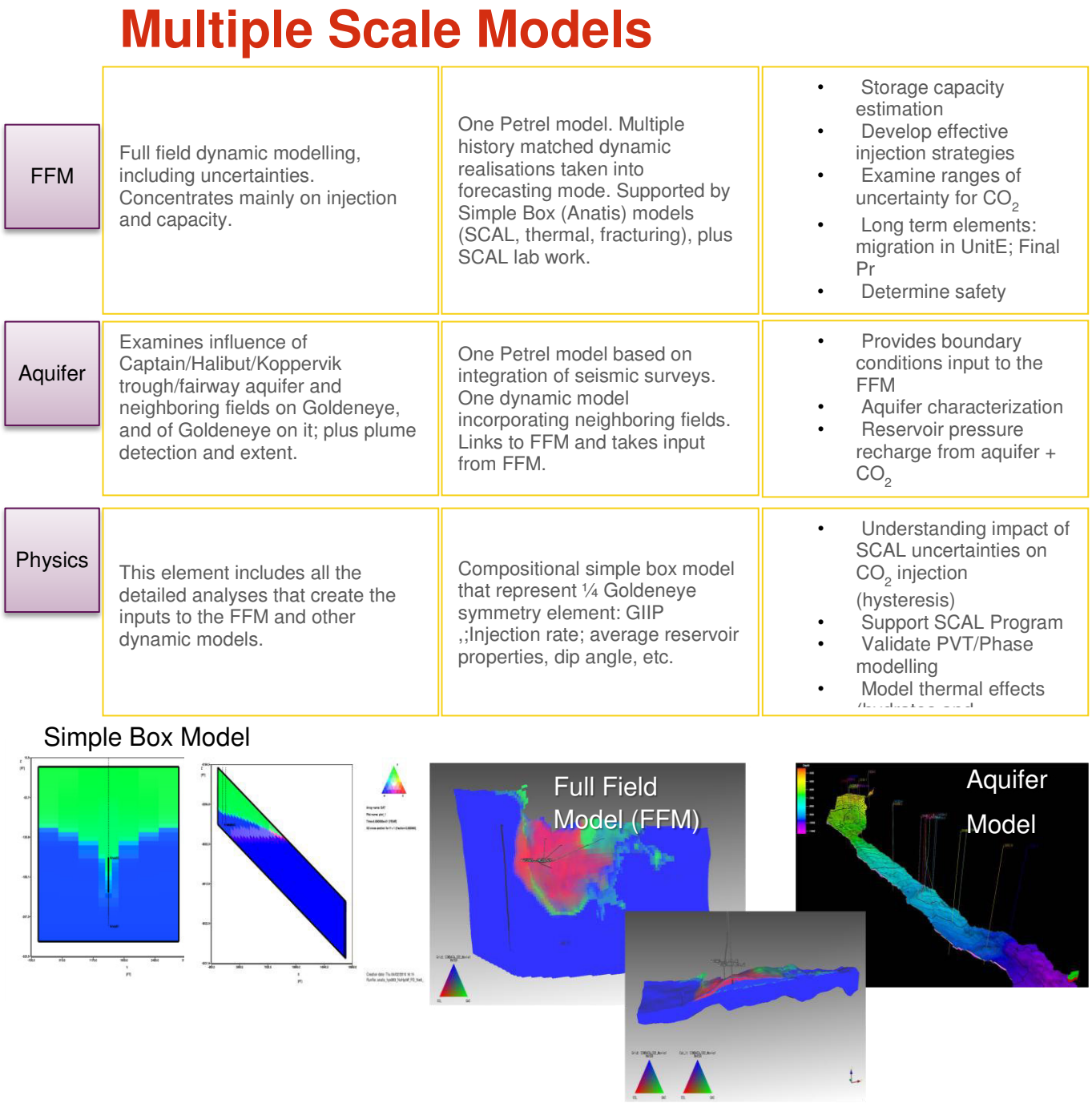

Figure 4-1. Multiple scale models approach.

5. Input for Full Field Simulation Models

5.1. Geological Model

The Goldeneye field is a gas condensate accumulation with a thin oil rim, located in the South Halibut Trough of the outer Moray Firth area, in the U.K. North Sea. Its reservoir, the Captain Sandstone Unit, comprises Early Cretaceous-aged sandstones deposited in a submarine environment. The trap is formed by a combination of structure and stratigraphic trapping. Figure 5-1 shows the field location with some regional structural elements.

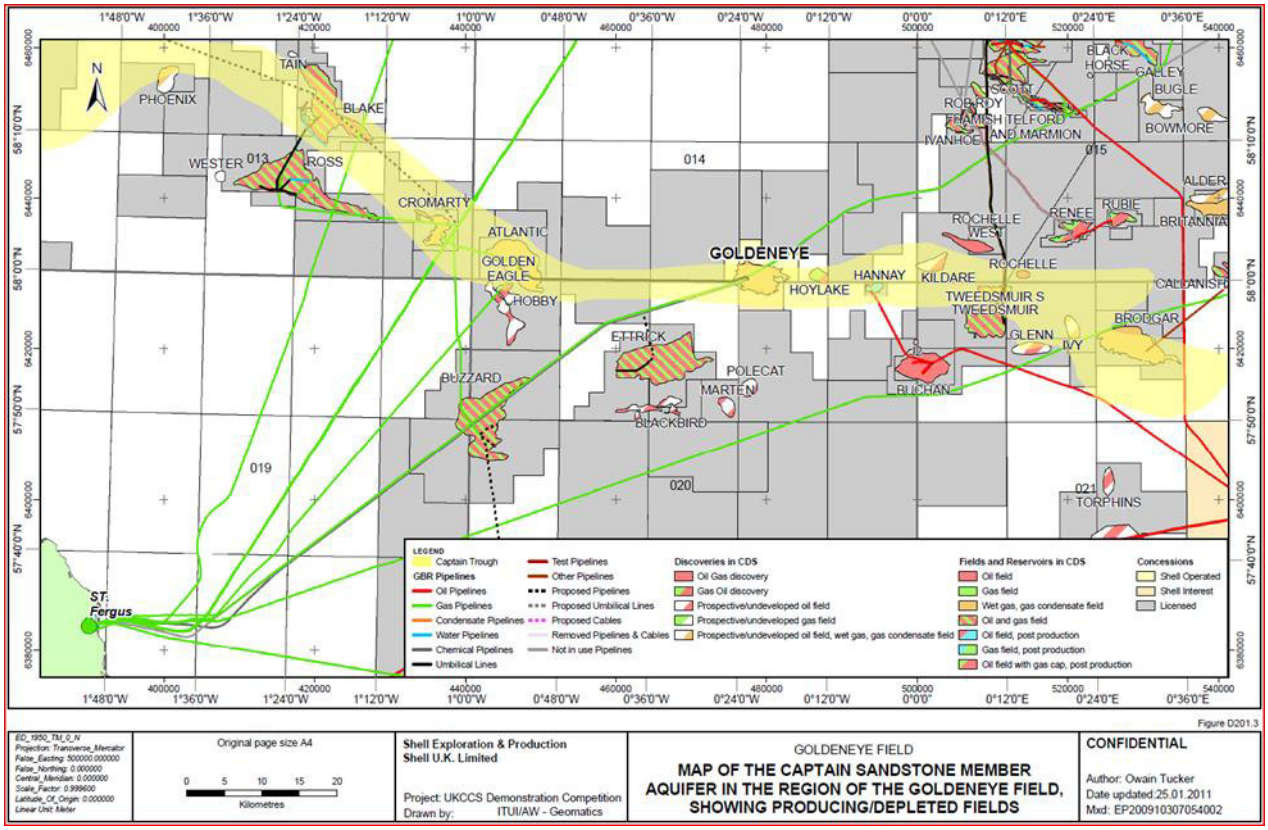

Figure 5-1. Goldeneye location map. The Captain Sandstone in the outer Moray Firth: Captain Fairway highlighted in yellow, basinal areas in pale green

5.1.1. Structural Model

The main reservoir is formed by a sandstone turbidite system with good reservoir properties (average porosity of Captain 'D' reservoir is 25% and average permeability is 1145 mD) containing hydrocarbons at normal pressure and temperature.

The Goldeneye field is a combined structural and stratigraphic trap (Figure 5-2). The trap is a three-way dip closed anticline to south, west and east, with a northerly up-dip pinch-out. The exact location of the northerly pinch-out cannot be resolved seismically, but Captain-aged sandstone is absent from well 14/29a-2 to the north. The sandstones lap onto and thin onto the Halibut Horst high, creating a pinch-out. The geometry is therefore interpreted to be a thinning wedge of sandstones formed during deposition. There is no significant faulting at top Captain level. There are many small scale faults interpreted, but these have minor throws.

The reservoir top-seal is formed from a combination of upper Valhall Formation and Rødby Formation shales. These two units combined comprise a 60-85m thick succession of laminated,

calcareous mudstones. The extent of the top-seal is significantly larger than the reservoir, and it therefore forms a regionally effective seal.

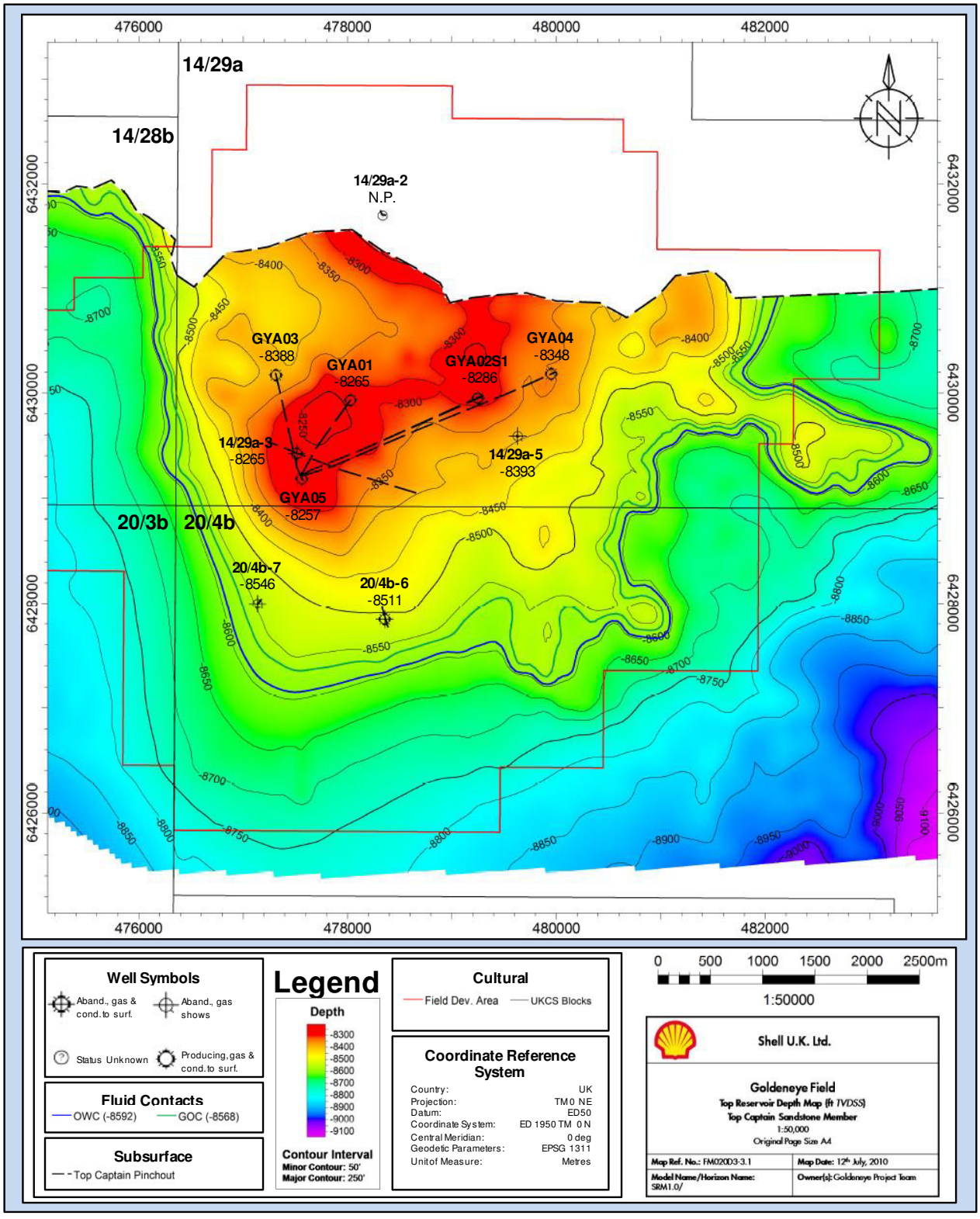

Figure 5-2. Goldeneye field top structure map.

The OOWC at 8592ft [2618m] TVDSS proves effective closure to at least this depth. All models therefore assume a structural-stratigraphic spill point in the north-west corner of the field at the OOWC, consistent with regional models of up-dip gas migration from east to west.

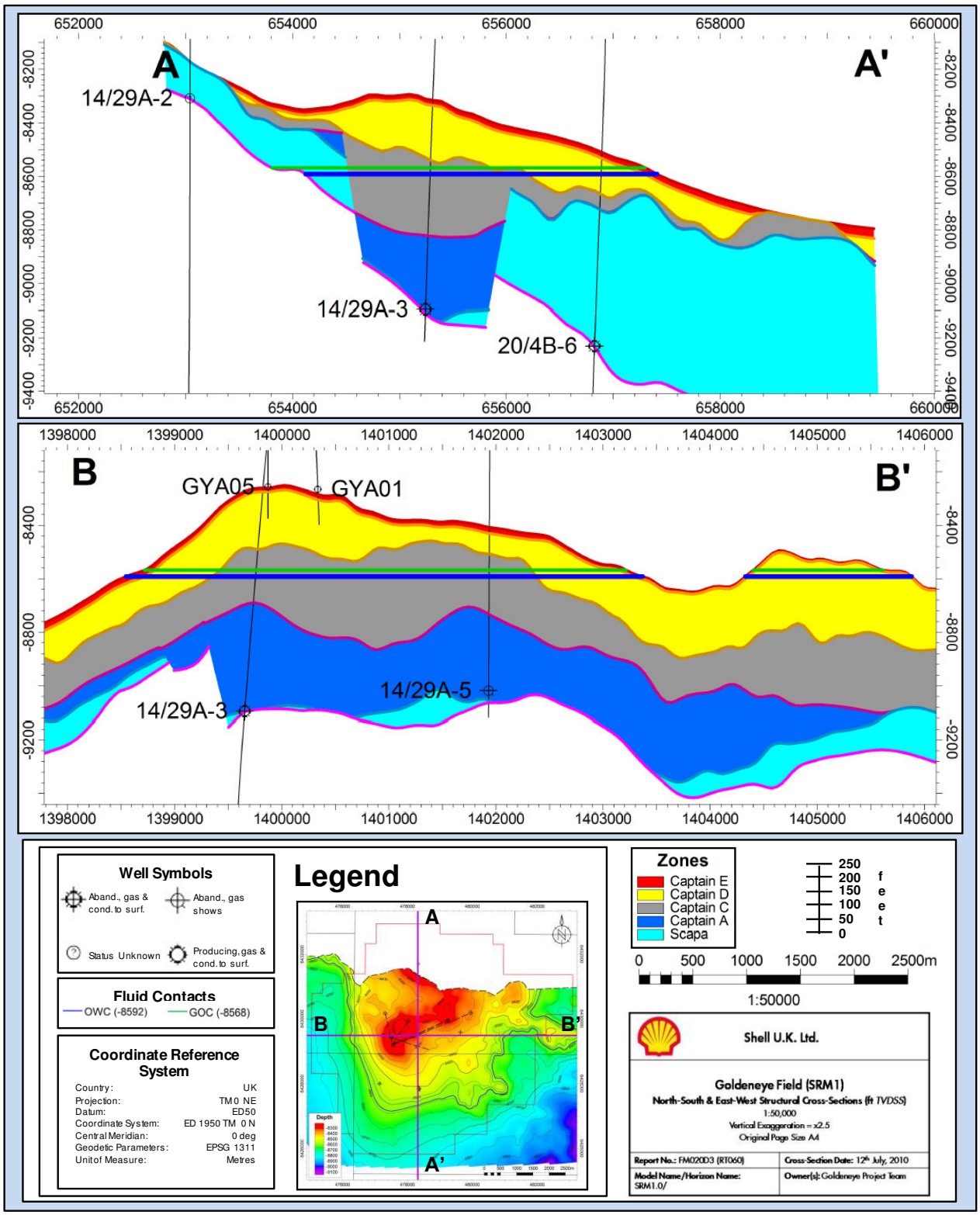

Figure 5-3. Representative structural cross-sections through Goldeneye field.

A suite of static reservoir models has been generated to evaluate key uncertainties impacting on CO_2 storage capacity and containment. The differences in the models have been generated by:

- including/excluding faults;
- differing seismic depth surfaces to represent the top and base of the reservoir;
- using seismic depth surfaces, isochores or well tops to define internal reservoir layering;
- varying the location of the northerly stratigraphic pinch-out;
- altering the zonation of the pre-reservoir stratigraphy and;
- adding (or ignoring) a top Captain 'C' pick to well GYA01.

In each case, the data and methodology used to construct the facies and petrophysical property models remained the same – with the exception that the vertical probability curve that controls facies distribution in each zone had to be modified to accommodate changes in zone layering.

5.1.2. Full Field Model Grid

The CCS Goldeneye field SRMs are all gridded at approximately 50 x 50m (voxel level). The model framework grid itself comprises irregular cells, and all models share the same grid. Models have 253 x 147 x 250 (number of layers varies), giving around 9.5 million cells.

The static model Petrel grid is the same as that used for the full field dynamic simulations but up-scaled mainly vertically. The full field model (FFM) has dimensions: 126 x 73 x 23 (211554 gridblocks). There are 23 vertical gridblocks divided over 4 flow layers as shown below in Figure 5-4 with an average thickness of 8m (25 ft) thick. The horizontal dimensions of the simulation gridblocks are 100 m x 100 m, twice the original size.

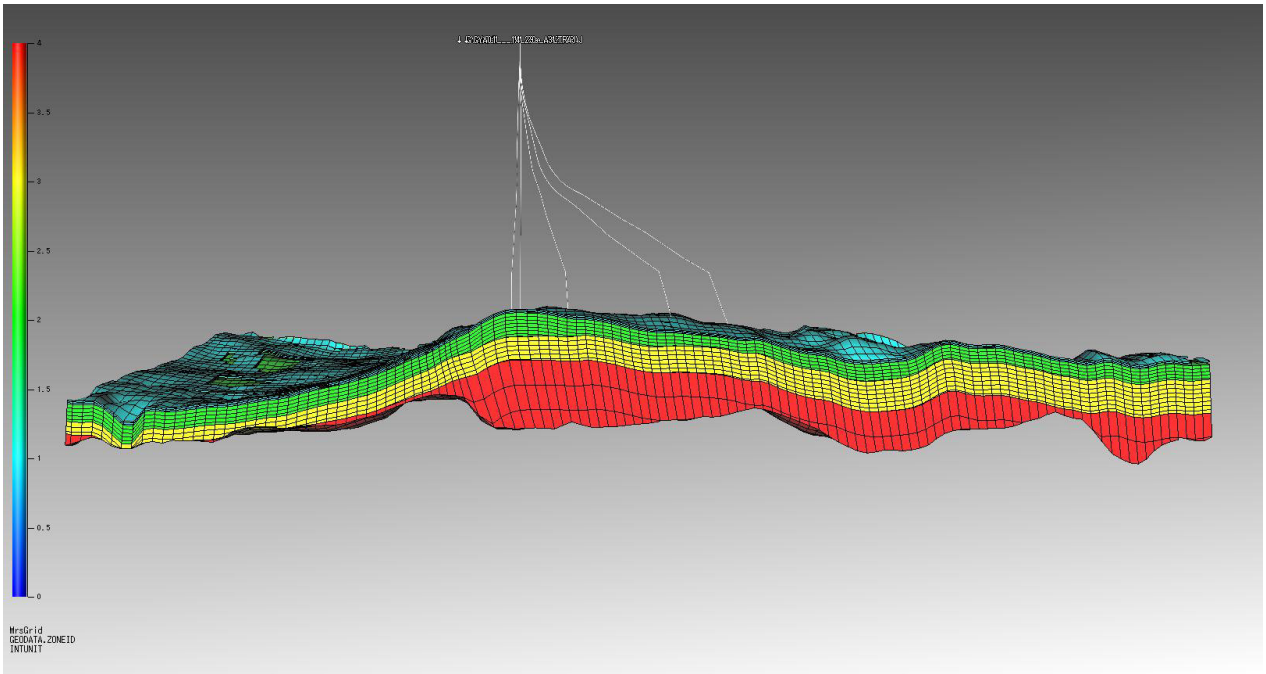

Figure 5-4. Cross-section of Goldeneye FFM Zones.

In order to model CO_2 flow, it is also appropriate to concentrate on higher resolution towards the tops of flow units, where buoyant CO_2 will collect and then migrate laterally. CO_2 tends to form thin expanding plumes below permeability barriers and to spread out laterally. It is important to have sufficient resolution to allow accurate plume modelling, and to have coherent cell layers to allow stable cell-cell calculations. This means that for the important reservoir layers, such as Captain 'C', 'D' & 'E', layering was always made top conformable or proportional to avoid cells collapsing laterally.

5.1.3. Static Properties

The Goldeneye reservoir may be sub-divided into four litho-stratigraphic units, from top to base as shown in Table 5-1 and Figure 5-5.

Table 5-1. Sub-Division of the Captain reservoir, Goldeneye area.

Reservoir Unit	Description
Captain 'E' Unit	Laterally variable thin heterogeneous unit
Captain 'D' Unit	Laterally extensive massive sand unit
Captain 'C' Unit	Laterally extensive, mudstone-rich heterogeneous unit
Captain 'A' Unit	Laterally restricted sand-rich unit

The Captain 'D' is the primary reservoir unit, into which all the development wells have been completed. It comprises medium grained massive sandstones that, with the exception of a fining-upwards sequence at the top seen in all wells in the field, show only subtle changes in grain size. Average Net-to-Gross from this interval is 94%, average net porosity is 25% and average (total) permeability is 1145mD. Captain 'D' is the most prolific flow layer with the highest permeability and largest HCPV. As a consequence, it is where most of the injected CO_2 is expected to be stored.

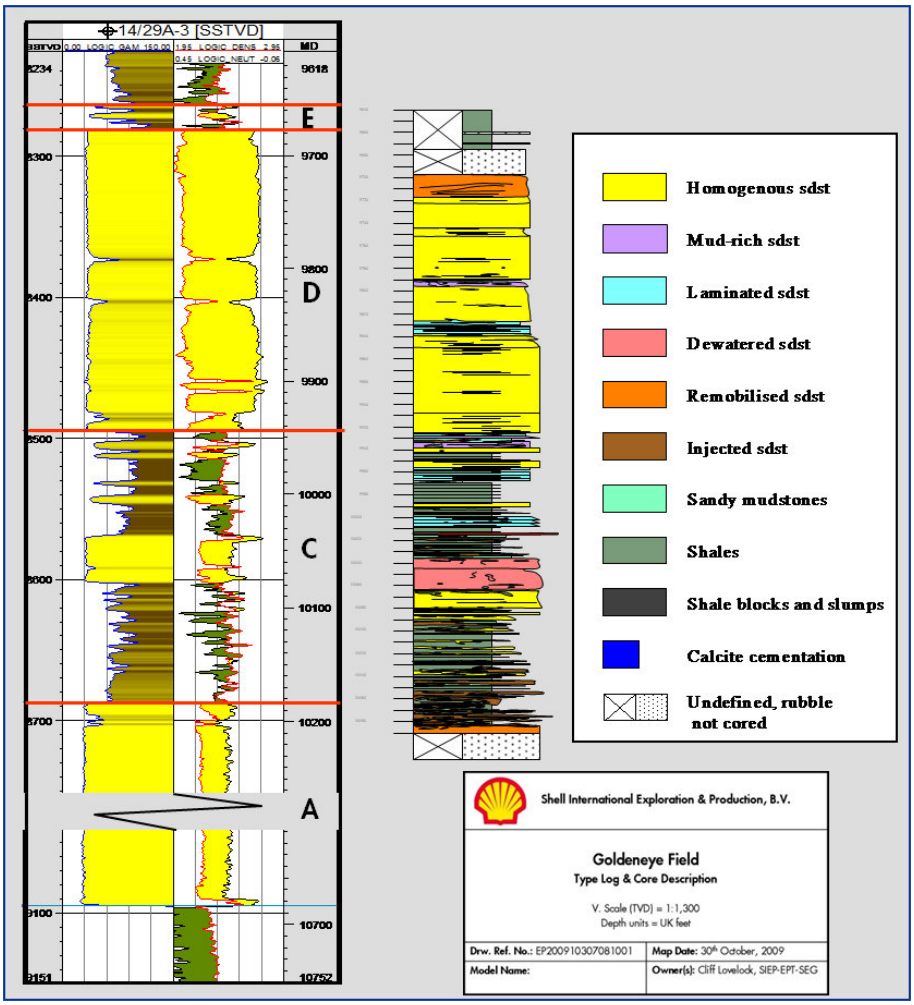

Figure 5-5. Goldeneye Type Log.

In order to generate the property model, input log data derived from petrophysical evaluations were up-scaled into the model layers by arithmetic averaging, and then a Sequential Gaussian Simulation (SGS) algorithm was used to populate the model. Property modelling follows a similar methodology to the facies modelling.

5.1.4. Net to Gross, porosity & permeability modelling

Property modelling was performed separately for each individual zone. The porosity, permeability and net/gross curves were up-scaled into the model layers using arithmetic averages. The three properties were distributed between wells using Sequential Gaussian Simulation and constrained via the facies model. This means that property distributions derived from the log data are maintained in the populated model.

The original input porosity curve has a cut-off applied at 0.14 pu, and ensures there are no zero values for porosity (they are set to undefined). The cut-off prevents net reservoir appearing in shale sections of the log data, and it is also noted that 0.14 gives the correct thickness of cements compared to core.

Permeability is co-kriged with the porosity model, to ensure that if a cell has a high porosity value; it is more likely to have a high permeability. The stochastic distribution of the properties is taken from the distribution seen in the up-scaled well logs for Unit 'E' and Unit 'D'. For the other zones the

number of well penetrations is very limited and the distribution found from the up-scaled well logs is not a statistically meaningful sample. In these cases a normal distribution using the mean and standard deviation taken from the up-scaled well logs is enforced upon the properties. The net-to-gross modelling uses a trend grid to decrease the net to gross seen in the wells from South to North.

For further details about the geological model of Goldeneye refer to the Static Reservoir Modelling (Field) Report (7).

5.1.5. Permeability reconciliation with dynamic data

The static permeability estimates were used during the field development and early CCS planning phases to achieve satisfactory history matches in the dynamic realm. However, recent Goldeneye dynamic history data and inclusion of information from the neighbouring Hoylake field show there is a need to increase reservoir permeability in Goldeneye by a factor of 1.8 to match re-pressurisation performance. An increase in the Goldeneye permeability requires offset by a reduction in the permeability of the aquifer east of the field to balance water encroachment and achieve a match of water breakthrough in the five Goldeneye production wells. The downscaling of permeability of the Eastern analytical aquifer model is corroborated by the regional dynamic aquifer model which suggests lower permeabilities in the eastern aquifer by up to 45% to match pressures in the Rochelle field prior to start of Rochelle production.

To enable this permeability reconciliation, alternative implementations of the porosity-permeability transform were employed. The static permeabilities were derived from porosity using a geometric relationship. The alternative arithmetic relationship was used for Goldeneye and supported the implementation of a permeability multiplier in the dynamic models. The new K/Phi relationship represent an increase in the permeability of 145 % compared to the old poro-perm transform, with an uncertainty band between 130% and 160%.

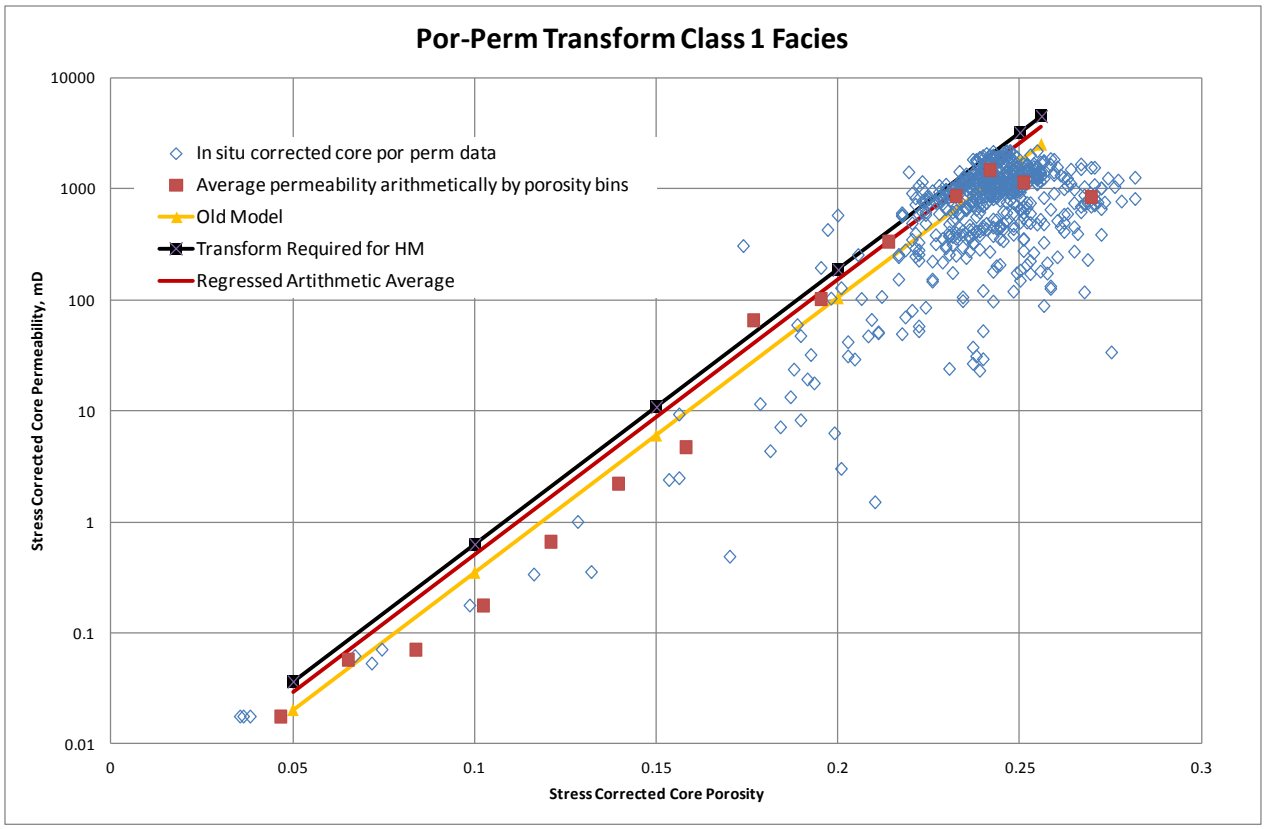

Figure 5-6 Alternative porosity-permeability relationships

The corresponding model permeabilities at well locations were found to be in line with the well test permeabilities derived for three flank wells, GYA05, 20/4b-6 and 20/29a-3 (Table 5-2). Other wells were not addressed as they lay in areas of varying reservoir thickness that would influence the permeability calculation.

Table 5-2: Well test/static permeability comparisons, Goldeneye flank wells

	Model K before correction mD	Model K before correction mD	Well Test K mD	% Difference after correction
GYA05	1007	1460	1430	2%
20/4B-6	351	508	553	-9%
20/29A-3	760	1102	1200	-9%

The required additional uplift to match dynamic performance can be found in alternative mechanisms for distributing permeabilities away from the wellbore in the static model. Sequential Gaussian Simulation (SGS) was employed for the production and early CCS work: the SGS methodology can produce significant lateral permeability changes from grid block to grid block in the model, thereby degrading permeability by 5-15% compared to a more uniform layered permeability system. To compensate for this effect the permeability in the FFM would need to be corrected by applying a multiplication factor to the model perms.

Modifications to the two factors (1) porosity permeability transform and (2) assignment of permeability in the static model enable permeability reconciliation between the static and dynamic realm. The dynamic data shows that in order to match recent re-pressurisation one would need to apply the upper end of the correction band, 1.6 x 1.15 = 1.84.

5.2. Fluid description (PVT)

In 1996 Shell discovered the Goldeneye field by drilling well 14/29-a3, finding a gas column of 303ft. In the following years three appraisal wells were drilled: 1998 Amerada 20/4b-6 (South), 1999 Shell 14/29-a5 (South-East) and 2000 Amerada 20/4b-7 (South-West).

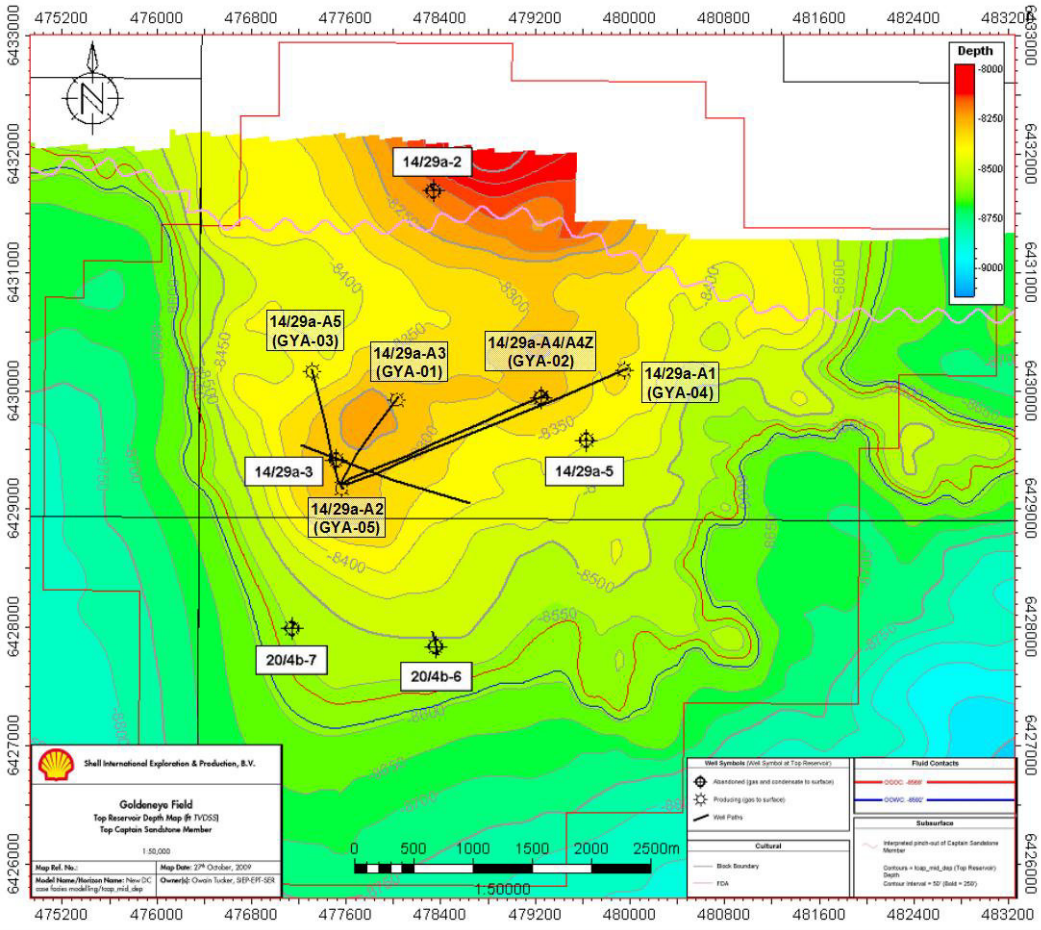

Figure 5-7 Goldeneye field top structure map showing well locations

In 2004 five development wells were drilled. The locations of the exploration and development wells are shown in Figure 5-7.

Fluid samples were taken from all four discovery/appraisal wells during RFT/MDT tests and surface samples from DST tests. PVT samples were taken from the test separator during clean-up of the five Goldeneye development wells (GYA01 to GYA05). Detailed analysis from two of the wells was carried out, GYA04 and GYA03, including geochemical analysis. Gas and liquid compositions were determined for the other wells.

All fluid samples considered representative showed that compositionally, all the gas samples exhibit a high degree of consistency. The calculated phase envelope also illustrated the similarity between all the different samples, as shown in Figure 5-8.

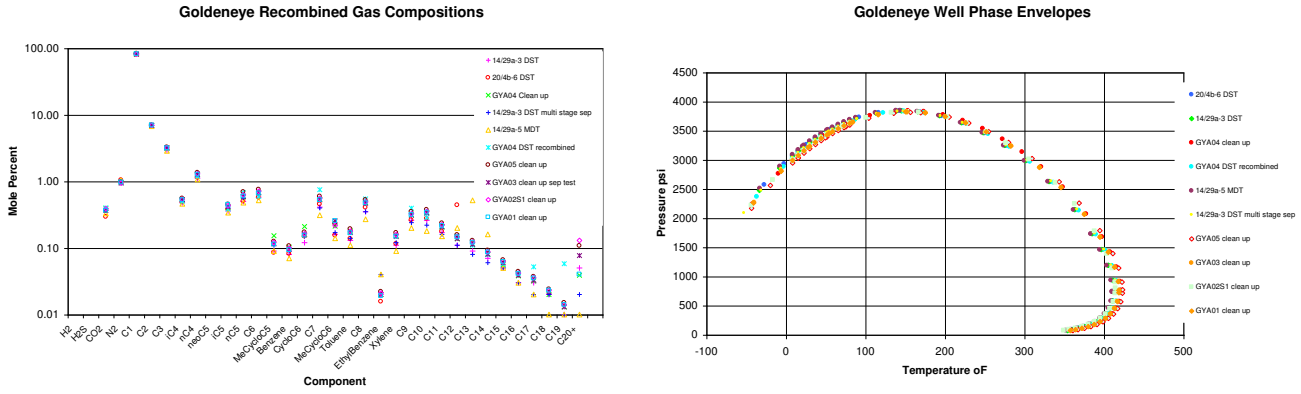

Figure 5-8. Representative Goldeneye recombined gas composition and phase envelopes.

Taking this into account and considering that only GYA03 and GYA04 have a complete PVT suite of experiments, the PVT model currently used by Shell for modelling full field and forecasting was generated based on the surface sample of well GYA03. GYA03 data was matched against the experimental Constant Mass Expansion (CME) and Constant Volume Depletion (CVD) data.

The EOS characterisation was modified to improve the predictions of measured data. Nonlinear regression was used to mathematically minimize the difference between Peng-Robinson 78 (PR78) Peneloux (8) predictions and measured PVT data. Adjustments of EOS parameters such as binary interaction parameters (BIPs) and heavy component critical properties were used. Interaction coefficients between C1 and C7+ pseudo-components were used to improve Saturation Pressure (Dew Point) representation. A decoupled Viscosity Experiment regression over Critical Volume on C7+ pseudo-components was used to match gas viscosity. A summary of the match results is presented in Figure 5-9.

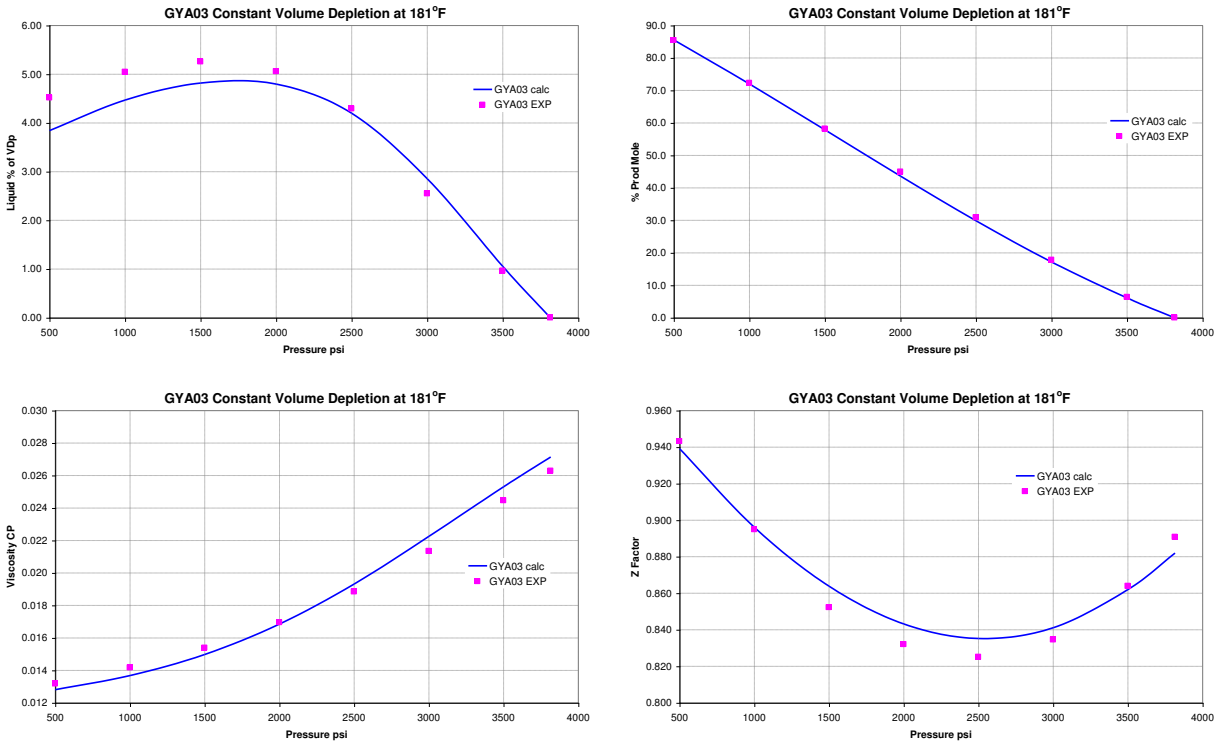

Figure 5-9. **(a) Retrograde condensate %VDp match; (b) Cumulative % volume of the initial wellstream produced; (c) Gas viscosity (calculated); (d) Gas compressibility Z-factor. CVD data with full characterisation.**

The original GYA03 composition was described up to C36+ and was reduced down to six pseudo-components following a stepwise pseudoisation procedure recommended by Whitson (9). It was possible to retune the EOS by regression of the newly reduced pseudo-components, so that the EOS predictability was maintained after the component reduction.

As a final action, additional modifications were introduced in order to improve the representation of CO_2 properties with the EOS. Pure component CO_2 properties were calculated using the thermophysical properties of fluid systems from the National Institute of Standards and Technology (NIST). (10) Comparisons with NIST and PVTSim show some differences in CO_2 physical properties in the pressure operation range within the reservoir (2000 – 3000 psi [13.19Mpa – 20.68Mpa]). At Goldeneye reservoir conditions, error in CO_2 density could be as much as 7% while in viscosity only 4.5%. It was decided to regress over the CO_2 volume shift parameter (C_{pen} after Peneloux) in order to minimize the error between PR78 Peneloux EOS and NIST. The following figure shows CO_2 density error function versus pressure, for a range of C_{pen} values.

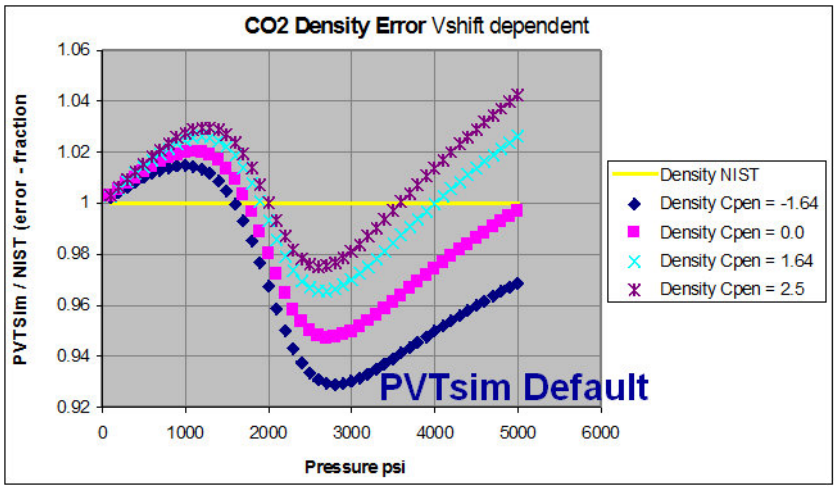

Figure 5-10. CO_2 Density error function versus pressure (psia) for a range of Cpen values

In order to get a balance between the error in density and viscosity a mid value of C_{pen} has been chosen. A value of C_{pen} = 1.64 cm^3/mol offers that midpoint between benefits, allowing a reduction of the density error from 7% to 3.2%, while keeping viscosity error around 2.5% in average for the pressure range of interest.

It is important to understand that these differences in CO_2 viscosities are small in comparison with the range of uncertainty of other parameters such as the relative permeability. For further details regarding the PVT modelling are discussed in the detailed PVT modelling report (11).

5.3. Saturation Functions

The Goldeneye Captain saturation height model is derived using the *Leverett-J* method (12) on both logging and capillary pressure data. The log input only includes clean sand which satisfies the following criteria:

- Porosity above 20 %
- Low clay content, CEC[15] less than 0.1 meq/ml[16]

The initial saturation model is calculated from clean sand logging data. It is then populated with overall log and capillary pressure properties to compare the results. Water saturations produced from both inputs show good agreement with uncertainty less than 0.05 s.u. within net intervals.

Subunit D, the main CO_2 container, is thoroughly uniform and clean. It also presents a massive and continuous sand across Goldeneye, meaning that the Archie method (13) is well suited. Archie log saturation is calculated to verify the Leverett-J model performance. The wells were drilled in different years with different logging tools, which impacts quantitative measurement and trigger the need for individual well Archie parameters.

Log data from wells 14/29-a3 and 20/4b-6 are used as input to the Leverett-J method producing two saturation models for gas and oil. The additional inputs are fluid gradients from the pressure plot, minimum saturation from log at infinite HAFWL, and default IFT reservoir based on hydrocarbon content.

[15] CEC refers to Cation Exchange Capacity.

[16] Meq/ml reads as milli equivalent per milli liter.

The input detail is listed in Table 5-3 for gas saturation and Table 5-4 for oil saturations. The equation is as follows:

$$J = \frac{HAFWL}{\sigma \cdot \cos\theta} \cdot \sqrt{\frac{K}{\phi}} \cdot (\rho_{water} - \rho_{hc})$$

Where: J = *Leverett-J function (unitless)*

$HAFWL$= *height above free water level (ft)*

σ = *interfacial tension (mN/m)*

θ = *contact angle (deg)*

K = *permeability (mD)*

ϕ = *total porosity (v/v)*

ρ_{water} = *water density gradient (psi/ft)*

ρ_{hc} = *hydrocarbon density gradient (psi/ft)*

Table 5-3. Gas reservoir parameter input

		14/29-a3	20/4b-6
FWL	*[ft tvdss]*	8590.9	8592
σ	*[mN/m]*	31	31
ρ_{water}	*[psi/ft]*	0.44	0.44
ρ_{gas}	*[psi/ft]*	0.103	0.103
θ_{gw}	*[deg]*	0	0
$S_{w\text{-}irr}$	*[frac]*	0.02	0.02

Table 5-4. Oil reservoir parameter input

		14/29-a3	20/4b-6
FWL	*[ft tvdss]*	8590.9	8592
σ	*[mN/m]*	25	25
ρ_{water}	*[psi/ft]*	0.44	0.44
ρ_{oil}	*[psi/ft]*	0.32	0.30
θ_{ow}	*[deg]*	50	50
$S_{w\text{-}irr}$	*[frac]*	0.02	0.02

The FFM dynamic model uses saturation height functions whereas the overburden uses chalk capillary entry pressure. In the FFM model porosity and permeability is fixed based on statistical value to create three saturation model representing three sand flow facies. These facies are described as follows:

- High porosity-permeability sand, porosity = 0.25 v/v and permeability = 1000 mD

- Interbedded unit, porosity = 0.15 v/v and permeability = 30 mD
- Debris flow, porosity = 0.07 v/v and permeability = 5 mD

Further details regarding the saturation model are discussed in the Petrophysics report for this project. (14)

5.4. Relative Permeability

The legacy SCAL data comprised relative permeability data measured on core from wells:

- Well 14/29-a3 and 14/29-a5
  - Corelabs study for Shell
  - SS imbibition gas/water relative permeability
- Well 20/4b-6
  - Corelabs study for Amerada Hess[19]
  - Wettability (well encountered oil rim)
  - SS imbibition gas/oil, SS drainage gas/oil, SS imbibition water/oil
- Well 20/4b-7
  - Study for Amerada Hess
  - Report on SCAL programme requested

Core data coverage is as follows:

Table 5-5. Core data coverage

Sample No.	Well No.	Reservoir interval	Porosity (%)	Brine Permeability (mD)
S1A	14/29-a3	Captain D*	18.2	1.7
S2A	14/29-a3	Captain D*	27.3	111
S3A	14/29-a3	Captain D	25.0	792
S4A	14/29-a5	Captain D	27.8	688
S5A	14/29-a5	Captain D	28.3	1224
S7	14/29-a5	Captain E	26.2	28.4
S47	14/29-a5	Captain C	23.3	27
11A	20/4b-6	Captain E	25.0	215
38A	20/4b-6	Captain D	26.8	1168
50A	20/4b-6	Captain D	26.4	1412
56A	20/4b-6	Captain D	26.3	1451

** Plug associated with thin shaly interval*

[19] Amerada Hess (currently the Hess Corporation) is a large American-based integrated oil company headquartered in New York City with exploration and production operations in the United States, United Kingdom, Norway, Denmark, Russia and Africa.

For the simulation modelling work, the 14/29-a3 curves are applied to the oil rim and a small interval above it where oil smearing will occur; the 20/4b-6 curves are applied to the gas column above this point.

Three different sets of relative permeability data are applied for the purpose of reservoir modelling based upon facies. Table 5-6 shows the relative permeability data used for the simulation model.

Table 5-6. MoReS relative permeability data input

Facies	s_{wc}	s_{orw}	s_{org}	s_{gr}	k_{rw}	k_{rwmax}	k_{ro}	k_{romax}	k_{rg}	k_{rgmax}	n_w	n_{ow}	n_{og}	n_g
Gas zone 1	0.07	0.23	0.01	0.25	0.25	0.73	0.2	0.77	0.98	0.98	5	3	5	2.5
Gas zone 2	0.14	0.23	0.01	0.23	0.25	0.73	0.2	0.77	0.98	0.98	5	3	5	2.5
Gas zone 3	0.17	0.23	0.01	0.23	0.25	0.73	0.2	0.77	0.98	0.98	5	3	5	2.5
Oil zone 1	0.07	0.23	0.01	0.23	0.70	1.00	0.2	0.77	0.98	0.98	2.1	3	5	2.5
Oil zone 2	0.14	0.23	0.01	0.23	0.70	1.00	0.2	0.77	0.98	0.98	2.1	3	5	2.5
Oil zone 3	0.17	0.23	0.01	0.23	0.70	1.00	0.2	0.77	0.98	0.98	2.1	3	5	2.5

A NORMALISED_STONE three phase model is used in order to avoid some convergence problems, even though SATURATION_WEIGHTED or LINEAR_ISOPERM are preferred models. Stone models usually create the concaved isoperms at low oil relperm isoperms (nearby straight-lines or convex at higher oil relperm isoperms). Experimental data sometimes indicates convex isoperm curvature even at low oil relperms. In this case, using Stone model(s) could significantly under-estimate oil phase mobility at low oil saturation (thus oil recovery). However, in the Goldeneye case the oilrim is not produced during depletion stage but, just smeared into the gas bearing interval by the aquifer influx, hence no major drawbacks expected by the implementation of Stone model. As a result, for an injection scenario of 10 million tonnes of CO_2, modelled three phase effects could be considered of second order.

On the other hand, the Stone models have the advantage of faster computation speed during the simulation. Therefore in situations where three-phase effects are not expected to play an important role, the Stone models may have some computational advantages.

This problem is not obvious in black-oil mode as it does not allow for three-phase behaviour. In EOS mode, the interaction between three phase behaviour and saturation functions is the cause of many convergence problems.

5.5. Initialisation

The model is initialised with a black oil representation of the fluids in place, with an oilrim of 24ft [7.3m] thick. Datum depth for reported pressures is 8400ft [2560m]. FWL is set to 8592ft [2619m] TVDSS and FOL at 8568ft [2612m] TVDSS.

The model has been initialised following a procedure of explicitly defining the oil and gas initial composition with a PX representation of the PVT data. The undersaturated oilrim is forced to be initialised with Rsi = 926.7 scf/stb, in line with the down hole samples of wells: FMT/ MDT of 14/29-a3, 20/4b-6, 14/29-a5. GOR (scf/stb) 818, 1005, 1029, respectively. In this way, even though the oilrim representation is a simplification (single PVT for the model properly describing the gas

condensate) it keeps the main properties in line with the downhole samples available. Otherwise, due to the use of a single PVT (gas condensate one) the oilrim would be a condensate dropout with different properties (lighter oil) such as viscosity and density than that from the downhole samples.

The initial pressure used in a model assumes partial depletion of the field due to communication with the neighbouring oil field Hannay which came onstream in March 2002. The decline rates for the five wells range from 0.019 psi/day [0.00131 bar/day] in GYA02s1 to 0.023 psi/day [0.00159 bar/day] in GYA04. This accounts for about 15 psi pressure drop from original pressure of 3815 psi measured in exploratory wells 14/29-a3 and 14/29-a5 and is further explained in detail in Section 11.

5.6. Production Data

Goldeneye has some of the best production data in the North Sea – having continuous flow and down hole pressure monitoring. Each of the Goldeneye production wells were completed with permanent downhole gauges which are connected to individual pressure, temperature and mass flow meters. As a consequence, reliable and precise data is available throughout all the production history of the field. All real time data is collected and captured by the SCADA system and can be extracted to an Excel database.

This data is then input to the simulation. The simulator is therefore fed with data directly from the well head where gas rates are measured by *Venturi* meters after the choke (checked in the offshore test separator) and from permanent real time pressure gauges at the well foot. Since cessation of production in 2010, the gauges have continued to be monitored, providing a further three years of pressure build-up data. Three out of the five gauges are still operating in 2014, while the other two have been isolated from the reservoir by suspension plugs.

5.7. In-place volumes from up-scaled static reservoir models

The suite of static reservoir models in use to investigate Goldeneye's suitability for CCS has a range of initially in-place volumes of between 706 and 797 Bscf (a spread of 86 Bscf). All of these models, therefore, have GIIP volumes that lie between the P15 and P85 expectation volumes as calculated by the Goldeneye production team (705 & 799 Bscf, respectively).

To create the full field simulation model, the static reservoir model was exported in Rescue format (v37) from the Petrel software application and imported into Shell's dynamic simulator (MoReS), via an up-scaling application – also software developed within Shell – called 'Reduce++'. The up-scaling process converts a fine-scale geological model into a model with fewer cells which can be used for history matching or forecasting with acceptable runtimes. The coarse gridblock properties are derived from the properties of the underlying geological model such that their behaviour closely reflects that of the geological model. Different up-scaling methods are used for different properties.

Table 5-7 shows the equivalent volumetric measurements in the static reservoir model and the full field simulation model. Fluid saturations in the FFM are not imported from the static reservoir model. Instead a capillary pressure curve is used (for the static reservoir model saturations are derived using a saturation height function derived to match the S_w curves calculated from petrophysical analysis). The gas formation volume factor (B_g) used in the static reservoir model is the one used by the production team and is not the same as the one derived from the latest PVT model discussed in section 5.2 - which is used in the full field simulation model.

Table 5-7. Equivalent quantities in Static Reservoir Model (SRM) and Full Field Model (FFM) used for simulation.

SRM	FFM
Bulk volume	Not available
Net volume	GBV : Net reservoir (rock) volume
Pore volume	GBV * porosity = Net pore volume
HCPV gas	Net pore volume * saturation of gas
GIIP	HCPV gas / B_g

In all three charts in Figure 5-11**,** the free gas initially in place (FGIIP) volumes from the SRM 3.1, geological model are calculated in the static reservoir modelling software (Petrel) and in the software which upscales the static model to a dynamic model (Reduce). The small differences between the volumes from Petrel and their equivalents in Reduce are largely due to the fact that Petrel can assign part of a voxel to, for example, net sand while Reduce specifies the whole voxel as either net or non-net sand. In addition, when generating the fluid saturations in Reduce++ the voxel centre height is used and constant values are assumed throughout each voxel. Petrel applies a "height above contact" which is set for the fraction of the voxel cell that lies above the contact.

The static reservoir model hydrocarbon volume was calculated with the production team's figure for gas formation volume factor (B_g). The production team's value for B_g is 4.3 rm^3/sm^3. For this project, a review of the available PVT information has led us to calculate a different figure of B_g = 4.4 rm^3/sm^3). To allow for a meaningful comparison, however, the figure used in the static reservoir model was used to calculate GIIP in MoReS. Using the production team's B_g figure, the Petrel model reports approximately 3% larger GIIP from the main reservoir zone (Captain 'D') than the equivalent MoReS model. Using the B_g calculated from the updated PVT analysis subtracts a further 2% from the FGIIP in MoReS, compared to that calculated in Petrel.

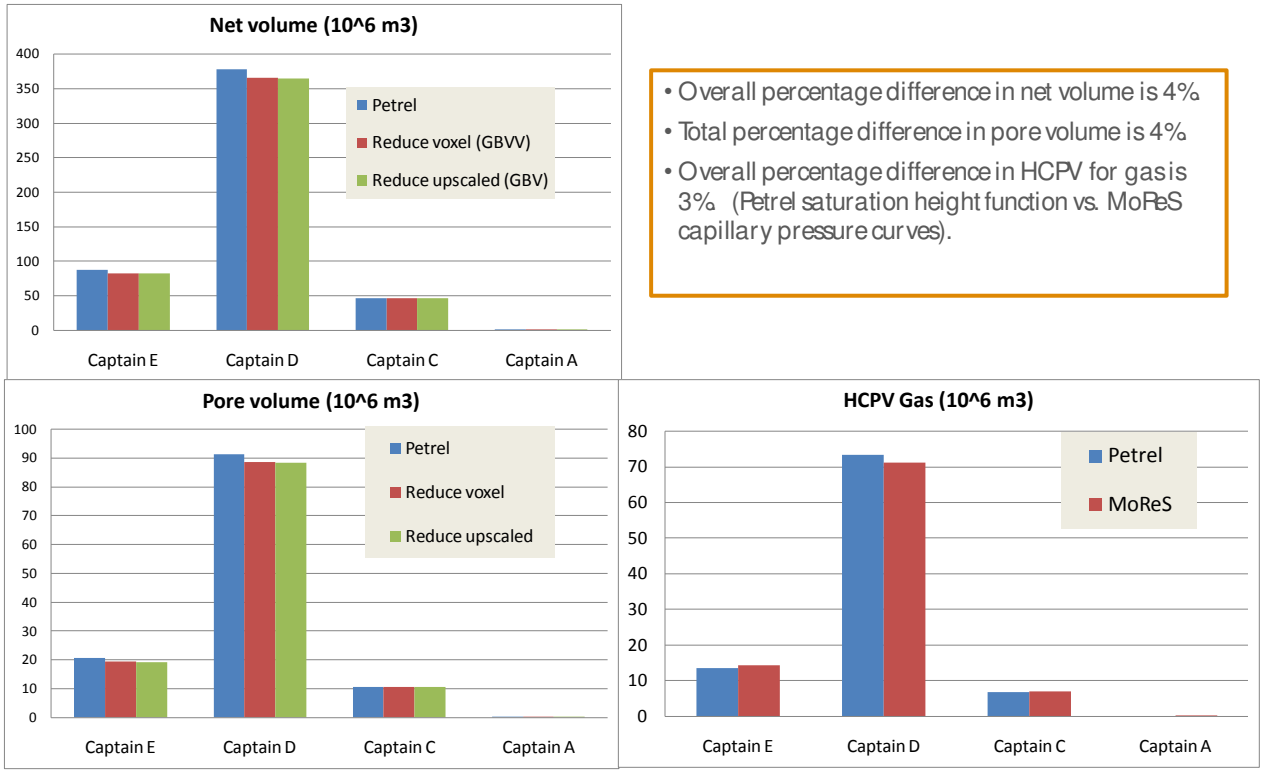

Figure 5-11. **Comparison of different volumes calculated from SRM3.1 in static reservoir model (Petrel), during initial import into dynamic simulator (Reduce Voxel) and after upscaling (Reduce up-scaled/MoReS).**

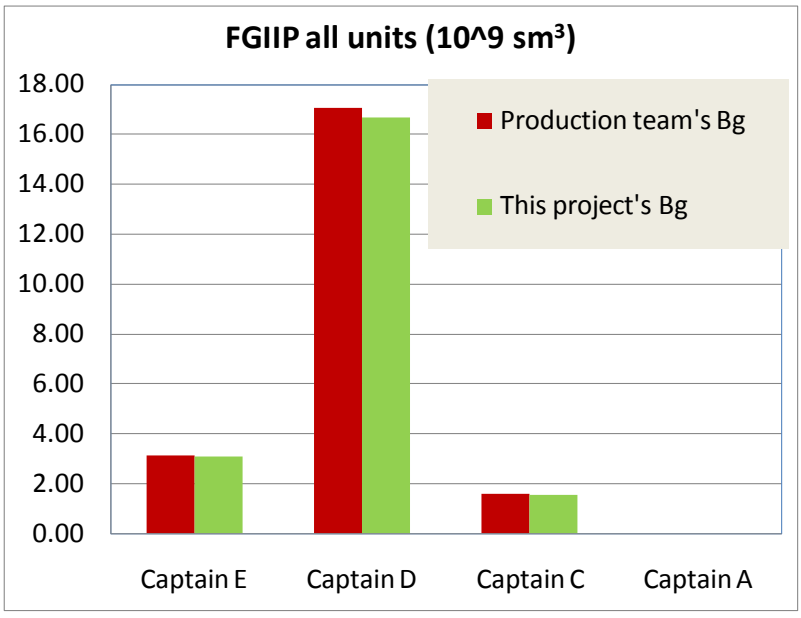

Figure 5-12. **SRM3.1 : Comparison of FGIIP calculated from Petrel hydrocarbon pore volume and two values for formation volume factor (B_g).**

The detailed comparison of the fine scale, static model volumes and those in the coarser simulation model is only shown here for the SRM 3.1 model. However, the same consistency has been demonstrated for the other models which have been exported to the dynamic realm (15).

The differences in volumes between static reservoir model and full field simulation model reported for this scenario are similar to those seen in other models and their causes are also believed to be the same. The volumes are listed in Table 5-8. Note that, as stated above, to calculate a figure for free gas initially in place the value of 0.765 rb/Mscf ($4.3x10^{-3}$ rm^3/sm^3) was used for the gas formation volume factor B_g. This is the value used by the production team and in the geological (Petrel) work.

Table 5-8: Net volume, net pore volume, hydrocarbon pore volume for gas and free GIIP in three geological models.

	Net volume (10^6 m^3)		Net Pore Volume above OOWC (10^6 rm^3)		HCPV gas ($10^6 rm^3$)		Free gas initially in place ($10^9 sm^3$)	
Geological model	Petrel	Reduce	Petrel	Reduce	Petrel	MoReS	Petrel	MoReS
FFM 3.1	514	495	123	119	94	93	22	22
FFM 3.15	514	496	123	118	94	91	22	21
FFM 3.05	518	524	124	126	93	96	23	22

The overall percentage difference in FGIIP between the static and dynamic models is down to only 3%. The discrepancies were reconciled with reasonable explanations such as: B_g, P_c, saturation height functions or even with slightly different approaches to estimate the in place volume, giving confidence that all elements involved in volumetric estimation are in place.

6. Uncertainty Framework

In order to understand the elements that impact CO_2 storage capacity, an uncertainty analysis of the key parameters affecting the storage complex was carried out. The objective was to identify what needed to be tested in order to demonstrate capacity, containment and injectivity of CO_2 within Goldeneye. The aim was to deliver a set of parameter ranges and subsurface realisations needing to be modelled (static and dynamic) to investigate if the Goldeneye storage area can accommodate 20 million tonnes of CO_2.

This may be demonstrated by showing that:

- Goldeneye can store more CO_2 within the storage area than we are injecting (storage margin)
- Goldeneye can take higher pressures and injection rates than we are using (injection margin)
- Ideally, a case may not reasonably be constructed where the CO_2 escapes to an unwanted area

The following uncertainty elements were identified for investigation and are shown in Table 6-1.

Table 6-1. Uncertainty elements identified.

Category	Element	Element	Element
Field area	Volume A,C,D,E	Properties, A,C,D,E (phie)	Lateral hetrogeneity
	Thickness, A,C,D,E	Shale breaks within D	Spill point location
	Extent (pinch out) A,C,D,E		
Aquifer	Permeabilty	Size	
Dynamic	Relperm and cap curves	Oil rim effects	Injection rates
	Trapped gas sat and other end points	Faults	Injection volume
	Kv/kh A,C,D,E	Skin	Injection well choice
	Properties A,C,D,E (perm)	Upscaling effects	Injection depths
	Initialisation	Neighbouring field effects	EOFL
Stress test	Aquifer plume – dense phase up dip	Ionic – down dip	
	Cap rock leaks (remove gas)		
Caprock and overburden	Rodby extent and thickness	Induced fractures	Caprock reactivity
	Secondary seals - extent	Injection well integrity	Geomechanical effects
	Secondary storage (vertical)	Abandoned wells in field	
	Faults and fractures	Other abandoned wells	
Other	Plume thickness for monitoring	Hydrates and plugging	Well cement debonding

Elements highlighted in green were considered important and fully investigated during the RE workflow. As for the rest, some were investigated and even used as part of the history match framework, but resulted in having a minor impact or been history match constrained.

Key uncertainty parameters were classified into two subgroups: *Static* and *Dynamic*.

6.1. Static Uncertainties

Based on the data available and the geological understanding of the area, a suite of static reservoir models was generated to evaluate key uncertainties impacting on CO_2 storage capacity and containment. The differences in the models were created by:

- Differing seismic depth surfaces to represent the top and base of the reservoir;
- Using seismic depth surfaces, isochores or well tops to define internal reservoir layering;
- Varying the location of the northerly stratigraphic pinch-out; altering the zonation of the pre-reservoir stratigraphy;
- Adding (or ignoring) a top Captain 'C' pick to well GYA01.

In each case, the data and methodology used to construct the facies and petrophysical property models remained the same – with the exception that the vertical probability curve that controls facies distribution in each zone had to be modified to accommodate changes in zone layering (16). As a result, several different geological realisations were built. The three main aspects identified as key uncertainties with a possible direct impact on CO_2 storage capacity and containment were:

- Extension of the stratigraphic pinch-out
- Structural dip on the western flank of the field
- Internal Captain stratigraphy (thickness)

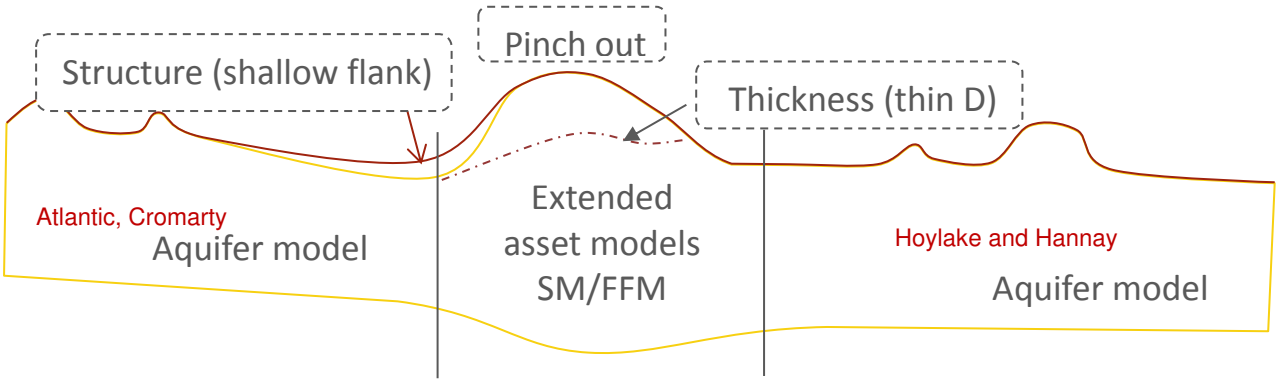

Figure 6-1. Key static uncertainties - cross section along Captain fairway, east to west (left to right)

The combination of these three parameters generated the main three geological realisations that were taken into dynamic simulation to assess the impact on capacity and containment. Their ranges and relative importance were assessed based on the geological information available.

- Extension of the stratigraphic pinch-out: precise identification of the stratigraphic pinch-out difficult to achieve due to scarce well density data from the field. Simulation is therefore required to investigate the impact of the pinch-out location in the CO_2 migration path. In the base case model the position of the pinch-out was selected with the PreSDM seismic data as the basis, with the extreme positions being controlled by the locations of the 14/29a-2 well (which saw no Captain Sandstone Member rocks) and GYA03 and GYA02, (the most northerly of the producing wells, both of which encountered Captain Sandstone Member stratigraphy).
- Structural dip on the western flank of the field: based upon uncertainty in the velocity model. Alternate supra-Beauly wedge interpretation sees the 'supra-Beauly wedge' migrated 750m to the west (17). This has the effect of reducing the structural dip on the western side of the field.
- Internal Captain stratigraphy (thickness): Two scenarios of internal Captain stratigraphy were considered. One scenario is generated when using constant isochores to create the reservoir zones, whilst the second scenario is associated with the use of well tops without isochores or seismically interpreted surfaces to divide the reservoir. This sensitivity has a large impact on the size of the in-place hydrocarbon volumes in the internal zonation of the reservoir. Re-allocating volume between the high net-to-gross 'D' unit and the low net-to-gross 'C' unit can change the in-place volume between -9.6% and +4.8% (15). As well as changing the size of the reservoir from which gas is being produced, this reallocation of rock volume will affect the full field simulation, swapping volumes between an easily accessible, high quality container and a less easily accessed, low quality one.

It is important to mention that additional geologic realisations with seismically interpreted surfaces were tested and it was not possible to achieve a history match. As a result, the models carried over were executed using constant isochores to create the reservoir zones.

The following static uncertainty matrix summarizes the scope of the study regarding this topic.

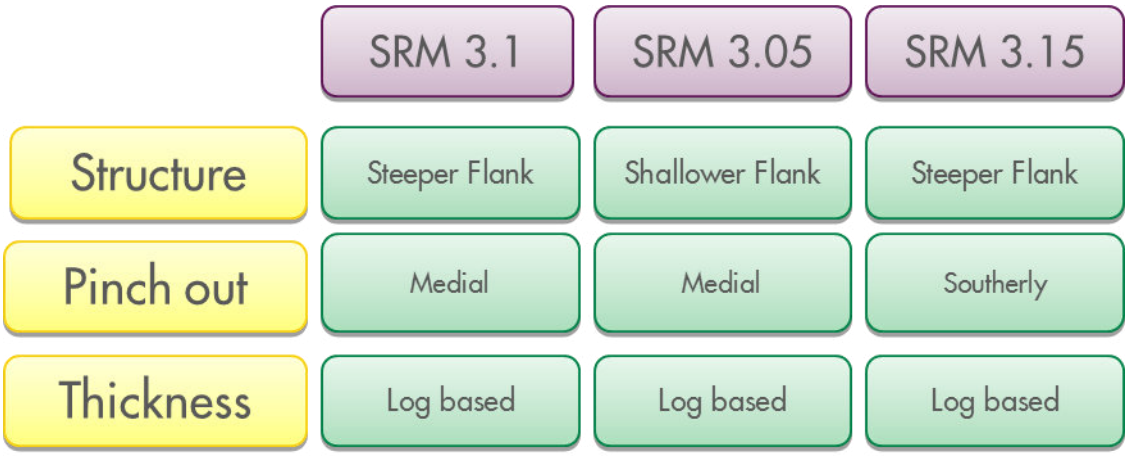

Figure 6-2. Static uncertainty matrix

A study of these key uncertainty elements is expected to assess:

- Structural dip on the western flank of the field: impact of the structure in the displacement process. Degree of instability of the CO_2 – water displacement process (Dietz tongue effect) with respect to the steepness of the west flank of the field, taking into account the fact that for a shallower flank there will be less gravity force to overcome when CO_2 is trying to reach the lowest structural point and escape out of the reservoir.
- Extension of the stratigraphic pinch-out: the precise geometry of the pinch-out and north boundary of the field, which is not accurately known, could have an impact in the possible lateral egression of CO_2. The geometry has an impact on the hydrocarbon volumes at the north-west corner of the field (the effects can produce a maximum reduction in GIIP of 5.3% and a maximum increase in volumes of 1.2%) and as a consequence, the CO_2 storage capacity and potential migration path.
- Internal Captain stratigraphy (thickness): this will also have an impact on hydrocarbon in place (a change in the in-place volume between -9.6% and +4.8%) and its distribution among the reservoir units, probably again impacting CO_2 storage capacity and migration path or accumulation.

The understanding of all of these static uncertainties in conjunction with dynamic variables, will assist with the definition of important project decisions such as the injection strategy, the injection well priorities, well completion designs, measurement, monitoring and verification strategies, amongst others.

6.2. Dynamic Uncertainties

In addition to static uncertainties, a number of dynamic parameters were also considered. The main concern from the fluid dynamics of CO_2 injection was related to the displacement processes that will

occur within the reservoir. The following figure depicts the displacement process in Goldeneye lifecycle under CO_2 injection post cessation of production.

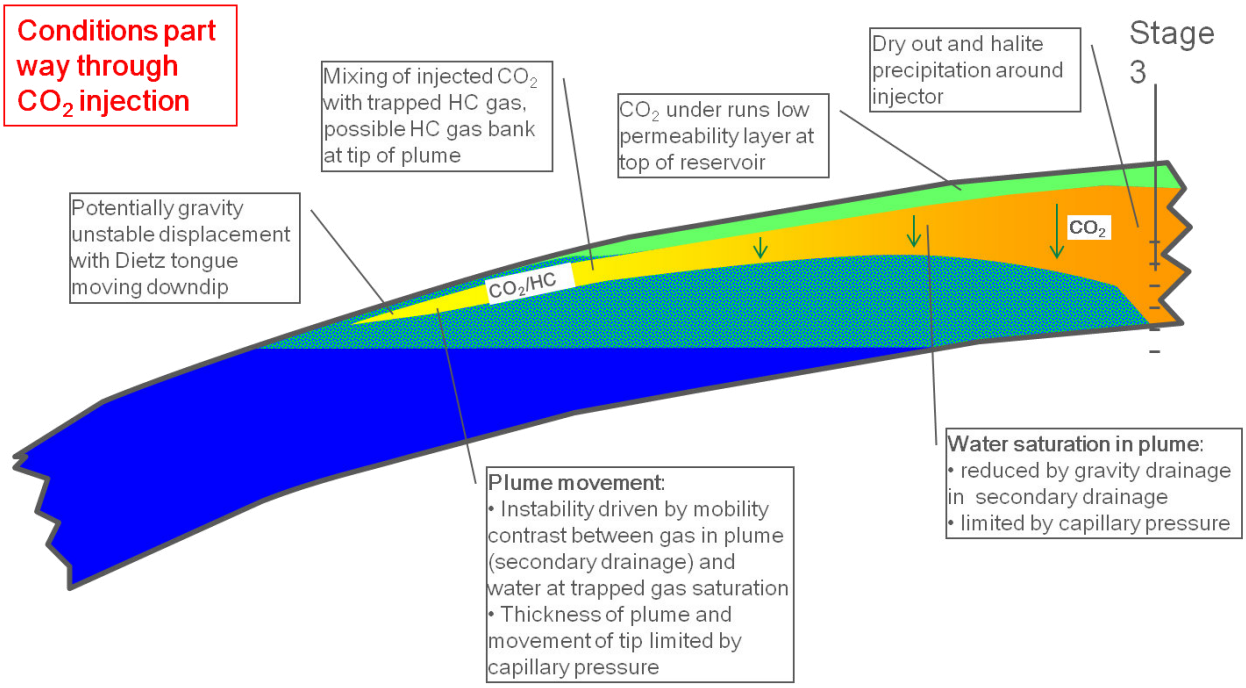

Figure 6-3. Displacement process in Goldeneye lifecycle

At Goldeneye pressure and temperature, the CO_2 dense phase is less dense than water and so, under equilibrium conditions it will overlay the brine filled part of the reservoir. During injection, the CO_2 displaces water under segregated flow conditions and can tongue and override the water (Dietz instability).

This will lead to a set of dynamic uncertainties dominated by relative permeability parameters such as:

- Relative permeability end points (both water and gas/CO_2)
- Residual gas saturation (S_{gr})

There could be additional dynamic uncertainties having an impact in the displacement such as:

- Oil rim. Impact of smeared oil rim area in complex displacement process (Three Phase effects)
- kv/kh ratio (ratio between the vertical and horizontal permeability) defining connectivity among reservoir units.

However, these will be, up to some extent, constrained by the history match of the model (water breakthrough time and pressure depletion behaviour).

In the displacement of water by CO_2 injection at the top of the structure and interval the interface between the fluids will be strongly gravity dominated due to the excellent vertical permeability and the density difference, as may be seen in the following figure.

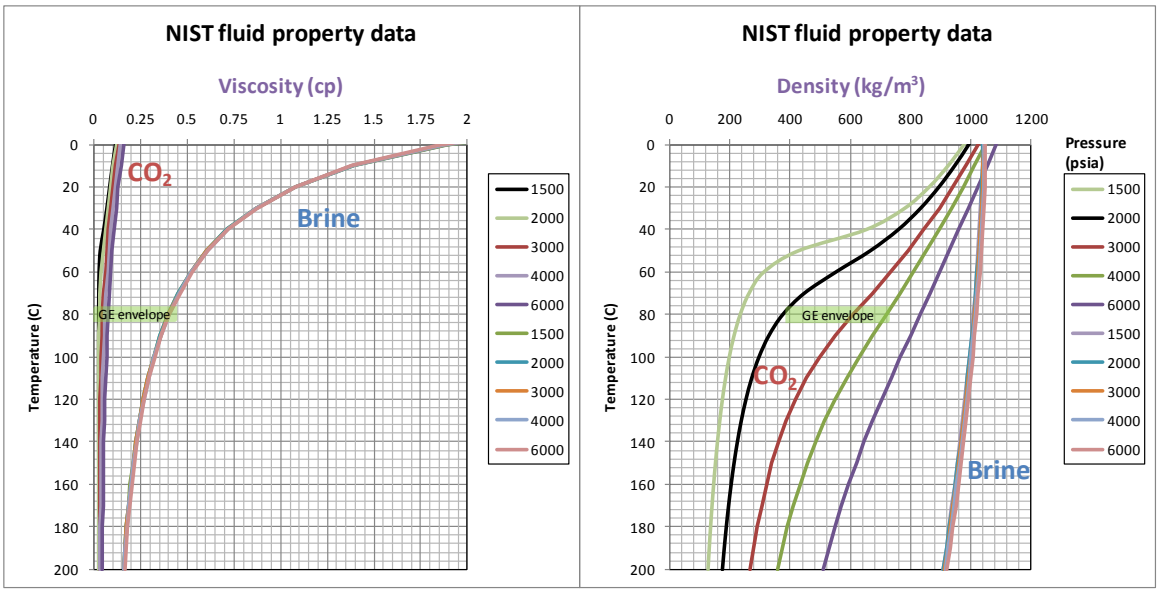

Figure 6-4. CO_2 and Water viscosity and density vs. pressure and temperature.

Pure water viscosity is strongly dependent on temperature, but this is not the case for CO_2. Study of the density plot shows that CO_2 density is strongly dependent on pressure/ temperature, but this is not the case for water. These general physical behaviours of both water and CO_2 will have a predominant impact on the way in which the CO_2 plume will behave, allowing worse or better displacement due to the viscosity ratio of the fluids.

The density of supercritical CO_2 is around 40 – 50 % lower than typical saline formation water under the same conditions. As a result of this density difference the lighter CO_2 will want to rise upwards, driven by buoyancy through the formation to accumulate at the highest possible place in the reservoir beneath the seal.

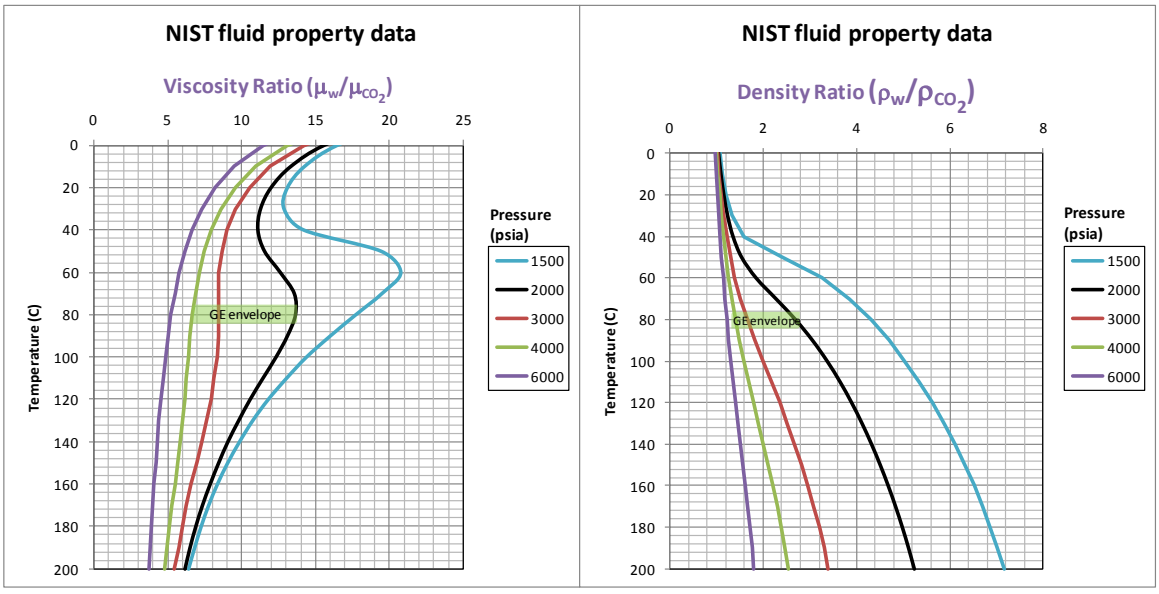

Figure 6-5. Viscosity (left) and Density (right) ratio as a function of pressure and temp.

This mobility ratio contrast between gas in the plume (secondary drainage) and water at trapped gas saturation will increase the instability of the displacement. Estimations at reservoir conditions reveal that a highly unfavourable mobility ratio in the order of 25 will be achieved.

During displacement under segregated flow conditions, the manner foreseen in Goldeneye, it is expected that:

1. In the CO_2 flooded part of the reservoir:
    - CO_2 alone will be flowing (moving laterally) in the presence of residual water saturation.
    - In this condition the effective permeability $k_{rg} = kk_{rg}'$, where k_{rg}' is the end point relative permeability to water (water will carry on draining under gravity)[24].
2. In the non CO_2 flooded zone:
    - Water will be flowing in the presence of residual gas saturation.
    - The effective permeability will be $k_{rw} = kk_{rw}'$, where k_{rw}' is the end point relative permeability at S_{gr} (residual gas saturation)

Different sets of relative permeability curves were used in order to assess the impact on the displacement.

Special Core Analysis (SCAL) data currently available in the field are as follows:

- Well 14/29-a3 and 14/29-a5
    - Corelabs study for Shell
    - Steady state imbibition gas/water relative permeability
- Well 20/4b-6
    - Corelabs study for Amerada Hess
    - Wettability (well encountered oil rim)
    - Steady state imbibition gas/oil, SS drainage gas/oil, SS imbibition water/oil
- Well 20/4b-7
    - Study for Amerada Hess

Land correlation for Captain D, using "corrected data" gives a range of residual gas saturation (S_{gr}) of 25% - 38% at maximum gas saturation.

[24] CO_2 here is labelled as "g" owing to the fact that supercritical CO_2 behaves in a similar manner to hydrocarbon gas, albeit with a different density and viscosity. CO_2 is miscible with hydrocarbon gas therefore what exists in practice is a mixture of CO_2 and hydrocarbon acting together as a gas with a properties in between those of CO_2 and hydrocarbon gas.

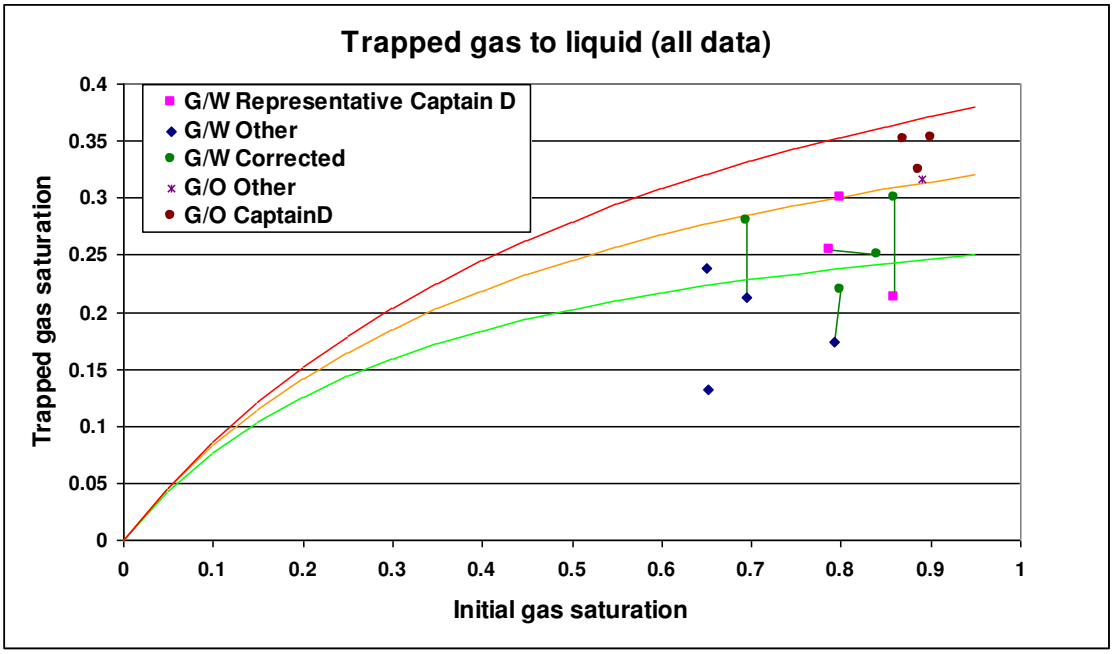

Figure 6-6. Trapped gas saturation to liquid. Land correlation.

Data taken from literature show a strong correlation between porosity and residual gas saturation. So for an average porosity of ~24% measured in Goldeneye Captain D, the residual gas saturation can be ~30%. A simulacrum[25] box model was set up with hysteresis in gas relative permeability resulting in S_{gr}=30%.

There is also uncertainty in the water relative permeability end point (k_{rw}'). Various sensitivities were performed to investigate this, with gas relative permeability and all other parameters held constant. Water relative permeability end point values, based on data currently available in the field that do not require correction, support a range of 0.05 to 0.25. Corrected data means that instead of using the average water saturation measured along the core, which in some cases was very variable and not representative of in situ conditions, the closest value to S_{wi} was chosen and the correspondent S_{gr} value was assumed to be correct.

[25] Described in detail in section 6.2.1

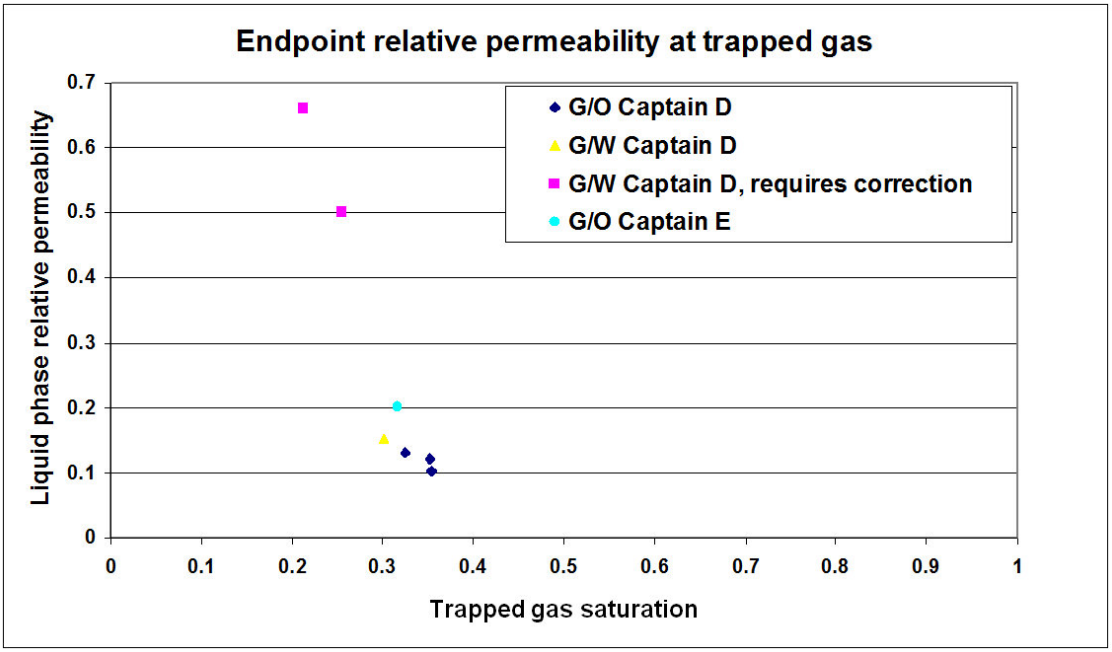

Figure 6-7. Endpoint relative permeability at trapped gas saturation.

Dynamic uncertainty parameters were investigated mainly in the simulacrum box model and not the FFM. This allowed a better understanding of their impact in a mechanistic manner. Variations of these parameters were found to yield a minor effect when compared to the effect of the parameters related to the fact that CO_2 was being injected and the reservoir processes were being turned from water driven gas depletion into gas injection (displacement process and overriding effect due to the mobility ratio being 25). As mentioned previously, dynamic parameters were also constrained by the history match.

The effect of these parameters (assessed in the simulacrum model) in comparison to the storage buffer size and the effects of the dominant parameters meant that it was not necessary to pursue an experimental design based sensitivity analysis including all minor parameters in the full field models. This analysis could be pursued at a later date if the volumes to be stored were to change in such a manner that the storage buffer was reduced.

Assessment of storage capacity and injectivity has been based on legacy SCAL data, making full use of the in-situ saturation data to account for laboratory artefacts. This allowed ranges to be developed as inputs for the storage assessment for:

- gas relative permeability at initial water saturation
- trapped gas saturation to brine
- water relative permeability at trapped gas saturation

History matches to Goldeneye production performance were achieved within the uncertainty range developed.

A new SCAL programme conducted in 2010 (18) comprised a combination of ambient condition measurements and reservoir condition floods with CO_2. The work was targeted at the key data uncertainties. Analysis of the results confirms the validity of the ranges used in the storage assessment based on the legacy data, so that there is no immediate requirement to update any of the existing reservoir models following the new SCAL study.

6.2.1. Unstable displacement

Analytical investigation of the displacement process taking place during CO_2 injection in the Goldeneye reservoir identified that the storage capacity could potentially be reduced by this effect in the short term (injection period).

As a consequence, a simulation model was constructed to investigate these effects. A dipping box model (termed the simulacrum model) representing approximately ¼ of Goldeneye in volume, with similar rock properties (permeability and porosity) and dip angle was used to simulate these effects. The model was conditioned with a 10 year depletion period, a further 10 years of recharge from the aquifer and finally, a 10 year CO_2 injection period. The simulacrum model was initially constructed during the modelling work for the UK CCS Demonstration Competition – for which a total injection of 20 Mt of CO_2 into the Goldeneye field was mandated. The model and basic physics results were carried forward to the current study work.

Phase behaviour was represented using a Peng Robinson 1978 equation of state (EoS), calibrated to match the Goldeneye hydrocarbon fluid description from GYA03, CO_2 properties (density and viscosity) at reservoir conditions (11) and CO_2 dissolution in brine.

Sensitivities were carried out on a range of values of effective water relative permeability at residual gas saturation (S_{gr} = 30%) within the observed data, varying between 0.1, 0.25 and 0.6.

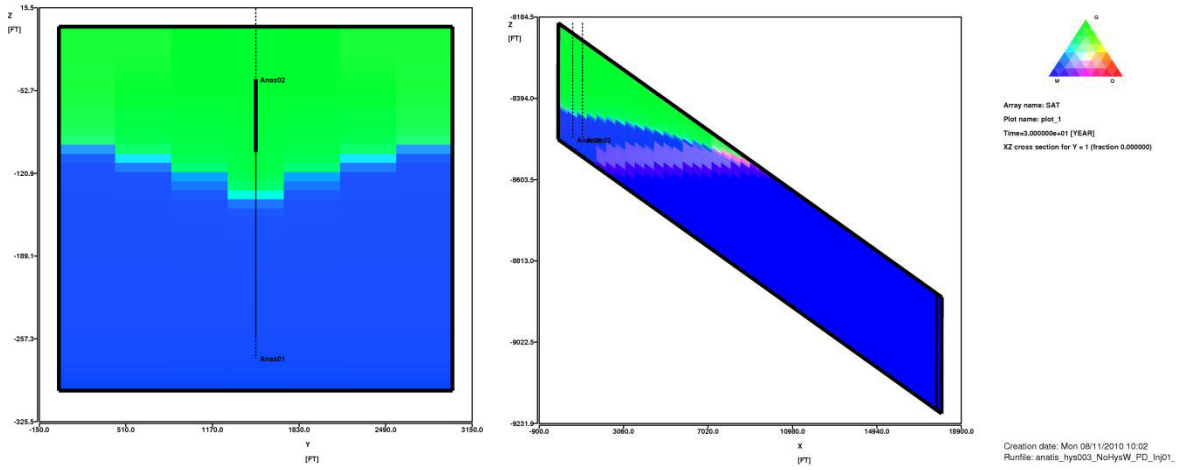

Figure 6-8. Cross section in ternary diagram. Sensitivity with k_{rw} = 0.6 @ S_{gr} = 0.30

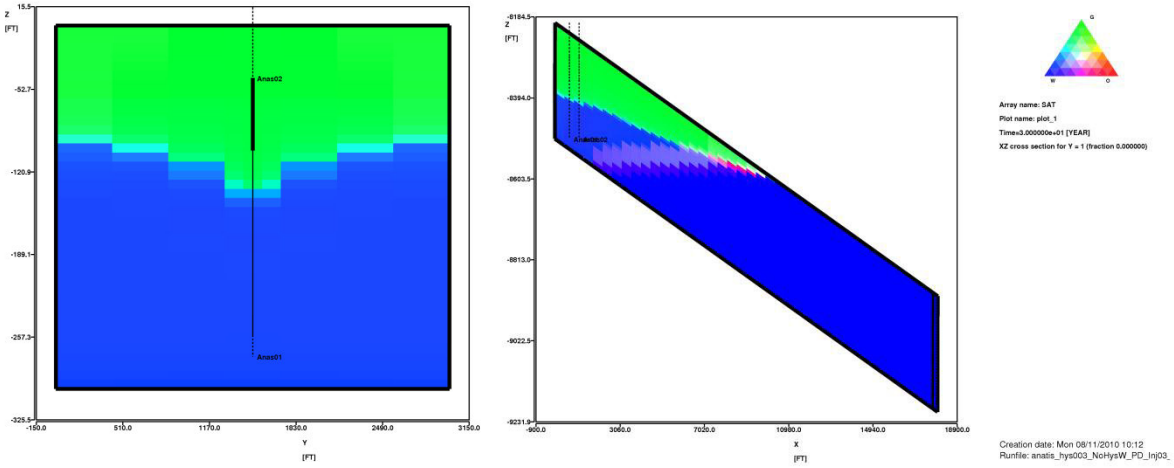

Figure 6-9. Cross section in ternary diagram. Sensitivity with k_{rw} = 0.25 @ S_{gr} = 0.30

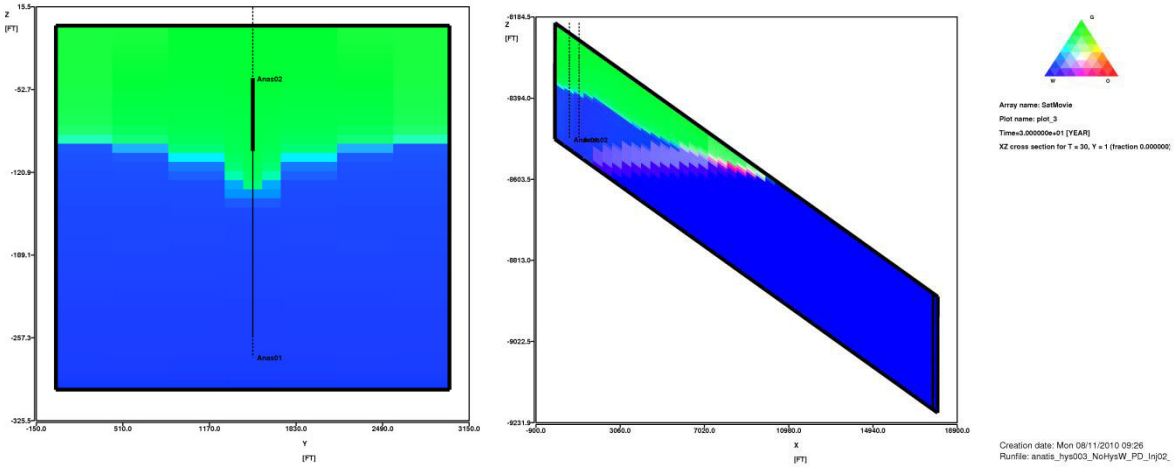

Figure 6-10. Cross section in ternary diagram. Sensitivity with k_{rw} = 0.10 @ S_{gr} = 0.30

Results from the model confirmed that a strong override of water by CO_2 will occur in the reservoir, producing a CO_2 tongue moving downwards due to the unstable displacement (a consequence of the unfavourable mobility ratio). As expected, the tonguing effect is enhanced in proportion to minimisation of the water relative permeability end point, creating a Dietz tongue that could be almost parallel to the top of the interval. This means that, during injection, the mobile CO_2 dense phase has the potential to extend below the original hydrocarbon water contact.

The simulacrum models show the impact of the water relative permeability endpoint on the Dietz tongue within the original hydrocarbon column, with the dip of the plume approaching the reservoir dip as the relative permeability reduces. However, once the plume has moved beyond the OWC the impact of trapped gas on water relative permeability is reduced, because the gas plume is then displacing 100% brine in the aquifer.

The impact on the CO_2 plume length is approximately 20% (of the total length), considering the range of values of effective water relative permeability (k_{rw}) at residual gas saturation analysed. As a

consequence, a change of only 20% in the CO_2 plume length due to the uncertainty in the effective water relative permeability end point, is considered minor and not necessary to be tested in the full field model at this stage of the project, because even in the worst case scenario it will not cause CO_2 to go over a local or structural spill point.

The refill dynamics are highly impacted. Probably less than 50% of Captain D will be flooded with CO_2 (in the vertical sense) before the CO_2 has moved under the original OWC. This effect that will happen only during injection because, once injection ceases, the viscous driving force will be removed leaving only the buoyancy force which will drive the CO_2 back up dip and back above the original contact.

The Dietz tonguing behaviour means that the tip of the CO_2 plume will reach the original OWC after injecting 10 to 12 million tonnes of CO_2, but if injection continues past this point (as was required for UK CCS Demonstration Competition) the structure will continue to fill until the total target tonnage has been injected. More details regarding this effect will be described in Section 10.3.1.

6.2.2. Secondary Drainage Relative Permeability

The secondary drainage relative permeability curve is expected to follow the primary drainage curve. However, the time required to bring back initial water saturation will be much longer than the injection period because there is insufficient time for gravity drainage to bring saturations into capillary equilibrium. A schematic of the displacement processes was shown in Figure 6-11. The following depicts with more detail the plume content.

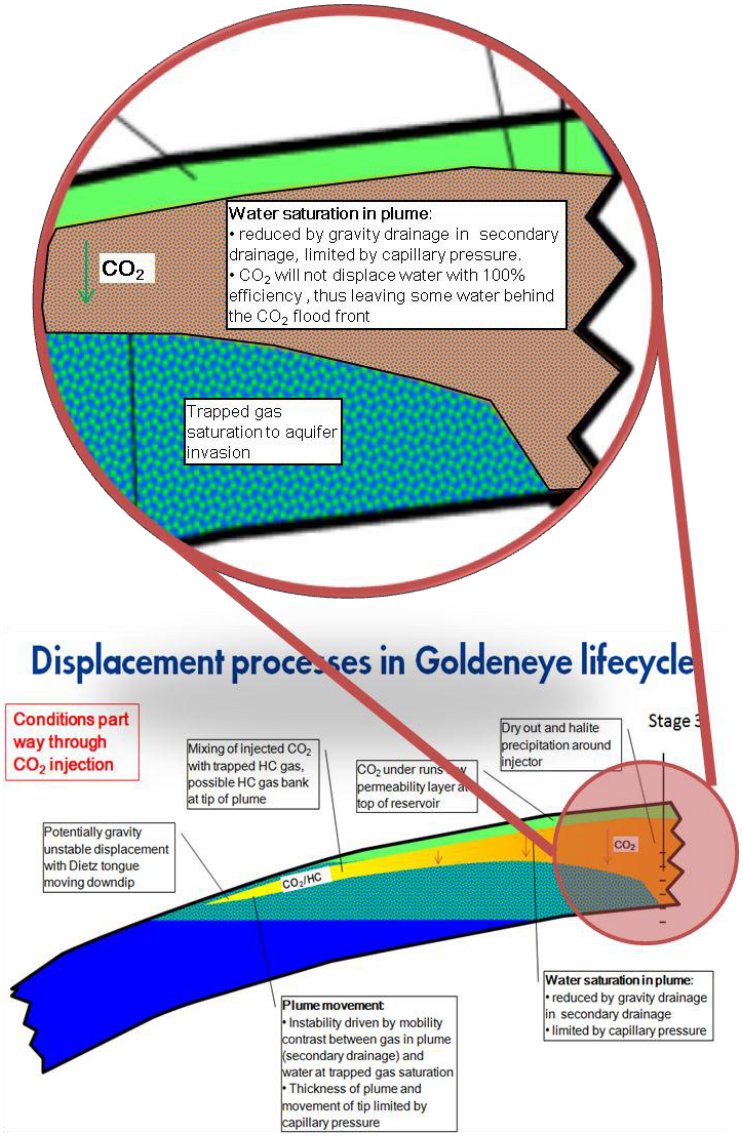

Figure 6-11. Displacement processes in Goldeneye lifecycle. Zoom in to S_w in the plume.

In order to estimate how large the effective "residual water saturation" (S_{wr}) left behind the CO_2 flood front could be, both analytical and numerical estimations were carried out. Buckley-Leverett displacement theory and fractional flow equations were applied for a process where gas (CO_2) is displacing water. Sensitivity analyses were carried out on the water relative permeability Corey Exponent.

Fractional flow analysis allows calculation of the average saturation of the displacing front (CO_2) and hence, the complemented displaced phase (in this case brine). Numerical simulation results have shown that an unstable gravity dominated displacement will occur in Goldeneye. Therefore, the fractional flow analysis was carried out incorporating gravity in order to take into account the gravity forces in addition to the viscous salvage displacement.

A set of relative permeability curves as well as rock properties were used taking into account Goldeneye basic data from logs and supported by legacy SCAL data and a tailored SCAL programme targeting the CO_2 flood. These included: S_{wi}, porosity, NTG, vertical permeability and thickness, among others. Corey exponents were used as sensitivities and CO_2 and brine properties were taken at Goldeneye reservoir conditions.

The average water saturation left behind once CO_2 injection has occurred can provide insight into the physics represented in the simulation model.

The following figures show the results of both Buckley–Leverett and fractional flow analytical calculations, as well as the numerical results from a simple box model in MoReS described in section 6.2.1.

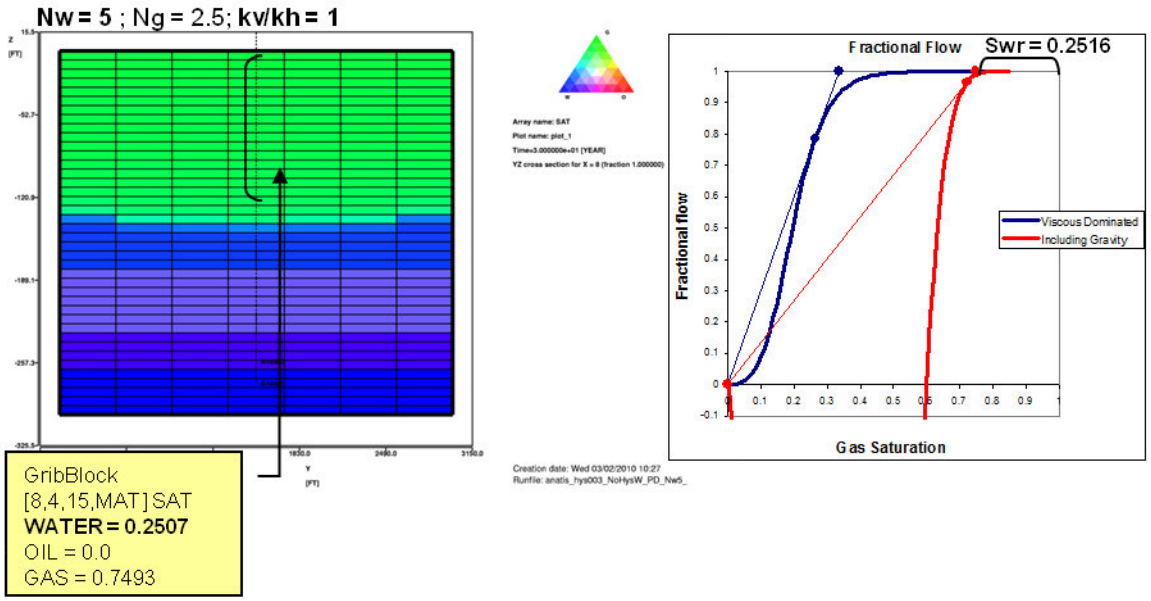

Figure 6-12. Cross section vs. fractional flow curve with B-L solution. N_w = 5.0

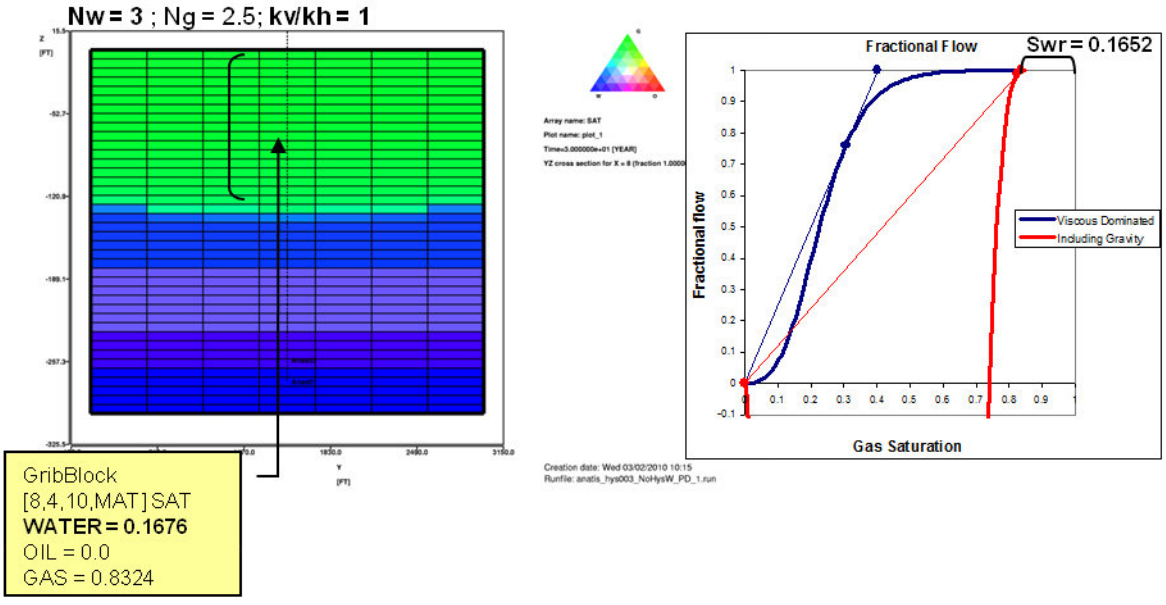

Figure 6-13. Cross section vs. fractional flow curve with B-L solution. N_w = 3.0

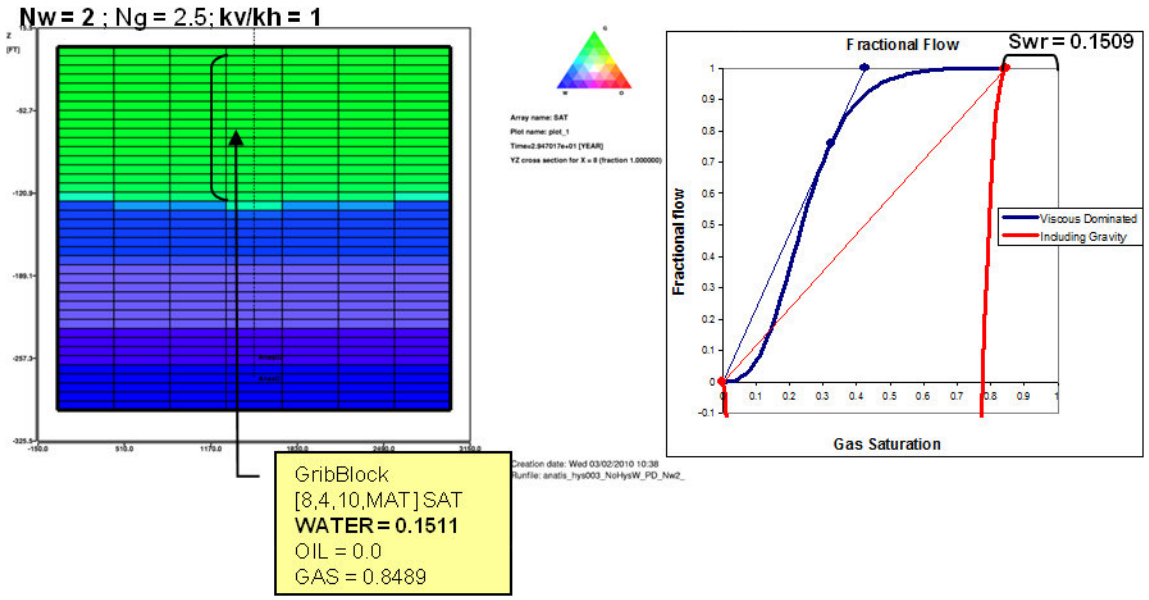

Figure 6-14. Cross section vs. fractional flow curve with B-L solution. N_w = 2.0

The cross section and fractional flow numbers agree, confirming that the physics represented in the numerical model is as expected. This traditional fractional flow curve combined with the Buckley - Leverett solution gives the average saturation behind the injection front. In this case, that will be the average CO_2 saturation within the plume, and as a consequence, the complement will be the average water saturation (Sw_{avg}) left behind the injection front. It may be observed that for a range of Corey exponents of 2, 3 and 5, Sw_{avg} can vary from 0.15 to 0.25, depending on how easy it is to displace the water during CO_2 injection. Based on literature and the unfavourable mobility ratio expected for the reservoir, a Corey exponent of 5 could be the more appropriate figure. This yields a higher water saturation left behind the injection front, considerably higher than the connate water saturation observed in Goldeneye (S_{wi} ~ 0.07). Accordingly, this factor represents an important storage capacity reduction element for Goldeneye, because in conjunction with S_{gr}, it will reduce the pore space available.

6.2.3. CO_2/water relative permeability end points

The injection rate can vary significantly for different relative permeability values and injectivity could also be sensitive to variables that define the relative permeability curves. In addition, the end point of the relative permeability curves conditioned the mobility ratio (M) of the fluids, and has a large impact on the CO_2 plume shape. As previously mentioned, water will be by-passed and gas tongues will develop, leading to an unfavourable displacement. In such conditions, the CO_2 plume will travel further away from the injection point, diminishing the average CO_2 storage density and requiring a larger volume to store. As a consequence, a proper assessment of the relative permeability variables is important for the refill efficiency of the system (19).

One of the challenges of properly modelling CO_2 injection is that relatively little is known about relative permeability end points of a CO_2/water system. Most published work refers to instances in Van Genuchten or the Brooks and Corey model (20). Yet until recently, no relevant data have been published regarding relative permeability and capillary pressure of CO_2/Brine systems at in situ conditions. One of the studies available is that by Bennion and Bachu (21), (22) reporting a series of laboratory measurements performed in the Western Canada sedimentary basin on six samples of carbonates and sandstones. These plugs all have low average permeability (sandstone samples with

permeability 0.55, 2.2 and 5.78 mD, and porosity of 11.7 %, 12.6 % and 12.5 %), and are not thought to be representative for good quality reservoirs like Goldeneye. The relative permeability end point for CO_2 measured at irreducible water saturation varied around 0.55, 0.12 and 0.33, respectively. No in-situ saturation monitoring (e.g. by imaging) was used, and no in-situ saturation profiles in the sample were available. The CO_2 endpoint relative permeability and the capillary end effect were determined by multi-rate end point floods.

Alternatively, Stanford University (23) also published the results of a study regarding physical modelling of CO_2 sequestration regarding relative permeability of CO_2/Brine system done using a Berea sandstone core with a porosity of 0.23 and permeability of 885 mD (similar to Goldeneye rock). Results show that CO_2 dissolution and evolution have very significant effects on the displacement of water by gas injection. Again the gas relative permeability end point was in the neighbourhood of 0.2, implying a reduced mobility of CO_2 in the presence of brine.

Alternative schools of thought express the idea that the relative permeability of CO_2/Brine should not be that dissimilar to that found in conventional experiments conducted with brine and a model fluid (i.e. decane).

This could have an impact in both injectivity and CO_2 displacement, therefore more work has to be carried out in order to corroborate this assumption. As part of the Goldeneye project, a SCAL program was assembled to analyse the most important variables impacting displacement, via direct measurement of Goldeneye reservoir rock with a CO_2 /Brine system (18):

- Trapped gas saturation to brine and end point relative permeability
  - Determines mobility ratio of displacement of aquifer brine by injected CO_2
  - Limits lateral migration of plume in aquifer by capillary trapping of CO_2
- CO_2 relative permeability in the plume at water saturations in range 25 to 35%

The SCAL programme was designed specifically for Goldeneye conditions and plume geometry:

- Combination of ambient (air/brine) and reservoir condition (CO_2/brine) tests
- Special procedures to reduce issues over component exchange between CO_2/brine
- It also has the bonus from a knowledge development point of view in that it may generate one of the first reliable published data sets.

The main impact of the CO_2/water relative permeability end points on the storage capacity is related to the displacement mechanism, affecting the behaviour of the Dietz tongue and potentially generating scenarios where the CO_2 can move to levels below the original OWC. In extreme cases it could eventually migrate under the spill point. As a result, it is difficult to assign a specific reduction factor to this effect. Addressing the direct impact of end point relative permeability on the refilling efficiency (based on how unstable the displacement is, i.e. extent of the Dietz tongue), will give an approximation of the storage capacity reduction.

Sensitivities were carried out, in the dipping box model, for a wide range of values of effective gas (CO_2) relative permeability (k_{rg}) at residual water saturation, of 0.8, 0.5 and 0.25, in order to covert both schools of thought and following the literature reviewed. The following figures show the results.

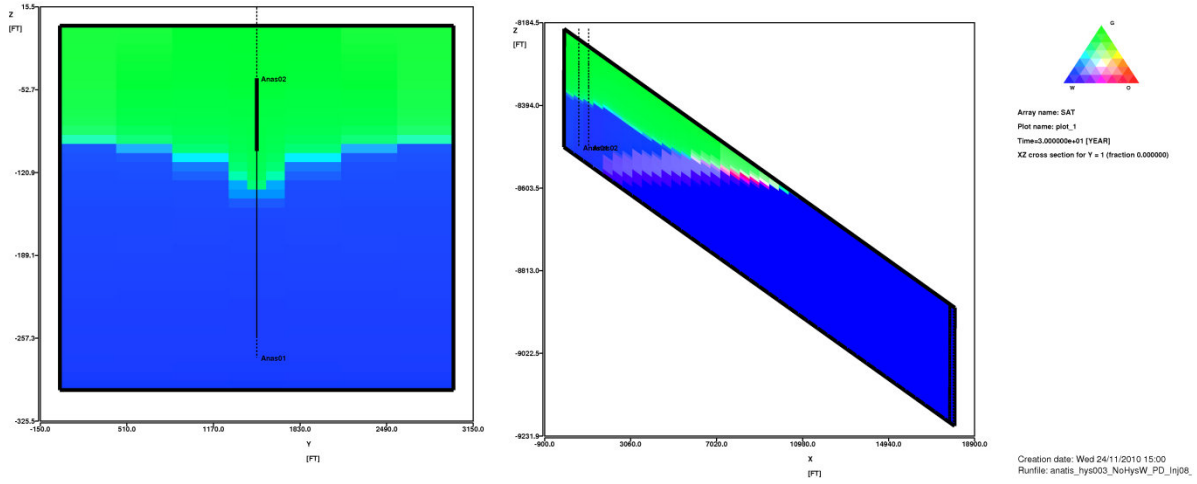

Figure 6-15. Cross section in ternary diagram. Sensitivity with k_{rg} = 0.8

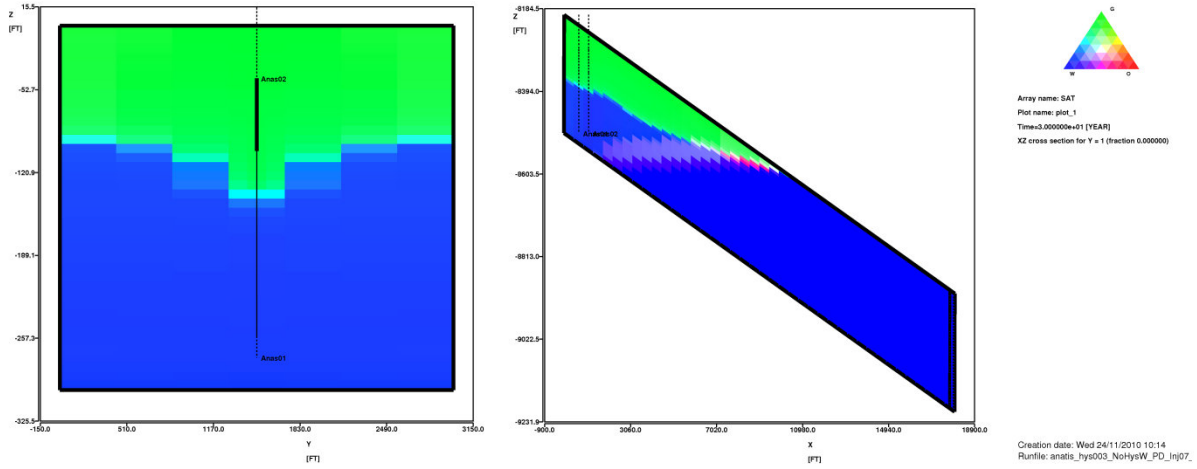

Figure 6-16. Cross section in ternary diagram. Sensitivity with k_{rg} = 0.50

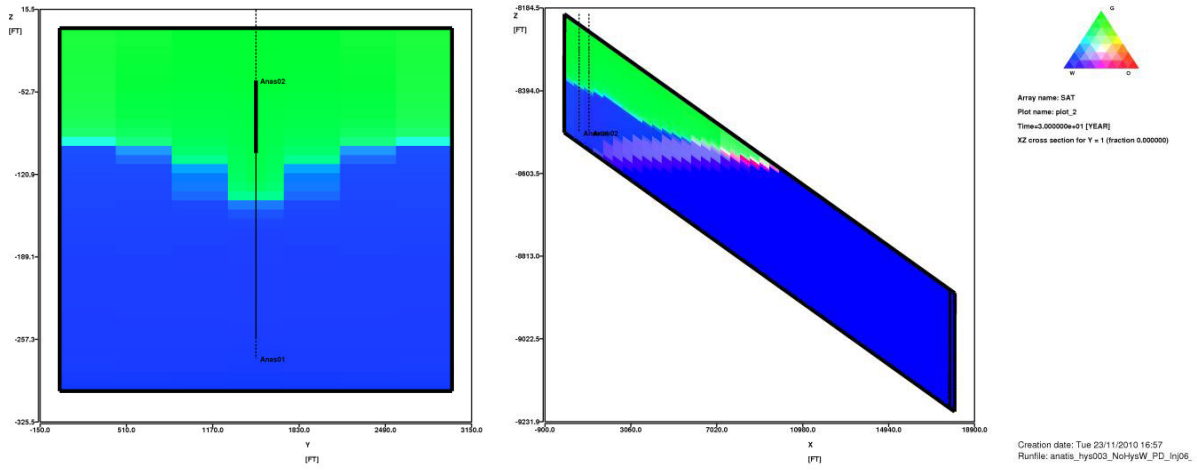

Figure 6-17. Cross section in ternary diagram. Sensitivity with k_{rg} = 0.25

As may be seen, the relative permeability end points have a minor impact on the displacement, making the plume go slightly further in the case where k_{rg} = 0.80 meaning that it will move easily, and the other way round when k_{rg} is restricted (as mentioned above by different publications) to lower values like 0.25. The impact on the CO_2 plume length is approximately 10%, considering the range of values of effective gas (CO_2) relative permeability (k_{rg}) at residual water saturation analysed. As a consequence, a change of only 10% in the CO_2 plume length due to the uncertainty in the effective gas relative permeability end point, is probably also considered minor and not necessary to be tested in the full field model at this stage of the project, because probably even in the worst case scenario it will not create an egression out of the storage site.

However, a bigger effect will be seen in injectivity, where the overpressure needed could be higher than expected. This topic is discussed in detail in a separate report (24).

7. Analytical estimate of Geological Storage Capacity

The Geological carbon storage capacity is an estimate of the maximum amount of carbon dioxide (CO_2) that can be stored in geological formations. The methodologies used to estimate geological carbon storage capacities vary depending upon the specific arrangement of the geologic formation to be used as a storage site. All methodologies start with and estimation of the pore space available for CO_2 injection based on standard volumetric assumptions.

Two main methods could be used to estimate the CO_2 storage volume in depleted oil and gas reservoirs: (1) a volumetric-based CO_2 storage estimate and (2) a production-based CO_2 storage estimate. For the purposes of this assessment, calculation was based on quantifying the volume of hydrocarbons produced (production-based) and assuming that the maximum storage capacity would be given by an equivalent volume of CO_2, where both hydrocarbon and CO_2 volumes were calculated at initial formation pressure. This theoretical maximum volume is modified by storage efficiency factors which accounts for the fact that CO_2 may not be able to completely fill this volume. In the case of Goldeneye, the need to displace aquifer water that has invaded the reservoir during production is the key consideration.

These storage efficiency factors are specific for each carbon sequestration project and depend mainly on the combination of both static and dynamic features present in the reservoir to be used.

Finally, the analytical storage estimation was compared with the results from a three-dimensional, three-phase, full field numerical simulation model.

7.1. Factors influencing the storage capacity of a depleted hydrocarbon reservoir

The major factor influencing storage capacity in a depleted hydrocarbon field is the voidage created – i.e. the volume of hydrocarbon and water extracted from the subsurface, less anything injected. Aquifers can flow into fields, however, in so doing they lose pressure – i.e. voidage is created in the aquifer as well.

This initial voidage cannot be completely refilled – there are factors that reduce the volume available and other factors that increase it. The following diagram summarizes the factors impacting the CO_2 storage capacity in a depleted hydrocarbon field – with some specific localisations for the details of the Goldeneye field.

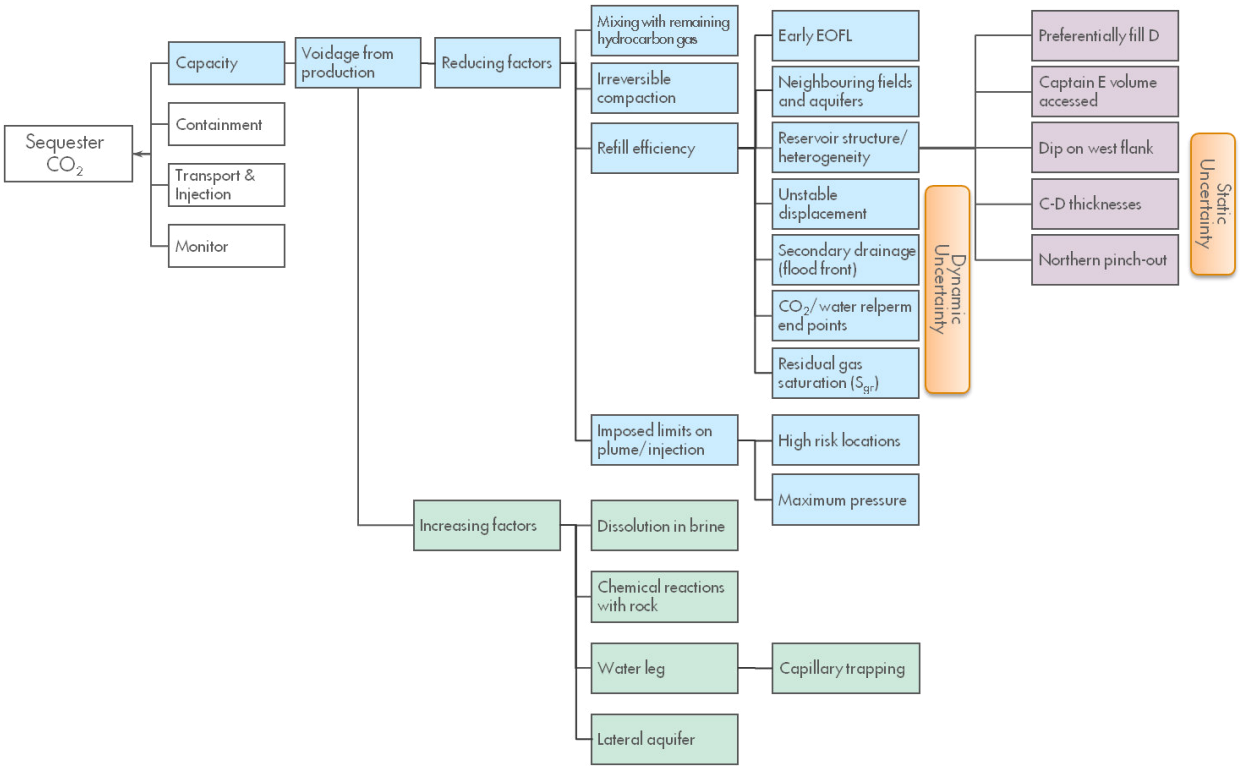

Figure 7-1: Factors impacting CO_2 storage capacity

7.1.1. Total pore volume available: voidage from production

The total pore volume available for CO_2 was determined by making the assumption that all the pore volume vacated by produced hydrocarbons is replaced with CO_2 using the following inputs:

- reservoir temperature of 83°C
- the characterised PVT properties of the Goldeneye fluids
- recharge to initial pressure at datum of 266 bara [3863 psia] at datum level of 2610m (8565 ft TVDss)

This calculation gives a storage capacity of 47 million tonnes of CO_2 using the total cumulative hydrocarbon production till cessation of production. This is substantially larger storage capacity than that required for the Peterhead to Goldeneye CCS Demonstration Project. However, it is a maximum theoretical storage capacity assuming a perfect refill of the Goldeneye container. In reality there will be a series of additional factors, some of which will increase the storage capacity, and some which will reduce it. The following section analyses and describes these elements in order to determine an estimate for effective storage capacity.

7.1.2. Possible increases in the sequestration capacity

Permanent sequestration ("immobilisation") of CO_2 is achieved in time through various factors such as:

- structural and stratigraphic trapping
- dissolution of CO_2 into the formation brine
- residual CO_2 trapping
- chemical reactions of CO_2 with minerals present in the formation

The last three processes increase the sequestration capacity and their significance grows with time. Of these, dissolution and residual trapping are discussed in some detail in the following sections.

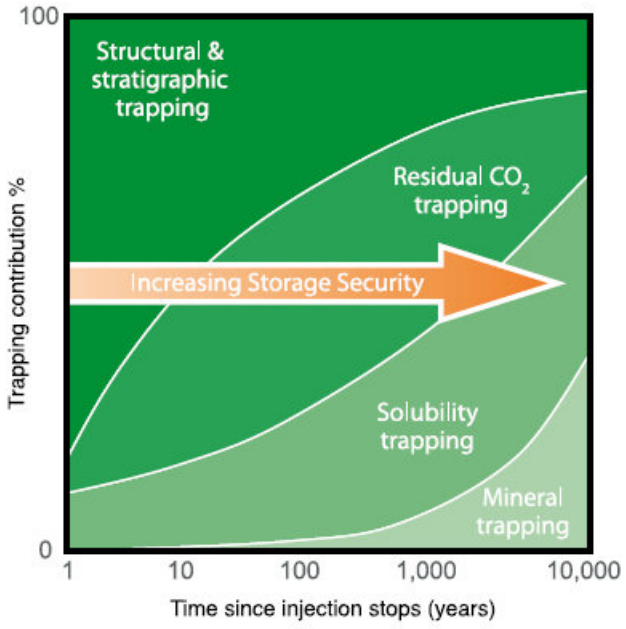

Figure 7-2: Storage security depends on a combination of different trapping mechanisms.

Mineralisation

This process is strongly dependent on the geochemical composition of reservoir rock and happens over very long timescales. Over time, reactions with clay minerals will also lead to a removal of CO_2 from the gas phase. The effect has been modelled for this system and found to work over longer time scales than the injection period, as shown in the figure above. Therefore, it will not be taken into account for the storage capacity. Nevertheless, mineralisation will work in favour of the project reliability over a large period of time. For more details on this topic, refer to the Geochemical Reactivity Report (4).

CO_2 dissolution in brine

CO_2 solubility in water is higher than that of hydrocarbon gases such as methane, and is a function of pressure, temperature and water salinity. In general, CO_2 solubility increases with pressure and decreases with temperature. An increase in salinity of the reservoir water decreases CO_2 solubility significantly. Dissolution of CO_2 is an important immobilisation mechanism.

Several correlations are available from literature regarding CO_2 solubility. One of them was published by Chang, Coats and Nolen in 1996 (25).

This correlation matches the solubility data of Wiebe (26) for liquid and supercritical CO_2 in water within ±10 scf/STB for temperatures between 54 °F and 212 °F and pressures up to 10000 psia. Above 212 °F the correlation can lead to unphysical behaviour.

The calculated solubility in distilled water can be adjusted further for the effects of salinity to obtain the solubility of CO_2 in brine.

Applying this methodology to estimate an average CO_2 solubility for the Goldeneye reservoir conditions (~3800 psi, 181 °F and 53.000 ppm of salinity) results in dissolution of 145 scf/bbl (7.7 kg/bbl, 4.6 % on weight). Goldeneye conditions are relatively favourable for CO_2 dissolution due to the low formation brine salinity.

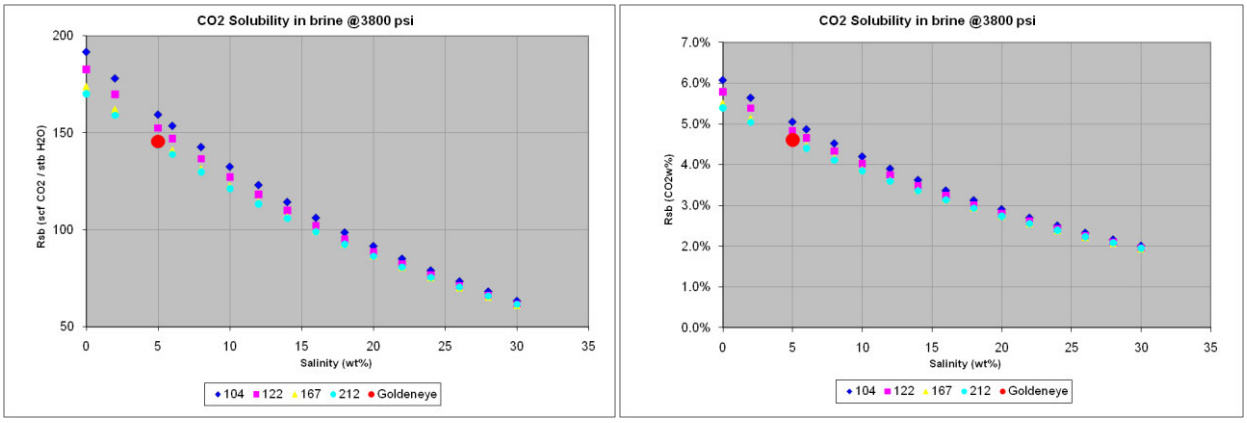

Figure 7-3: Calculated CO_2 solubility in NaCl brine at 3800 psi.

The increment in storage capacity has been estimated as 2.2%, taking into account a CO_2 solubility of 4.6% (weight) and that CO_2 will contact approximately 25% of the brine due to the nature of the displacement process (the remaining water saturation behind the CO_2 injection front is about 25%, estimated by fractional flow and Buckley-Leverett solution - see discussion in section 6.2.1.

Water leg and Lateral Regional Aquifer

Additional factors that could increase the storage capacity are related to the aquifer. The lateral regional aquifer surrounding Goldeneye is not part of the current analysis; nevertheless it represents a large opportunity for CO_2 aquifer storage. To the east of Goldeneye, the Captain sandstone extends approximately another 40-60 km and continues to deepen. To the west of Blake the formation starts to widen and eventually outcrops at the seabed about 50 km to the west of Blake. This situation may produce opportunities for further developments in the fairway and is under study by the Scottish Centre for Carbon Storage.

On the other hand, there is also the possibility of increasing the storage capacity by considering the water leg beneath the Goldeneye structural trap *Possible reductions in the pore volume available to CO_2*

Three effects were identified that reduce the vacated hydrocarbon pore volume available to CO_2:

- Mixing of the CO_2 and Goldeneye gas
- Irreversible compaction of the reservoir sands
- Efficiency of refilling:
    - Reservoir heterogeneities (Volumetric Sweep)
    - Unstable displacement (Dietz efficiency)
    - Water from the aquifer ingress that has become effectively immovable to CO_2 injection within the pores (Secondary drainage relative permeability effects – Water displacement)
    - CO_2/water relative permeability end points

Additionally, there are other elements (for example End of Field Life (EOFL) and the interaction with neighbouring fields), which could also impact the storage capacity. Nevertheless, if current conditions are maintained, no major impact is expected.

There may also be downside injection scenarios with high risk locations for injectors (although no such locations are currently identified) that could reduce capacity. These may include restrictions in maximum injection pressure in order to prevent fracturing the structural seal, or reservoir back pressure that could restrict the storage capacity. Nevertheless, current assessment indicates that these scenarios are unlikely.

Mixing of the CO_2 and Goldeneye gas

CO_2 will be injected in a depleted predominantly methane gas reservoir. Due to the aquifer encroachment, there will be some residual hydrocarbon gas saturation (S_{gr}) in addition to the free gas saturation left in the top of the structure. Residual gas saturation has been estimated to be between of 25% and 38%, based on laboratory data. CO_2 will become mixed in, mobilising and displacing remaining hydrocarbons from the rock as in an Enhanced Gas Recovery (EGR) process. During this process CO_2 and Goldeneye gas will interact, and at reservoir conditions they will be miscible. The degree of mixing is unknown; however, the mixture will have a different density to that of pure CO_2.

By the time CO_2 is injected into the reservoir, part of the pore space will be filled with brine as a consequence of the aquifer ingression. During the process of CO_2 displacing brine, part of that brine will become effectively immovable due to secondary drainage relative permeability effects that are discussed in section 6.2.2. The time required to bring the system back to initial water saturation will be much longer than the injection period because there is insufficient time for gravity drainage to bring saturation into capillary equilibrium., This situation leaves an *"effective residual water saturation (S_{wr})"* behind the CO_2 front (just as a residual oil saturation to water is left in a normal waterflood) over and above S_{wi}, also because of reduced column thickness. It may be shown that the residual water saturation S_{wr}, could be around 25%, based upon fractional flow and Buckley-Leverett solution calculations.

If there is no mixing of CO_2 and hydrocarbon gas, 25% of the pore space will be filled with brine *("effective residual water saturation", S_{wr})* and another 25% will be filled with hydrocarbon gas (residual gas saturation, S_{gr},. This latter figure tends to be reduced to 20% due to gas compression when the reservoir is re-pressurised with CO_2 during injection). This leaves between 50-55% of pore space available for CO_2 storage. Nevertheless, an additional reduction of capacity is expected to occur once CO_2 eventually becomes mixed with the trapped hydrocarbon gas.

In order to evaluate this effect, the Real Gas theory was used. The equation has the following form:

$$pV = znRT$$

where, p = *absolute pressure, psia*

V = *volume, ft^3*

T = *absolute temperature,* °R

n = *number of moles of gas, lb-mole*

R = *the universal gas constant which, for the above units, has the value 10.730 psia ft^3 / lb-mole* °R

z = *gas compressibility factor z is a dimensionless quantity and is defined as the ratio of the actual volume of n-moles of gas at T and p to the ideal volume of the same number of moles at the same T and p*

By understanding the variation of the compressibility factor z at different concentrations of mole percentage of CO_2 and hydrocarbon gas (mainly methane), we can estimate the capacity reduction from the mixing effect as a function of the actual moles of CO_2 in an ideal mixing scenario, compared with a no mixing theoretical scenario.

Based on this approach, the reduction in capacity has been estimated to be as much as 6%. This assumes 100% mixing between CO_2 and the remaining hydrocarbon gas; however simulation has shown that instead of a perfect mix, a hydrocarbon gas bank is formed at the tip of the plume. This results in imperfect mixing and hence the reduction will be smaller than 6%, (i.e. classifying it as a small reduction factor).

Irreversible compaction of the reservoir sands

The reservoir is currently grain supported, therefore compaction is minimal. Additionally, the depletion during hydrocarbon production is forecast to be from ~263bara to ~138bara [~3815 psi – 2000 psi]. Irreversible compaction is expected to be minimal.

When CO_2 is injected in the Captain sandstone, the small amount of calcite in/around the pores will be dissolved. However, there is not much carbonate cement in the reservoir parts that will be used for the CO_2 injection. So, the pore space will increase a small amount (greater volumetric injection will be available) and the matrix will become slightly weaker, although the risk of pore collapse is avoided.

Compaction experiments carried out in 1998-1999 showed that the compaction of cores from Goldeneye sands is partly elastic (i.e. reversible) and partly plastic (i.e. irreversible). Results from the experiments showed minimal compaction, and the porosity change was about 0.3%. As a result this effect can be considered to have negligible impact. For further details regarding this topic, refer to the Goldeneye Geomechanical Report on Results of Lab Experiments (1).

7.1.2.1. Efficiency of refilling

Refill efficiency has been divided into macroscopic and microscopic fill efficiency. The microscopic efficiency has been partially discussed under the last point above, but macroscopic efficiency also includes the impacts of permeability variations in the subterranean formation and dynamic stability of the flood fronts due to mobility ratio (viscosity and relative permeability).

- **Reservoir heterogeneities**
  There is substantial permeability contrast between the Captain D sand and other sands in Goldeneye. The D sand contained ~78% of the original hydrocarbon (Figure 7-4). Injected CO_2 will tend to follow the path of least resistance. Full field simulation has confirmed that, during the injection phase, the CO_2 preferentially fills and follows the D sand. If the D-sand were the only body available for filling, the storage capacity would be reduced by 9.7 million tonnes CO_2.

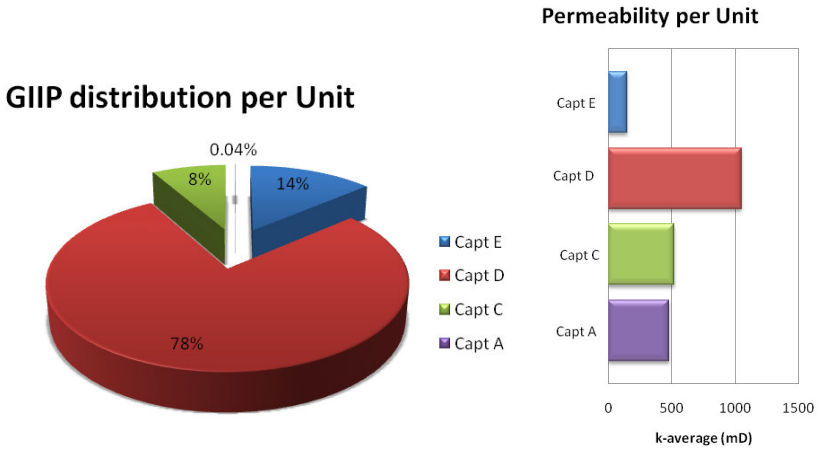

Figure 7-4. Goldeneye GIIP distribution and average permeability per geological unit.

After injection, buoyancy forces dominate, and the CO_2 contracts back into the original gas cap. It also begins to fill the overlying Captain E sand. The Captain E sand accounts for a further 13.7% of the original hydrocarbons in place and could potentially add an additional

3.4 million tonnes CO_2 if 100% refilling efficiency is considered (based on an estimated gas ultimate recovery of 60 Bscf). However, part of it will be filled with the remaining undeveloped hydrocarbon gas, and when the effects of some of the reducing factors that affect the Captain D unit are taken into account, just a part of Captain E will be finally flooded with CO_2 (mainly the bottom part). Furthermore, this will occur after injection ceases, and it could take a long time for the buoyancy forces to overcome the capillary forces and slowly fill the Captain E sand. Numerical simulation results show that 2.5 Mt of CO_2 makes its way into Captain E, 20 years after injection stops.

- **Unstable displacement**
  The effects of unstable displacement during CO_2 injection process in Goldeneye could potentially reduce the short term (i.e. during injection) storage capacity.
  A dipping box simulacrum model representing roughly one quarter of Goldeneye in volume, with similar rock properties (permeability and porosity) and dip angle was used to simulate these effects. Phase behaviour was represented using a Peng Robinson 1978 **(8)** equation of state (EoS), calibrated to match the Goldeneye hydrocarbon fluid description from GYA03, CO_2 properties (density and viscosity) at reservoir conditions (11) and CO_2 dissolution in brine.

Considering both increasing and reducing factors, the effective storage capacity can be estimated as a function of voided volume (from production) and refill efficiencies based upon the most important reducing and increasing factors mentioned above, which are later multiplied together.

$St_{Capacity}$ = *Available Volume * Volumetric Sweep * Dietz efficiency * Water displacement *Mixing * Dissolution*
where:

- Available volume total pore volume voided by production
- Volumetric sweep: considering where the CO_2 will preferentially go in based on reservoir quality (heterogeneities)
- Dietz efficiency: related to the unstable displacement of CO_2 displacing water under an unfavourable mobility ratio
- Water displacement: "residual water saturation" (S_{wr}) left behind the CO_2 flood front
- Mixing: of CO_2 with remaining hydrocarbon gas saturation (undeveloped + trapped)
- Dissolution: of the CO_2 in both the pore water and the underlying aquifer

Mineralisation has been identified as a potential increasing factor, but makes significant contributions over timescales long after the injection period has finished. It is therefore not considered further here. Other factors, such as irreversible compaction, are considered negligible. Additionally, processes such as the possible filling of Captain E sand when buoyancy forces dominate after cessation of injection, may be added at the end of the capacity estimation.

It is important to highlight that the unstable displacement factor (Dietz efficiency) will be in play only during injection, and will determine the point in time when the tip of the CO_2 plume reaches the boundary of the OOWC. As a consequence, we will define an effective storage capacity *post injection*, not considering the unstable displacement or Dietz tonguing effect. Nevertheless, it must be stressed that this discount factor could have an important role depending on the reservoir structure, as will be explained in more detail in Section 10.3.1. In addition to the storage capacity defined by the structural trap of Goldeneye, the water leg beneath the reservoir that lies within the storage site, could potentially add some extra capacity. As the capacity added depends on the exact trajectory of the Dietz tongue mentioned above this estimate is based on numerical simulation results. Finally, an areal sweep efficiency will exist that should also be taken into account. This will be difficult to estimate

analytically due to the non-uniform shape of the CO_2 plume, but it will be evident in the numerical simulation results.

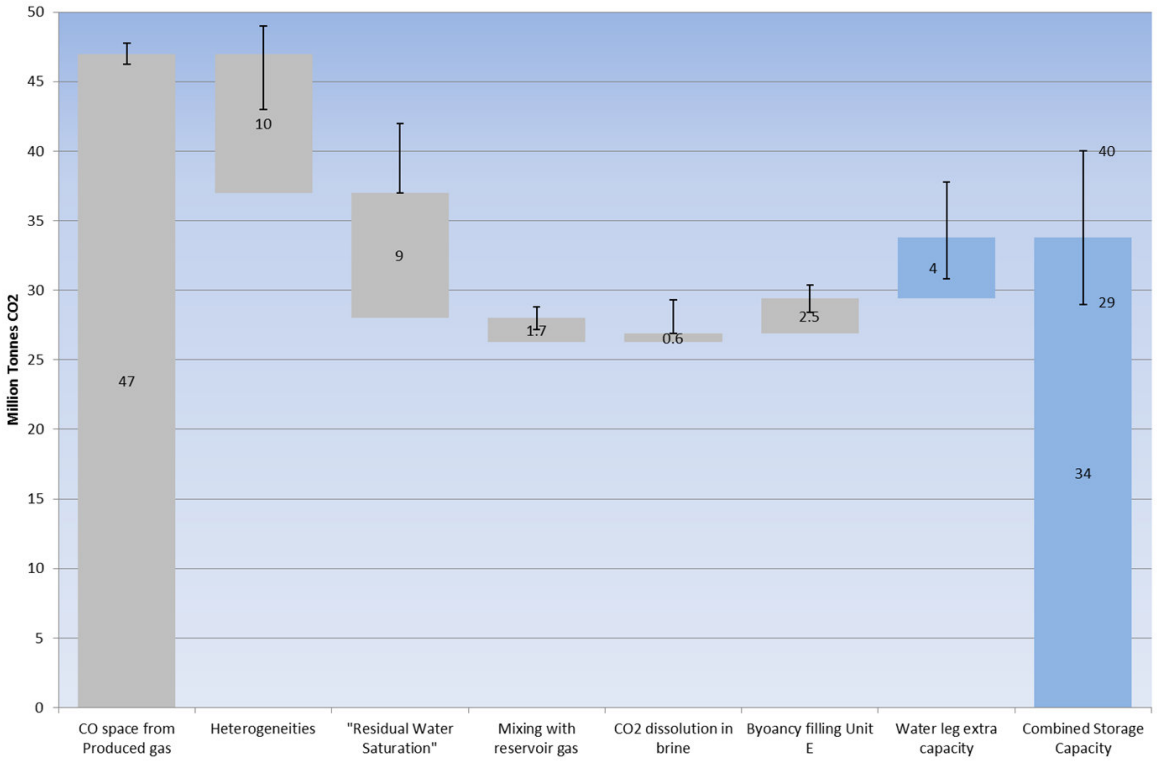

Figure 7-5. Post-injection effective storage capacity of Goldeneye

Using this equation and taking into account the additional capacity of the original water leg beneath the field and inside the storage site, Goldeneye's effective, post-injection and combined geological carbon storage capacity can be estimated as 34 million tonnes of CO_2, which is more than adequate to store the 10 or 20 million tonnes intended.

The uncertainty bars in each of the elements of Figure 7-5 represents the uncertainty observed.

- **Heterogeneities:** reservoir heterogeneities were highlighted in Goldeneye by the permeability contrast when comparing Captain E and C with the Captain D sand. This led to the assumption that most if not all of the CO_2 will be injected in Captain D. This sand contained ~ 78% of the original hydrocarbon, however, this factor has a range among all the geologic realisations available for Goldeneye that ranges from 70% to 82% and consequently this uncertainty bar represents that span.
- **Residual water saturation:** the size of the effective "residual water saturation" (S_{wr}) factor left behind the CO_2 flood front, was estimated by Buckley-Leverett displacement theory and fractional flow equations. S_{wr} ranged from 15% to 25% depending on the Corey exponent to water, and this uncertainty bar represents that span.
- **Mixing with hydrocarbon gas:** the reduction in capacity was estimated to be as much as 6%. This is assuming 100% mixing between CO_2 and the remaining hydrocarbon gas, however, simulation has shown that instead of a perfect mix, a hydrocarbon gas bank is formed at the tip of the plume, meaning that mixing is not perfect. As a consequence the reduction will be smaller than 6%, making it a minor reduction factor. 4% was taken as a lower end for this element, which is a relative small figure overall.

- **CO_2 dissolution in brine:** the increment of storage capacity was estimated as 2.2%, taking into account a CO_2 solubility of 4.6% (weight) and that CO_2 will contact approximately 25% of the brine due to the water saturation left behind the CO_2 injection front. Nevertheless, dissolution is considerably more complicated than the obviously instantaneous dissolution described before. In addition there will be diffusion of the carbon dioxide dissolved in the water, allowing more CO_2 from the gas phase to dissolve in the aqueous phase below the plume. There will also be a convective mixing effect because the density of water saturated with CO_2 is greater than that undersaturated, hence density instability is created and eventually plumes of CO_2 laden water flow downwards through the formation. Assuming this, a maximum dissolution reduction was calculated to be 11.2% considering that not only the height of the CO_2 plume (residual water saturation) is contacted but in the long term the whole reservoir thickness.
- **Buoyancy filling of Unit E:** after injection, buoyancy forces dominate. The CO_2 contracts back into the original gas cap, and it also begins to fill the overlying Captain E sand. It was seen in simulation that Captain E will eventually be flooded with CO_2 but mainly only the bottom part. A refill efficiency for Unit E of between 33% and 66% was assumed in order to create the span for this uncertainty bar.

Water leg extra capacity: in this case the bar shows an uncertainty margin dominated by the static uncertainties regarding the structural west flank of the field and is also sensitive to the injection pattern. The alternative realisation SMR3.05 (shallower west flank) allowed only 2 Mt of CO_2 to be stored in the water leg, while SMR3.15 (pinch-out sensitivity) allowed 7 Mt and the reference case (SRM3.1) 4 Mt for the reference case injection scenario.In contrast to a traditional E&P approach (where a probabilistic distribution will define a P10-P50-P90), in a sequestration project capacity must be demonstrated in at P0 or near certainty. The summation of all the positive and negative uncertainty bars gives the total uncertainty range for the storage capacity at the end of injection. The extremes represent the unlikely scenarios where all the elements decreasing or increasing the storage capacity all happen in the downside or upside cases.

The final capacity and the extremes are for the specific injection pattern using the current Goldeneye well penetrations and currently proposed store rock volume. If for example, more CO_2 were to be injected, an alternative pattern with new penetrations could yield a higher post injection capacity by forcing more CO_2 to be stored in the water leg.

8. Goldeneye Full Field Reference Case Model

Flow processes under gas injection are extremely complex and are, like many things, only approximated in three dimensional finite difference simulations (or Full Field Models), with existing levels of computing power. However, Full Field Models (FFMs) do have a role when considering the overall material balance, approximate fluid flow and field operability. With care, the results of FFM runs can be compared against sector models with both simplified and detailed physical representations in order to obtain an understanding for the field-wide scope for gas injection.

For several years Shell has had a successful FFM of the Goldeneye Field. This has been used for well planning and recovery estimates. Although adequate for asset modelling, the grid resolution in the existing MoReS model was considered too low to adequately represent gas injection. Unfortunately, it also used a grid up-scaled within the Petrel® model and applied history match modifications post upscaling. As a result a rapid reconfiguration was required in order to obtain something suitable for

gas injection. It was also important to obtain a model that was flexible enough to allow alternative geological realisations to be examined. The general approach taken was:

- Export the geological model from Petrel® and upscale in Reduce++,
- Configure and history match in a grid independent manner,
- Avoid local well modifications, instead take a field wide approach to history matching,
- Use a finer grid all round,

A basic history matching exercise was performed. The general aim was to obtain a reasonable match without local modifications. The CO_2 project required a model where the general flow processes were correct but individual wells did not need to be perfectly matched. This meant that it was not necessary to make local changes, which always ran the risk of providing the correct behaviour at an existing well without correcting any general behaviour in the rest of the reservoir.

8.1. Model Behaviour

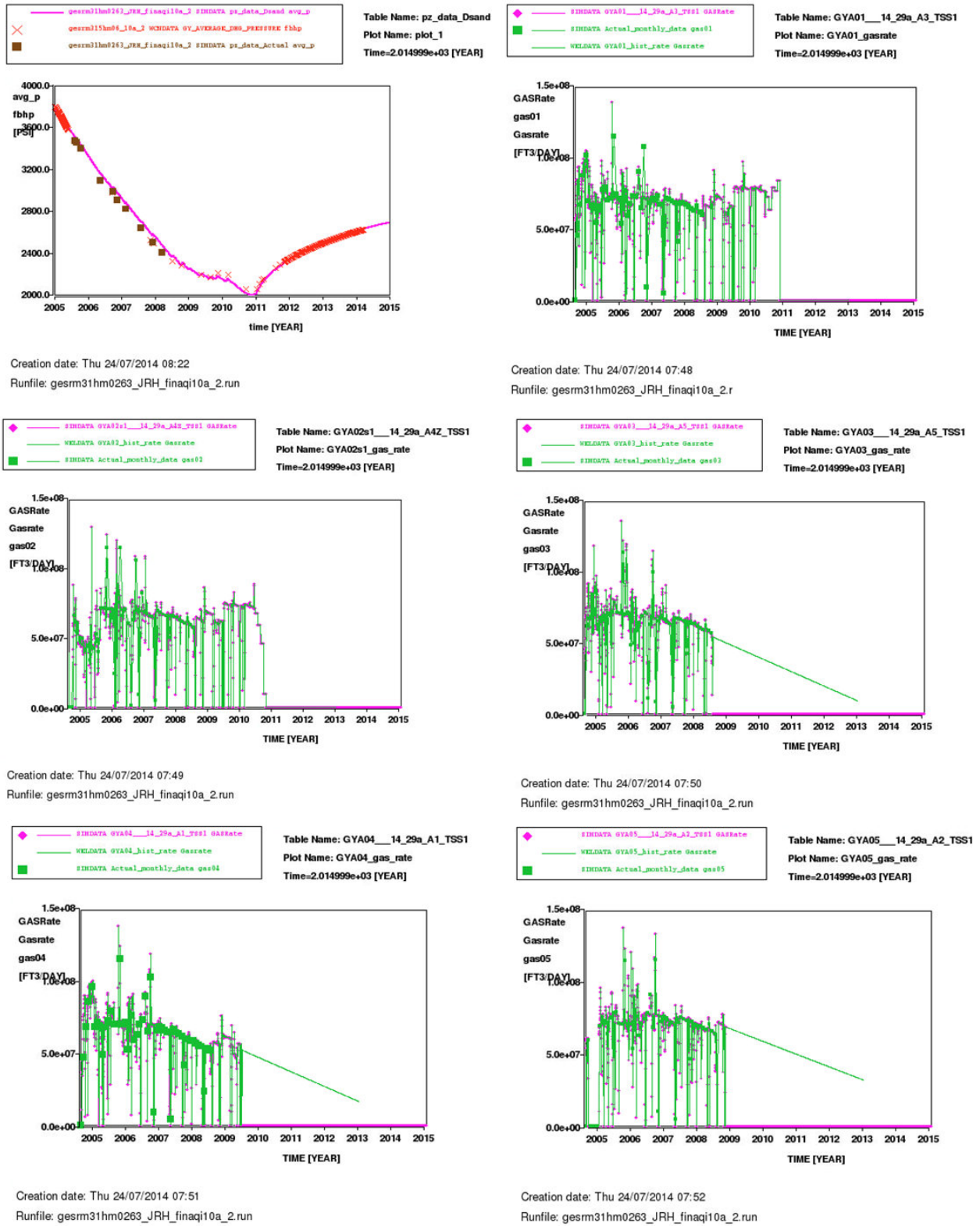

Figure 8-1: FFM diagnostics – reservoir pressure and wells rate.

Figure 8-1 shows a series of standard diagnostic figures that were used during the history matching process. The main aim was to achieve a pressure match in order to get a general material balance

within the field. Once that was achieved, the work continued to match the water breakthrough time of the wells.

Key:

Bottom hole pressure figure:

- Pink line Simulated average pressure for gas in the Captain D unit.
- Red crosses SBHP data (from PDHG corrected to reservoir datum) 2004 – 2014 period.
- Brown squares SBHP data (from PDHG corrected to reservoir datum) 2005 – 2008 period.

Production figures:

- Pink diamonds monthly gas production simulated
- Green Solid lines daily history gas production
- Green squares monthly history gas production

Major Issues were:

- Insufficient hydrocarbon volume in the main reservoir units (E,D,C) to maintain the reservoir pressure.
- Lack of connectivity within the three main reservoir units such as Unit E, D and C.
  - Causing early water breakthrough and mismatch of energy in the system
- Permeability of the Captain D sand
  - Need to increase the permeability to match recent re-pressurisation performance 2011-2014,
- Aquifer strength both in the East and the West.
  - An increase in permeability of Captain D was offset by a reduction in the permeability of the Eastern aquifer to balance water encroachment

8.2. History Match

Experimental design or assisted history matching techniques were not used. Instead the approach was to initially work to understand the key drivers in the system and then to enforce this using a traditional history matching approach. During the history match the model is constrained on gas rate.

Once the model was properly set up, reflecting both the geologic and dynamic data, relatively few history match modifications were required:

- Vertical connectivity of main reservoir units (E,D,C)
- GIIP volume and distribution among main reservoir units (E,D,C)
- Aquifers characterization both East and West of the Field
- Residual gas saturation (S_{gr}) and $k_{rw}@S_{gr}$

8.2.1. Vertical connectivity of main reservoir units (E,D,C)

Initial history matching runs began to show a lack of connectivity among the main reservoir units. This was observed through different depletion levels at each unit, especially Unit C and below. The following figure shows a W-E cross section in the middle of the field with the history matched model at the left and the initial history match run at the right.

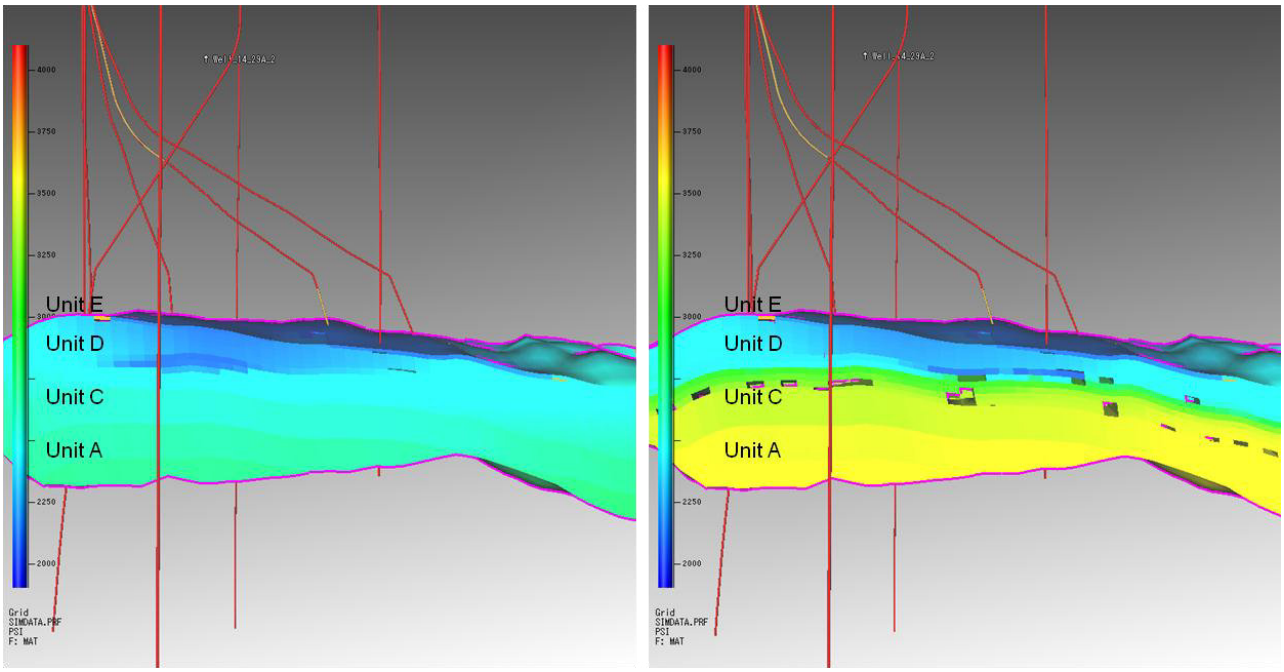

Figure 8-2: FFM cross section showing pressure depletion level

Data from wireline formation pressure data showed that pressure variation with depth was insufficiently significant to infer compartmentalisation among Goldeneye geologic units. On the contrary, a continuous pressure trend along the reservoir was observed in all wells. The following figure shows well 14/29-a3 FMT pressure data with log curves and pressure data points from the well test gauge.

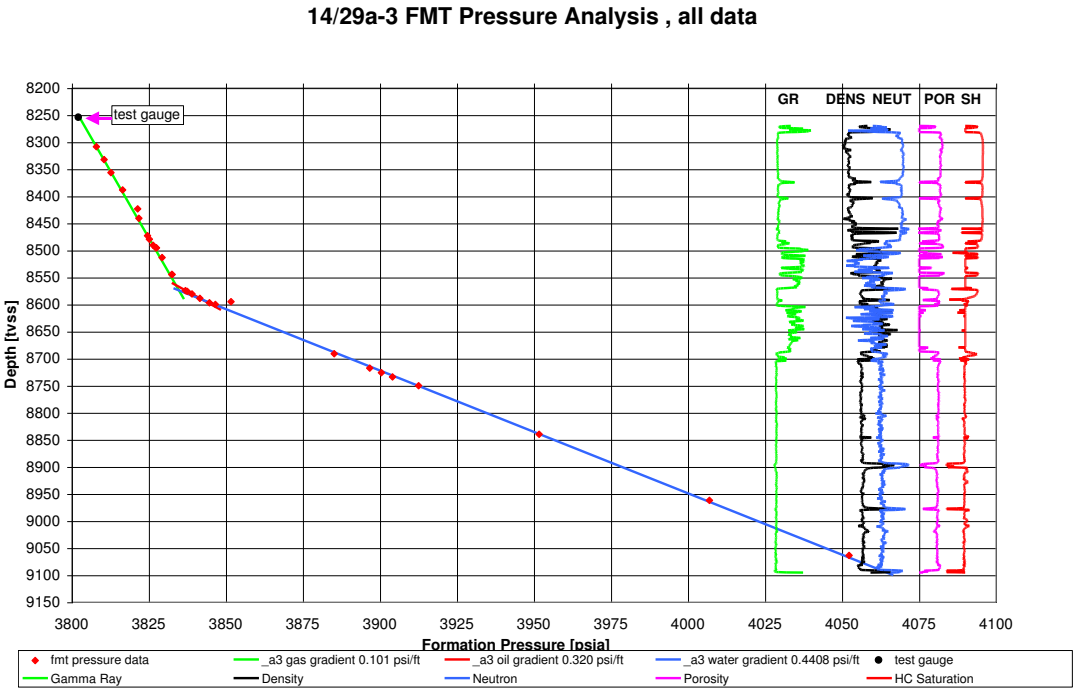

Figure 8-3. 14/29-a3 FMT pressure data with log curves.

All wells in the field showed good alignment and no vertical pressure difference among the units, at least under initial conditions (pre-production). A common OWC and GOC were also observed in all the wells. Unfortunately RFT/MDTs are not available at different stages post-production to corroborate the vertical connectivity result.

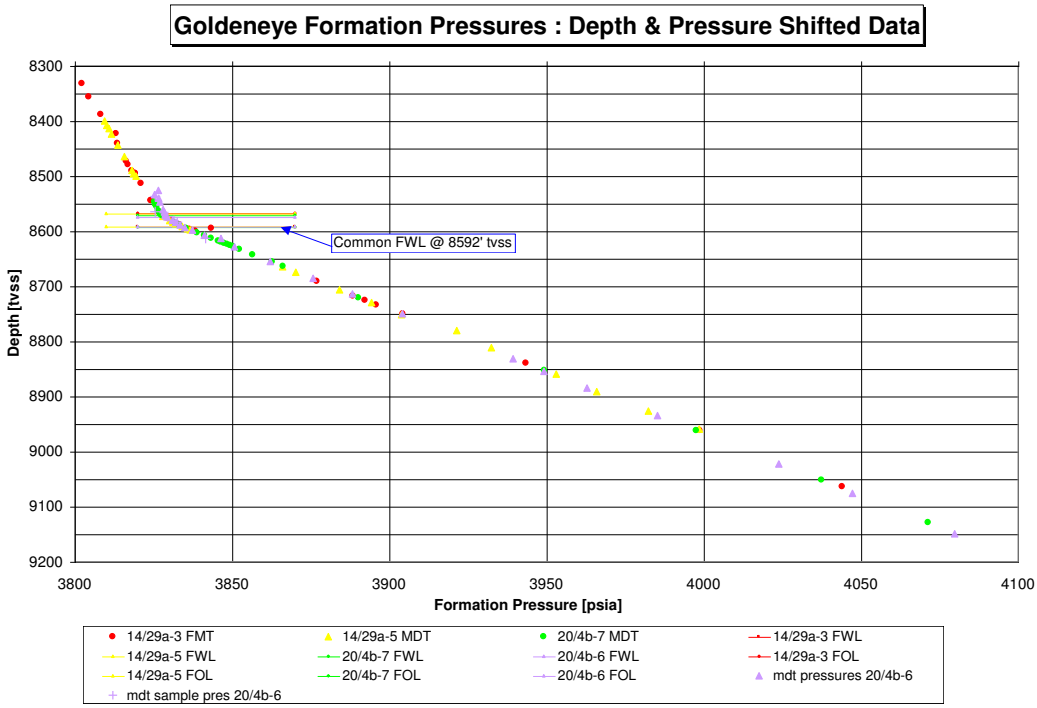

Figure 8-4. Formation pressure data.

In order to improve the connectivity among Captain geologic units, seal factors of "geological surfaces" in MoReS (interface between Unit E, D and C) were opened, which was supported by static and dynamic data. This allowed better communication, based upon the premise that high mobility gas will eventually find a way of moving in order to hydraulically connect the volume.

8.2.2. GIIP volume and distribution among main reservoir units (E,D,C)

Improving communication among the geologic units proved to be insufficient to obtain a pressure match of historical measurements. The model lacked sufficient hydrocarbon volume in order for the wells to produce the reported gas levels and avoid early water breakthrough.

Initial material balance studies showed a larger GIIP in the field than that resulting from the detailed geological model. However, in many cases the basic P/Z plot for a waterdrive gas field can overestimate the initially in place volumes. It will appear to be linear until a very advanced stage of depletion, causing a misleading extrapolation. If the plot is made with an enlarged P/Z scale then it can often be seen that the only linear portion of the plot occurs very early in the lifetime of the field, before the water influx is significant. Extrapolation of this early trend will give a more reliable value of the GIIP. The latter technique was applied in the case of Goldeneye, using early shut-in data from well GYA05 from Oct 2004 to Feb 2005. The following figure shows the result.

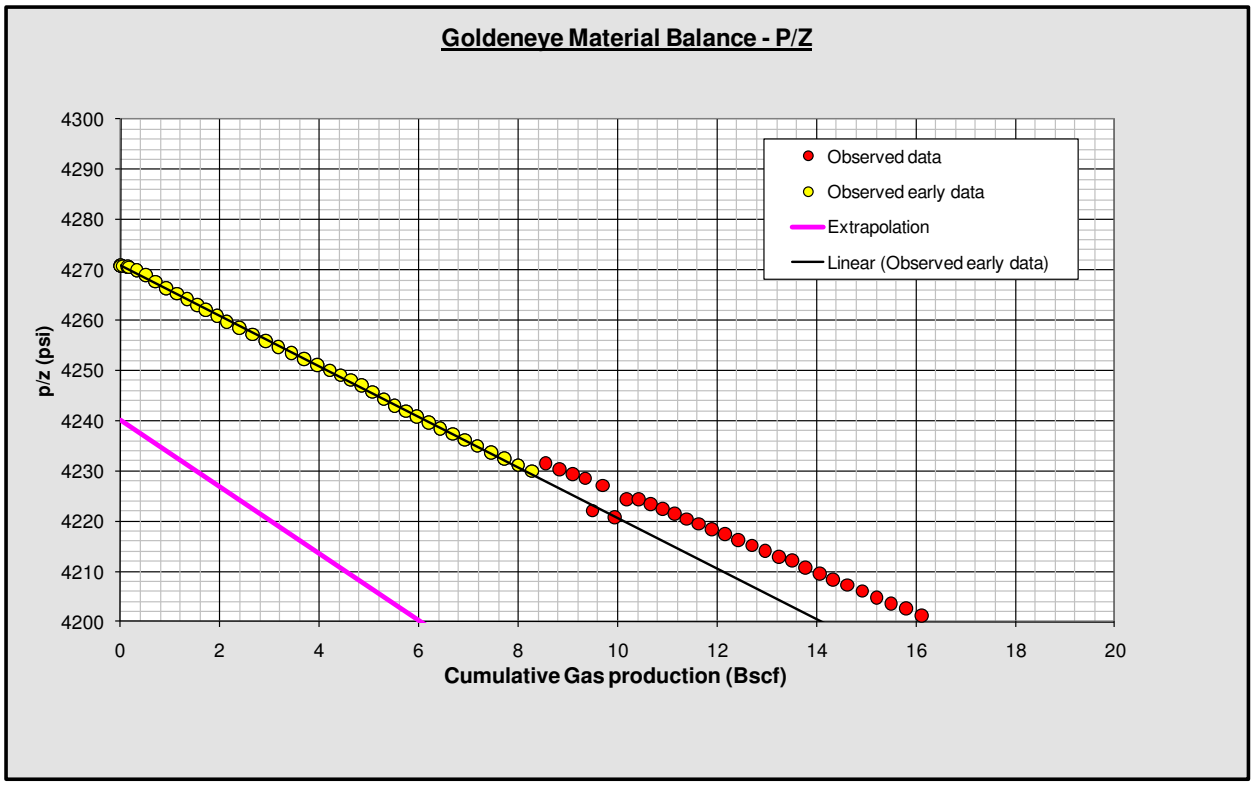

Figure 8-5. Goldeneye Material Balance P/Z plot. Zoom at early shut-in pressure period.

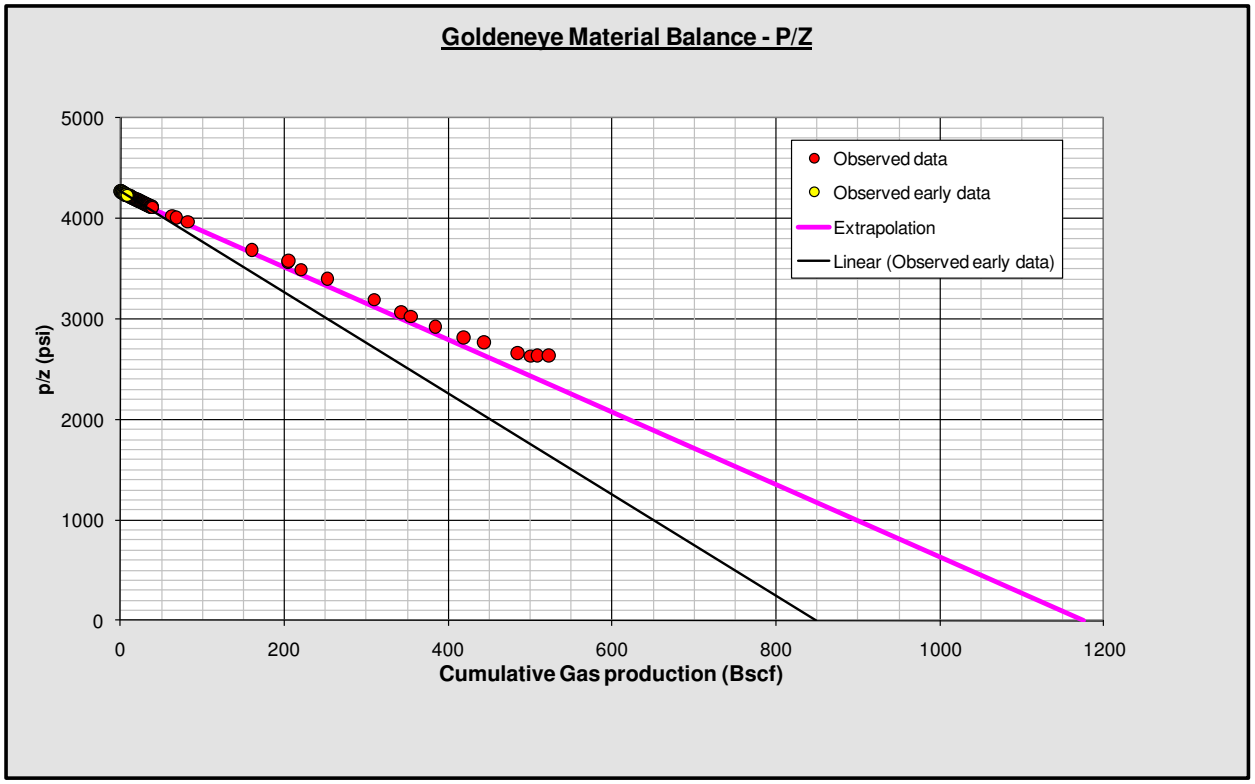

Figure 8-6. Goldeneye Material Balance P/Z plot. GIIP extrapolation.

The Havlena-Odeh technique works better when assessing a waterflooded gas reservoir, trying to reduce the uncertainty of the P/Z plot by doing a reverse extrapolation of the GIIP. It can be expressed as follows:

$$\frac{F}{E_g} = G + \frac{W_e B_w}{E_g}$$

Where,

$F = G_p B_g + W_p B_w$ = *total gas and water production (rcf)*

$E_g = B_g - B_{gi}$ = *underground gas expansion (rcf/scf)*

$W_e B_w$ = *water influx*

The following figures show the Havlena-Odeh plots for Goldeneye, which indicates water influx and a total connected GIIP of between 775 Bscf and 945 Bscf. In addition, the analysis implies that the aquifer is likely to be moderate-to-strong. In a material balance approach, the response will see the total energy of the reservoir. In the case of Goldeneye the gas in solution in the oilrim will also contribute to the mass balance.

Stochastic distribution of the oilrim volume placed it in the following range: 27.5 MMstb (P90), 31.5 MMstb (P50) and 35.5 MMstb (P10). The reference case model has 32.3 MMstb in the oilrim, initialized at 926.7 scf/stb yields roughly 30 Bscf at initial conditions, of which is expected to come out of solution approximately some 14 Bscf during depletion when pressure went from bubble point (P_b = 3531 psia) to abandonment pressure of ~2000 psia. This represents 1.7% of Goldeneye GIIP, becoming a minor effect.

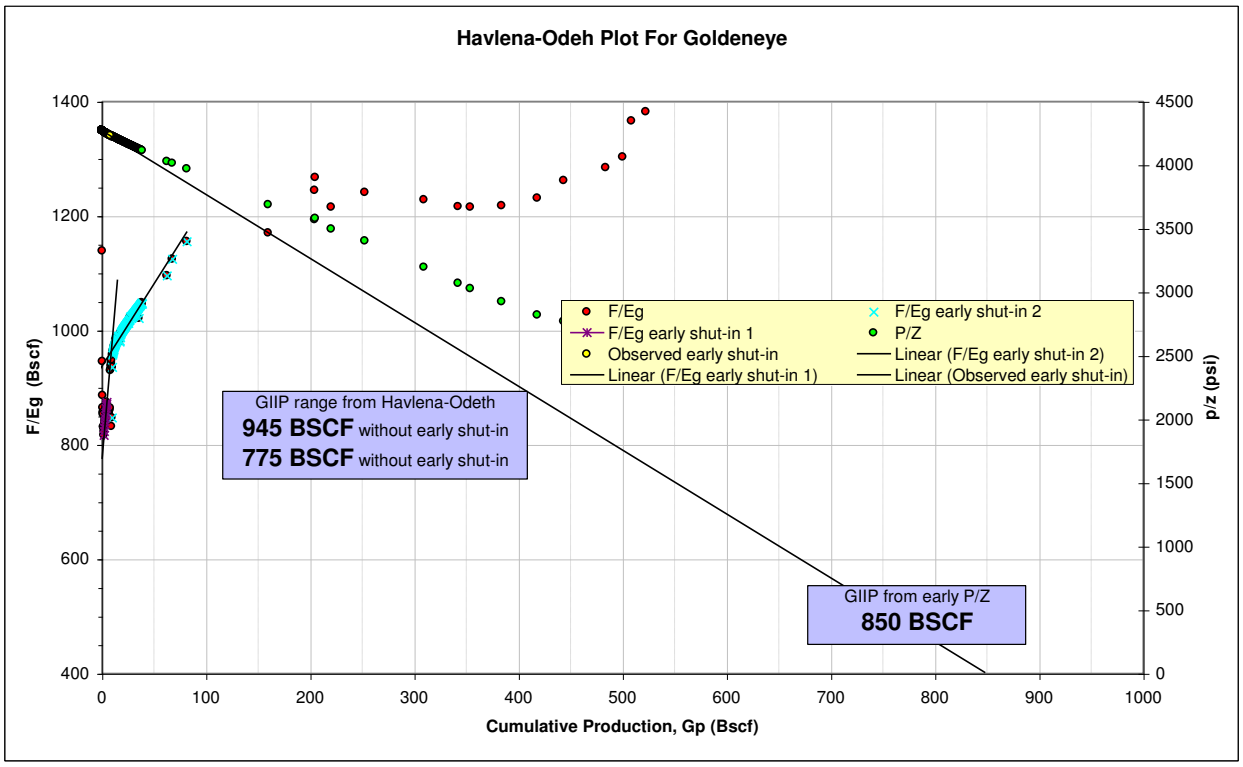

Figure 8-7. Havlena-Odeh material balance plot.

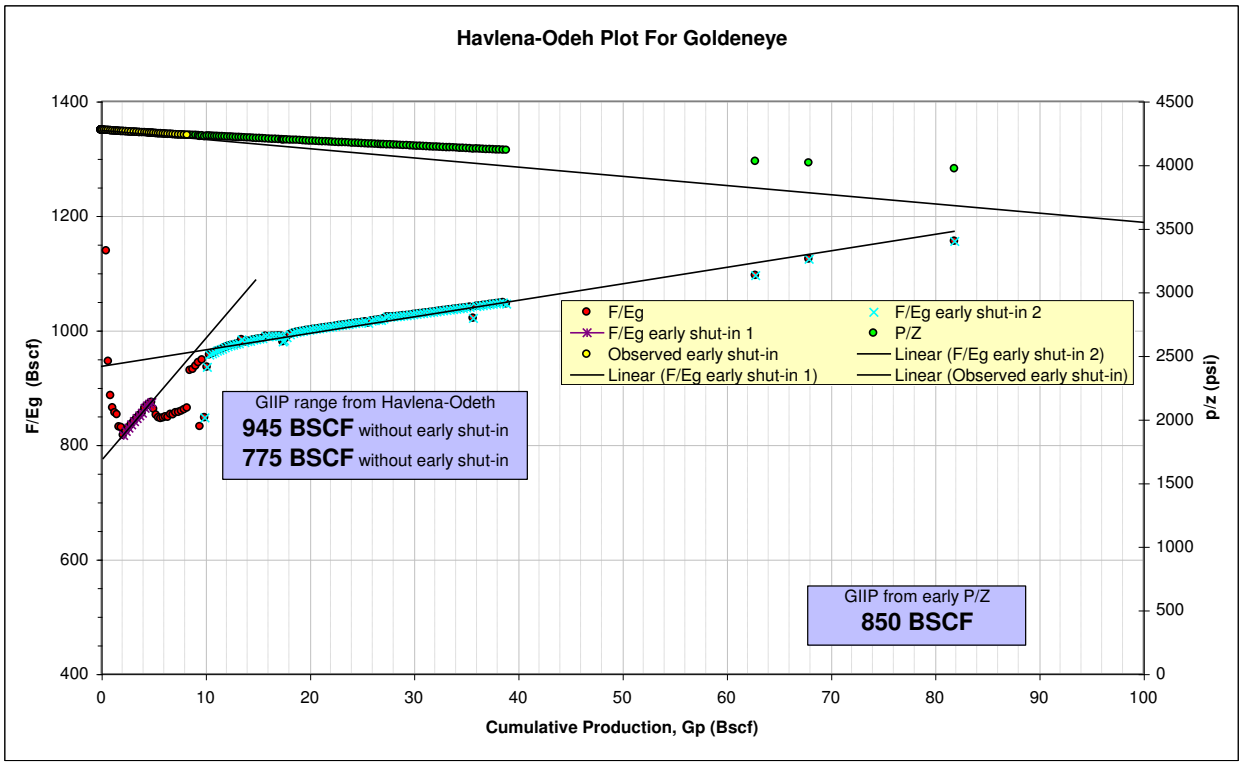

Figure 8-8. Havlena-Odeh material balance plot. Zoom in.

The Havlena-Odeh results can be compared to the static volumes estimated for the field: the stochastic distribution of total gas initially in place (gas column + solution gas in the oilrim) ranges from 723 Bscf to 846 Bscf. This is in line with the material balance analysis. Both parameters support the use of the range of GIIP as a history matching parameter. The following figure shows the probabilistic distribution of GIIP in Goldeneye field.

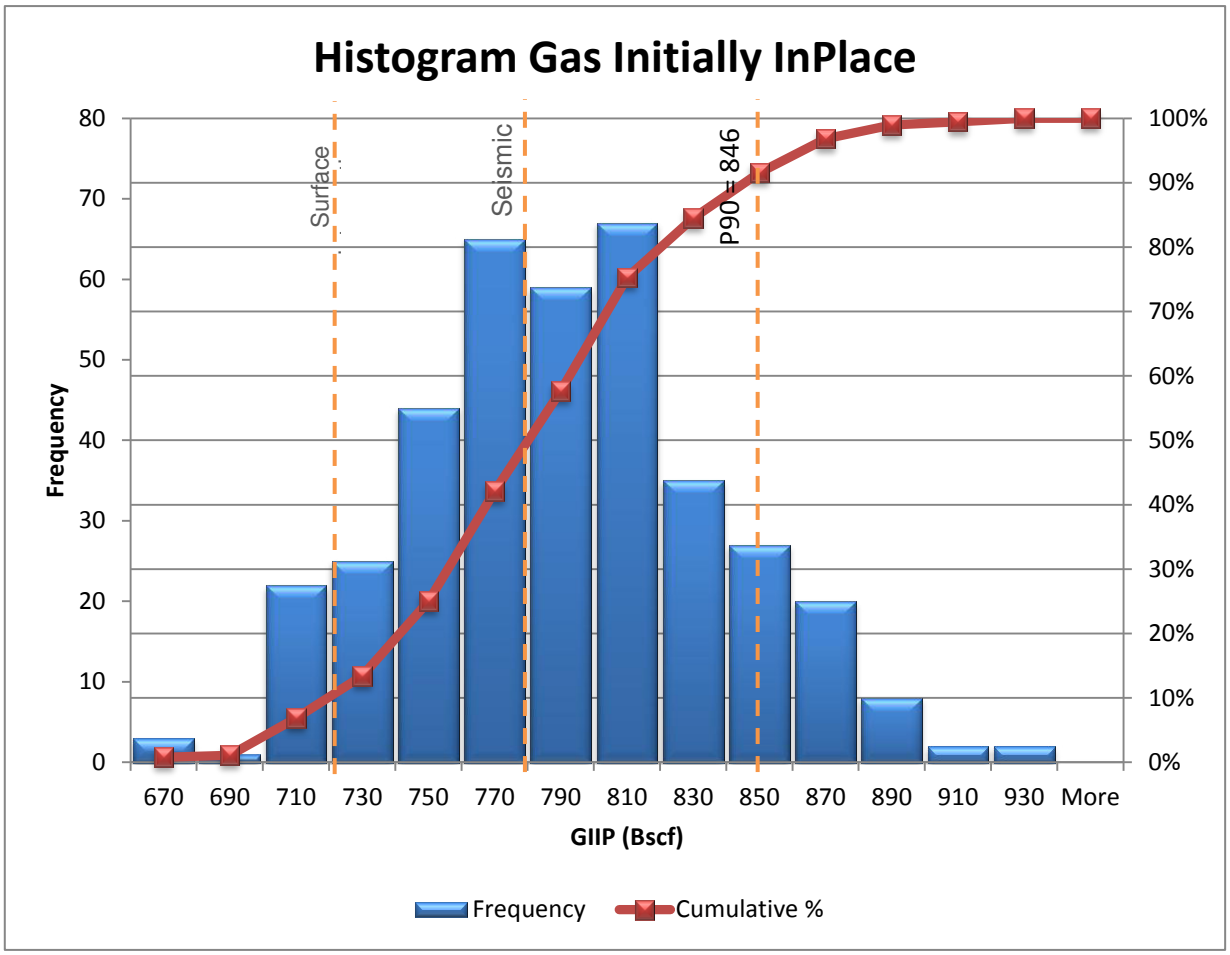

Figure 8-9. GIIP probability distribution based on 381 runs of the geologic model.

Taking into account both analyses, the GIIP in unit D (main reservoir geologic unit) and unit C were increased by 10% in order to compensate for the pressure depletion observed in the initial model behaviour, and enlarge the gas availability to wells trying to retard the water breakthrough. Final history matched GIIP = 815 Bscf.

8.2.3. Aquifers characterization both east and west of the Field

The history matching process of the Goldeneye field is heavily influenced by the aquifer fluxes both from the east and the west. These fluxes are complex due to a combination of depletion resulting from production and subsequent shut-in from the nearby Hannay oil field in the east and, production effects from the adjacent Atlantic and Cromarty gas fields in the west. In order to improve the understanding of the pressure history a regional aquifer model has been constructed. This includes the production of neighbouring fields in addition to the aquifer. By understanding the pressure history and characterising the aquifer fluxes to the east and west of the Goldeneye Field, the dynamic simulation of the aquifer constrains and improves the history match in the Goldeneye full field simulation model for both pressure response and water breakthrough of the wells.

The aquifer static model over the Captain fairway covers approximately 100 km of the Captain sandstone but the aquifer continues to the east and west. To the east the Captain sandstone extends for further 40-50 km approximately and continues to deepen. To the west of Blake the formation starts to widen and eventually outcrops at the seabed about 50 km to the west of Blake. The aquifer is

therefore potentially infinite (effectively) to the west but finite to the east. The following figure shows the extent of the Captain Fairway highlighted in yellow; with basinal areas in pale green.

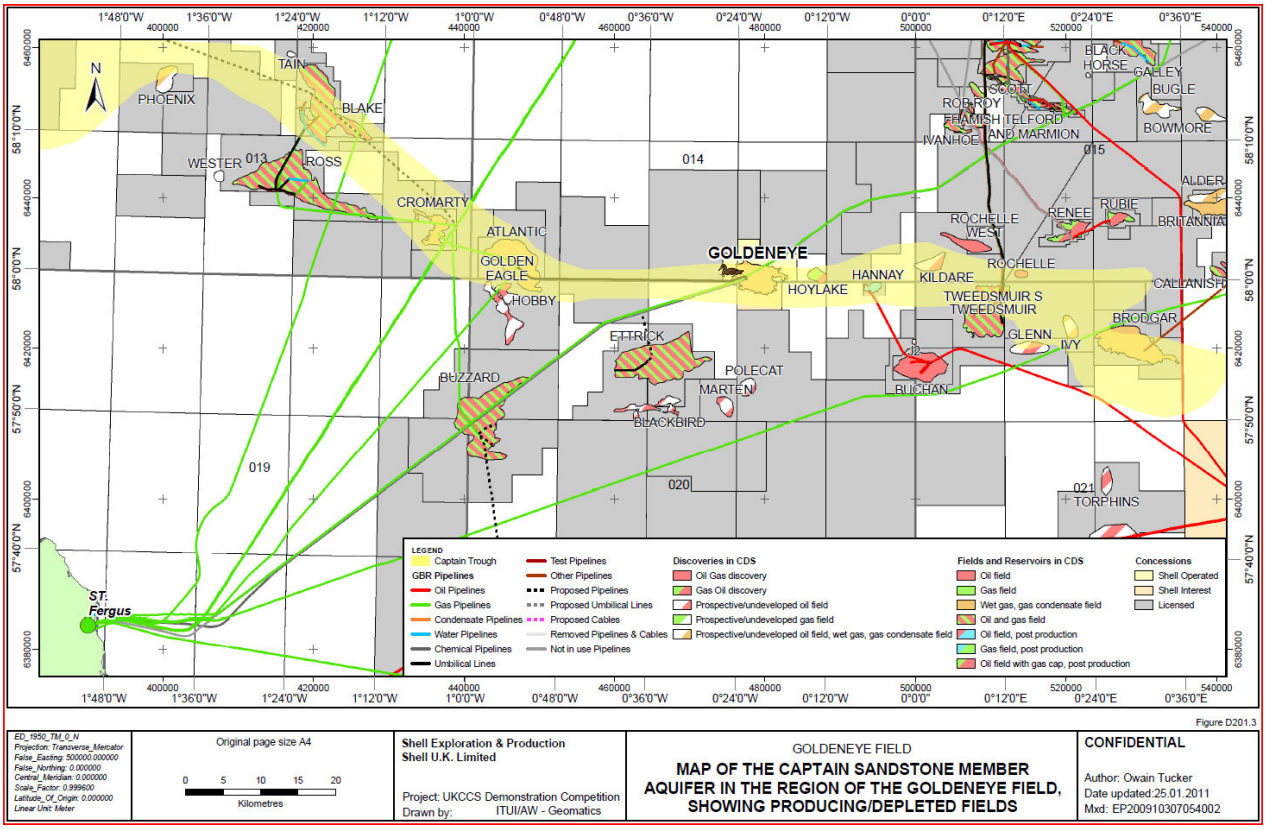

Figure 8-10. Distribution of Captain sandstones across the outer Moray Firth.

Owing to computer processing power constraints much of the detailed modelling of CO_2 movement within the store has been carried out using a standalone model, matching the analytical aquifer strength to the pressure response observed. An intrinsic problem in the use of this method is that this model cannot match the initial depletion observed from Hannay, which is a very useful data set in matching aquifer size, response and lag times. At the same time, whilst Hannay is producing, it is extracting water, both reducing the pressure support from the eastern aquifer and pulling water away from Goldeneye producer. Additionally, the western aquifer will be matched using the full pressure of the Cromarty and Atlantic gas caps, whereas the apparent strength of the western aquifer should be significantly reduced from the point where these fields started production. Accordingly, in an ideal situation a dynamic pseudo-aquifer would be implemented. These issues become more important when attempting to forecast water production in Goldeneye.

As a consequence, the aquifer characterization in the FFM is a pseudoisation of the actual fairway aquifer. A detailed regional aquifer model was built which incorporates fields in the Captain sandstone: Hannay, Atlantic, Cromarty, Blake and Rochelle. All of these fields are assessed as being likely to be in communication with Goldeneye and can potentially influence its pressure. In addition Hoylake gas field, in proximity of Goldeneye to the east, was included in the aquifer model, to address pressure interference effects with Goldeneye. This will be discussed in detail in Section 11.

For the Goldeneye FFM the aquifer representation was specifically a history match parameter varied within the regional known parameters, but focused upon achieving a pressure and water breakthrough match. The intention with the FFM is to understand the displacement mechanisms

during CO_2 injection, while the general material balance, production – aquifer balance and pressure behaviour will be properly assessed with the regional aquifer model.

The following table describes the ranges in aquifer properties that were used during the FFM history match. It is based on a regional study and is in line with the latest aquifer model used for the regional aquifer numerical model described in Section 11.

Table 8-1. Regional aquifer static characterization

Scenario	Length	Width	h	h	N:G	Por	kh	W_i	W_i
	(km)	(km)	(ft)	(m)	(ratio)	(%)	(mD)	($e6m^3$)	(MMStb)
No	8.8	4.5	550	167.7	0.72	23%	800	1099.6	6.9
Low	18	4.7	430	131.1	0.75	23%	750	1913.2	12.0
Mid	65	7.5	350	106.7	0.75	23%	500	8778.3	55.2
High	140	7	320	97.6	0.76	24%	850	17584.5	110.6
H High	230	11	400	122.0	0.71	26%	1500	57832.1	363.8

Final aquifer parameters used in the history matched model were for an infinite acting linear aquifer of: 190 km length (150km west + 40km east), 625 mD west, 250mD east. The background to this is a stronger more permeable aquifer to the west and a weaker less permeable aquifer (permeability trend in the region) to the east and in order to compensate for the effects from Hannay oil field which produced around 30 million reservoir barrels of fluid.

8.2.4. Residual gas saturation (S_{gr}) and $k_{rw}@S_{gr}$

Data availability for residual gas saturation and the effective end point of water relative permeability was discussed in Section *6.2*. For reference, S_{gr} could vary between 25% and 38% and $k_{rw}@S_{gr}$ between 5% and 25%, based on the SCAL data available at the moment. The impact of these two variables during the history matching process differs from that described for CO_2 injection in Section 6.2. Residual gas saturation to water by aquifer intrusion during depletion will impact the amount of mobile gas available for production (during CO_2 injection this will define how much CO_2 will get trapped). Also the water relative permeability end point at residual gas saturation during the depletion stage, will define how easily the aquifer will move through the hydrocarbon column impacting both reservoir pressure as well as water breakthrough time for wells (during the CO_2 injection phase, $k_{rw}@S_{gr}$ defines how easy it will be for CO_2 to push water away, having an impact on the Dietz tongue and unstable displacement).

As a consequence, these two parameters are also constrained by the history match itself and were used as parameters to achieve it. Final values were S_{gr} = 25% and $k_{rw}@S_{gr}$ = 0.25, both within the ranges available for them.

Sensitivities were carried out in order to test the effect of higher S_{gr} (meaning less mobile gas available) and therefore also having a higher GIIP in order to compensate. However, GIIP values were pushed to the higher end limits and the whole history match process is more complicated than just a simple balance of these two parameters. There is also an oil rim between the aquifer and the gas column that acts as a baffle restricting the aquifer response and impacting the reservoir pressure. The oil rim also becomes smeared during the depletion stage, which also affects the mobility ratio within the gas leg. Accordingly, a combination of a possible reduction of residual oil saturation in the gas leg due to the presence of trapped gas, and the reduction of residual gas saturation in the oil leg due to the presence of trapped oil, will define the balance of residual saturations and GIIP in order to achieve a reasonable history match.

8.3. History Match Results

After introducing the changes discussed above, a reasonable history match was achieved in the Goldeneye reference case full field model. The following figures show the results. The plot key is the same as stated before in Section 8.1.

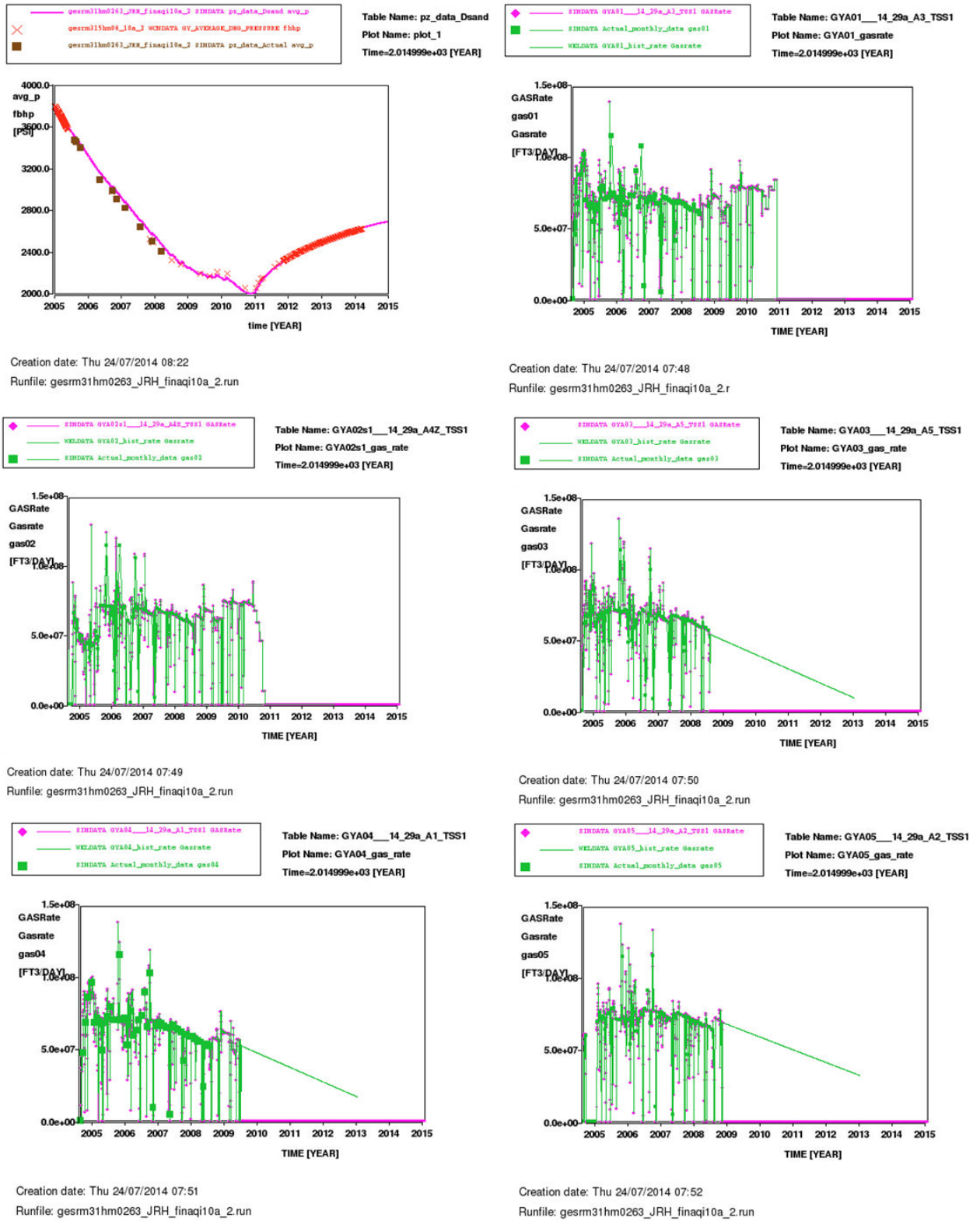

Figure 8-11. FFM 3.1 diagnostics – reservoir pressure and wells rate. History matched.

The following aspects should be highlighted:

- **Average reservoir pressure** A reasonable match is achieved during most of the history including initial pressure and depletion up to the beginning of 2010, with minimum variation between observed pressure measurements (red crosses) and average pressure for gas in the Captain D unit (pink line). Observed pressure measurements are taken from the permanent downhole gauges which are located slightly above the top perforations in Captain D unit and then corrected to a datum of 8400 ft TVDSS. As a consequence, this represents the geologic unit being directly monitored. In the late time period, simulated pressure diverges from observed pressure. This effect is explained by the interaction of Goldeneye, aquifer support and neighbouring fields cessation of production during Q2 of year 2009 (Hannay, Atlantic and Cromarty). When the neighbouring fields of Hannay, Cromarty and Atlantic cease production the effective strength of the eastern and western aquifers changes. The neighbouring fields no longer block the aquifers which are now free to repressurize Goldeneye. Further study of this would require a better representation of the aquifer in the full field model: probably by pseudoising the aquifers with dummy wells that recreate the changes in aquifer intrusion or by explicitly representing these effects numerically in a larger model, for example in a refined version of the fairway regional model discussed in Section 11.
- Water breakthrough time in all wells GYA01, GYA02S1,GYA03, GYA04 and GYA05 was precisely matched by general adjustment of the aquifer strength on the east and west (described above in Section 7.2.3). The field ceased to produce in December 2010 when the last well GYA01 watered out.

This represents a remarkable achievement for the modelling phase and provides the best possible foundation for predictive behaviour under CO_2 injection. Nevertheless, CO_2 injection represents a different physical process and so, a careful modelling approach is still needed to ensure that the facts controlling CO_2 movement are properly represented.

9. Goldeneye Full Field Alternative Realisations

Several different geological realisations were built to address the three main aspects identified as key uncertainties with a possible direct impact on CO_2 storage capacity and containment. These aspects were:

- Extension of the stratigraphic pinch-out
- Structural dip on the western flank of the field
- Internal Captain stratigraphy (thickness)

These realisations were built and are summarized in the Static Uncertainties in Section 6.1.

Each realisation was (approximately) history matched to provide stability and confidence in the prediction results. It also served to screen out unrealistic realisations. The approach taken to address the history match of the three realisation models, attempted to follow the same strategy that was implemented during the calibration of the Reference Case.

As described previously, the main modifications made to the Reference Case in order to reproduce the history were:

- Vertical connectivity of the main reservoir units (E,D,C)

- GIIP volume and distribution among the main reservoir units (E,D,C)
- Aquifer characterization both east and west of the field
- Residual gas saturation (S_{gr}) and $k_{rw}@S_{gr}$

These modifications were included in the alternative realisations which were then run to compare with results from the FFM reference model in order to determine the impact of these changes upon the history performance.

9.1. Behaviour of alternative realisations

As in the reference case, the main aim was to achieve a pressure match in order to get a general material balance within the field. Once that was achieved, the work continued to match the water breakthrough time of the wells.

Major issues found in the alternative realisations were:

- Insufficient hydrocarbon volume in the north-west area of the field, causing early water breakthrough of GYA03. This is mainly due to the modification introduced by bringing the northern pinch-out towards the south (SRM 3.15).
- Excess of energy in realisation SRM 3.05. The shallower west flank increases the total GIIP by 2.5%, impacting the general pressure match of the field.

9.2. History Match

Although a similar approach as that taken with the reference case was employed, some rather local modifications were required in addition to the same changes already introduced in the reference case history match.

Additional history match modifications in the alternative realisations were:

- GIIP volume was modified in the main reservoir unit D, specifically in the north-west corner of the field in order to increase the gas availability to wells and avoid an early water breakthrough (SRM 3.15: pinch-out sensitivity). The increase in volume in this small region was compensated with the total volume multiplier in main reservoir Unit D, so that the total GIIP remained the same as in reference case.
- Weaken aquifers to east and west of the Field in SRM 3.05 due to the excess of energy caused by the shallower western flank. Both aquifers were modelled as finite acting, the western permeability was reduced to 600mD and the eastern permeability was reduced to 175mD There is uncertainty regarding the aquifer characterization and it is not clear from the data if it exhibits infinite or finite behaviour. This realisation also allows testing a different approach to the overall energy balance in the system.

After introducing the changes mentioned above, a reasonable history match was achieved in the Goldeneye alternative realization cases of the full field model. The following figures show the results. The plot key is the same as stated before in Section 8.1.

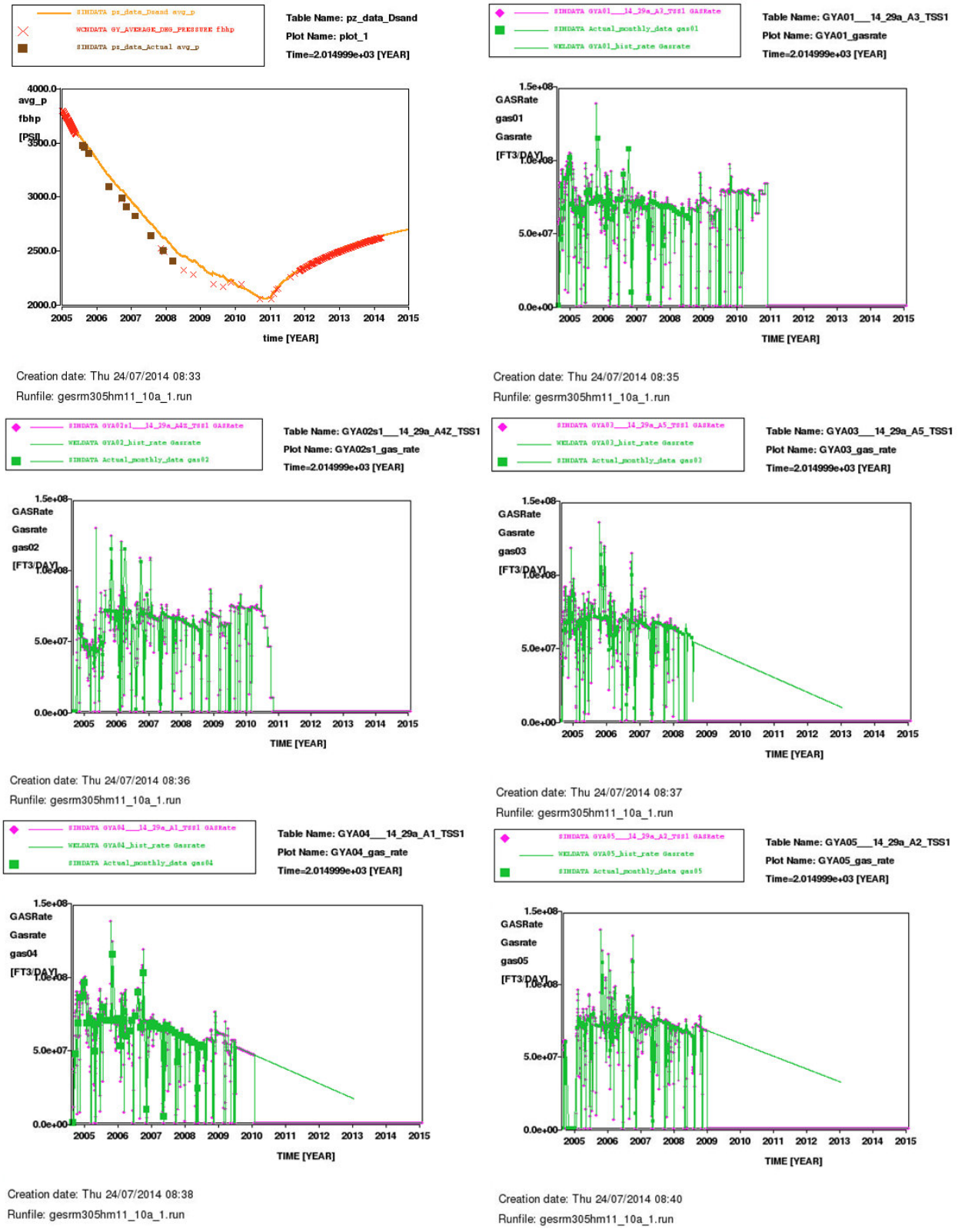

Figure 9-1. FFM 3.05 diagnostics – reservoir pressure and wells rate. History matched.

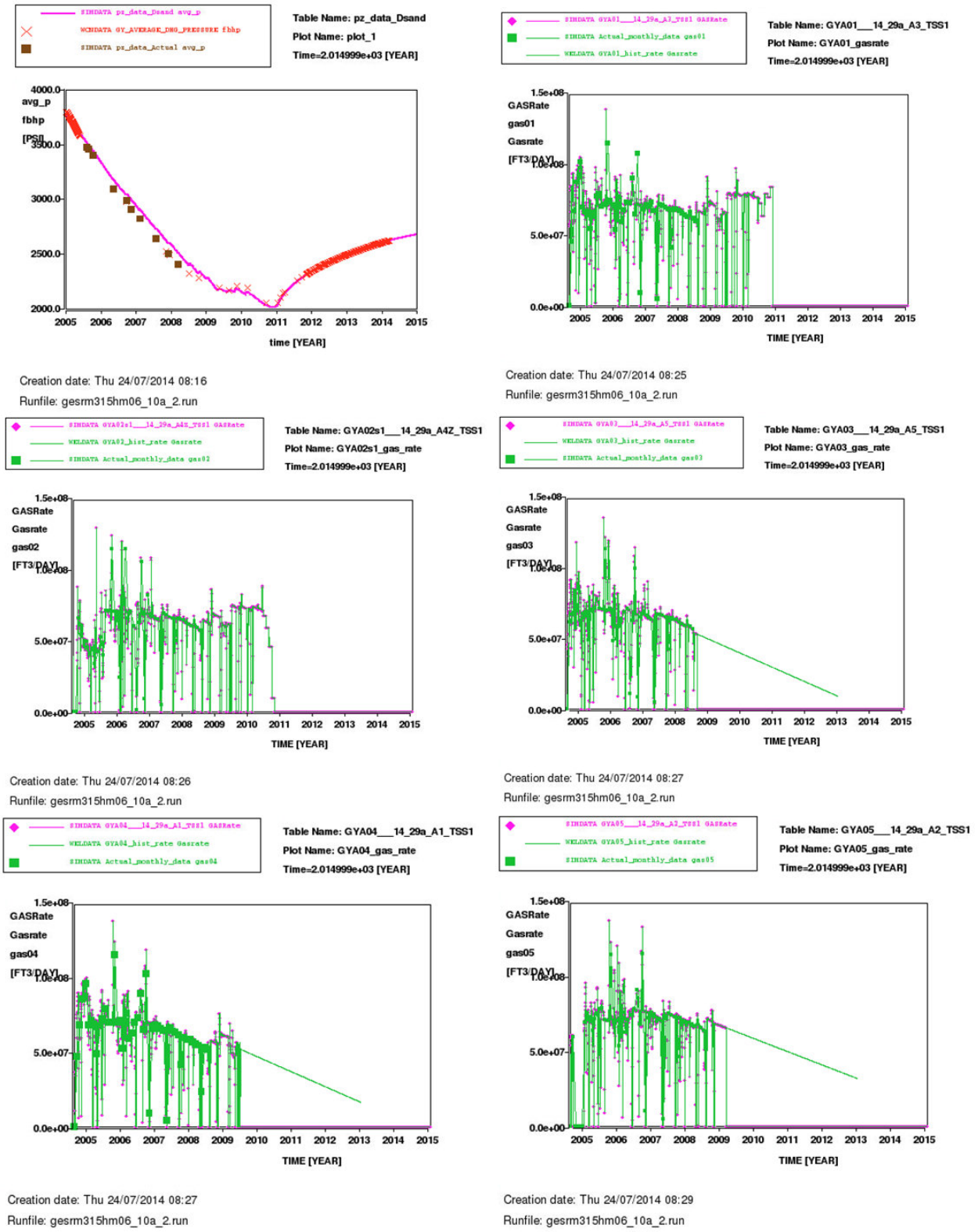

Figure 9-2: FFM 3.15 diagnostics – reservoir pressure and wells rate. History matched.

Aspects to highlight are as follows:

- **Average reservoir pressure** behaviour is very similar in the three realisations after history match changes were introduced. It demonstrates that a balance can be achieved by modifying the aquifer characterization but still reflecting permeability trends and aquifer strengths within the fairway.
- **Water breakthrough time in wells GYA03 and GYA04** is not perfect in the alternative realisations but it is close enough to be acceptable. In realisation SRM 3.05 (western flank sensitivity) GYA03 breaks water four months earlier than history, however, GYA04 does it five months later. Thus, in the end the total gas produced is the same. Realisation SRM 3.15 (pinch-out sensitivity) properly capture the water breakthrough time of the wells. An important aspect to be stressed regarding the water breakthrough time, (which is briefly mentioned during the description of *Static Uncertainties* in Section 6.1) is that geologic realisations with seismically interpreted surfaces were tested and was not possible to achieve a history match. The scenario where internal Captain stratigraphy was generated using seismically interpreted surfaces to divide the reservoir (SRM 2.1, not documented in this report), yielded an early water breakthrough in wells GYA03 and GYA05, that could not be fixed without local modifications which were poorly supported by geologic evidence. Whilst scenarios with internal reservoir distributions that were developed with thickness maps derived from log based data, fully reflected the lateral water front displacements that cause water breakthrough in the two western wells (only three month of difference) exactly at the time history said (SRM 3.1, 3.05, 3.15 documented in this report).

These results give confidence that the FFM and its alternative realisations are suitable to take forward into CO_2 injection, having been properly calibrated and reasonably adjusted to be run in forecast mode.

10. Goldeneye full field forecast

The analytical calculations discussed in Section 7 show in the base case that there is about 20 million tonnes of spare capacity inside the original hydrocarbon gas field in the long term (post injection), which is sufficient to allow for additional discounting effects, without including the additional storage capacity of the water leg.

Full field dynamic modelling of the system was undertaken to check that the interaction of the geological system and the dynamic system did not produce effects that reduced the capacity. The dynamic models are based on three 3D geological realisations (Section 6.1) and include all the discount elements previously mentioned (Section 7). The models have confirmed the applicability of the analytical calculations.

The modelling is described below.

10.1. Final production phase

The three models were matched to historical production data up to December 2010 when the field ceased to produce. Since cessation of production the pressure gauges have continued to be monitored, providing a further 3 ½ years of pressure buildup data. Three out of the five gauges GYA01, GYA02S1 and GYA05 are still operating while the gauges in GYA03 and GYA01 are isolated from the reservoir by suspension plugs. All the pressure data have been history matched up until April 2014.

Table 10-1. End of production life in different models

Geological model	
FFM 3.1	December 2010
FFM 3.05	December 2010
FFM 3.15	December 2010

10.2. Injection wells

For the Peterhead CCS project, the target for CO_2 injection is 10 Mt CO_2 in a period of between 10 and 15 years starting in January 2019. In order to make best use of existing resources all CO_2 injection is planned to be via the existing wells, which will be converted from production to injection service. In the model no changes have been made to the completions of the wells. For the initial sensitivity work, the flow of CO_2 into the wells is governed by injection tables, designed to represent 4½ inch completion tubing. The high permeability of the reservoir means that the capacity results are insensitive to minor variations in the completion characteristics of the wells.

CO_2 injection is modelled from 1st January 2019, with ramp up to 1.00 Mt CO_2/year within a day of starting up the Peterhead plant to reach steady state conditions.

In all cases, the wells are further constrained by a maximum BHP when injecting. For the initial simulation work, this has been set as 4000psi at datum of 8400ft [2560.3m] TVDSS. It is recognised that the pressure immediately around the wellbore will be higher than that further away. For the purposes of reporting the results the datum corrected average pressure for gas (hydrocarbon and CO_2) in the Captain D is used.

10.3. Injection scenarios

Several injection scenarios were modelled to test the storage margin referred to above in Section 6. In each case, the maximum reservoir pressure (after injection) and the total mass of CO_2 injected are determined. Also, the extent of the CO_2 plume (with respect to the location of the structural spill point) is checked. The aim is to establish that it is possible to inject 10 million tonnes of CO_2 in 10 years and the additional capacity for 20 million tonnes of CO_2, without risk of egression from the store and . The scenarios are:

a) **Base case**: staged injection starting with western injector GYA05, injecting for 5 years and then switching to eastern injector GYA02S1, injecting for another 5 years, with an even injection rate for a total of 10 years.GYA03 is not used for injection in this scenario and may be used as a monitoring well.

b) **Test risk of egress over the western and eastern flanks of the field (1):** inject the same total rates as above, but equally divided between only wells GYA02S1 and GYA04 (eastern wells) or GYA01 and GYA05 (western wells).

c) **Test risk of egress over the western and eastern flanks of the field (2):** Check risk of egression from store by injecting at double rate, while injecting same volume as under (b)

d) **Worst case of well availability**: attempt to inject the entire target CO_2 into one well only

e) **Maximum available storage:** inject at the same total rates as under a) but equally divided between only wells GYA02S1 and GYA04 (eastern wells) or GYA03 and GYA05 (western wells)Check the injected volume required to cause an egression from the store or to exceed initial (pre-production) average reservoir pressure. All scenarios were run in each of the three geological realisations – 3.1 (reference case), 3.15 (northern pinch-out sensitivity) and 3.05 (west flank sensitivity).

The key points to note for each scenario are:

- Total mass of CO_2 which was injected
- Extent of CO_2 plume outside the original hydrocarbon/water contact, at the end of injection
- Average reservoir pressure for gas in Unit D (the main storage unit)

A total of nine scenarios were run, in each of the three models. Results are given in Table 10-2 to Table 10-4.

The data in the tables is as follows:

- CO_2 injected: the mass of CO_2 in millions of tonnes delivered by all wells in period 2019 to 2029.
- Injected CO_2 in the Original Gas Zone: CO_2 resident immediately after cessation of injection (1st January 2029) within the original gas/oil contact.
- Plume extent beyond original OWC on 1st January 2029 – to both east and west of field: approximate distance from OOWC to the tip of the CO_2 plume, at top Captain D. This estimate is limited by the granularity of the dynamic model – the gridblocks are 100m x 100m areally. A positive number here means that the plume extends outside the OOWC, negative means it lies within the contact.
- Sensitivities extending the injection period until 2039 to a total injected volume of 20 Mt.

Table 10-2. Storage capacity results. Summary table for FFM 3.1 (reference case)

FFM 3.1	CO_2 injected (Mt)	Injected CO_2 in original gas zone (Mt)	% CO_2 outside original OWC after injection	Plume extent beyond original OWC –west (m)	Plume extent beyond original OWC –east (m)
Base case	10	10	0%	-400	-600
GYA01 and GYA05	10	10	0%	-300	-700
GYA02S1 and GYA04	10	10	0%	--600	-500
All in well GY01 failure	10	10	0%	-300	-700
GYA02S1 and GYA05	20	20	1%	0	-400
GYA01 and GYA05	20	19	3%	200	-500
GYA02S1 and GYA04	20	20	0%	-200	0
Double rate	20	18	8%	500	-800
Inject to **2060**	40	32	20%	1000	500

Table 10-3. Storage capacity results. Summary table for FFM 3.05 (west flank sensitivity)

FFM 3.05	CO_2 injected (Mt)	Injected CO_2 in original gas zone (Mt)	% CO_2 outside original OWC after injection	Plume extent beyond original OWC –west (m)	Plume extent beyond original OWC –east (m)
Base case	10	10	0%	-200	-800
GYA01 and GYA05	10	10	0%	-200	-800
GYA02S1 and GYA04	10	10	0%	-500	-500
All in well GY01	10	10	0%	-200	-800
GYA02S1 and GYA05	20	20	1%	0	0
GYA01 and GYA05	20	19	3%	200	-500
GYA02S1 and GYA04	20	20	1%	0	0
Double rate	20	18	8%	600	-800
Inject to 2060	40	30	24%	800	200

Table 10-4. Storage capacity results. Summary table for FFM 3.15 (northern pinch-out sensitivity)

FFM 3.15	CO_2 injected (Mt)	Injected CO_2 in original gas zone (Mt)	% CO_2 outside original OWC after injection	Plume extent beyond original OWC –west (m)	Plume extent beyond original OWC –east (m)
Base case	10	10	0%	-400	-800
GYA01 and GYA05	10	10	0%	-400	-800
GYA02S1 and GYA04	10	10	0%	-500	-100
All in well GY01	10	10	0%	-400	-800
GYA02S1 and GYA05	20	20	1%	100	0
GYA01 and GYA05	20	19	4%	200	-600
GYA02S1 and GYA04	20	20	1%	0	0
All in well GY01	20	19	3%	0	-500
Double rate	20	18	9%	400	-600
Inject to 2060	40	30	24%	800	200

Relevant scenarios are described here in more detail in the following sections.

10.3.1. Base case injection pattern – 10 Mt.

When the base case injection pattern (described in (a) above) was run in any of the geological models, the target of 10 million tonnes of CO_2 was injected, with no egression from the store. For model FFM 3.1, the target was achieved with no backing out of any of the four injection wells and the model indicated no CO_2 moving outside the original OWC at the end of injection. The CO_2 plume reached roughly 400m away from the original contact in the west, and roughly 600 m away from the contact in the east.

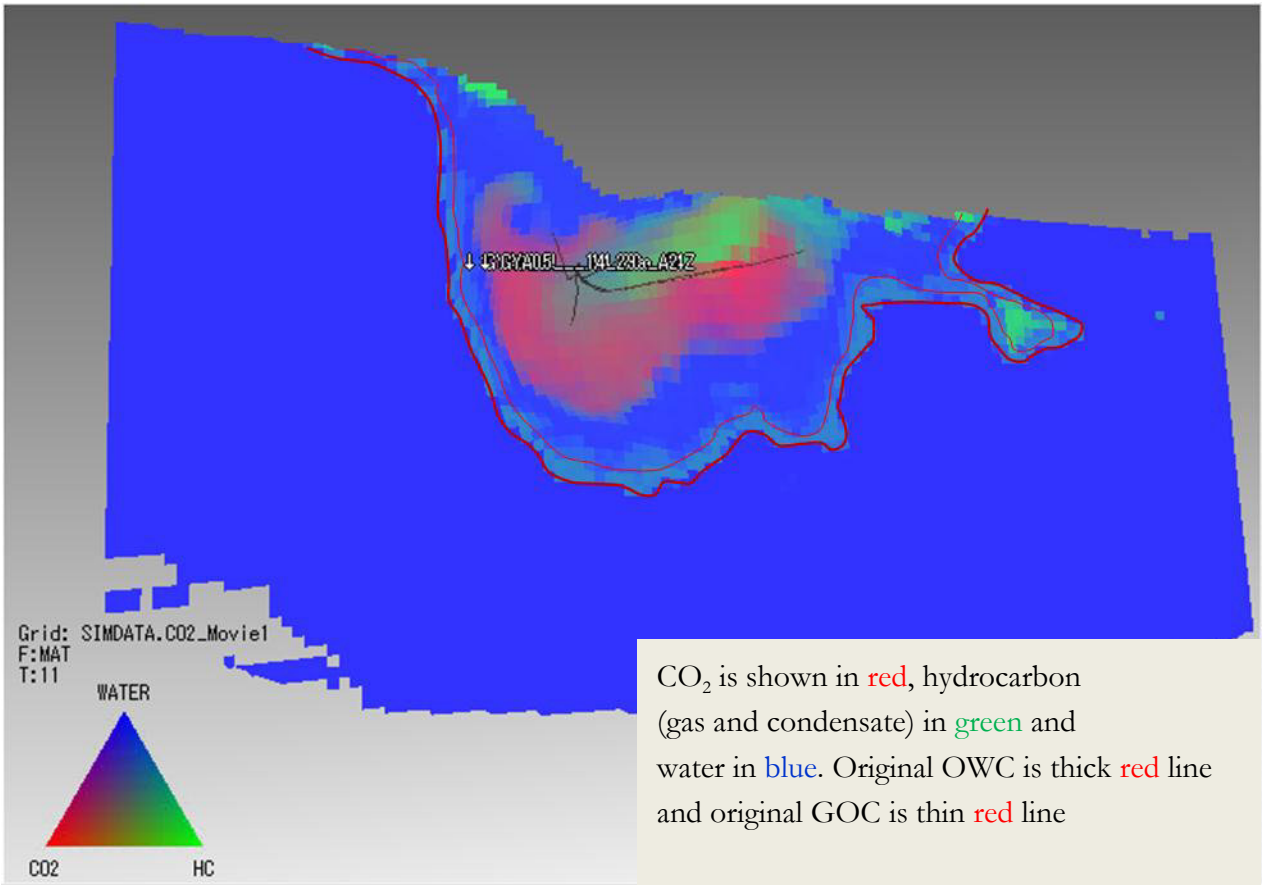

Figure 10-1. FFM3.1: Extent of CO_2 plume at top Captain D, at end of injection (2029).

Note that the colours in all screenshots of fluids in the Goldeneye CCS FFM follow the scheme noted in Figure 10-1– namely that CO_2 is shown in red, green represents remaining gas or condensate hydrocarbon, water is blue. Original oil/water and gas/oil contacts are shown as pink lines.

Figure 10-1 shows the prediction, from model FFM 3.1, of where CO_2 will be, after injecting a total of 10 Mt in 10 years, using as injectors wells GYA05 and GYA02S1, with the CO_2 injected equally by each well in a staged manner. For the purposes of this modelling exercise, injection tables representing 4½ inch completions were used. For the simulation, all injectors operated with a BHP constraint of 4000 psi.

It is important to highlight that during injection the tip of the CO_2 plume never reached the original oil water contact (OOWC), as shown by the base case realisation after 5 years of injection (approximately 5 million tonnes of CO_2), Figure 9-2 (A) and after 10 years of injection (approximately 10 million tonnes of CO_2) Figure 9-2 (B).

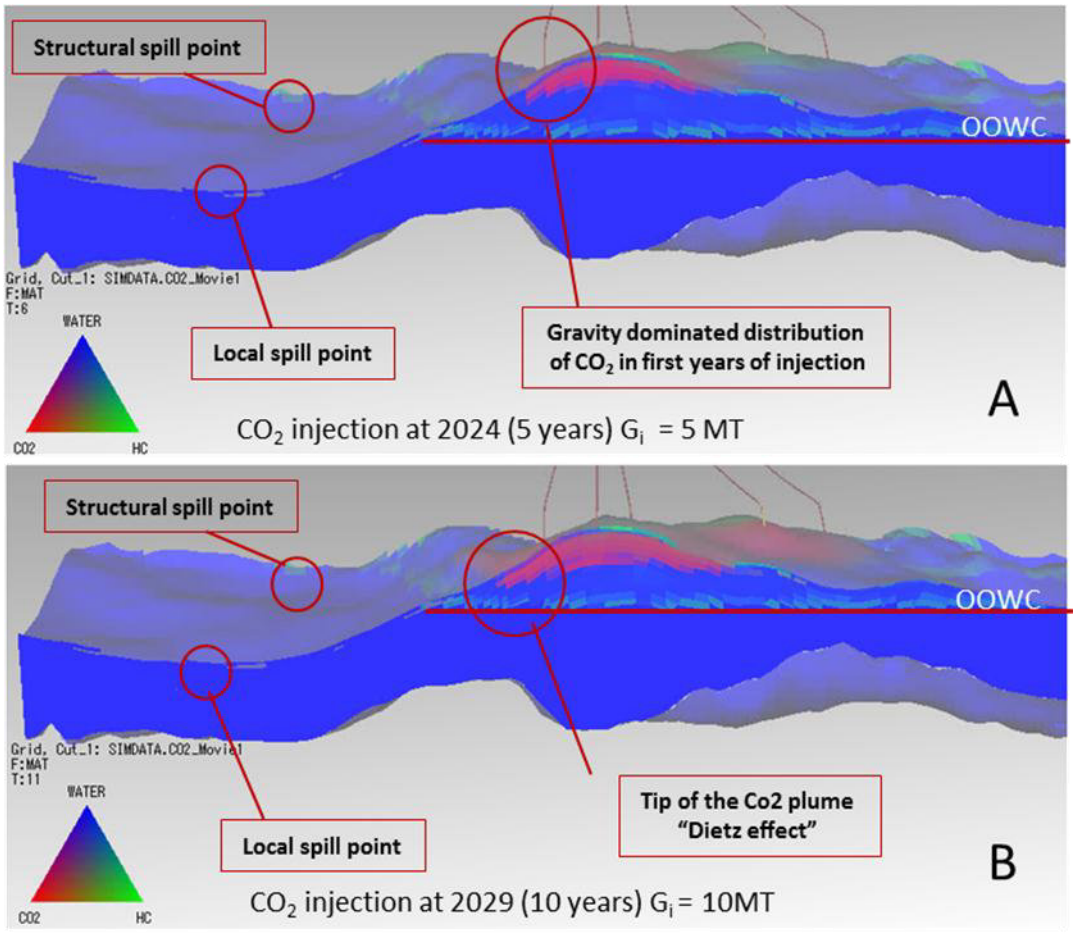

Figure 10-2: FFM 3.1 - CO_2 plume, (A) after 5 years of injection and (B) after 10 years of injection.

Additional simulations were run to assess how the system behaves after cessation of injection. For example in FFM 3.1all the mobile CO_2 moves back into the hydrocarbon column due to aquifer re-charge (see Figure 10-2 A and B). No CO_2 is present beyond the contact at any time during or after injection. At the maximum extent the CO_2 plume reaches to within 400 metres of the oil water contact as the "Dietz tongue" is starting to form.

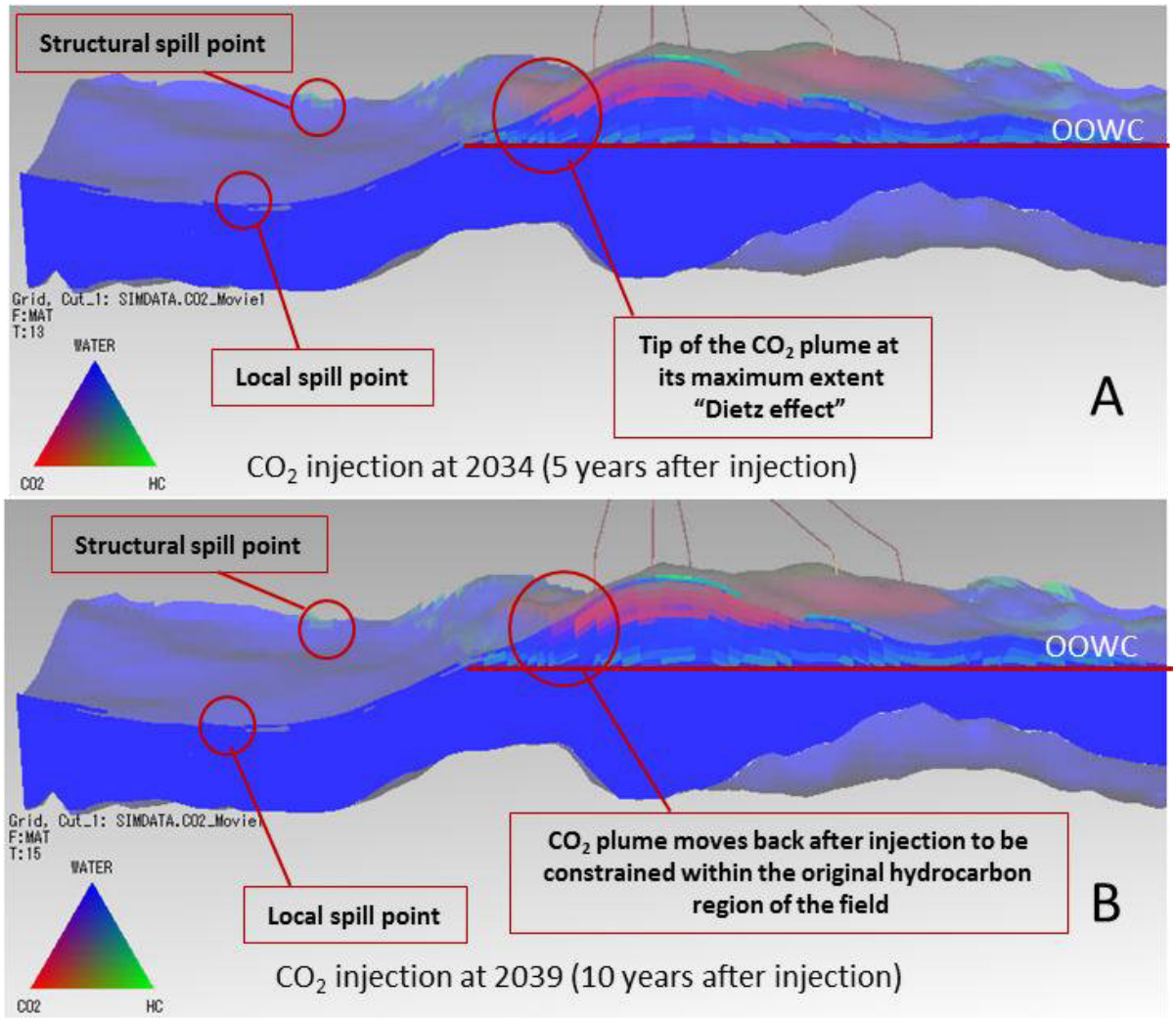

Figure 10-3: FFM 3.1 - CO_2 plume, 5 (A) and 10 (B) years after end injection

The average reservoir pressure relaxes in the first three to four years after stopping injection (Figure 10-4). In the longer term, the pressure decline slows and becomes a slow recharge, as the larger, and more distant, extended aquifer dominates. This result is supported by work carried out with the extended dynamic model of the larger Captain Fairway aquifer described in Section 11.

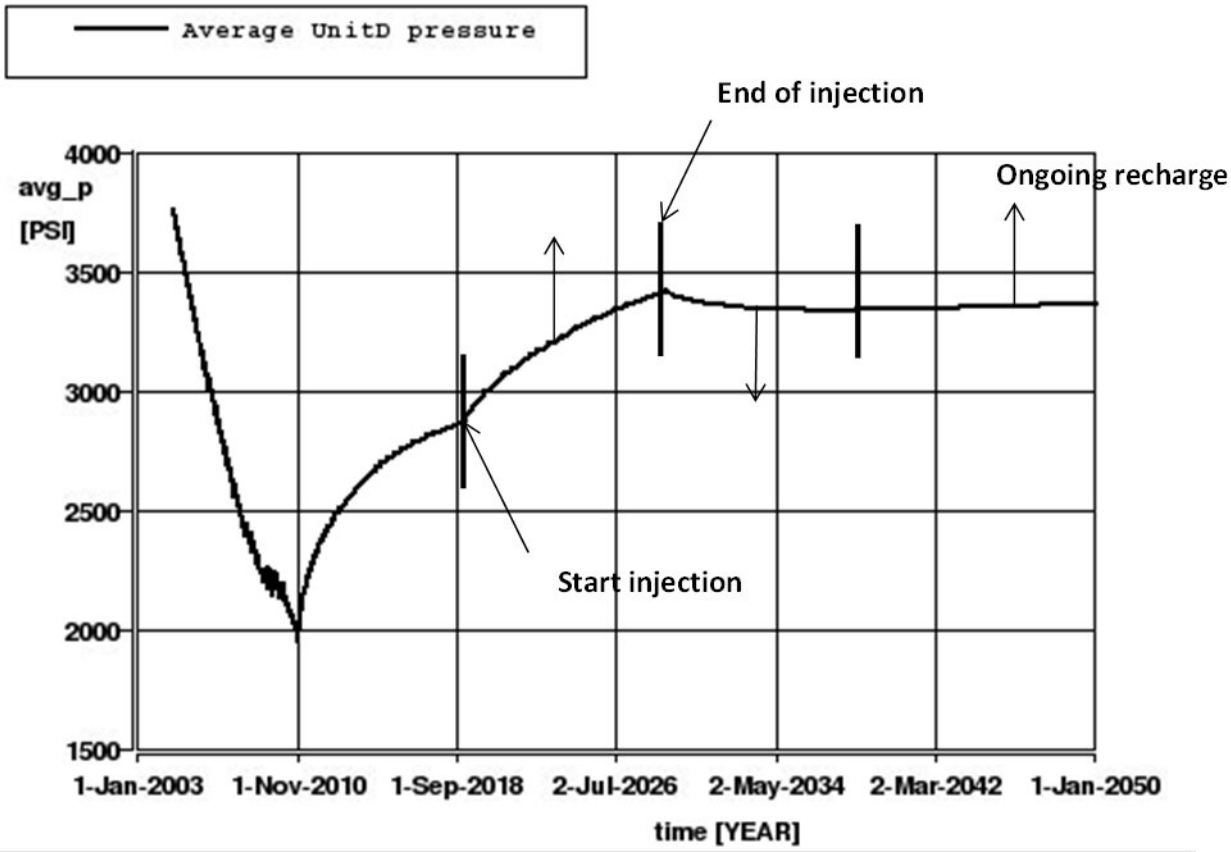

Figure 10-4: FFM 3.1 – recovery of average reservoir pressure (Unit D) after injection

When the same sensitivity was run in the other two models, the results were very similar. The basic plan of injecting 10 million tonnes of CO_2, in ten years, using two of the existing wells in Goldeneye, demonstrates no risk of egression when considering alternative geological realisations, meaning that even with a shallower west flank (SRM 3.05) or with a more southerly pinch-out (SRM 3.15) that could make easier for the CO_2 to egress, it still remains within the storage site (see Figure 10-5). As a result, the reference case is a robust CO_2 injection scenario.

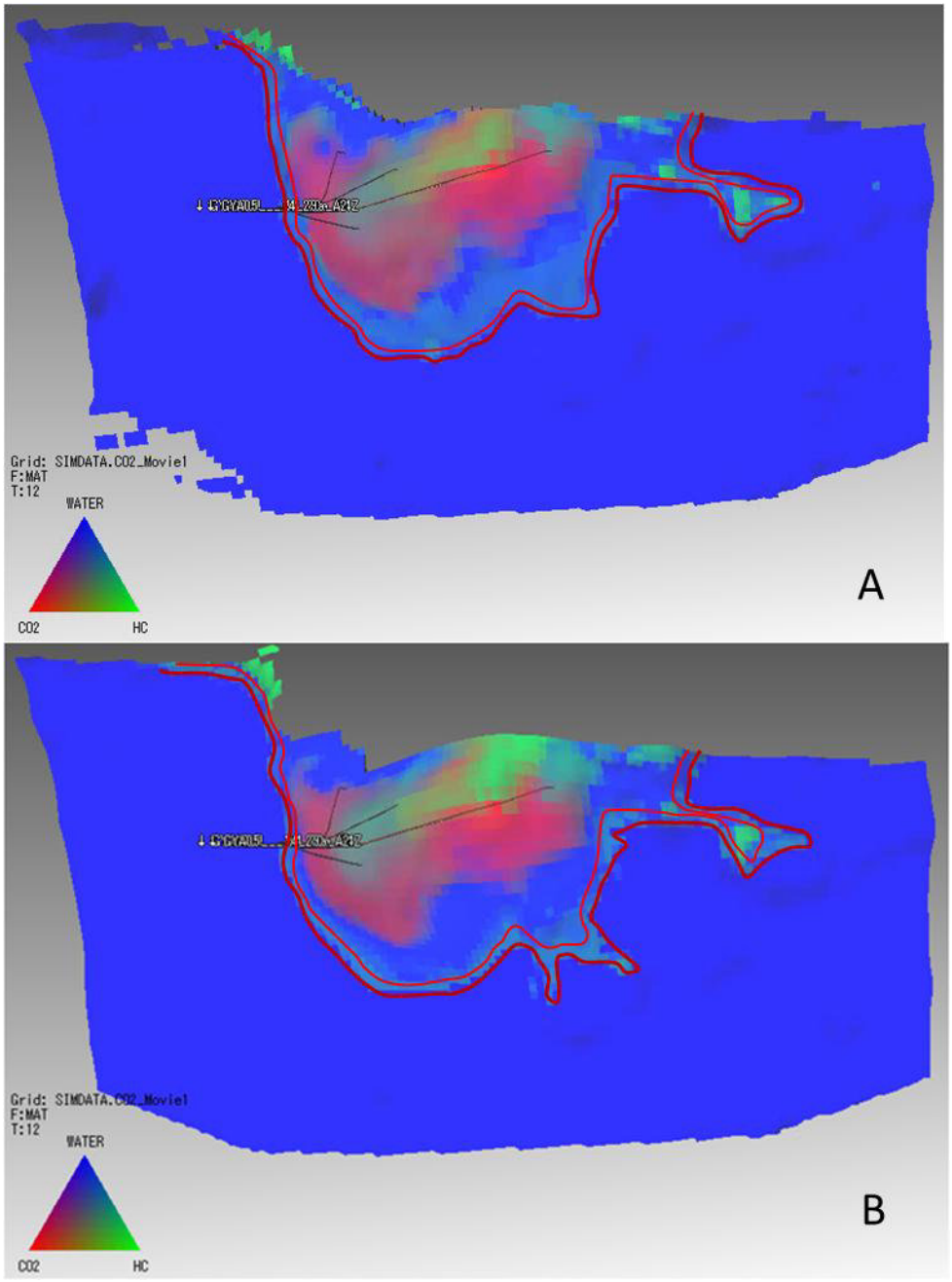

Figure 10-5. FFM 3.15, northern pinch-out sensitivity (A) and FFM 3.05, shallower flank (B) - Extent of CO_2 plume at top Captain D at end of injection (2029).

10.3.2. Base case injection pattern – 20 Mt of CO_2

There is a provision to extend CO_2 injection up to a total volume of 20 million tonnes.

The base case injection pattern (described above) was run in each of the geological models, targeting a 20 million tonne injection volume over 20 years. No egression from the store could be observed (Figure 10-6). For model FFM 3.1, the target was achieved with no backing out of either of the two injector wells and the model indicated a small proportion (1%) of the injected CO_2 moving outside

the original OWC at the end of injection. The CO_2 plume reaches the original contact in the west, and is roughly 400 m away from the contact in the east.

Figure 10-7 also shows how even though 1% of the CO_2 injected goes beyond the original oil/water contact into the virgin aquifer beneath the field, extending the plume only a few meters (one grid block) (reference case) outside the initial hydrocarbon area (due to the "Dietz" tonguing effect), it moves back after injection to be constrained within the original hydrocarbon region of the field.

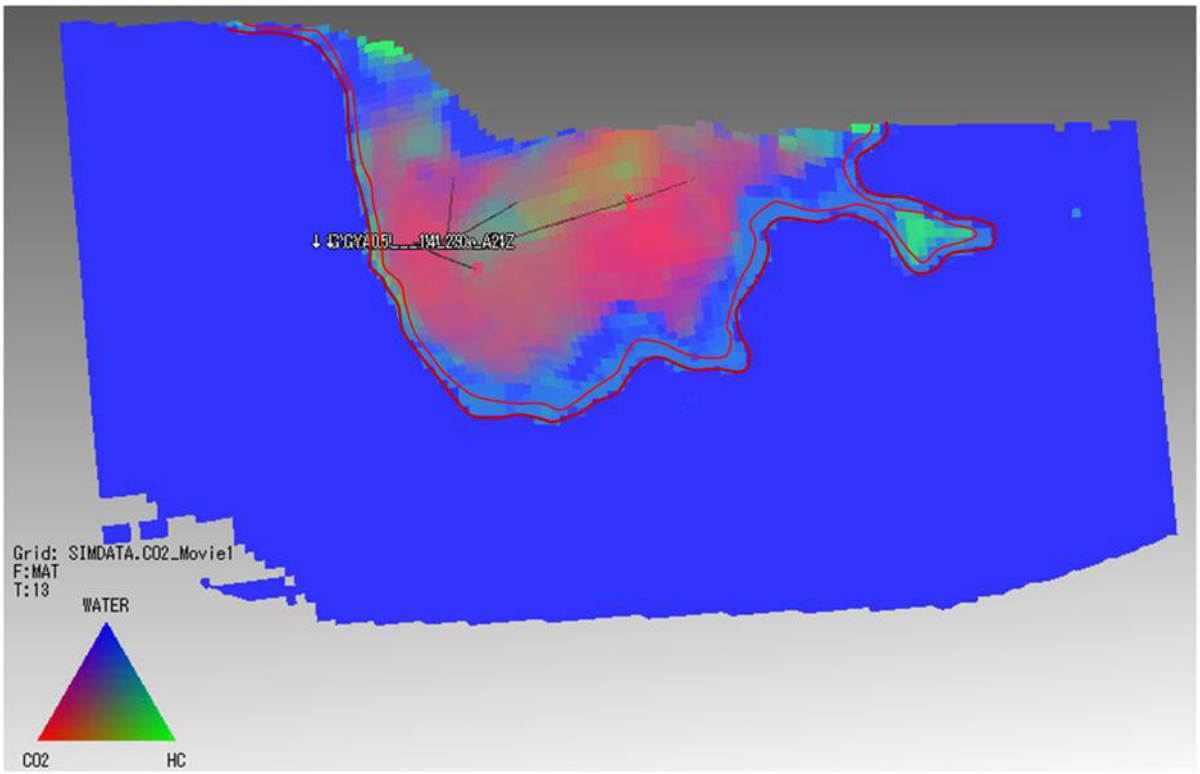

Figure 10-6: FFM 3.1 - Base case injection pattern - 20 Mt of CO_2

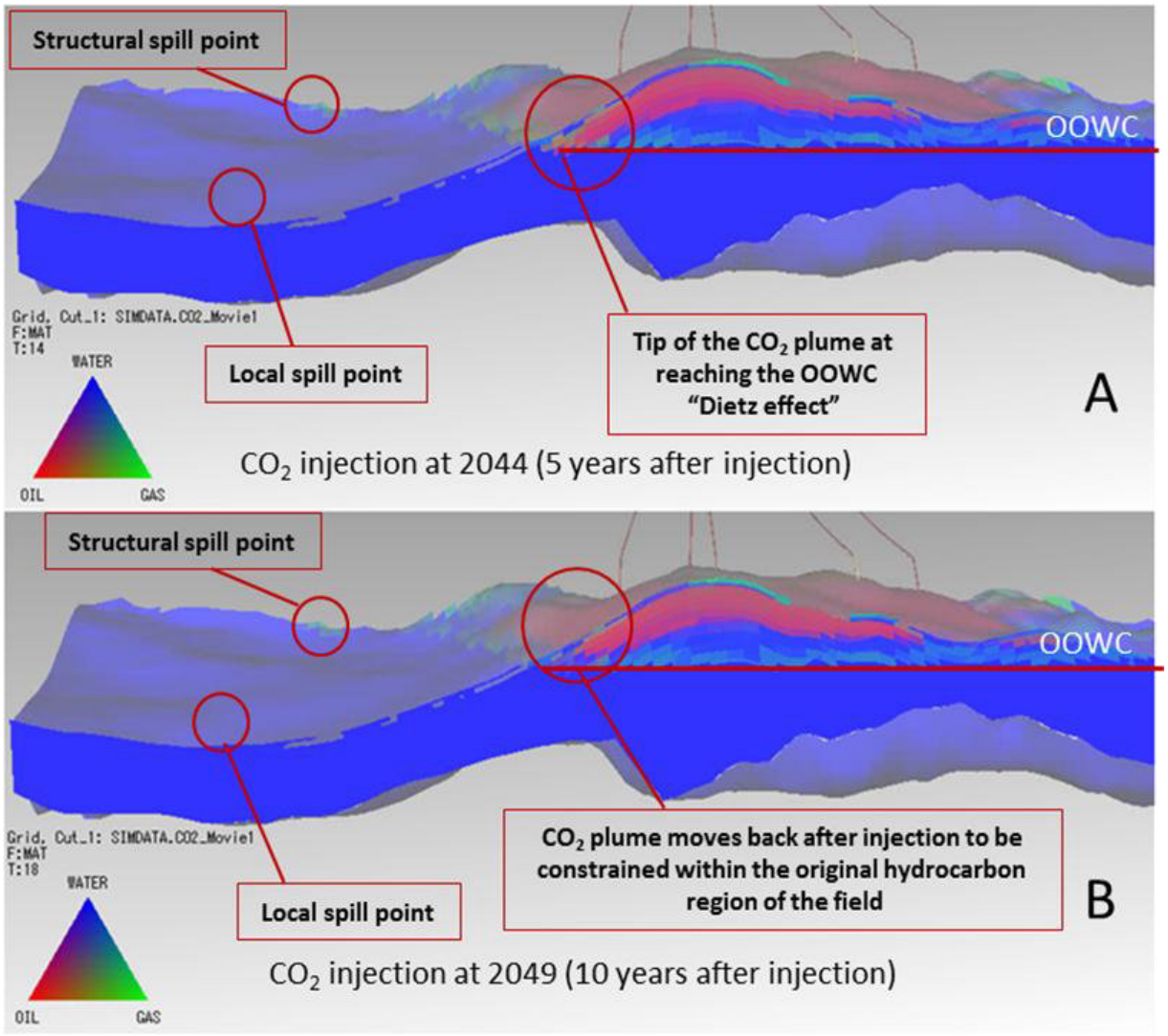

Figure 10-7: FFM 3.1: CO_2 plume, 5 (A) and 10 (B) years after end injection

In Goldeneye, even after injecting the second 10 Mt of CO_2 (Figure 10-7) the tip of the CO_2 plume still does not reach the structural spill point or move far enough downdip to reach a local spill point located under the saddle at the West, hence there is no egression or constraints to the storage capacity due to the Dietz tonguing effects. The Goldeneye structure is favourable to this process because the structural spill point is located far in the north-west corner of the field at the OOWC (consistent with regional models of up-dip gas migration from east to west), away from the injection wells. In a four-way dip structure that is filled to spill, egression of CO_2 would be much more likely at the time the CO_2 first goes below the OOWC as a result of a Dietz tongue, and so the Dietz factor would need to be retained in the storage capacity estimation.

10.3.3. Sensitivity to rate of injection

To investigate the dependency of the system to the (mass) rate of injection of CO_2, the base case injection pattern was run with the two injectors running at double the base rate (i.e. double 1.0 Mt/year/well). This will not be carried out in reality, as the contract requires 2 Mt/year of injection.

Again the extent of the CO_2 plume was checked, plus the average Unit D reservoir pressure, in particular at the point in time when this exceeded the initial pressure (if at all).

The average reservoir pressure, after start of injection, does not reach above initial for any of the three models. With the high rate scenario the models reach 3600psi midway through year 2016 for FFM31, midyear through 2027 for FFM 3.05 and 6 months later for FFM 3.15. The lateral extent of the CO_2 plume is also rate dependent. Figure 10-8 illustrates a snapshot of the CO_2 plume at the point in time when 20 million tonnes had been injected, either at the base case rate or the double rate. This occurs in year 2039 in the base case, and in year 2029 for the high rate case. It can be seen that the Dietz tongue extends a further 200m to the west in the high rate case, illustrating the rate dependence of the CO_2 tongue.

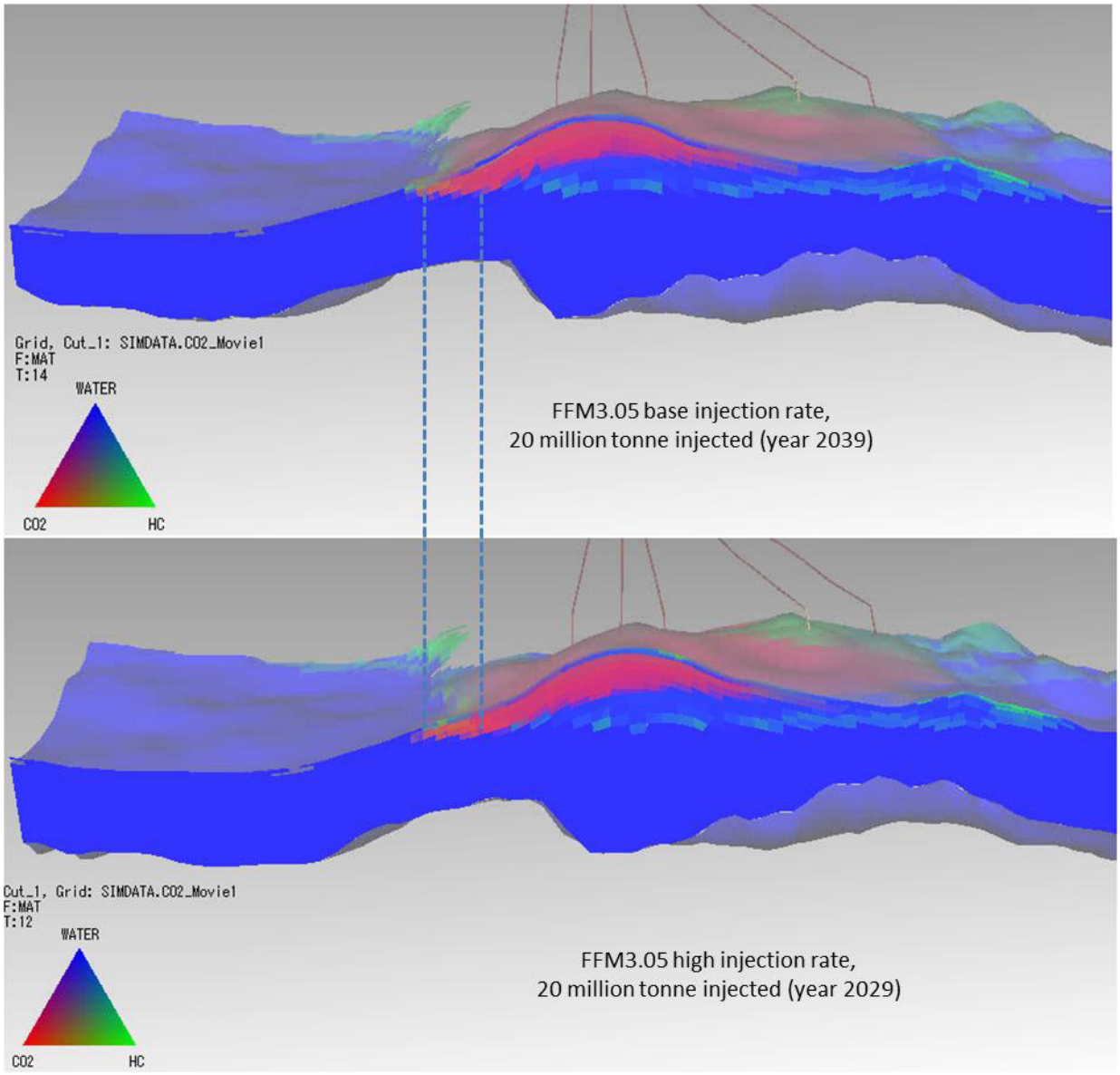

Figure 10-8: FFM 3.05 – Cross section illustrating the Dietz effect.

A higher risk of an egression arises if the total CO_2 is injected at high rate (double the base case rate) for a full 10 years, in the flattest geological realisation (FFM 3.05). However, as shown in Figure 10-8, even in this scenario, the tip of the plume does not reach the structural spill point or a local spill point located under the saddle at the West, hence there is no egression.

10.3.4. Maximum storage capacity

To determine a result for the maximum quantity of CO_2 which can be injected without egression from the store, the base case injection scenario was continued past 2029 until the CO_2 plume reached a point from which it could spill out of the store. It was seen that for all geological models, the mass of CO_2, which had to be injected to reach this situation, was significantly higher than 10 Mtor with the provisional expansion up to 20 Mt..

The maximum storage capacity was estimated by injecting at a total rate of 1Mt CO_2 /year (at this rate, the target of 10 Mt CO_2 can be injected in 10 years). Injection is stopped when the tip of the CO_2 plume nears the structural spill point. The wells are then shut in and the system allowed to relax until year 2115. To get an estimate for the maximum storage capacity, which can be made available by appropriate use of the available injection wells, different injection patterns were tested out.

a) Base Case: Injecting into one western injector GYA05 and one eastern injector GYA02S.
b) Maximum storage injection was done in only wells GYA02S1 and GYA04 – the furthest downdip wells. This is the situation where, the CO_2 plume will be as far away from the structural spill point as possible for each geological model.
c) Minimum Storage: - Inject into only one well on western flank GYA01 – this is the situation where the risk of egress over the western flank is the highest

For the reference case model (FFM 3.1) Figure 10-9 illustrates the extent of the CO_2 plume (at top Unit D) when the maximum storage capacity is reached for the one well only injection scenario. With the well pattern and rates described above, this occurs in year 2050 in this case.

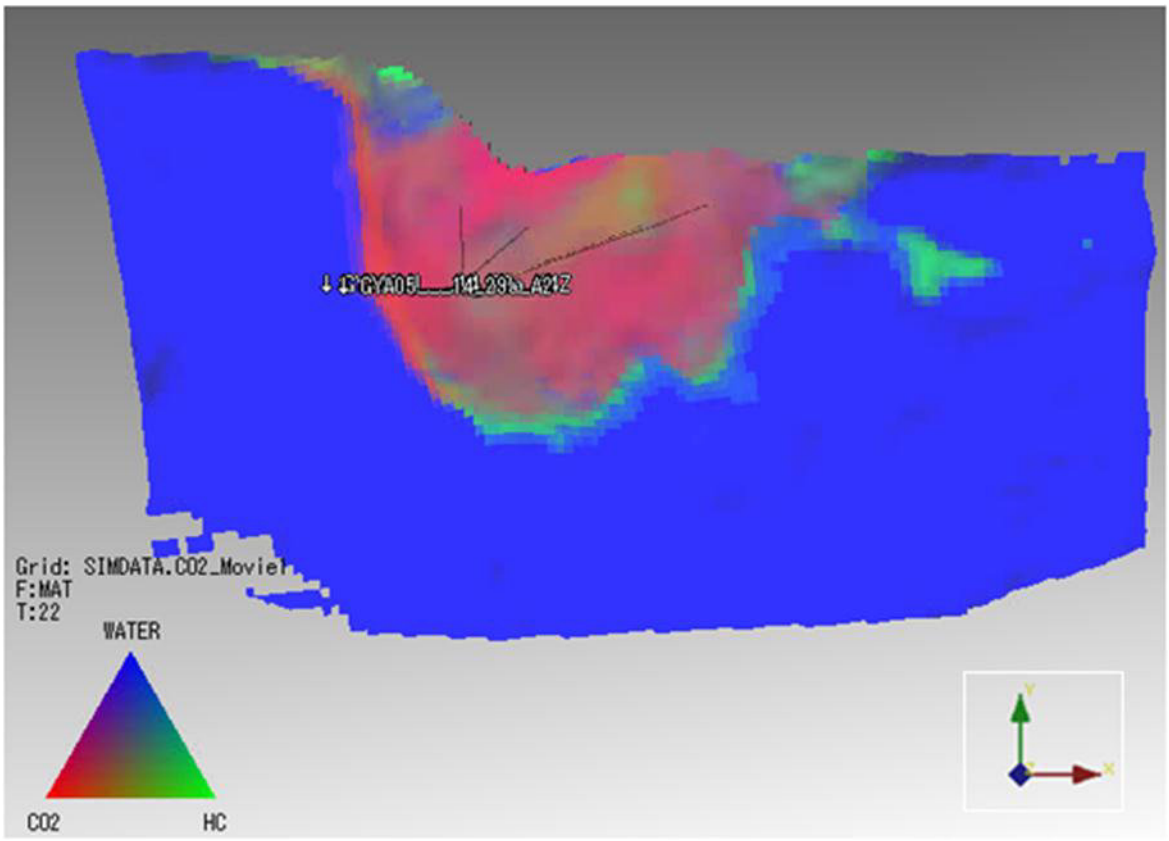

Figure 10-9: FFM 3.1 (reference case): CO_2 plume at top D, when maximum storage capacity is reached for injection in GYA01 - Year 2050.

Figure 10-10 shows the extent of the plume (at Top D) when the system has relaxed for five years after reaching the estimated maximum storage capacity for the case injecting into GYA01. The CO_2 is moving back into the original gas cap.

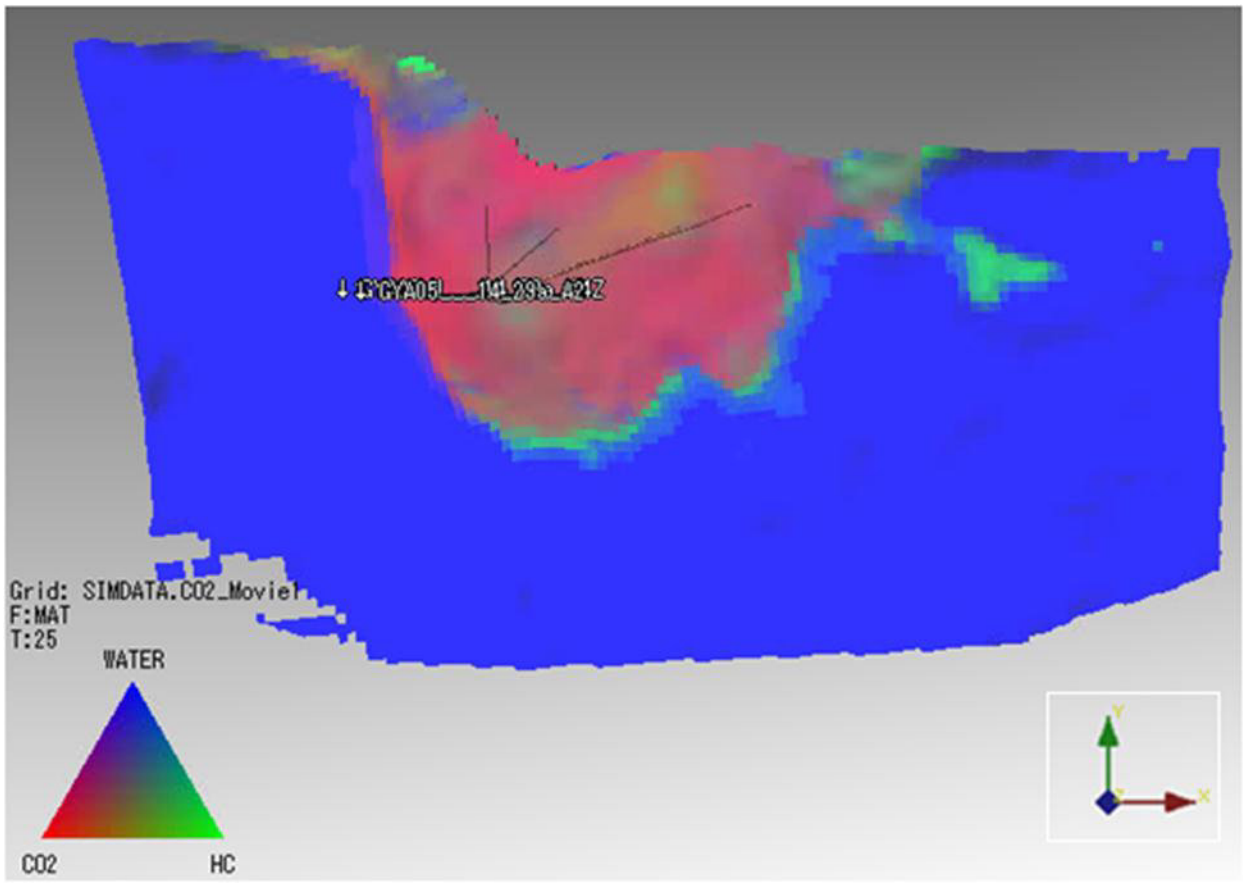

Figure 10-10: FFM 3.1, CO_2 plume extent five years after ceasing injection in GYA01 when maximum storage capacity was reached - Year 2055

The same effects may be seen in the other geological models FFM3.05 and 3.15. For the case of FFM 3.15, Figure 10-11 shows how the CO_2 redistributes over time between the original water leg and original hydrocarbon gas leg. In this case, which uses GYA01 as injector well, 30 Mt are still resident in the original gas zone after 100 years, and 3 Mt in the original water zone.

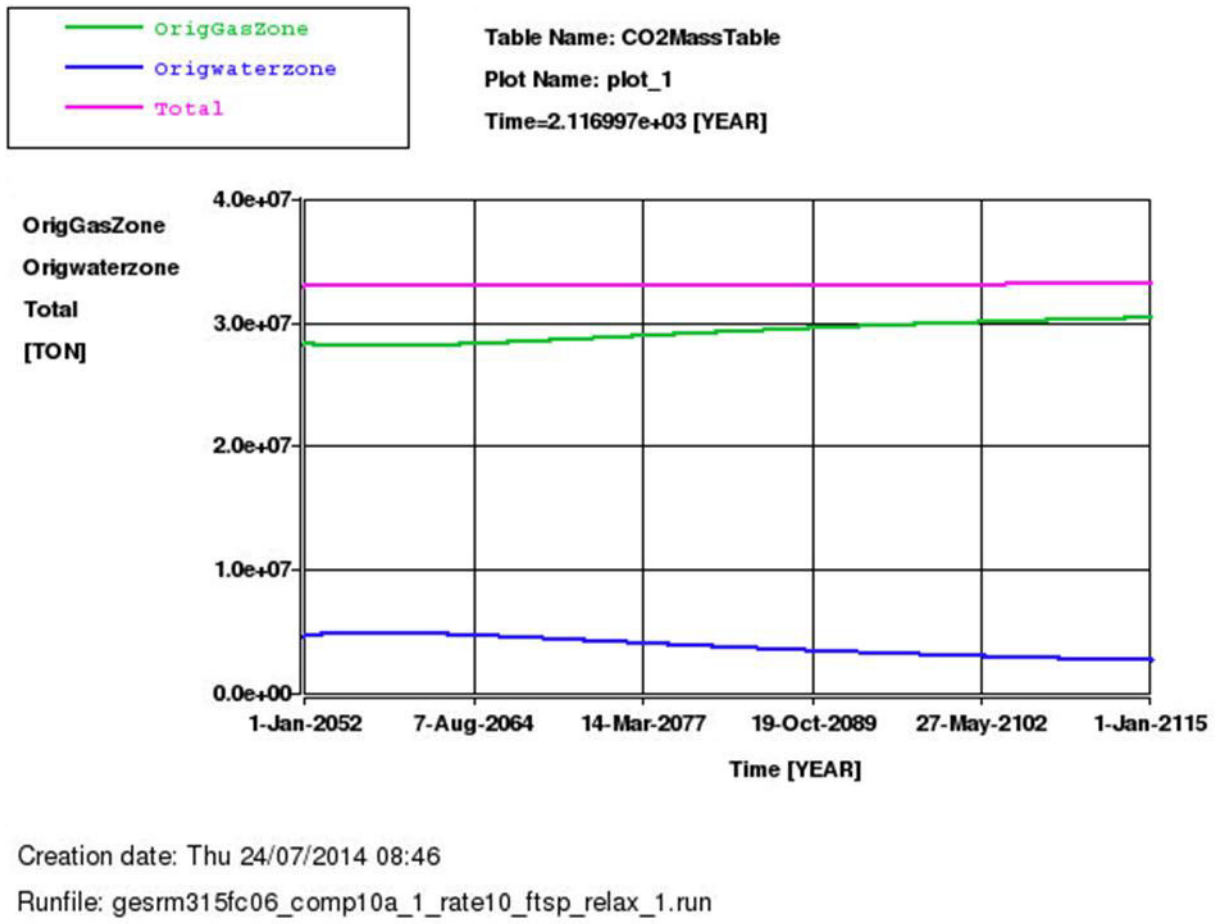

Figure 10-11: FFM 3.15 - redistribution of CO_2 with time after cessation of injection assuming injection in western flank well GYA01.

The maximum injected tonnage which does not give rise to egression from the primary store is recorded in Table 10-5 for the geological scenario FFM3.1.

In each case, the total CO_2 stored is listed, together with the mass of injected CO_2 which is resident in the original water zone at 1.1.2115 (i.e. excluding the CO_2 present in the reservoir before injection). The lowest estimated storage capacity here occurs when injecting into GYA01 closest to the spill point on the western flank.

The three injection patterns were repeated for each geological model. The variance relative to FFM 3.1 is summarised in Table 10-5. The lowest estimated storage capacity here occurs for FFM 3.05. This model was constructed with a shallower slope on the western flank, and it was expected that it would be easier for CO_2 to leave the geological storage (section 5.1). The highest estimated storage capacity occurs for the FFM3.15. This model was constructed with a deeper spill point on the western flank and hence it was expected that it would be more difficult for CO_2 to leave the geological store.

Based on above considerations there is a substantial storage margin – it is possible to inject between 19 Mt and 30 Mt CO_2 over that required for the mandated part of the Peterhead CCS project and between 9 Mt and 20 Mt over the requirement for the additional volume of 10 Mt of CO_2.

Table 10-5: Estimate of maximum storage capacity for FFM3.1 and variances for FFM3.05 (-) and FFM 3.15(+).

Injection Scenario	Maximum CO_2 injected to reach spill (Mt) - in original gas and water zones.	Injected CO_2 resident in original water zone after relaxing to 1.1.2115 (Mt)
GYA01	31 (+/-2)	2 (+/-1)
GYA02S & GYA05	33 (+/-2)	4 (+/-1)
GYA02S & GYA04	38 (+/-2)	7 (+/-1)

10.3.5. Well injection pattern

This is a test of the sensitivity of the system to the exact selection of the wells used for injection. In one case, all the CO_2 is injected equally into wells GYA01 and GYA05, to the west of the field. In another, the same condition was run with wells GYA04 and GYA02S1 – to the east. A series of further sensitivities pushed this idea to the extreme by injecting all the CO_2 in one well only (each of the five wells was tested in this way).

10.3.5.1. Injecting into GYA01 and GYA05

In none of the runs with this injection pattern did the CO_2 plume reach the spill point. The extent of plume for the models considered are shown in Figure 9-13 to 9-15 for the 10 Mt and 20 Mt CO_2 injection scenarios. The plume shape shows little variance between different models and therefore the injection pattern is robust w.r.t the structural uncertainty.

Table 10-6. Injection in wells GY01 and GYA05 only

Geological model	CO_2 injected using GYA01 and GYA05 only (Mt)	CO_2 outside original OWC at end of injection (Mt) (% total injected)
FFM 3.1	10	0 (0%)
FFM 3.05	10	0 (0%)
FFM 3.15	10	0 (0%)
FFM 3.1	20	1 (3%)
FFM 3.05	20	1 (3%)
FFM 3.15	20	1 (4%)

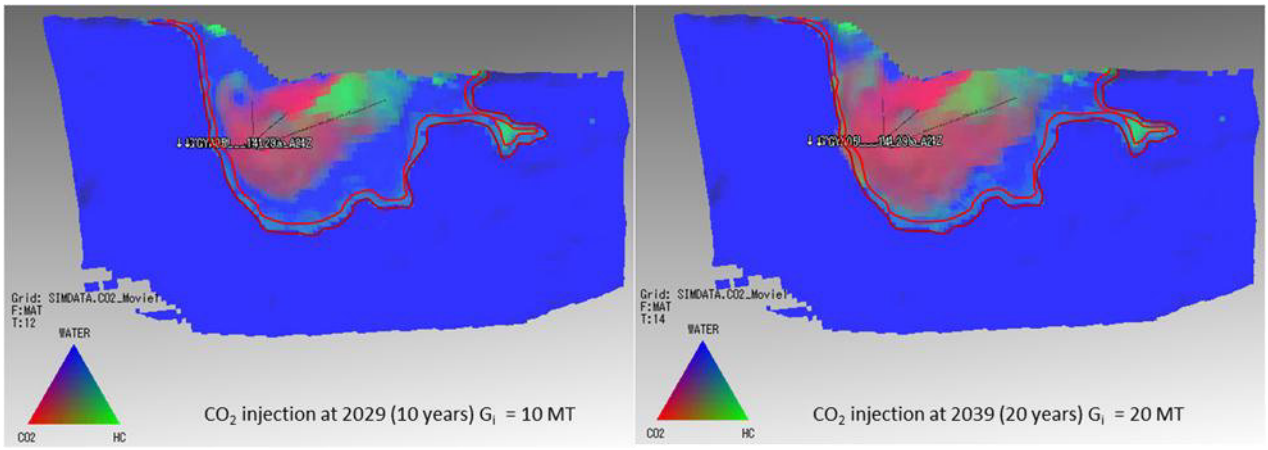

Figure 10-12: FFM3.1, injecting in GYA01 and GYA05 only

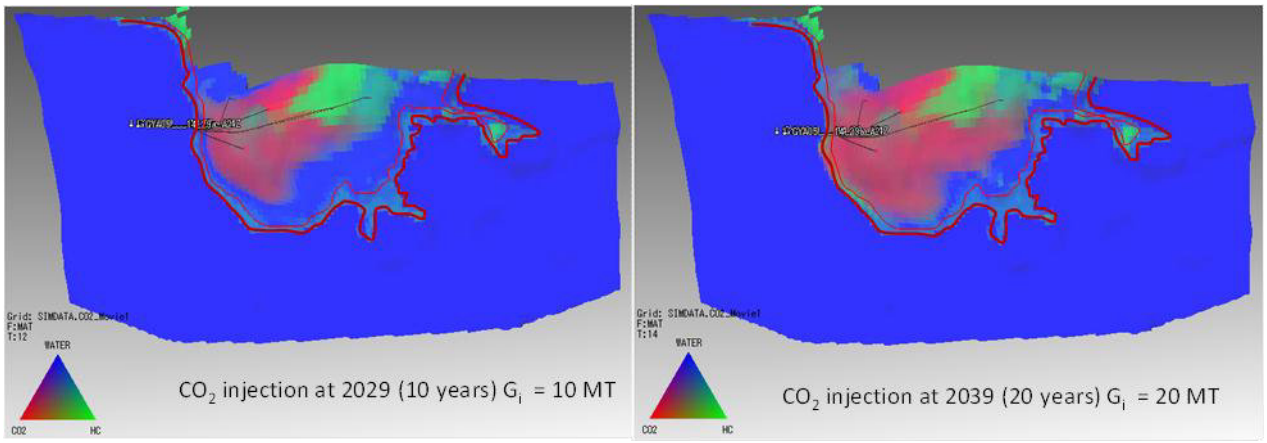

Figure 10-13: FFM305, injecting in GY01 only and GYA05 only

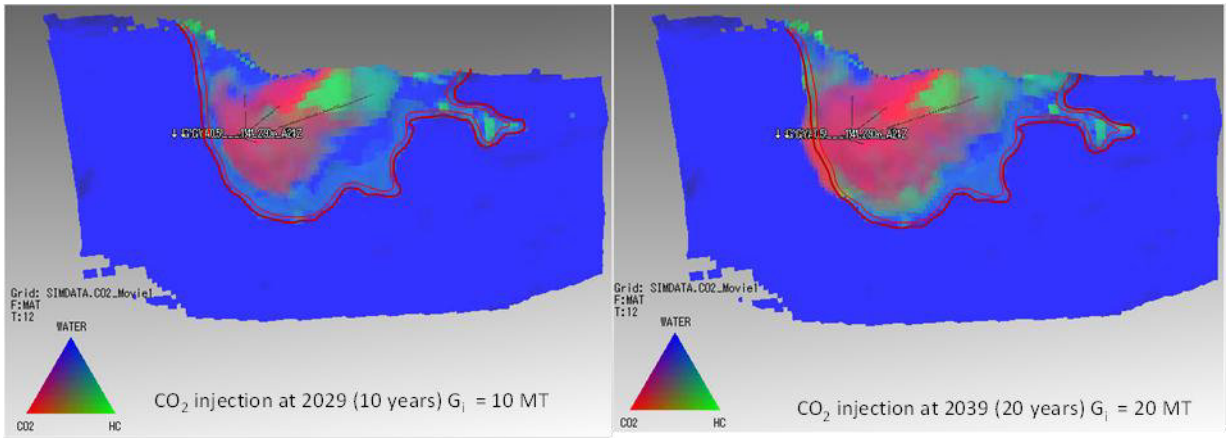

Figure 10-14: FFM 315, (northern pinch-out sensitivity), injecting in GYA01 and GYA05 only

10.3.5.2. Injecting into GYA02S1 and GYA04

All cases studied were able to achieve the target of 20 million tonnes CO_2 with good containment. The results for mass stored are shown in Table 10-7. There were few differences in the key results for each case.

The more favourable results for containment (compared with the reference case or injection in wells GYA01 and GYA05) are largely due to the location of these two wells, being more centrally located

and higher in the structure. They are less dependent on the nature of the western flank or northern pinch-out (both key geological uncertainties). However, using wells GYA02S1 and GYA04 does cause greater degree of egression at the eastern flank. If the total injection is spread more evenly over the structure, there is less impact on the east. The example of FFM 3.15 is shown in Figure 10-19.

Table 10-7. Injection in wells GY02S1 and GYA04 only

Geological model	CO_2 injected using GYA02S1 and GYA04 only (Mt)	CO_2 outside original OWC at end of injection (Mt) (% total injected)
FFM 3.1	10	0 (0%)
FFM 3.05	10	0 (0%)
FFM 3.15	10	0 (0%)
FFM 3.1	20	0 (0%)
FFM 3.05	20	0 (1%)
FFM 3.15	20	0 (1%)

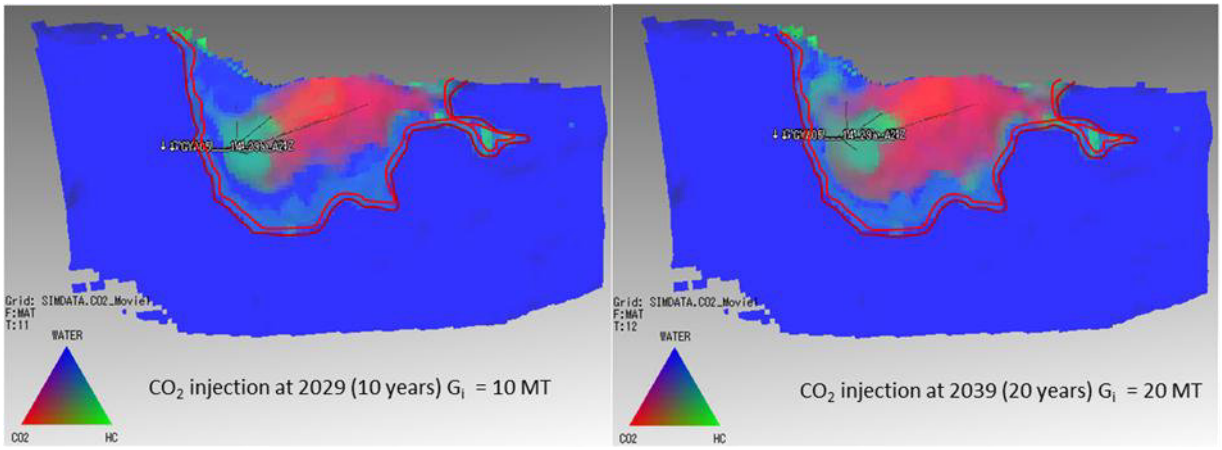

Figure 10-15. FFM 3.15 - injecting equally in wells GYA02S1 and GYA04 only. CO_2 plume after 10 years and 20 years injection (top Unit D),

10.3.5.3. Injecting into one well only

As an extreme case, simulations were run attempting to inject 20 million tonnes CO_2 into one well only. In general, it was not possible to meet the target completely with only one well. However, this situation is unlikely to be attempted in reality.

For example – injecting in well GYA01 only – a crestal well. The results for mass stored are shown in Table 10-8.

Table 10-8. Injection with one well only (GYA01)

Geological model	CO_2 injected using GYA03 and GYA05 only (Mt)	CO_2 outside original OWC at end of injection (Mt) (% total injected)
FFM 3.1	10	0 (0%)
FFM 3.05	10	0 (0%)
FFM 3.15	10	0 (0%)
FFM 3.1	20	0 (0%)
FFM 3.05	20	0 (1%)
FFM 3.15	20	0 (1%)

Even when the sequestration target of 20Mt is achieved, the test of injecting the highest volume into a single well still does not result in egression from the container. (Figure 10-16)

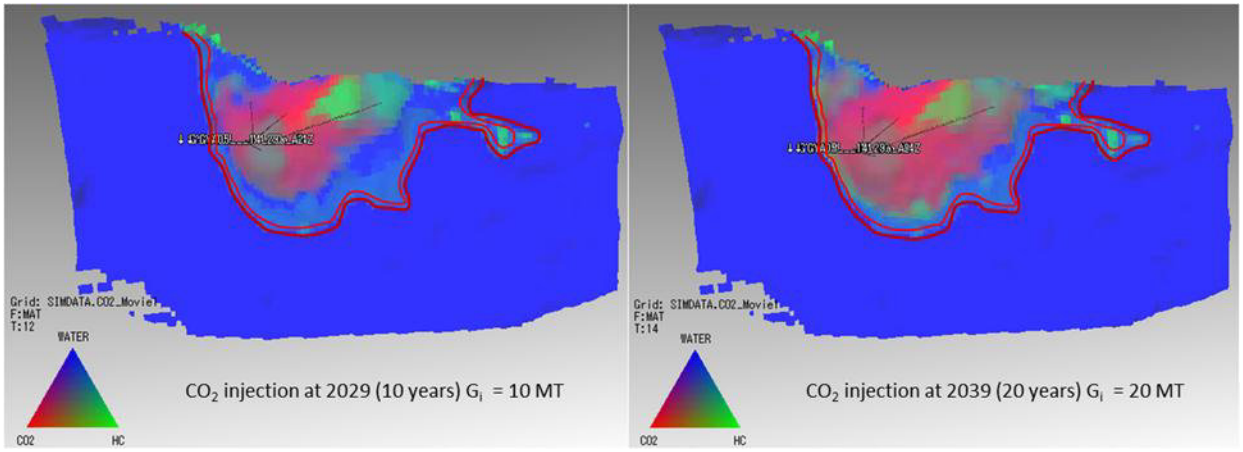

Figure 10-16: FFM 3.15 (northern pinch-out sensitivity) – injection in well GYA01 only. CO_2 plume after 10 years and 20 years injection (top Unit D)

10.4. Well completions

The injection tables which had been used for the study up to this point were designed for generic 4½ inch completions. Once information on the proposed well re-completions becomes available, well injection capacities will be tailored to plant capacities.

10.5. Implications of delayed start-up of injection

Some alternative injection scenarios were run to look at the impact on pre-injection and post-injection reservoir pressure if the start of CO_2 capture is delayed for some reason. Geological realisation FFM 3.1 (reference case) was used, with the base case injection pattern (ref. Section 9.3). Figure 10-17illustrate the differences between reservoir pressure in Unit D, immediately before the delayed start of injection and immediately after end of injection (having injected 10 Mt CO_2 in 10 years) compared to the equivalent pressures in the reference case (starting injection in January 2019).

In all cases, the Unit D pressure drops after cessation of injection (as illustrated in Figure 10-4). Delay to the planned date of injection start-up does not significantly alter the project. As recompletion of the existing wells, and conversion to injectors, will take place within a year of start-up, it will be possible to tune the completions to the observed pressure.

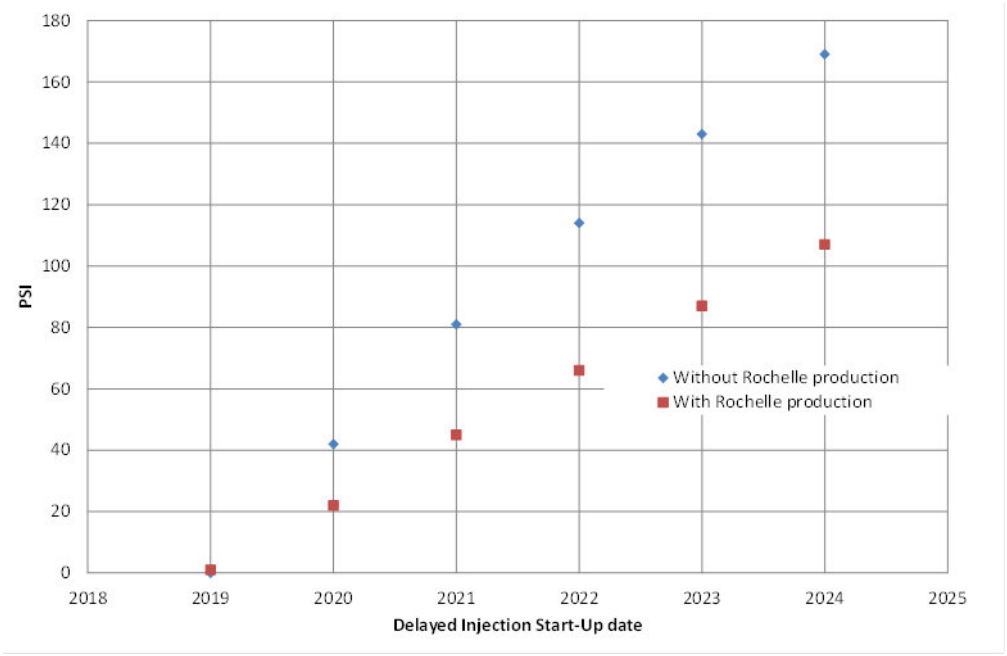

Figure 10-17. Difference in pre-injection pressure for delayed start dates.

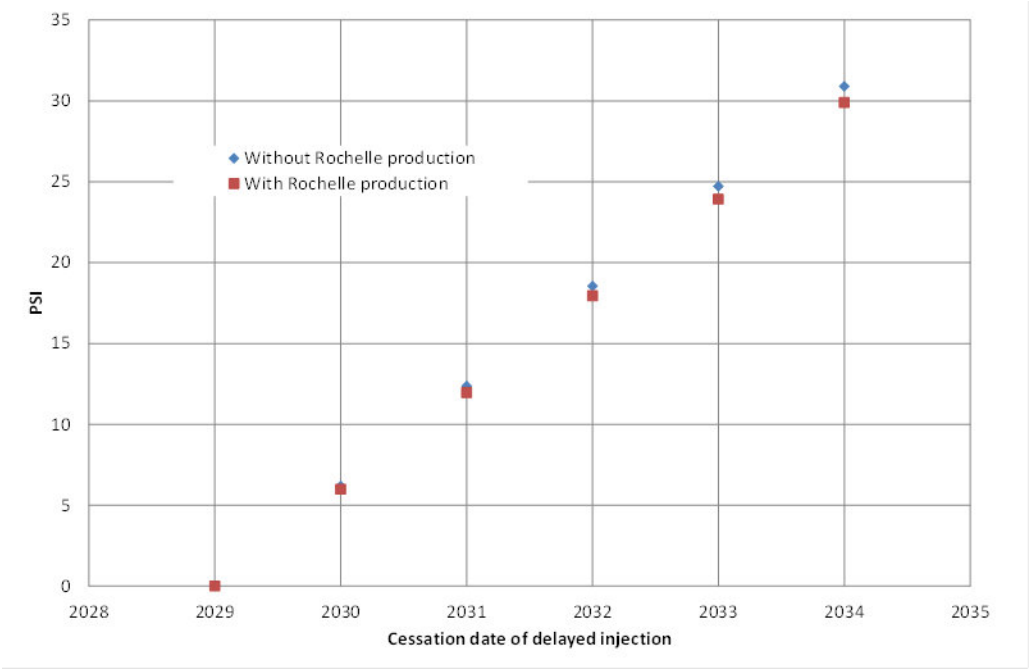

Figure 10-18. Difference in post-injection pressure for delayed injection.

10.6. CO_2 Dissolution

Most of this work was carried out during the 2011 Longannet to Goldeneye CCS project, and consequently many sensitivities are based on a target of 20 Mt CO_2 being injected into the Goldeneye store at a rate of 2 Mt p.a.

Most of the sensitivities do not include CO_2 dissolution in water. This effect will increase the storage capacity of the reservoir and trap more of the CO_2 over time after injection ceases. As well as trapping CO_2 in solution, dissolution also results in an increase in the water density which can introduce buoyancy driven convection currents, although this is only significant over time periods longer than the 10 year injection period. MoReS includes a CO_2 dissolution option and this has been used to investigate the effect of dissolution by re-running the injection Base Case with CO_2 dissolution switched on.

Figure 10-19 illustrates an example from a 20 Mt run, showing the CO_2 distribution after 20 Mt CO_2 was injected in a period of 10 years, with CO_2 dissolution active. CO_2 is shown in red. Green represents remaining gas or condensate hydrocarbon. Comparison with Figure 10-1 shows that there is very little difference in the extent of the CO_2 plume.

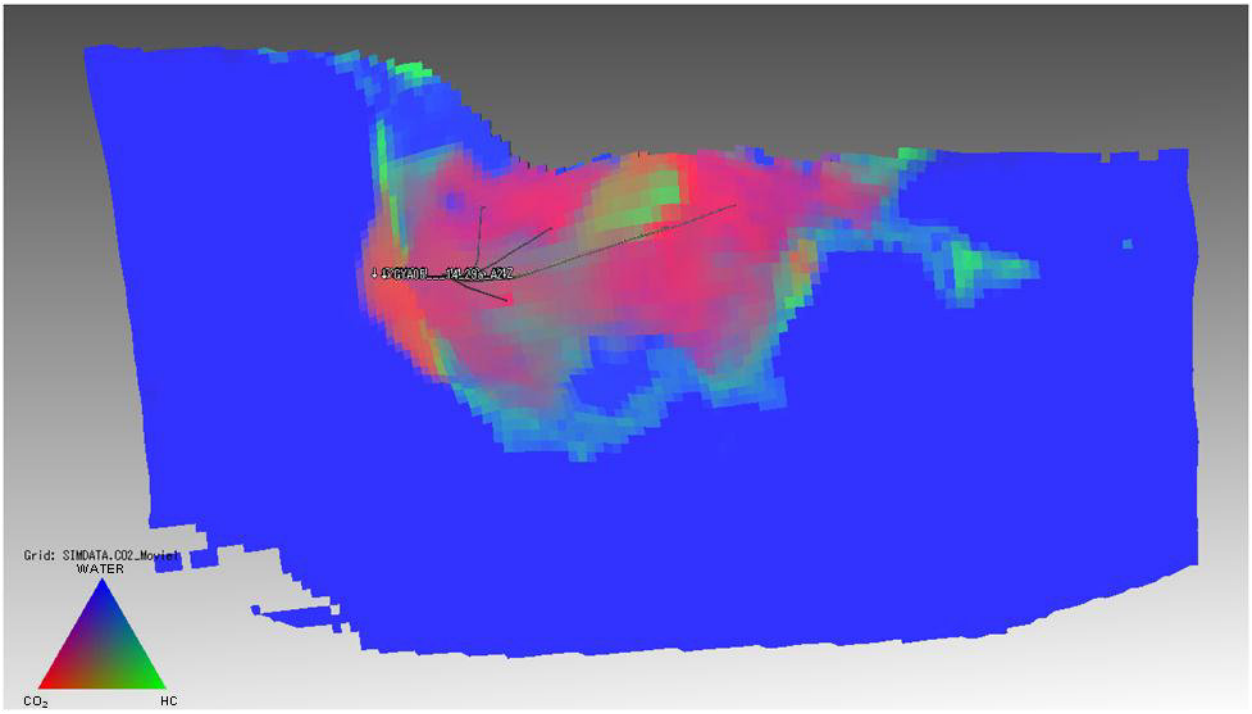

Figure 10-19. FFM 3.1: Extent of CO_2 plume at top Captain D at end of injection with dissolution (20 Mt CO_2 injected)

Figure 10-20 illustrates, for the same 20 Mt run, the mass of CO_2 dissolved in water in both the gas zone and the water zone outside the gas plume. After 10 years injection, 0.1 Mt CO_2 has dissolved in water outside the gas plume while 0.9 Mt of CO_2 has dissolved in water in the gas plume. A total of ~1 Mt of CO_2 is dissolved in water (approximately 5% of the injected volume).

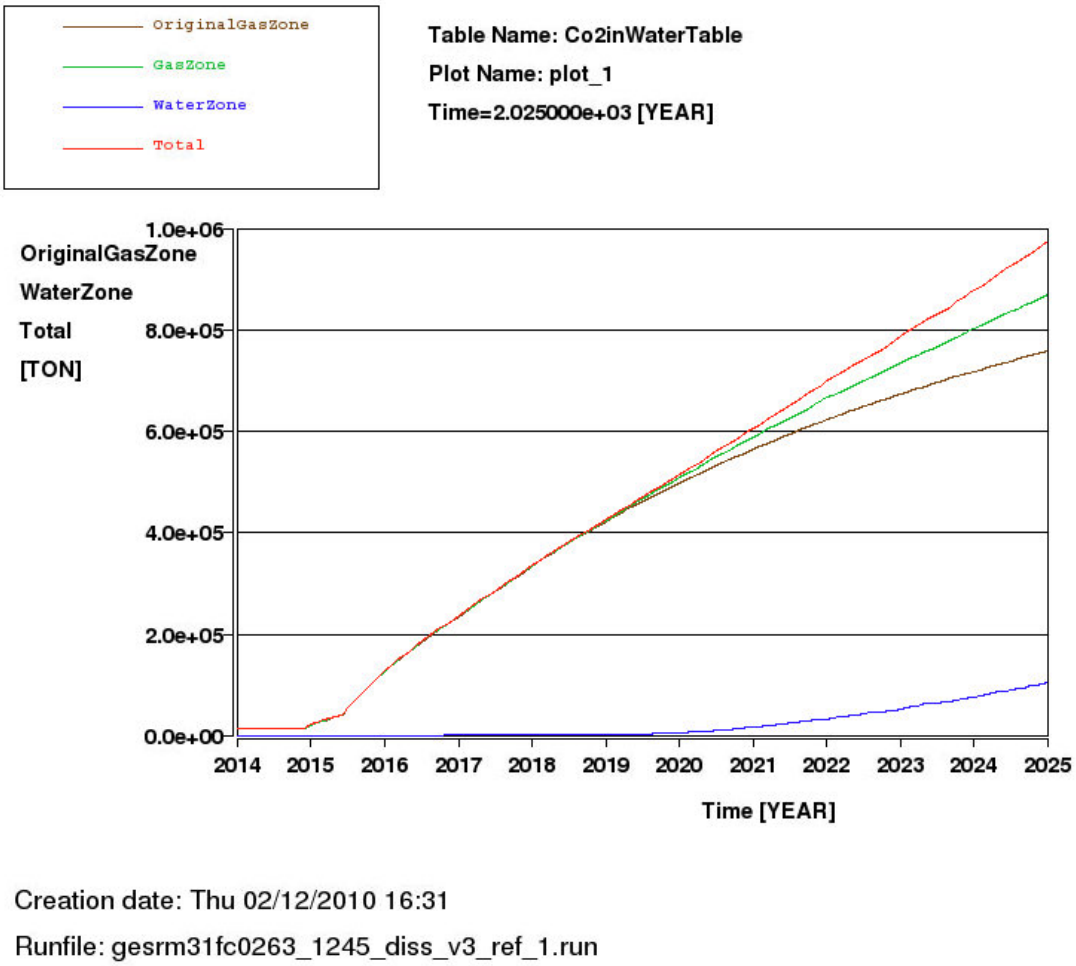

Figure 10-20. FFM 3.1: Mass of CO_2 dissolved in water during 10 year injection period (20 Mt case).

In Figure 10-20 the Gas Zone is the part of the reservoir where the original S_g>0.01[41] and the Water Zone is where S_w>0.99[42].

Figure 10-21 shows the change in the mass of CO_2 dissolved in water when the reservoir is left to equilibrate for 1000 years after injection. The total volume dissolved in water gradually increases to 1.9 Mt over the period, nearly double the initial amount of CO_2 dissolved in water. Nearly all of the extra dissolution takes place in the Water Zone as the water in the gas plume is already saturated.

[41] Gas saturation

[42] Water saturation

The volume of CO_2 dissolved in water is overestimated in the simulation mainly due to the fact that all the CO_2 in a block is assumed to be in contact with the water and the CO_2 saturation of the water immediately increases to the maximum amount allowed by the mass of CO_2. In reality, the CO_2 will not be in immediate contact with the water. The solubility is higher than that calculated using the correlation of Chang, Coats and Nolen (27) [Spreadsheet calculations using this correlation suggest that only 2.2% of the CO_2 will initially dissolve in water]. More detailed modelling of CO_2 dissolution and mineralisation are reported in the Geochemical Reactivity Report (2).

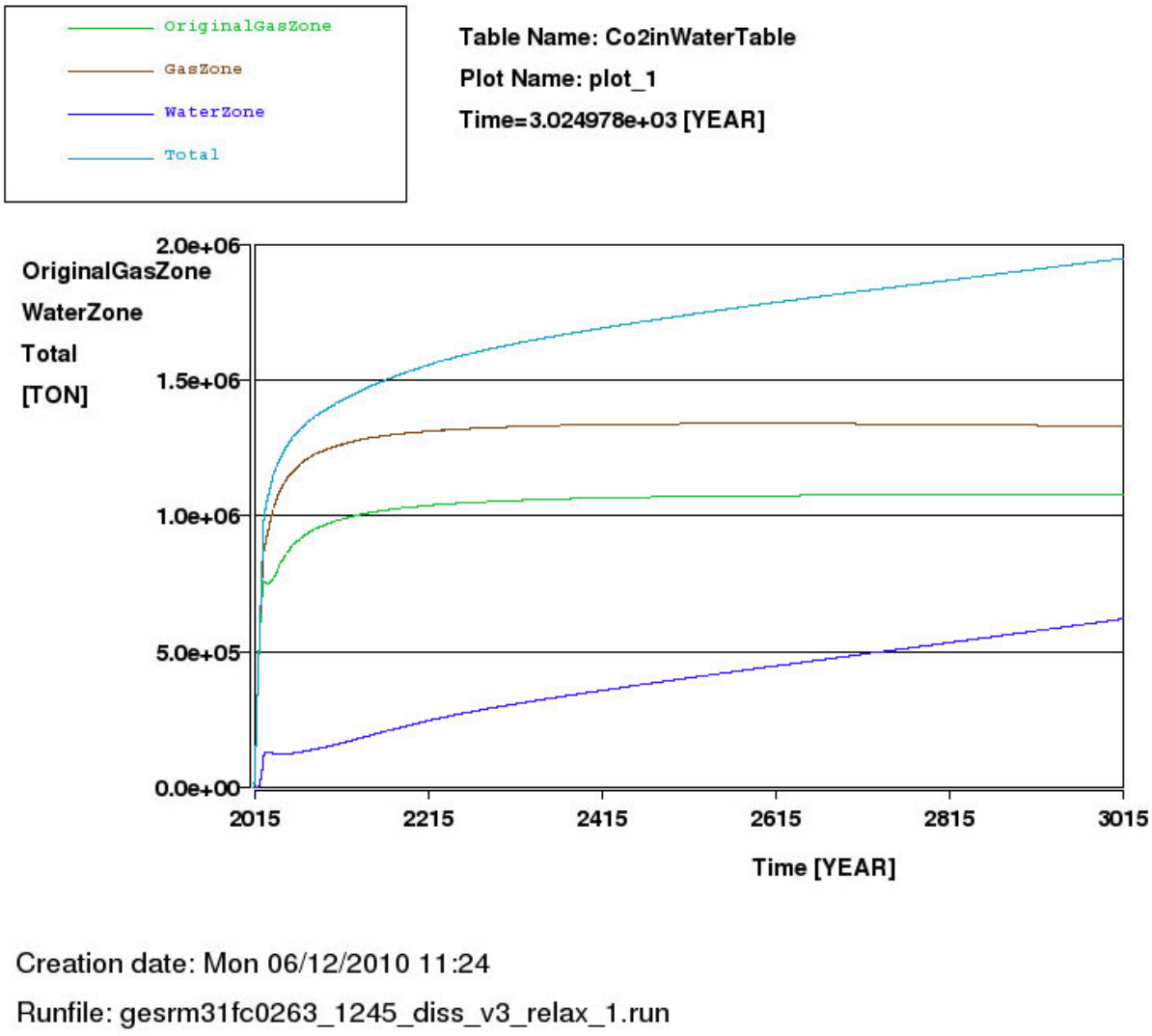

Figure 10-21. FFM 3.1: mass of CO_2 dissolved in water during 1000 years, after 20 Mt CO_2 injected..

In Figure 10-21, the Gas Zone is the part of the reservoir where the original S_g>0.01 and the Water Zone is where S_w>0.99.

10.7. Reservoir Compartmentalization

Over the years of hydrocarbon depletion the Goldeneye reservoir has exhibited a tank behaviour, with all the wells reacting together to any perturbation in the field. Nevertheless, Pressure Transient Analysis (PTA) has shown some limited effects in the derivative that to some extent could be

correlated with some of the seismically interpreted faults in the field. Historically, faults have been modelled as fully transmissible features in order to achieve a history match, so faults are present in the model but don't prevent fluid flow through them. The highly favourable mobility ratio of water displacing gas during the production period could have masked any tortuous path the gas could have taken while reaching the producers. The reverse process of gas displacing water has a highly unfavourable mobility ratio; therefore these seismically interpreted faults could play a different role in the CO_2 migration path, causing a distortion in the CO_2 footprint within the field. This possibility is outlined and explored in this section.

10.7.1. Pressure Transient Analysis

Exploration well 14/29-a3 tested gas/condensate from the interval 9,730 - 9,760 ft along hole below drill floor (AHBDF) in the Kopervik 1 reservoir (now called the Captain sands) and is the discovery well of the Goldeneye field. Initial PTA suggested that a period of declining pressure during the build-up could be interpreted as the presence of flow barriers. Further studies conclude that in view of the large deviation and the uncertain definition of the geometry no firm link could be made between the analysis and the seismic map. One possibility could be a wedge with the east-west running faults just north of the well forming one (semi-)sealing flow barrier and with the north-south running fault some 2200 ft to the west forming the other flow barrier.

Similarly, Well 20/4B-6 was drilled early in 1998 some 4000 ft south of the discovery well 14/29-a3. The GWC at top reservoir is 1500 ft further to the south. The map shows possible faults at 2900 ft to the north/east and at 3200 ft to the south/west. Studies concluded that the fact that the boundary effects in the late build-up cannot be matched with a constant pressure boundary opposite the GOC in the south suggests that there could be a short (4000 ft long) sealing barrier to the north. The constant pressure boundary is then a combination of the end of this barrier and the increase in gas column at that end. The sealing barrier opposite this constant pressure boundary is possibly the fault to the west of the well, which intersects with the short fault to the north.

10.7.2. Fault interpretation

One of the seismic fault patterns interpreted for the field is shown in the following figure.

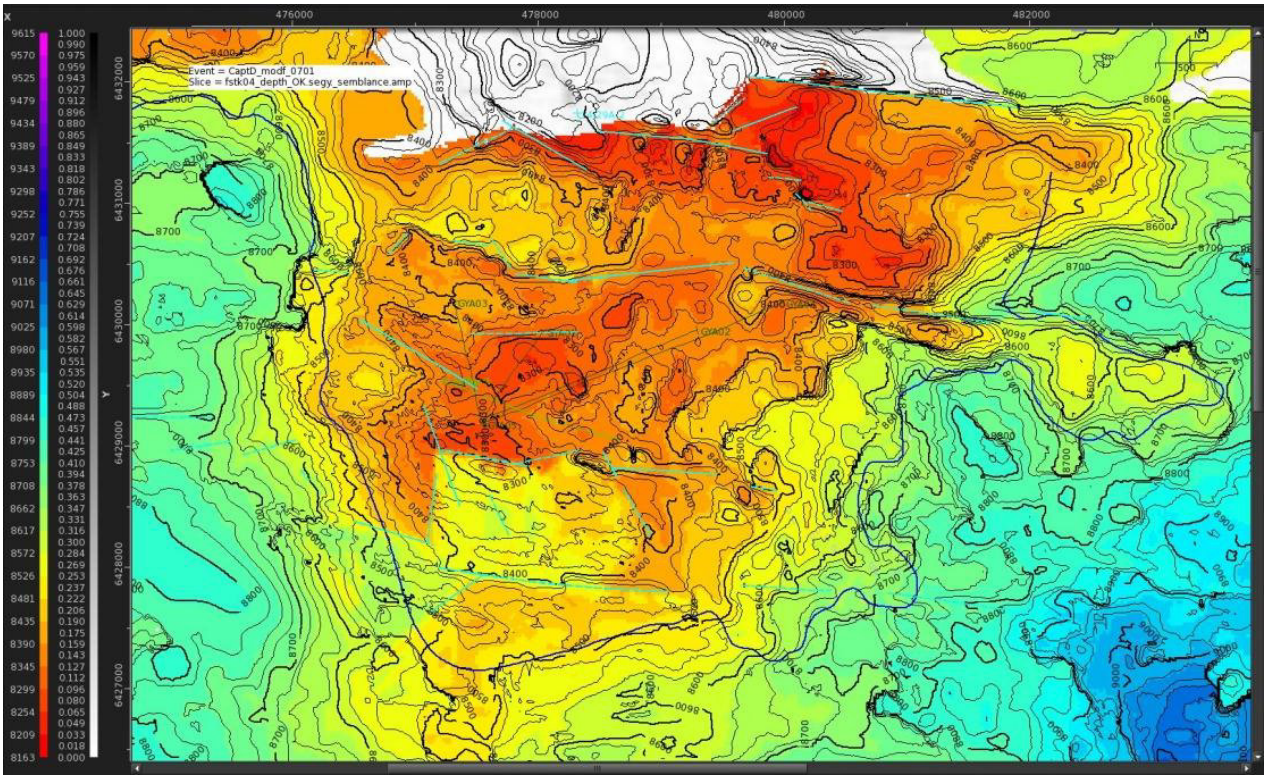

Figure 10-22. Seismic fault pattern Top Goldeneye Reservoir.

Fault offsets are observed at top reservoir and in overburden but remain small throughout. There is no evidence that faults have acted as pathways for fluid to escape from the reservoir (7). The impact of these faults toward fluid flow varies. These barriers are not considered to create isolated compartments. Latest studies have mapped and identified some of these barriers as being partially sealing to non-sealing faults. In general, the throws of most faults are very small at reservoir level.

10.7.3. Permanent Downhole Gauges Bottom Hole Pressure data

Goldeneye has Permanent Downhole Gauges (PDG) available in every well in the field, which represents a great opportunity for well and reservoir management implementation.

The following figure shows all five Goldeneye wells downhole pressure continuous measurements during the history of the field.

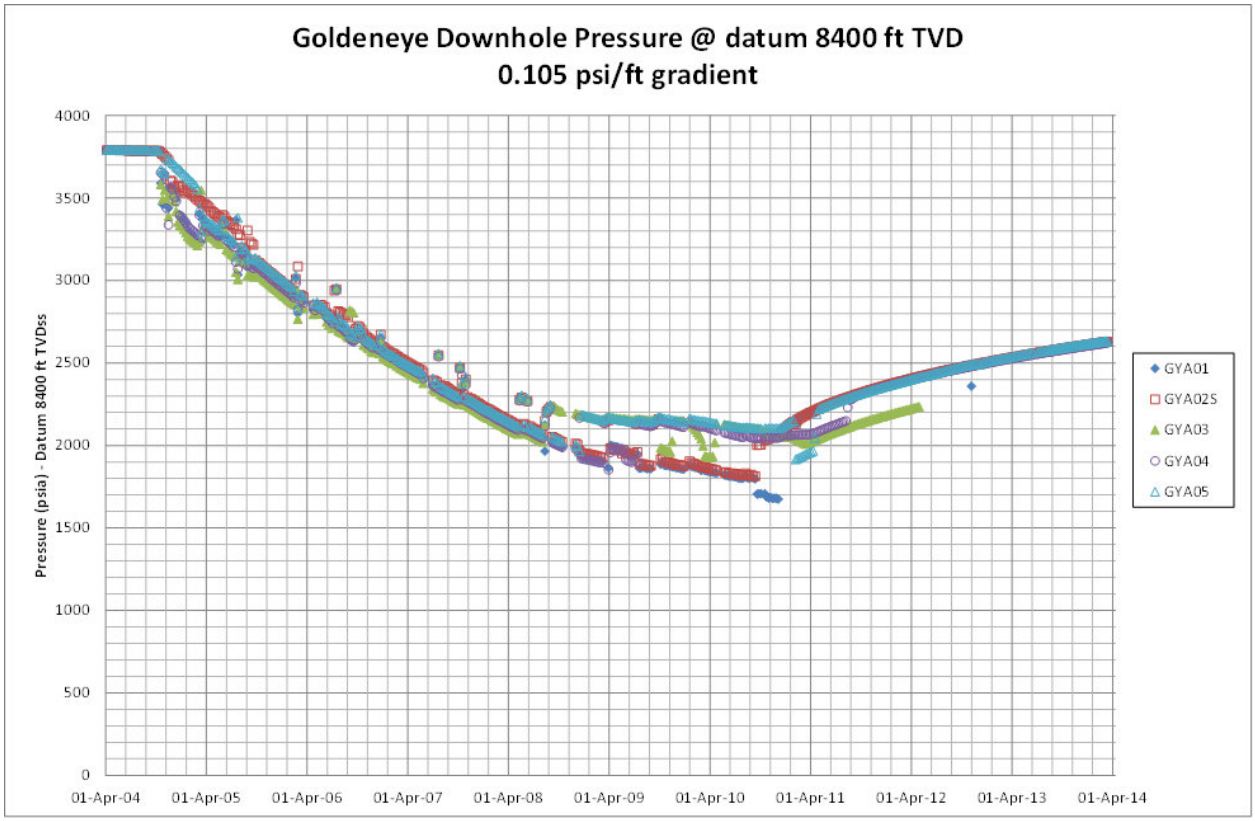

Figure 10-23. Downhole pressure for GE wells @ datum from PDHG.

During production it may be seen that all the wells show a single pressure depletion trend consistent with excellent reservoir communication of all sectors of the field. Even during shut-in periods, it is demonstrable that the reservoir pressure builds up in all wells together at the time, also corroborating the evident lack of compartmentalization within the reservoir.

Additionally Figure 10-24 shows one of the latest prolonged shut-in periods in the field, during September and October 2009. All Goldeneye wells were closed and downhole gauge pressure measurements (corrected to datum at a gas gradient) show remarkably similar behaviour whilst the reservoir pressure was building up towards stabilization.

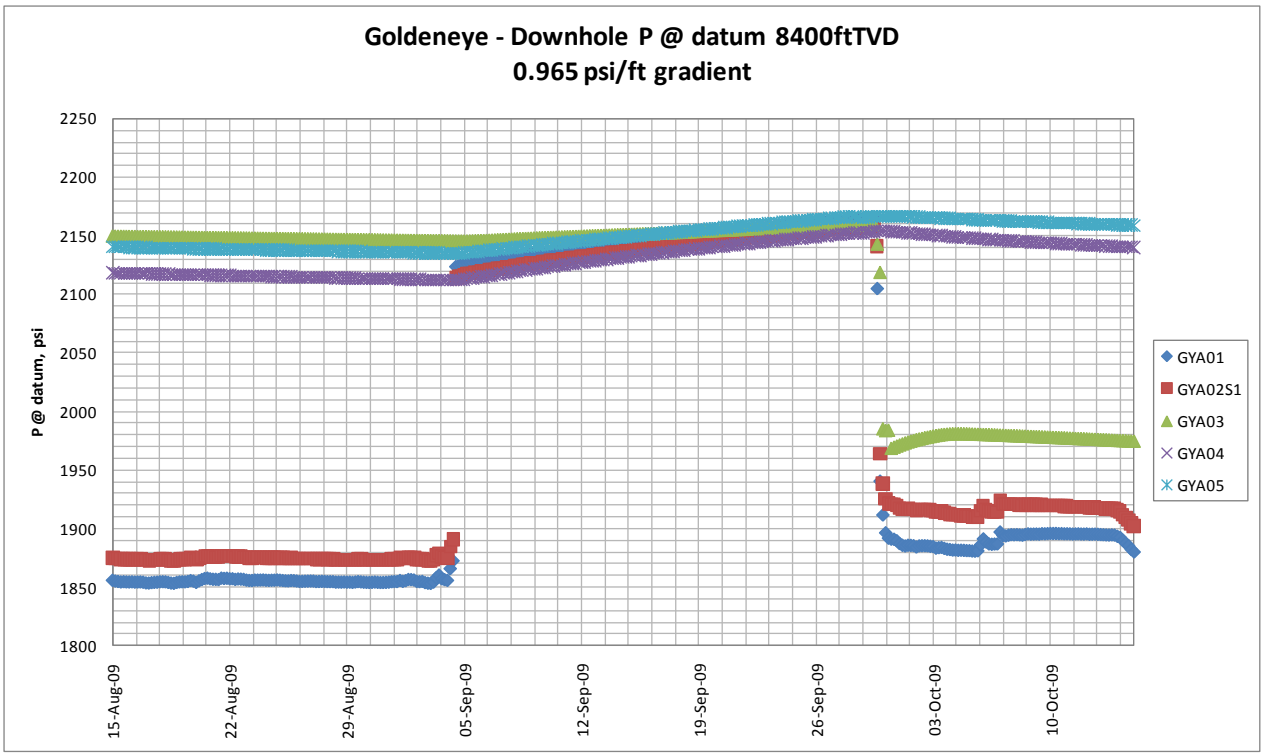

Figure 10-24. Field pressure Build-up from Sep-2010 until October 2010.

Small differences among the pressure measurements during the build-up period (± 30 psi) may be explained by differences in the fluid level in each well and also slight errors in the reported serring depth. The already watered-out wells (GYA03, GYA04, and GYA05) may have part of the perforations covered by water and in this plot all pressures are corrected to datum using a single gas gradient, which introduces a small error.

This is a highly convincing piece of evidence that supports the no compartmentalisation behaviour of the Goldeneye reservoir.

10.7.4. Sealing faults sensitivity scenario

Although, field behaviour points towards a communicating reservoir with no compartmentalisation, an additional sensitivity with the seismic interpreted faults completely sealing was tested in the full field model reference case, in order to assess the impact on the CO_2 migration path. It is important to highlight that a history match was not achieved while introducing the sealing faults, in terms of water breakthrough per well and overall reservoir pressure behaviour. As a consequence, a simplification was adopted by introducing the sealing faults only during prediction, in order to assess their impact in the CO_2 migration path with a proper fluid distribution.

The following figures show CO_2 injection sensitivity with seismic faults included. The injection scenario is a case with 20 Mt of injection equally distributed among four wells (GYA01, GYA02S1, GYA04 and GYA05).

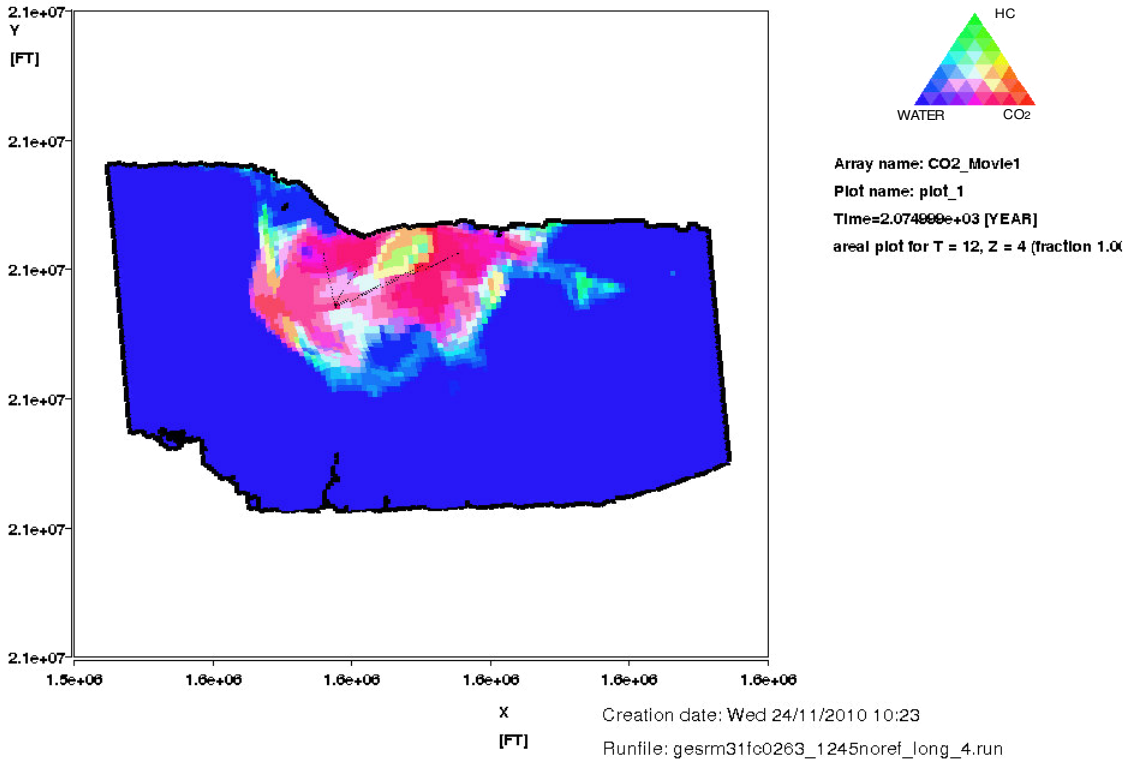

Figure 10-25. FFM SRM3.1: 20 Mt CO_2 injection at end of injection, no seismic faults.

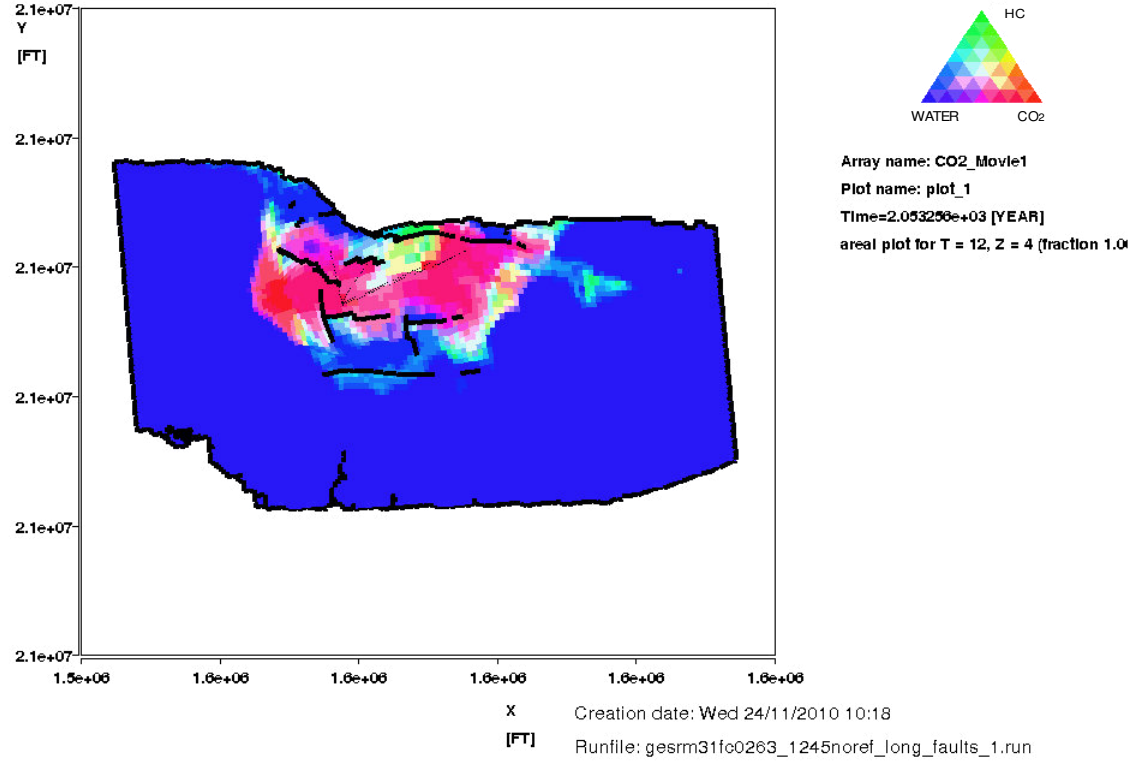

Figure 10-26. FFM SRM3.1 : 20 Mt CO_2 injection at end of injection, with seismic faults included.

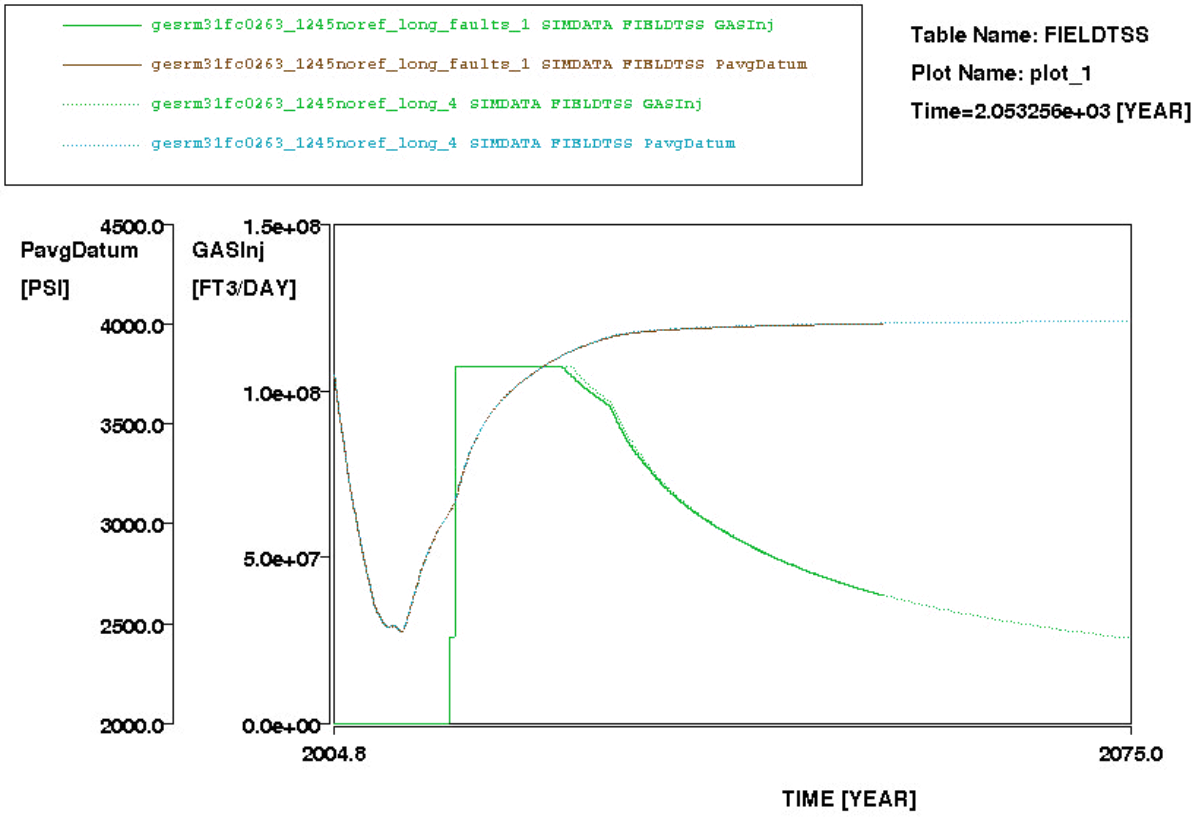

Figure 10-27. CO_2 Injection rate and field average reservoir pressure.

Key: Green solid line = modified faulted model injection rate
Green dash line = reference case injection rate
Brown solid line = modified faulted model average reservoir pressure
Blue dash line = reference case average reservoir pressure.

Examination of the plots above shows that there is very little difference to injection rates or field average pressure when faults are introduced. There is also a negligible effect on the Dietz tongue in the west, although it is a little more pronounced with a little less CO_2 in the south. However, because in general because the faults don't create compartments within the field, the CO_2 (as hydrocarbon gas did) finds it way around the faults to move along the field. There is no threat to the project because the effects on the migration path are minimal and do not create a preferential path that could originate an egression or any overpressure in specific regions that could impact injectivity via back pressure.

10.7.5. Thief zone

Although, the geological model has permeability aligned to depositional trends, there is no evidence to suggest presence of undiscovered high permeability thief zones within such an environment. An additional sensitivity with a high permeability "thief zone" through the spill point was tested in the full field model reference case, in order to assess the impact on the CO_2 migration path and its impact on the overall history match. The thief zone concept as shown in figure 9-28 was tested out in the model by introducing a high permeability corridor 3 x perm of the original perm in the model. The thief zone follows the general depositional trend NW-SE. The thief zone connects up one injector well with the spill point.

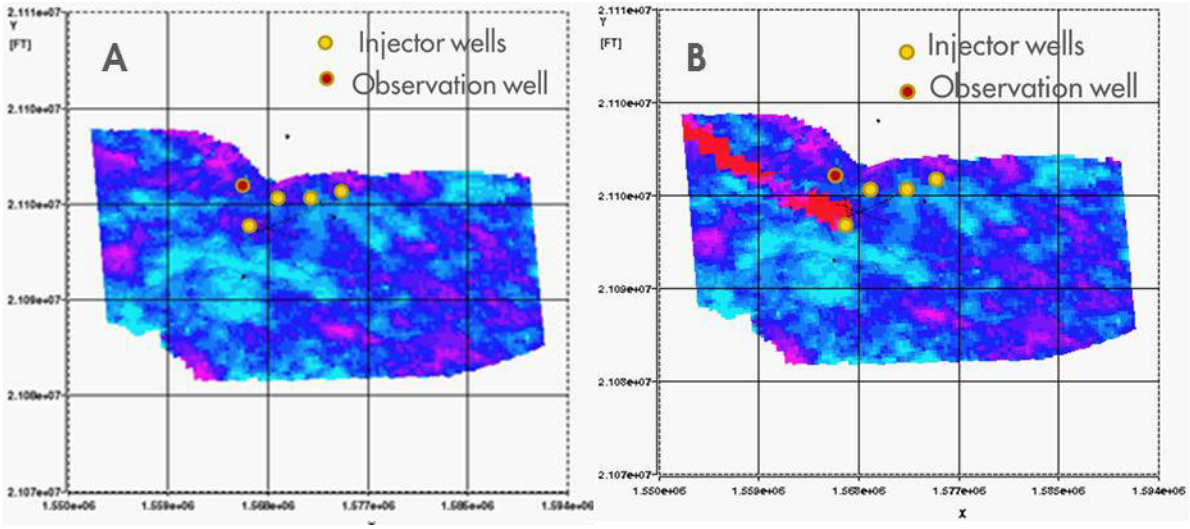

Figure 10-28: Permeability map of top unit D for FFM 3.1 model without thief zone (A) and for model with thief zone (B).

Once more a history match could not be obtained with pressure and water breakthrough matches in the FFM. Upon injection there is no evidence to suggest that a thief zone will provoke significant CO_2 fingering. This is explained by the fact that CO_2 fingering within the high perm corridor will not change as gravity forces tend significantly to counteract the fingering effect when viscous forces within the thief zone remain unchanged.

The following figures show a CO_2 injection sensitivity with a thief zone included. The injection scenario is also a case with 20 Mt of injection equally distributed among four wells (GYA01, GYA02S1, GYA04 and GYA05).

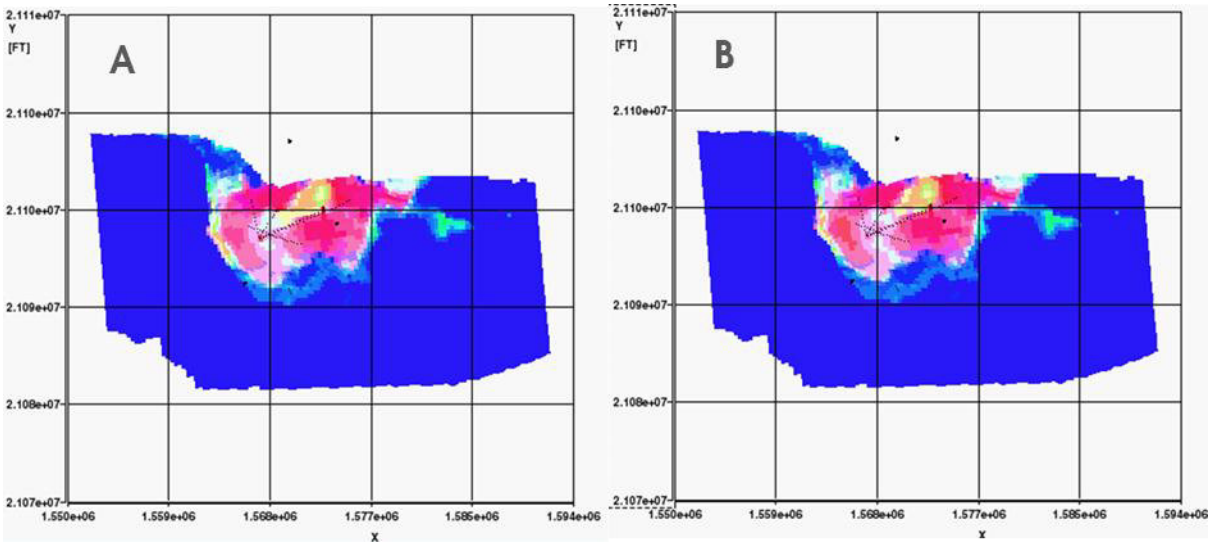

Figure 10-29: CO_2 plume after injection 20 Mt for FFM 3.1 model without thief zone (A) and for model with thief zone (B).

10.8. Vertical Grid Refinement

Owing to its buoyancy relative to water and the unfavourable mobility ratio, the CO_2 migration is sensitive to numerical gridding at the top of flow zones. An important assessment was the determination of what numerical layer thickness element is appropriate for predictions. Considering the high permeability levels of the main sand Captain D, vertical gridding effects will likely dominate over reservoir heterogeneity. Features in the model were as follows:

- Unit D total thickness approximately 225 feet.
- Voxel level 15 layers x 15' each
- MoReS level 9 layers x 25' each

Preliminary CO_2 injection scenarios in a coarse model showed that CO_2 flows through preferentially the top three layers of Unit D. As a consequence, only the top three layers of Unit D were refined in order to test its sensitivity.

Table 10-9. Vertical grid sensitivities.

CASE	No. of layers	Layer Thickness
Base Case	2	25 feet
Sensitivity 1500	3	15 feet
Sensitivity 900	5	9 feet
Sensitivity 500	9	5 feet
Sensitivity 375	12	3.72 feet
Sensitivity 225	20	2.25 feet

The model was re-run under history match mode using the black oil PVT representation with different vertical grid resolutions, replicating the same results as the coarse model. Afterwards, the model was converted to compositional form and run in forecast mode under the CO_2 injection reference case as described in Section 10.3.1. The results are shown in the following figures. Refinement was tested in the SRM 3.15 pinch-out sensitivity model.

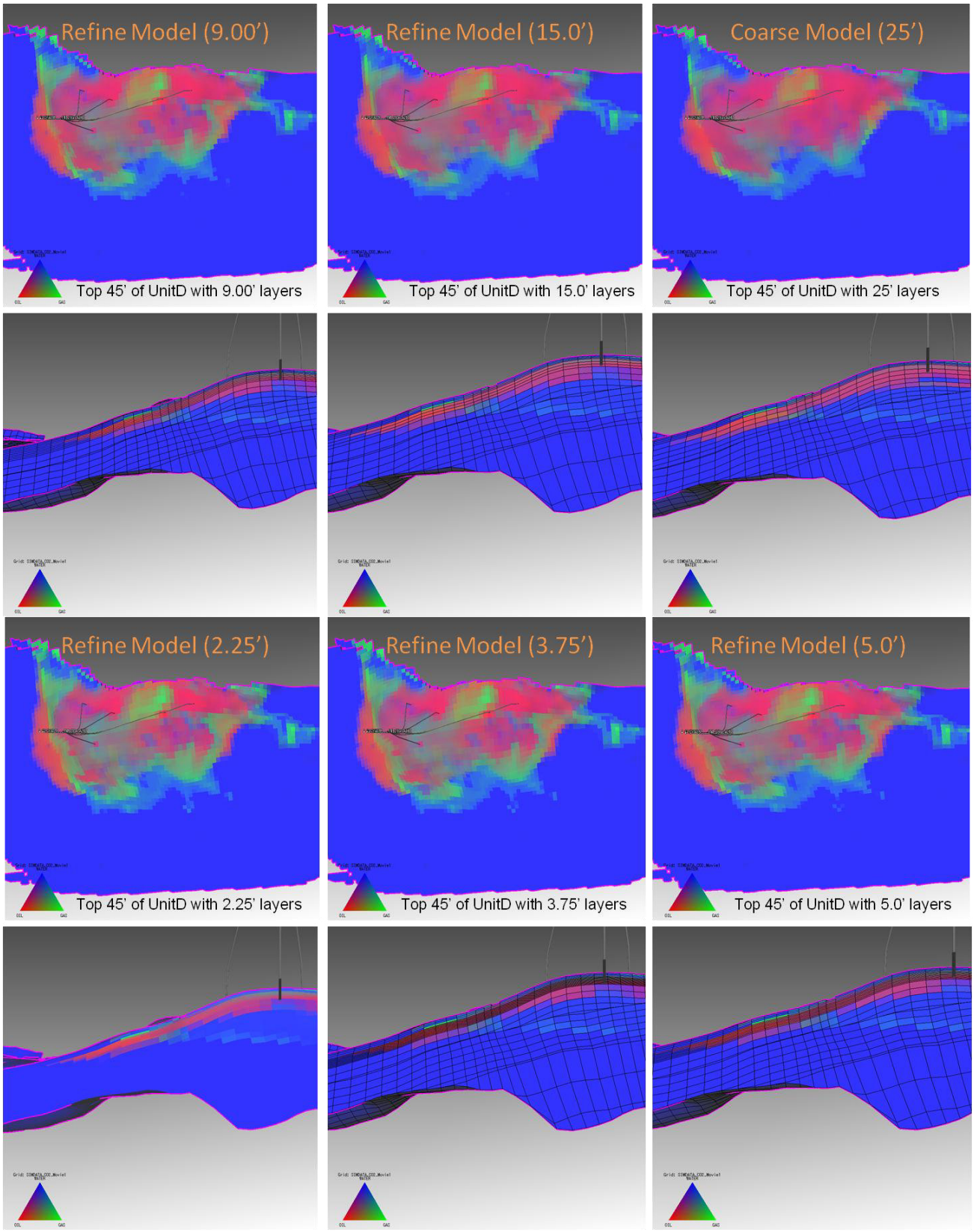

Figure 10-30. XY and YZ view of FFM SRM 3.15 with different vertical grid refinement levels.

The impact of the level of refinement was assessed by measuring the distance between the original OWC and the tip of the CO_2 plume that tongues into the aquifer. The following figure shows the results for different levels of vertical refinement.

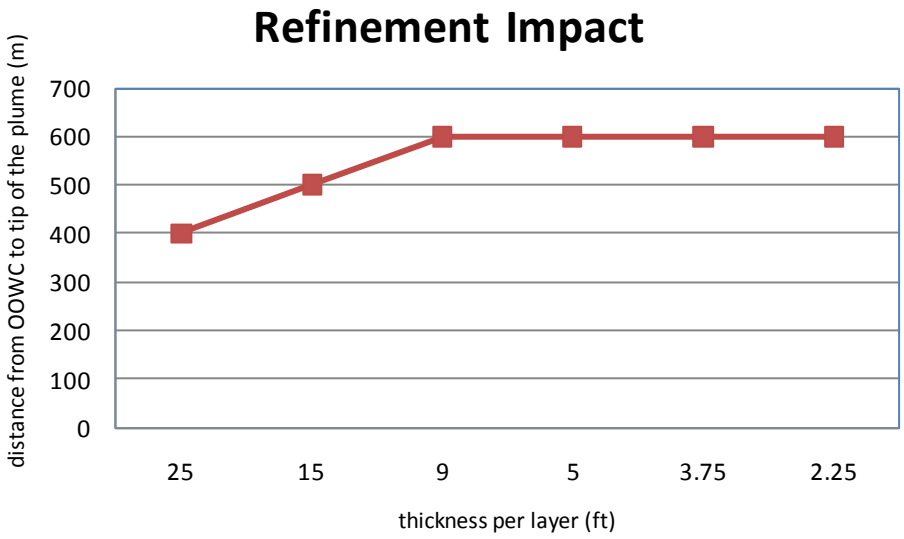

Figure 10-31. Vertical grid refinement impact on CO_2 modelling.

Main observations regarding the results are:

- The level of refinement ranged from the base case coarse model with 25' thick layers, up to 2.25' thick layers in the most refined case.
- Results show that for a level of refinement greater than 9' per layer there is no improvement in the solution of the plume.
- This is because the CO_2 is migrating from the top of the structure downwards, meaning that it has to overcome the gravity forces which constrain the CO_2 from moving further and allowing the tip of the plume to keep shooting farther. Therefore, this effect counterbalances the level of refinement required to properly model the CO_2 displacement.

As a result, it was considered not necessary to run all the scenarios in a more refined grid. The solution of the tip of the CO_2 plume with a difference of 200 meters, considering that the plume extends over the whole field, represents only 3.5% which is a small figure compare with the uncertainty in other parameters such as relative permeability and residual gas saturation.

On the other hand, the run time for a base case CO_2 injection scenario is 5.1 times longer (4.4 hours vs. 22.5 hours) for a grid of 9ft thick and 10.5 times longer (46.5 hours runtime) for the finest 2.25ft grid, which makes difficult to adopt a fine scale version to simulate all the sensitivities investigated with small improvements in the accuracy of the solution.

11. Fairway Regional Aquifer Model

11.1. Scope and Objectives

The performance of the Goldeneye reservoir has been significantly influenced by the surrounding aquifer. This can be seen in the early pressure drop before production started (which is due to the neighbouring Hannay field) and also in the longer term pressure history of the field which indicates significant aquifer support. As well as the Hannay field, three other fields have produced from the Captain sandstone: Atlantic, Cromarty and Blake (see Figure 4 1). In addition, the Rochelle West field which is approximately 35 km east of Goldeneye and inside aquifer model, started production in October 2013 followed by Rochelle East in January 2014, which is just outside the aquifer model. All six fields are interpreted to be in communication with Goldeneye and might have the potential to influence its pressure, if not at present then in the future. In addition Hoylake gas field, 5 km east of Goldeneye, has been included in the aquifer model to address pressure interference effects with Goldeneye. Buffalo, a prospect mapped by Premier Oil further to the east was also tested in the model to address pressure interference effects with Goldeneye. A summary of these fields and prospects is given in Table 10 1.

Table 11-1. Details of neighbouring fields to Goldeneye. (28)

Field	Operator	Type of Field	First Production	Date of Cessation of Production	Peak Production Rate	Total Hydrocarbon Production
Blake	BG	Oil plus Gas Cap. Water Injection	May 2001	Still producing. Estimated life 14 years.	54000 stb/day March 2002	74.3 MMstb at April 2009
Hannay	Talisman	Oil Field	March 2002	March 2009	7400 stb/day August 2003	8.5 MMstb
Cromarty	Amerada Hess	Gas Field	June 2006	July 2009	109 MMscf/day October 2006	59.7 Bscf
Atlantic	BG	Gas Field	June 2006	May 2009	116 MMscf/day October 2006	68.5 Bscf
Rochelle West (incl. in model) **Rochelle East (not in model)** **Buffalo Prospect (incl. in model)**	Endeavour	Gas Field with Oil Rim Gas prospect[38]	October 2013 January 2014	2020-2023	N/A	35 MMboe[37] Greater Rochelle area 50 – 75 MMboe (29)
Hoylake	Premier Oil	Gas Field with rim	Relingusihed in 2013	N/A	N/A	42-64 Bscf (30)

Injected CO_2 could potentially spill out of the Goldeneye reservoir and move along the aquifer. The movement of the CO_2 will depend upon the properties and structure of the aquifer as well as the pressure gradients due to production from the various fields. For these reasons a dynamic model of most of the regional aquifer has been created and used to investigate the reservoir pressure and the potential migration of CO_2.

The model does not cover the whole aquifer and so does not explicitly include the Rochelle East field which lies one km outside the eastern edge of the model. The Rochelle East field was modelled as part of the Rochelle West field, which lies inside the aquifer model. This model also enables the aquifer representation and history match of the FFM to be evaluated which improves confidence in the storage capacity estimate.

The Brodgar gas field, which is located at the eastern edge of the Captain fairway and outside of the aquifer model, 30 km east of Rochelle, is not thought to be in communication with the other fields in the Captain fairway. The field is located south of a major fault, the Glenn fault, and there is evidence to suggest that the field, which started producing in August 2008, is not under influence by the Captain fairway aquifer. The pressure depletion seen in Rochelle East (December 2008) and Rochelle West (October 2010) is not reflecting Brodgar production

11.2. Static Model

The Goldeneye field static model only extends for a few kilometres outside the oil water contact. For this reason a static model (31) of the regional aquifer has been created which stretches for approximately 100 km from the west of Blake to the east of Hannay. This model is gridded at a fairly coarse 200 x 200m resulting in a total of 25 million cells (488 x 240 x 213). The model grid is aligned with version SRM 3.1 of the Goldeneye static model to facilitate the inclusion in the model of a more detailed representation of the Goldeneye field based on the FFM. This is done in the up-scaling step when building the dynamic model as described below.

11.3. Up-scaling and Inclusion of FFM

The static model was up-scaled in Reduce++ to create a MoReS model. The areal grid is the same as in the static model (i.e. no horizontal up-scaling) but the vertical grid is coarser with the layering as illustrated in Table 11-2. This is a finer layering than used in the FFM, which uses half the number of layers in units A and C. The thickness of the different units varies across the model and a finer layering is necessary to give sufficient vertical resolution in those parts of the model where units A and C are much thicker than at Goldeneye. The finer resolution is not needed in the Goldeneye reservoir. The resulting grid is 488x240x34. Due to much of the grid being inactive, the number of active blocks is only 241609.

Table 11-2. Vertical layering of dynamic model.

Unit	Number of Layers
E	3
D	9
C	16
A	6

The ratio of vertical to horizontal permeability is set equal to 0.1 throughout outside Goldeneye. The generally high permeability and porosity would indicate a high value of Kv/Kh over most of the model but 0.1 was chosen to allow for the inclusion of small shale laminations. The shale layers separating the different geological units (A, C, D and E) are modelled explicitly in the static model and are vertical barriers to flow over most of the model. There are no faults in the model and there was therefore no need to specify fault multipliers.

As the Goldeneye region of the aquifer model is less detailed than the FFM, the Goldeneye area in the up-scaled model has been replaced with an up-scaled version of the Goldeneye static model. This is created by up-scaling version SRM 3.1 of the Goldeneye static model to a 200m grid and then copying the resulting properties and corner points into the up-scaled static model. This results in a similar representation of the Goldeneye area as in the FFM, but at a coarser scale as the FFM has a horizontal grid of approximately 100 m x 100 m. The history match modifications to the FFM model grid are included in this coarser representation of Goldeneye. These modifications are described in Section 8.2 above. These modifications are not extended to the remaining parts of the aquifer model.

Figure 11-1 illustrates the aquifer model with the Goldeneye and other reservoirs marked.

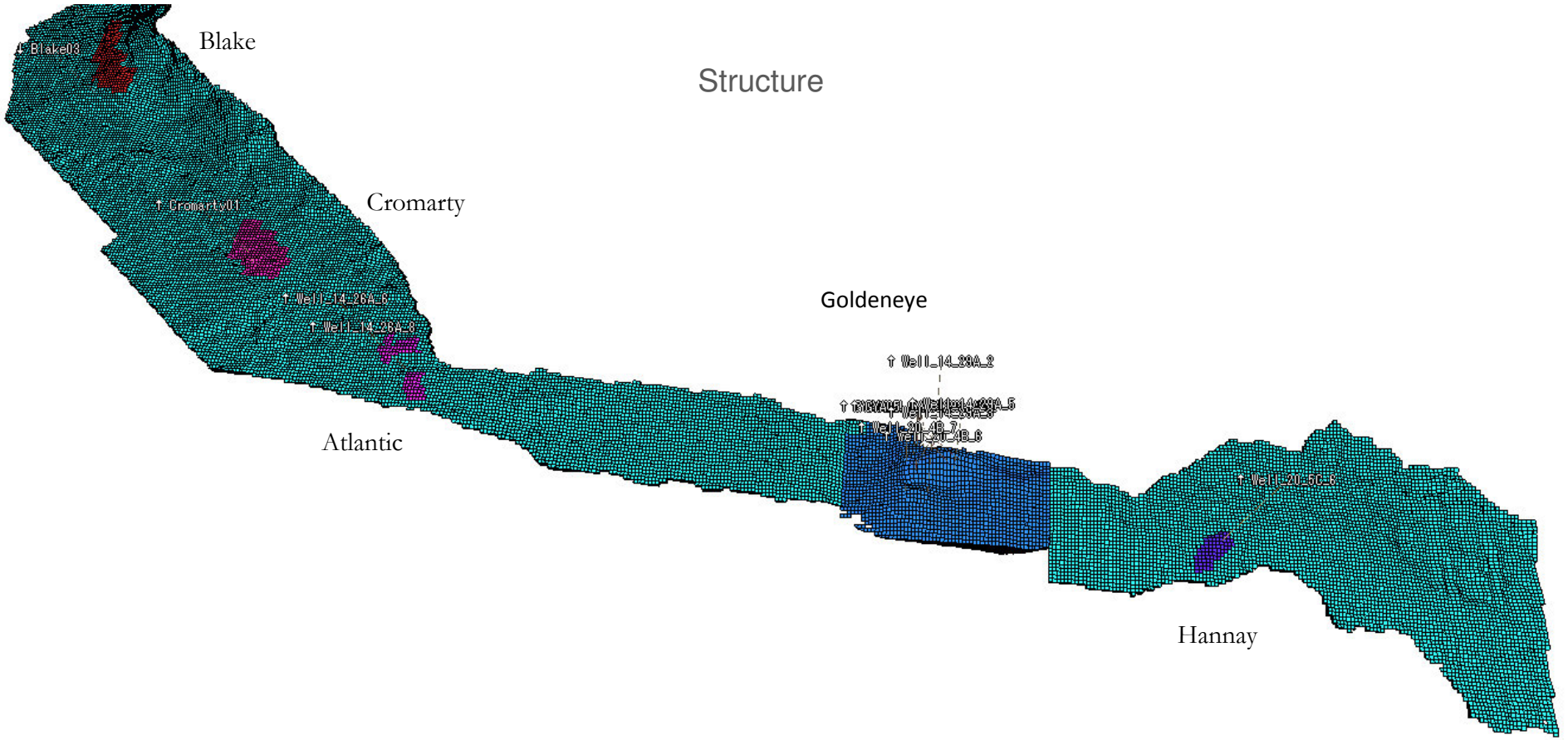

Figure 11-1. Goldeneye aquifer model grid (Goldeneye and other regions highlighted).

11.4. Aquifer extent

The static model covers approximately 100 km of the Captain sandstone but the aquifer continues to the east and west. To the east the Captain sandstone extends approximately another 40-60 km and continues to deepen. To the west of Blake the formation starts to widen and eventually outcrops at the seabed about 50 km to the west of Blake (32). The aquifer is therefore potentially infinite to the west but finite to the east. Porosity and permeability would be generally expected to increase updip to the west and decrease downdip to the east.

Additional analytical aquifers were attached to the eastern and western edges of the model to represent the aquifer outside the model. These aquifers had the same properties as the edge blocks of the model, but their horizontal extent was varied during the history match. The analytical aquifers were modelled as linear aquifers in most cases, but for some cases a radial aquifer was used on the western edge of the model as it was thought this might better represent the widening of the Captain formation and the potential connection of the aquifer to the sea.

The detailed extent and connectivity of the aquifers is uncertain. Detailed pressure measurements from the fields in the Captain sandstone would be needed in order reach definite conclusions.

11.5. Relative Permeability Data

The relative permeability model for the Goldeneye region was taken from the FFM and is described in Section 5.4. For the rest of the model a separate relative permeability model was used with separate imbibition and drainage curves using the Killough hysteresis model (33). This relative permeability model is similar to that used in the simulacrum box model used for many of the relative permeability sensitivities (see Section 6.2 above). The parameters used in the relative permeability model are given in Table 11-3.

Table 11-3. Aquifer model relative permeability parameters.

Parameter	Imbibition Value	Drainage Value
K_{rw}	0.4	1.0
K_{row}	0.8	0.8
S_{orw}	0.2	0.0
N_w	2	5
N_{ow}	4	5
K_{rg}	0.8	0.8
K_{rog}	0.8	0.4
S_{gc}	0.05	0.25 (trapped gas saturation)
N_g	2.5	2.5
N_{og}	5	5

The non-Goldeneye fields are only represented coarsely in the model and therefore cannot be expected to match the observed behaviour very well. For this reason, separate relative permeability

tables were used in these locations where the parameters were adjusted in order to give a better match to fluid production. In particular, the oil and gas relative permeability were made more favourable in order to reduce water production.

11.6. Capillary Pressure Data

For Goldeneye, the capillary pressure data was identical to the FFM as described in Section 5.3 above. For the rest of the model a single curve was used except for Hannay where a separate curve was used to give a better match to the STOIIP. The only significance of the Hannay curve is to provide figures for the initial fluids in place in the field, it does not affect flow in the aquifer.

11.7. PVT Data

11.7.1. Black Oil

When the model was run in black oil mode for history matching separate black oil PVT models were used for each field. Detailed PVT data for the non-Goldeneye fields was not available so PVT data was created as follows.

- The Hannay PVT was based on Gannet D which has similar properties.
- Cromarty , Atlantic , Rochelle, Hoylake and Buffalo PVT was based on Goldeneye data but with the CGR adjusted to a value believed to be representative of the fields.
- The Blake PVT was created using estimated values for the field.

11.7.2. Compositional

When the model was run in compositional mode only one equation of state was used, this being the equation of state used in the Goldeneye FFM (see Section 5.2 above). For the other fields in the model, the Goldeneye equation of state was also used. For the two gas fields (Atlantic and Cromarty) the errors introduced are small but for the oil fields (Hannay and Blake) the errors will be larger. To compensate for this the initial composition in these reservoirs was adjusted to obtain approximately the same GOR and Bo as in the black oil case. In all fields the GBV was scaled to match the STOIIP or GIIP. Very little difference was noticed in the history match pressures between the black oil and compositional cases.

11.7.3. Water properties and CO_2 Dissolution

The salinity of the Goldeneye formation water is 50,000 ppm. The MoReS option to calculate water properties from salinity was used with salinity set to this value throughout the model. In reality, the salinity varies across the aquifer, but data was not available to accurately model this. CO_2 solubility is a function of salinity, but the CO_2 injected into Goldeneye is unlikely to move far enough from the reservoir for this variation to be significant.

MoReS contains an option to model the dissolution of CO_2 in water. This option was used in a number of cases to investigate the sensitivity of the results to this mechanism. As described in Section 10.6, the model used in MoReS will tend to overestimate the effect due to two reasons.

- The simulator assumes all the CO_2 and water in a grid block are in contact, whereas in reality contact will be made with only some of the CO_2 and water.
- MoReS uses Henry's law to estimate the amount of CO_2 which dissolves in water. This calculation may overestimate the amount of CO_2 which dissolves in water compared to experimental results unless some fine tuning of Henry's coefficient is done.

11.8. Pressure Data

Pressure data for Goldeneye is available from a number of exploration wells as well as the five production wells. RFT data from six exploration wells is plotted in Figure 11-2. All the wells were drilled before production started in any of the fields under consideration and so should represent virgin conditions. There is a small amount of scatter between the wells – and between different runs in the same wells – but this has not been interpreted as due to compartmentalisation, rather it is a result of tool calibrations and temperature compensation, especially in the measurements from 1996. The difficulty of history matching the model with sealing faults as highlighted in Section 10.7.4 support this.

All five Goldeneye production wells have permanent downhole gauges (PDG) which were installed at least six months before the start of production. As illustrated in Figure 11-3, these gauges show a slow decline of approximately 0.02 psi/day [0.00138 bar/day] which is matched as presumably due to production from Hannay which started in March 2002. The decline rates for the five wells range from 0.019 psi/day [0.00131 bar/day] in GYA02s1 to 0.023 psi/day [0.00159 bar/day] in GYA04. The pressure in GYA02s1 deviates from the trend from June 2004 and cannot be relied upon after that. Figure 11-4 shows the pressures from two of the initial exploration wells together with the PDG data.

Extrapolating the PDG data back to 2002 brings the model approximately in line with the exploration well pressures. This strongly suggests the pressure decline is due to Hannay production, especially when considered with the fact that the largest decline is in GYA04, which is closest to Hannay.

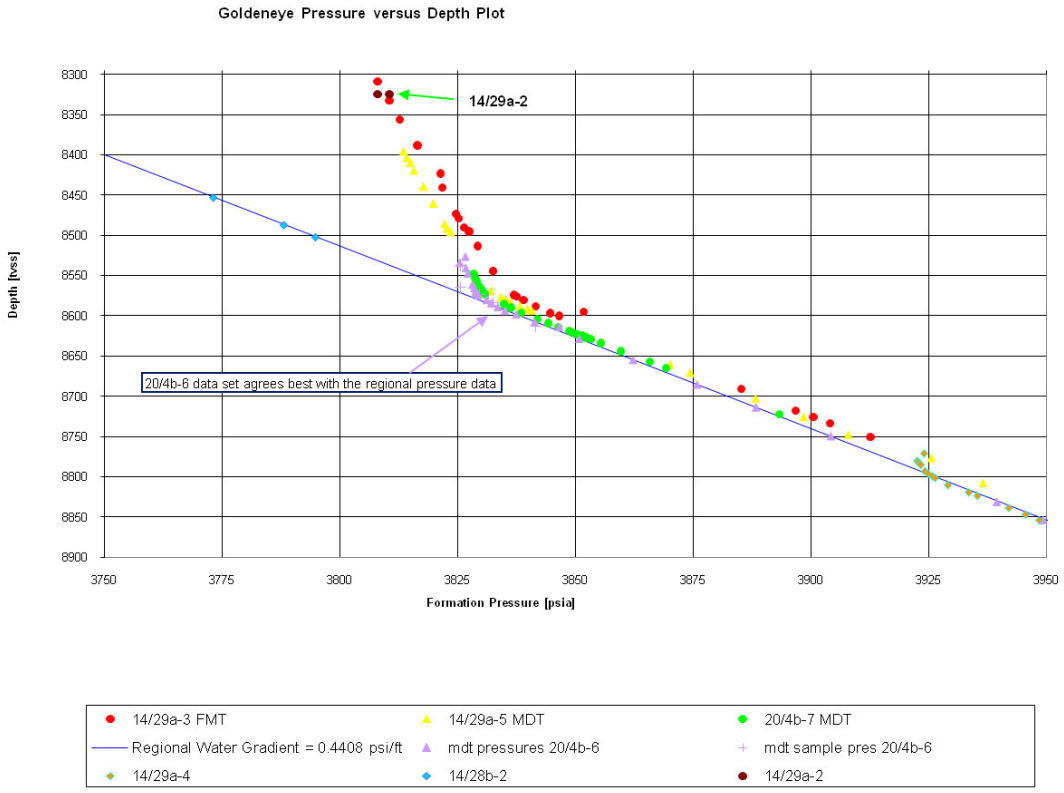

Figure 11-2. Goldeneye RFT data.

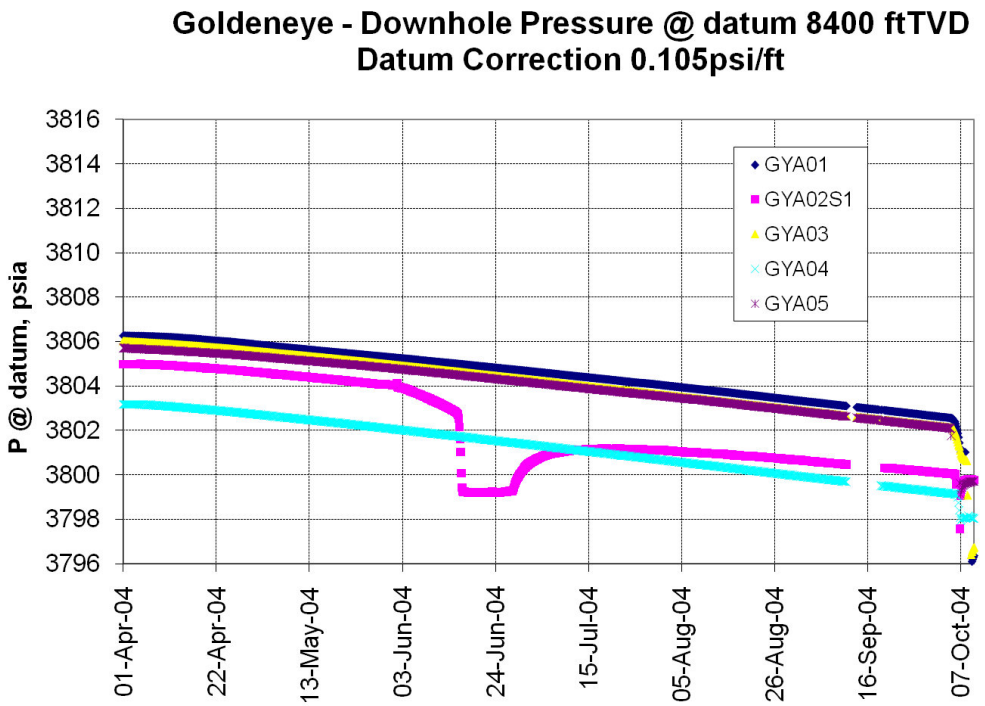

Figure 11-3. Initial decline in Goldeneye Pressure from downhole gauges.

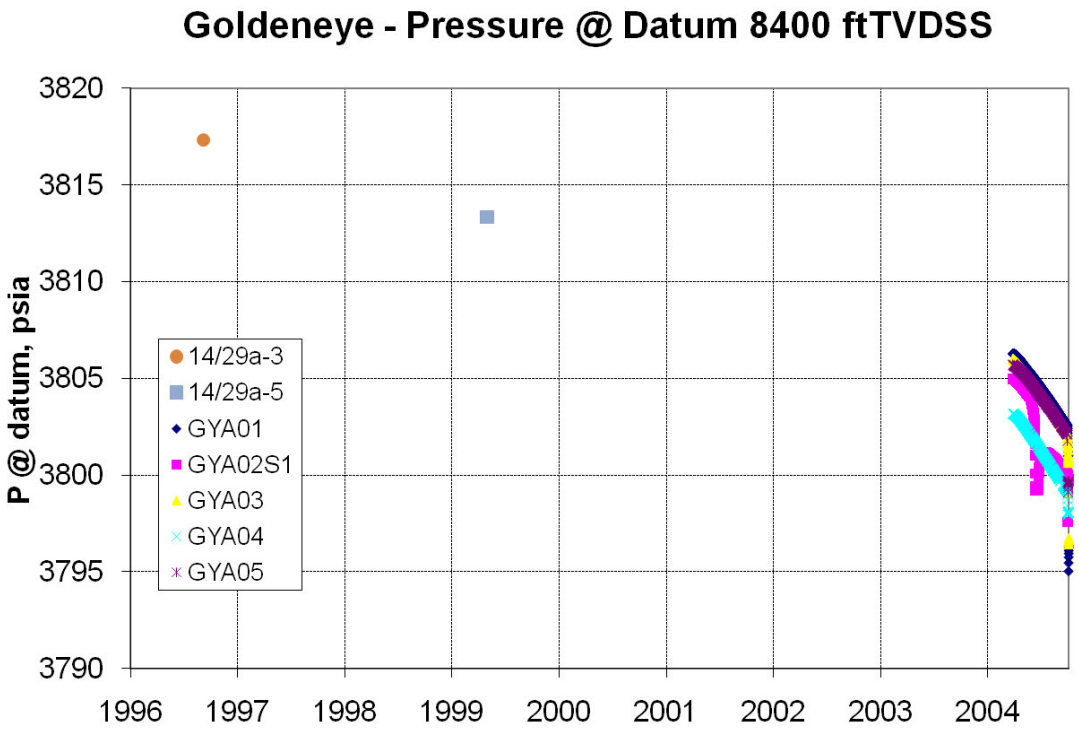

Figure 11-4. Change in Goldeneye pressure from 1996 to 2004.

11.9. Well and Production Data

Production data for Goldeneye was included in the model, but was averaged over monthly intervals rather than daily intervals as in the FFM. The Goldeneye production data was taken from the same source as the FFM (Section 5.6). For the other fields some production data is available from the DECC website (34) but this does not include water production or injection data. For this reason some data was obtained from a neighbouring operator.

The only field still in production is Blake, which has an estimated life of 14 years from start-up in 2001. As the field has water injection support, it was assumed that future voidage would be balanced by injection and there would be no net production after April 2009, when no more production or injection data were available.

The Goldeneye production wells were included in the model with their correct perforations and allocated production. For the other fields, detailed well information was not available and in most cases notional wells were added to the model to produce the allocated fluids. Blake has six production wells in the main field and two in the Blake Flank development. There are also two injection wells; these were modelled by two horizontal injection wells and one horizontal production well. One vertical well was used for Cromarty and one each for the Atlantic North and South accumulations. Hannay has two horizontal production wells (35) but only one notional well was included in the model.

Production from Rochelle East and West was included which corresponded to reserves of 35 MMboe. The model does not cover the whole aquifer and so does not explicitly include the Rochelle East field which lies 1 km outside the eastern edge of the model. The Rochelle East field was modelled as part of the Rochelle West field, which lies inside the aquifer model, 2 km away from the Rochelle East field. The in-place volumes and the gas off-take from Rochelle West therefore represents the combined Rochelle West & East. Rochelle West started production in October 2013, followed by Rochelle East in January 2014 . There is no impact of Rochelle production on the Goldeneye pressure history match until April 2014 due to a delayed response of the Captain fairway aquifer.

11.10. Initialisation

To ensure that the whole model was in hydrostatic equilibrium, the separate reservoirs were initialised with a water pressure of 4242 psia [292.5 bara] at a common datum depth of 9500 ft TVDSS [2896 m]. This corresponded to the pressure of 3835.5 psia [264.4 bara] in Goldeneye measured by the exploration well 14/29-a3 at a datum depth of 8573 ft [2613 m] TVDSS. The contacts and pressure data are given in Table 11-4. Some of the contacts were adjusted to ensure closure in the model, the coarse grid meant that otherwise fluids could spill into the aquifer (35) (36).

Table 11-4. Initialisation data used in model.

Field	Oil Water Contact (ft)	Gas Oil Contact (ft)
Goldeneye	8592 [2619 m]	8568 [2612 m]
Hannay	9450 [2880 m] ((35) has 9498 ft [2895 m])	N/A
Atlantic	N/A	6420 [1957 m]
Cromarty	N/A	6230 [1899 m]
Blake	5270 [1606 m]	5170 [1576m]
Rochelle West	10073 [3070 m	10094 [3077 m]
Hoylake	8801 [2683 m]	8796 [2681 m][3]

The resulting fluid distribution is illustrated in Figure 11-5.

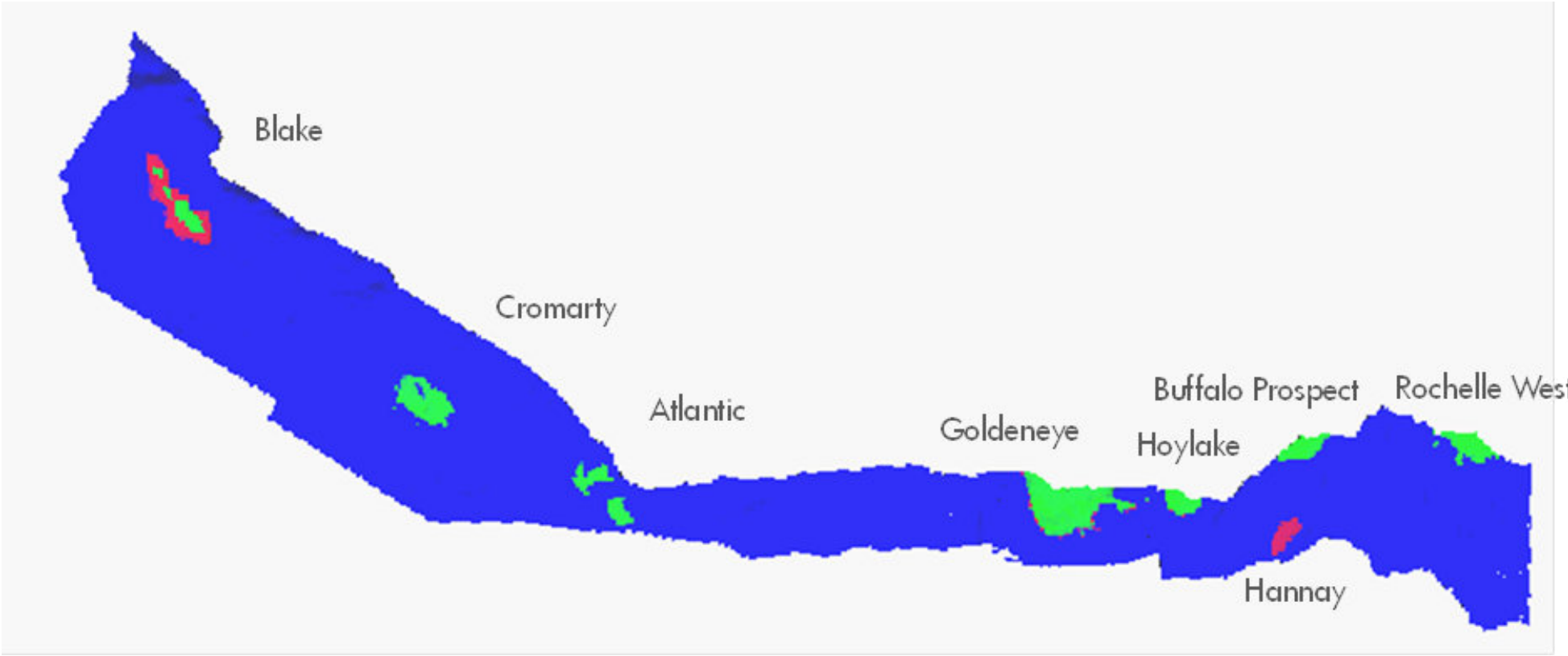

Figure 11-5. **Goldeneye model with initial fluid distribution.**

11.11. History Match

11.11.1. History Match Philosophy

Three different Goldeneye models have been history matched (Section 9 above) but only one aquifer model has been constructed which uses the SRM 3.1 model. The representation of Goldeneye in the aquifer model is taken directly from the history matched SRM 3.1 FFM, although at a coarser resolution, and no changes have been made to this part of the model. History matching has concentrated on matching the pressures in Goldeneye and the neighbouring fields by adjusting the strength and size of the aquifers to either side of Goldeneye. Water breakthrough times in Goldeneye wells have not been explicitly matched except by ensuring that no wells water out early. In any case, the coarseness of the Goldeneye representation makes detailed predictions of water breakthrough at wells difficult. The available data is insufficient to obtain a single match, and so a range of models have been investigated instead, all of which give a reasonable match to the pressure data.

11.11.2. Initial Goldeneye Pressure Decline

The history match to the pre-production pressure decline is illustrated in Figure 11-6 for a history match case, with an additional 40 km eastern aquifer and an infinite linear western aquifer. The pressure decline rate is well matched, but the pressures are about 5psi [0.35bar] too low. No cases run matched the observed pressure values, so the shortfall in pressure is probably due to inaccuracies in the initial pressure specified in the model (which may be about 5psi [0.35 bar] too low). Alternatively, the gauge depth for the wells could be slightly inaccurate. The other feature the model does not reproduce is the difference between the pressure in GYA04 and the other wells. The downhole gauge data shows this well to have a pressure approximately 3psi lower than the other wells, presumably because this well is farther east and closer to the pressure sink at Hannay. In the model GYA04 is only about 1 – 2 psi [0.07 – 0.14 bar] lower that the other wells. No attempt was made to match the difference pressure response of the wells, as the purpose of the aquifer model was to investigate the long term response of the aquifer.

Figure 11-7 and Table 11-5 show the decline rates of a number of other cases with varying aquifer size and with a number of different permeability modifications. Cases with no additional aquifers such as 9 show too high an initial pressure decline, indicating the need for more aquifer support than in the model. A 40 km eastern aquifer is enough to give the required decline rate, but there is little difference between this case and cases with larger aquifers to the east and west. With the initial pressure decline data it is therefore only possible to say that at least a 40 km aquifer is needed on the eastern side of the model.

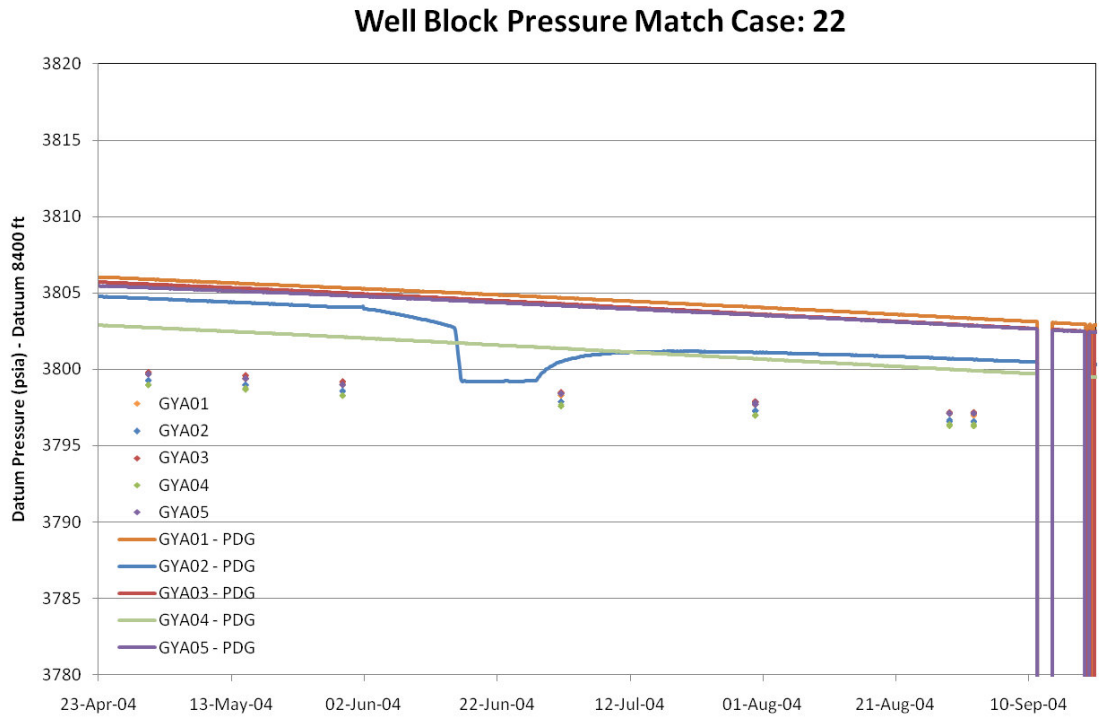

Figure 11-6. Pre-production Goldeneye pressure decline for history match case 22 with additional eastern and western aquifers compared to PDG data.

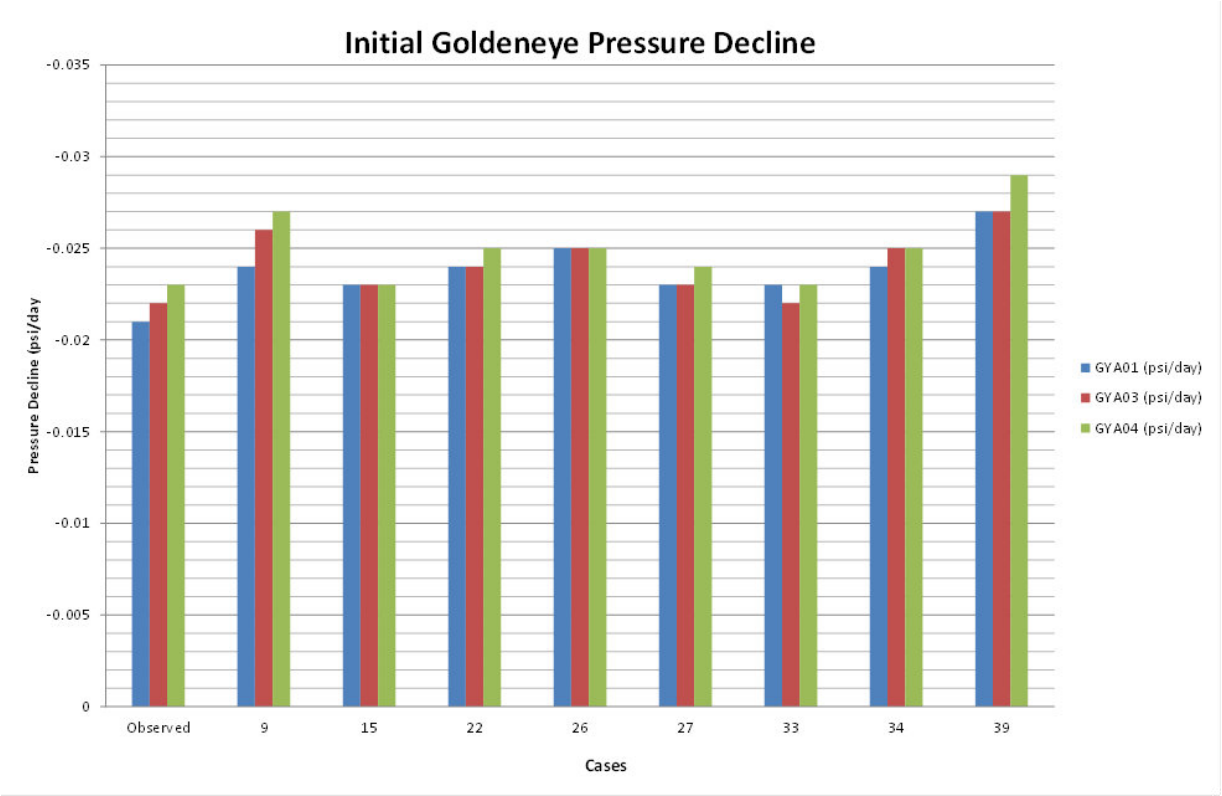

Figure 11-7. History match to pre-production Goldeneye pressure decline for history match cases (see Table 11-5 for details).

Table 11-5. Pressure decline in GYA01, GYA03 and GYA04 from April 2004 to August 2004 before start of Goldeneye production.

Case	Western Aquifer	Eastern Aquifer	Permeability Changes	GYA01 psi/day	GYA03 psi/day	GYA04 psi/day
Observed				-0.021	-0.022	-0.023
9	No additional aquifer	No additional aquifer	None	-0.024	-0.027	-0.027
15	No additional aquifer	40 km aquifer	Permeability in east x 0.55	-0.023	-0.023	-0.023
22	infinite linear aquifer	40 km aquifer	Permeability in east x 0.55	-0.024	-0.024	-0.025
26	infinite linear aquifer	50 km aquifer	Permeability in east x 0.55	-0.025	-0.025	-0.025
27	No additional aquifer	40 km aquifer	Permeability in east x 0.55 and Blake to Cromarty x 2	-0.023	-0.023	-0.024
33	infinite radial aquifer	40 km aquifer	Permeability in east x 0.55	-0.023	-0.022	-0.023
34	infinite radial aquifer	50 km aquifer	Permeability in east x 0.55	-0.024	-0.025	-0.025
39	Model sealed at Grampian Arch	40 km aquifer	Permeability in east x 0.55	-0.027	-0.027	-0.029

11.11.3. Match to Field Pressures

Figure 11-8 illustrates the match to Hannay pressures for a range of cases. It can be seen that with no additional aquifers attached to the model the pressure decline is too steep and additional support is therefore needed. A 40 km extra aquifer in the east is sufficient to match the long term pressure decline. A 50 km extra aquifer provides slightly more support with the pressure rising just above the measured pressure in 2010. Additional aquifer support to the west has very little effect on the match to Hannay. If the model is sealed at the Grampian Arch (just east of Atlantic) the pressure in Hannay is slightly too low towards the end of the history match even with an additional aquifer to the east.

The pressures for Goldeneye for the same cases are illustrated in Figure 11-9 where the same pattern is seen, the match for the cases with additional aquifers is satisfactory while the pressure is too low in the cases with no additional aquifers or with the model sealed at the Grampian Arch.

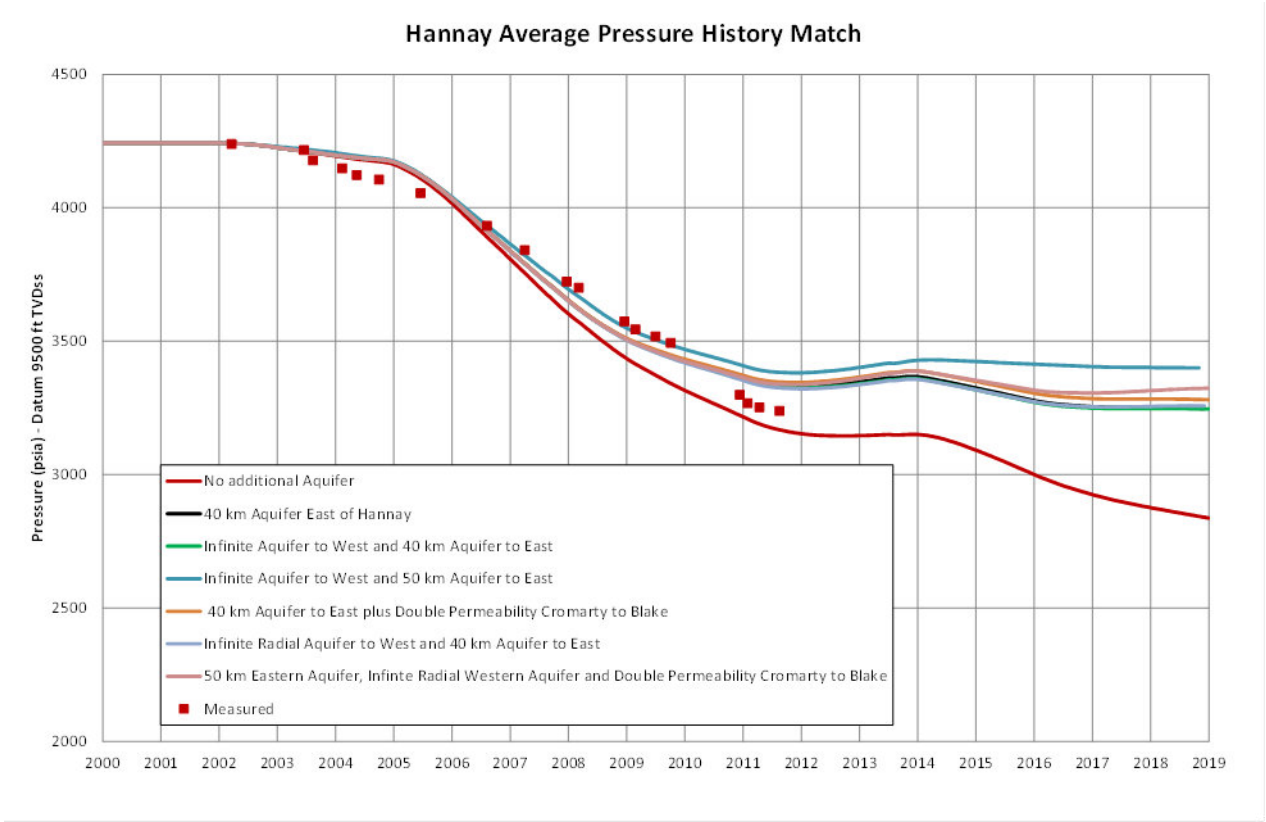

Figure 11-8. Hannay pressure match.

The pressure for Goldeneye for the same cases are illustrated in Figure 11-9 where the same pattern is seen, the match for the cases with additional aquifers is satisfactory while the pressure is too low in the cases with no additional aquifers or with the model sealed at the Grampian Arch. The latter is not shown on this plot.

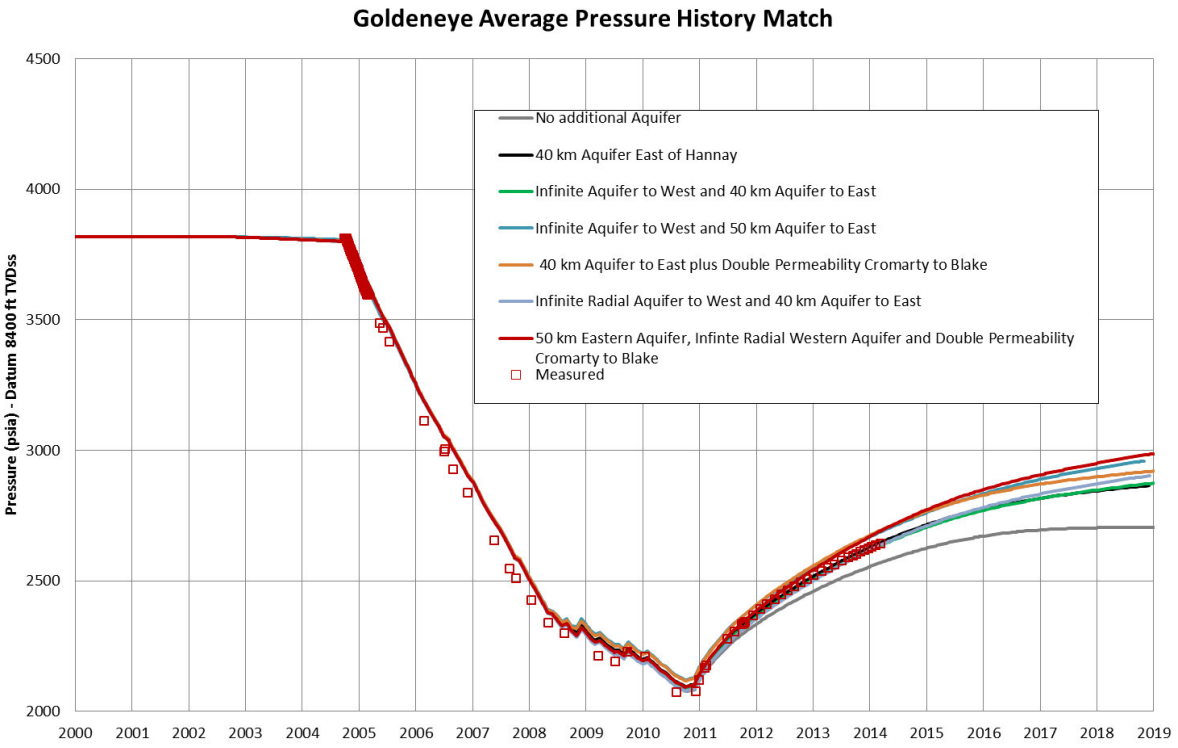

Figure 11-9. Goldeneye pressure match.

A sensitivity without Hoylake and the Buffalo prospect in the model is shown in Figure 11-10. The sensitivity shows that Hoylake, which constitutes a high energy source in proximity of Goldeneye need to be accounted for in the regional aquifer model. After Goldeneye de-pressurization the Hoylake gas cap expands and contributes to Goldeneye re-pressurization. The Buffalo prospect, which is further away, has a similar but a smaller impact. The pressure increase caused by Hoylake in Goldeneye had to be offset by lower perm in the eastern aquifer.

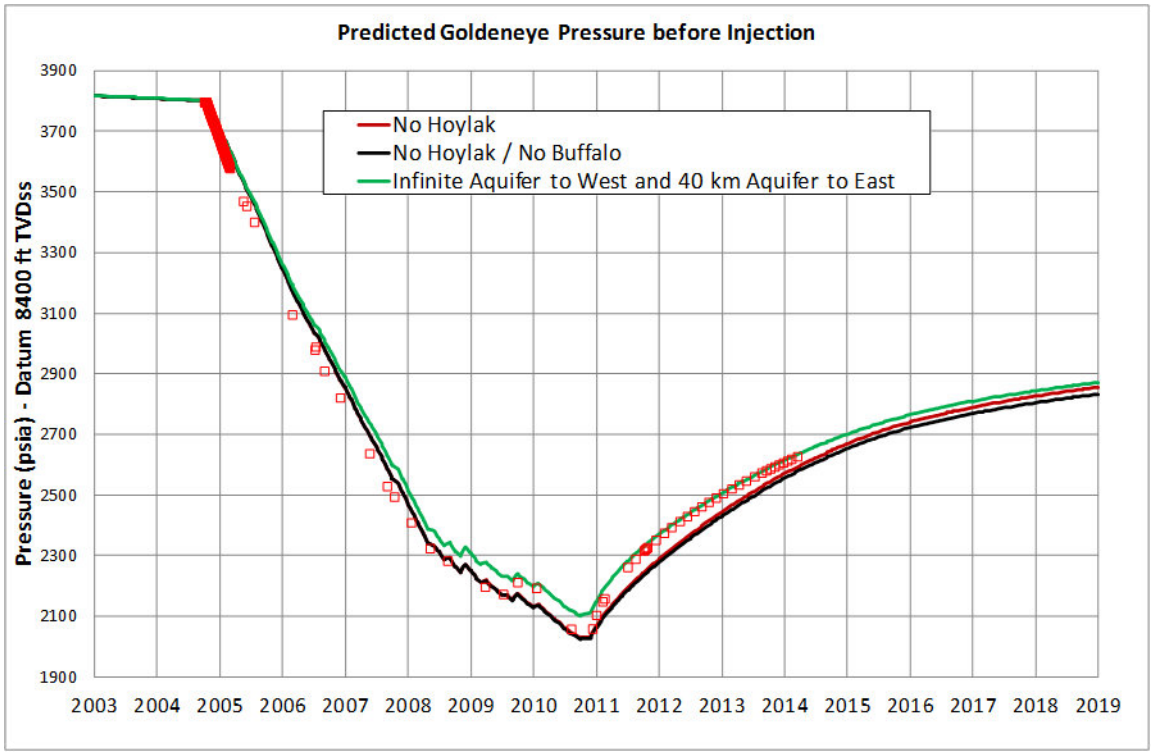

Figure 11-10: Predicted Goldeneye Pressure with and without Hoylake and Buffalo Prospect included in Regional Aquifer model

The match to the Rochelle West discovery well MDT pressure point from October 2010 referenced at datum 9500 ft TVDSS is reasonable as seen in Figure 11-11 except for the no additional aquifer case which gives too much depletion. The downscaling of permeability of the Eastern aquifer model is corroborated by the regional dynamic aquifer model which suggests lower permeabilities in the eastern aquifer by up to 45% to match pressures in the Rochelle field prior to start of Rochelle production. Given the relative coarseness of the por-perm relationship used to derive aquifer permeabilities (see Section 4 in the petrophysical report (14) this is not unreasonable.

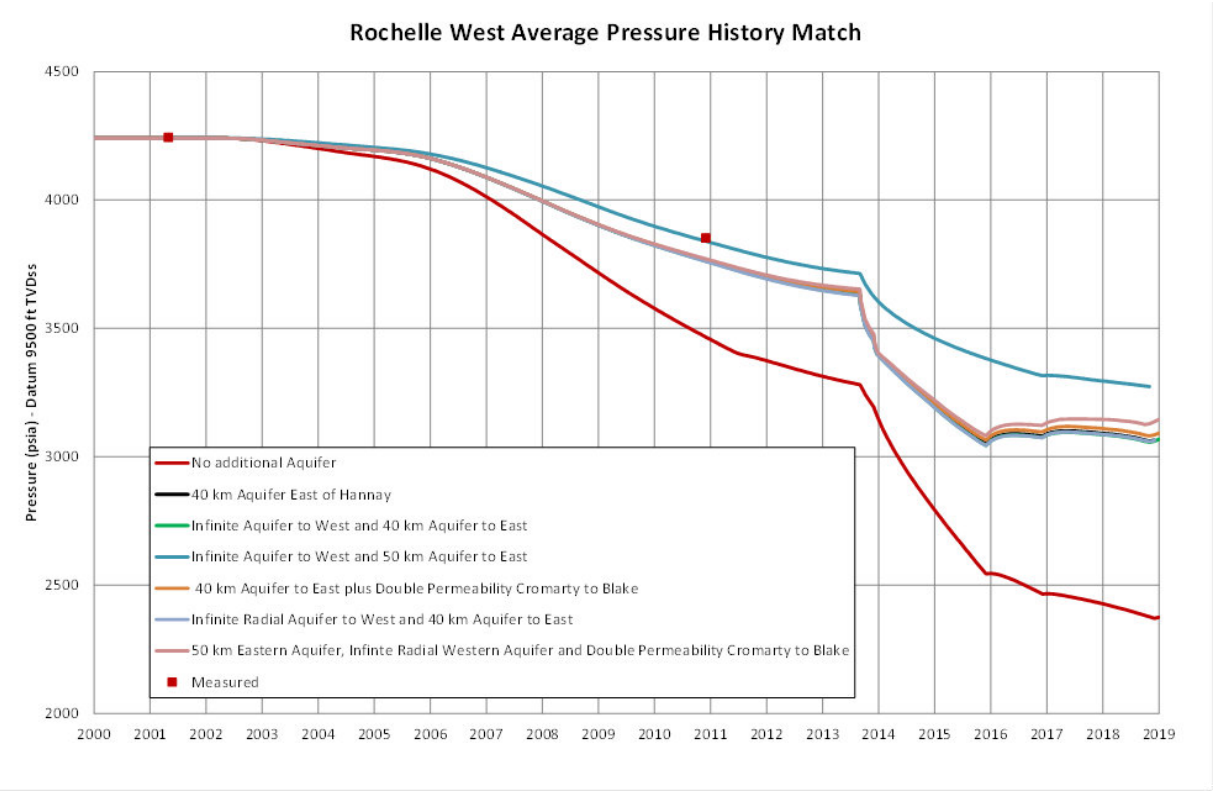

Figure 11-11: Rochelle West Pressure Match

For the other three fields in the model, only approximate (possibly inaccurate) pressure data are available.

For Blake the data were not felt to be accurate enough for matching purposes.

The match to Cromarty and Atlantic data is reasonable. Figure 11-12 and Figure 11-13 illustrate the match to these fields. The match to Cromarty in many cases is good whilst the match to Atlantic tends not to be as good with the pressures being 100 psi too low. A better match to the Atlantic pressure is obtained by increasing the permeability between Blake and Cromarty as in case 36 although this tends to raise the final pressure in Cromarty too much. As with Goldeneye and Hannay, cases with no additional aquifer support give pressures that are too low.

Due to the uncertainty about the pressures at Cromarty and Atlantic, and especially Blake, no definitive history match case was chosen and instead a variety of cases were used for further predictions.

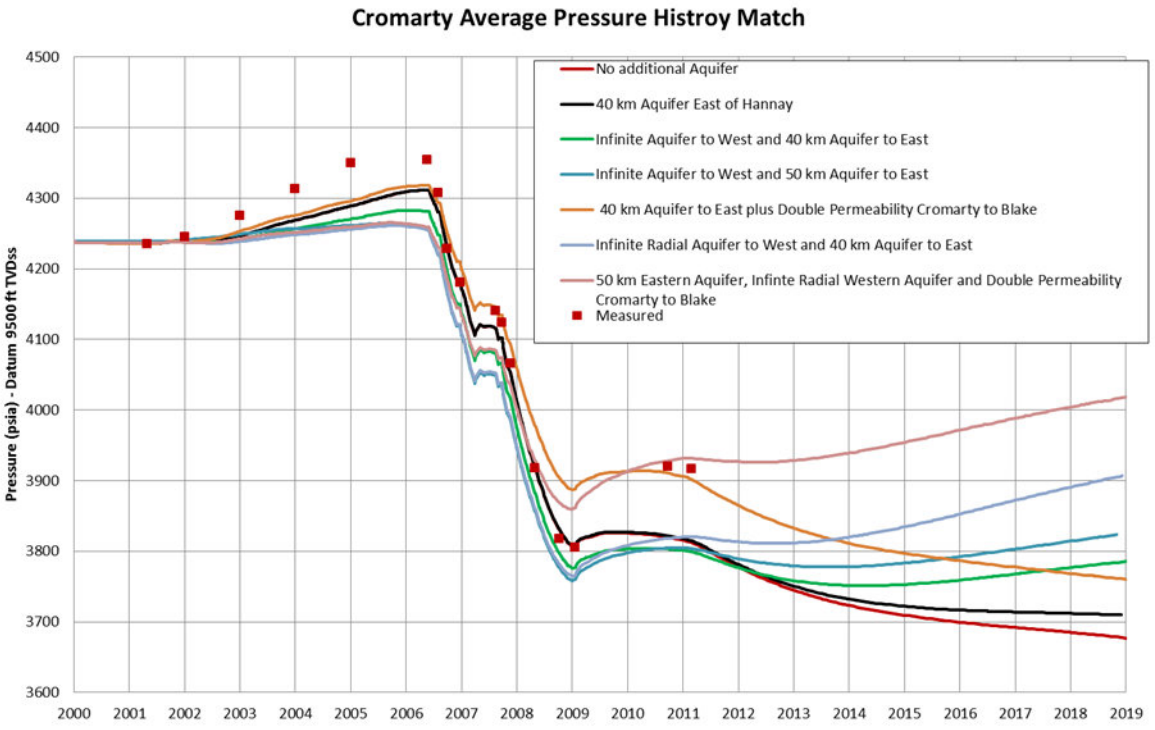

Figure 11-12. Cromarty pressure match.

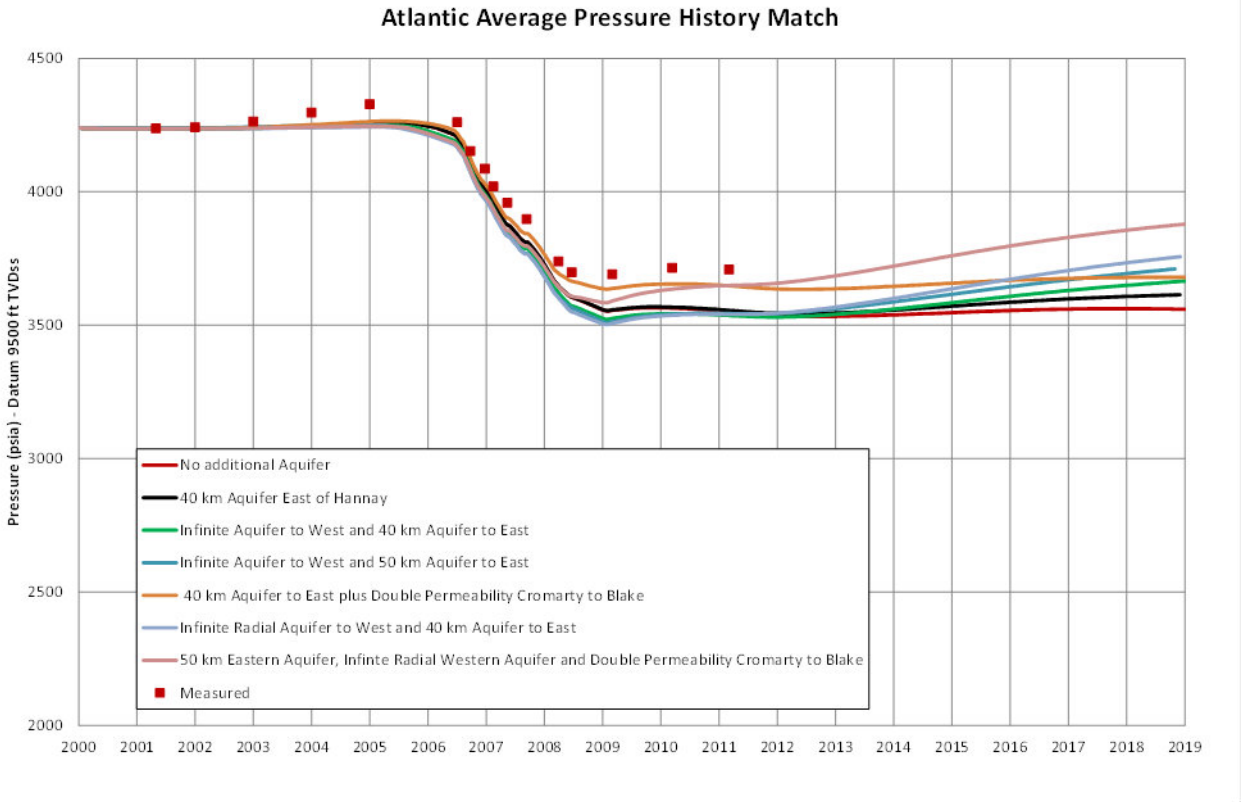

Figure 11-13. Atlantic pressure match.

11.12. Comparison of history match with FFM

The Goldeneye Fairway Regional Aquifer model pressure match is very similar to the FFM. However, there are differences between the models in the aquifer description and the resulting flows from the eastern and western aquifers. The FFM (Section 7.2.3) has a weak finite aquifer to the east and a stronger finite aquifer to the west. This contrasts to the Fairway Regional Aquifer model cases where the eastern aquifer is finite but slightly stronger and the western aquifer significantly stronger in some cases. The effects of these differences are illustrated in Figure 11-14 and Figure Figure 11-15 where the flows from the eastern and western aquifers into Goldeneye are illustrated for the FFM and the Fairway Regional Aquifer model.

The aquifer model case is case 34 (Table 11-5) with an infinite radial western aquifer and a 40 km additional eastern aquifer. The flows in the aquifer model are the fluxes across the boundary into the Goldeneye region which corresponds to the locations of the aquifers in the FFM. The aquifer model has a larger influx from the eastern aquifer than in the FFM and a correspondingly smaller influx from the western aquifer. One reason for the difference is the need to match the Hannay pressure in the aquifer model which results in a stronger (although smaller) eastern aquifer. The early production from Hannay reduces the early influx into Goldeneye but by 2007 the aquifer model has overtaken the FFM.

In order to investigate the effect of changing aquifer extent, a case was run with the FFM where the 40 finite eastern aquifer was replaced with a 50 km finite eastern aquifer, the history match was very similar showing that it is not possible to detect whether the aquifer is larger than 40 km.

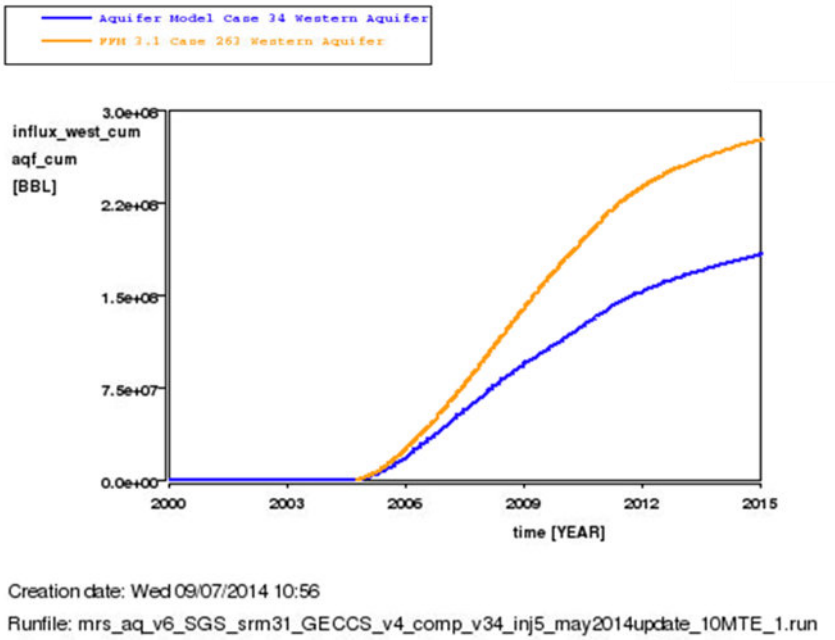

Figure 11-14. Comparison of flows from western aquifer for FFM and aquifer model.

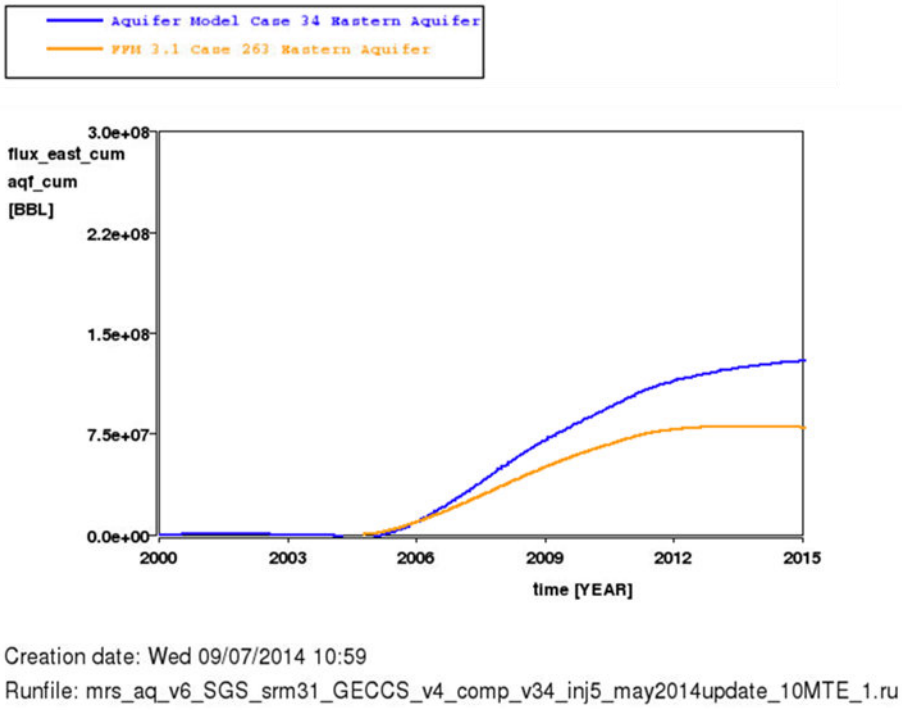

Figure 11-15. Comparison of flows from eastern aquifer for FFM and aquifer model.

11.13. Pressure Rise Following Shut in

A wide range of the cases discussed in the previous section were used to predict the pressure in Goldeneye over the period between hydrocarbon production ceasing at the end of 2010 and the start of CO_2 injection in 2015. These are illustrated in Figure 10 14 and listed in Table 10 6. The graph shows that there is little difference in the predicted pressures during the history match period, except for the case with no additional aquifer which has too low a pressure. During the shut-in period the different cases start to separate and the pressure in 2019 varies from 2703 psia to 2987 psia [186.4 bar to 206.0 bar] if Rochelle West and East production is accounted for and from 2873 psia to 3132 psia [198.1 bar to 216.0 bar] if Rochelle production is neglected, shown in Table 11-6. An additional case (infinite radial aquifer) is illustrated in Figure 11-14 (red dotted line) where the production from the Rochelle field has been excluded with an estimated increase in shut in pressure of 90 psia.

Part of the Rochelle East reservoir is outside the area of the model and the effect of Rochelle East was simulated by including the estimated reservoir volumes of Rochelle East into Rochelle West and producing the estimated reservoir volume of Rochelle East through the Rochelle West gas producer. The estimated reserves for the combined Rochelle fields are 35 MMboe.

For comparison with the aquifer model, the FFM pressure in 2019 is 2875 psia [198.3 bar].

The higher FFM pressure is partly due to the flow from the infinite eastern aquifer which, although quite weak, does not decrease as quickly as the finite eastern aquifer in the aquifer model.

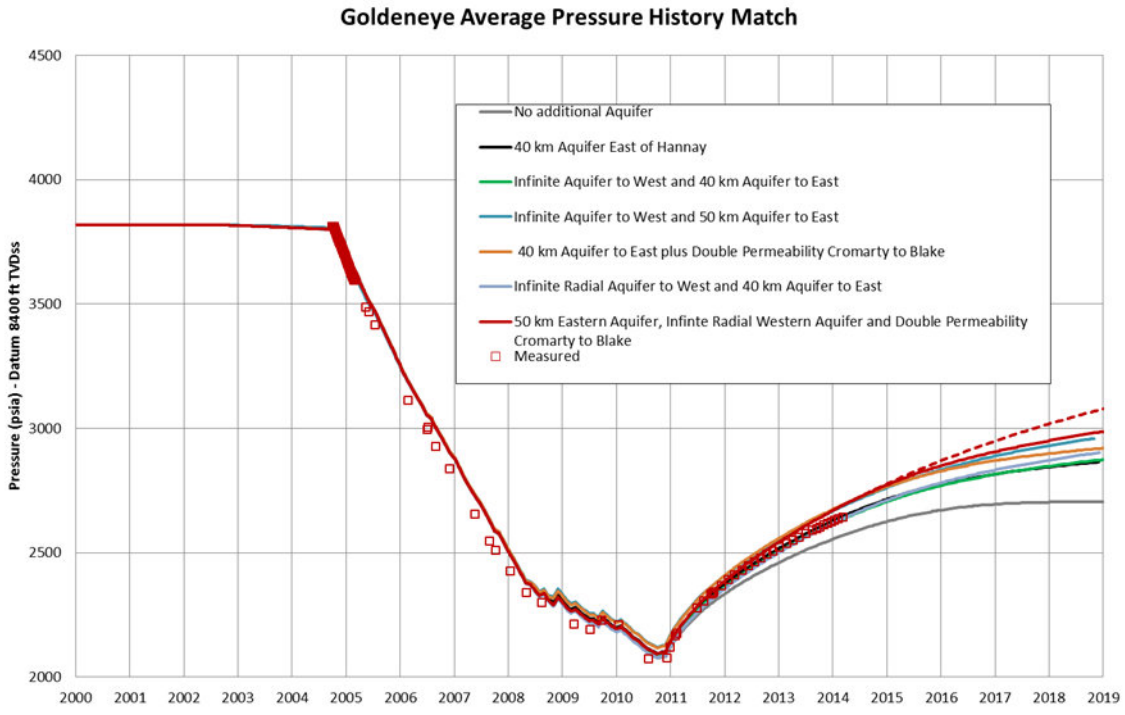

Figure 11-16. Predictions of Goldeneye pressure from field shut in at end 2010 to 2015.

Table 11-6. Predicted Goldeneye pressure at 1 January 2019.

Case	Western Aquifer	Eastern Aquifer	Permeability Changes	D Sand Pressure 1/1/2019 (psia)
9	No additional aquifer	No additional aquifer	None	2703
15	No additional aquifer	40 km aquifer	Permeability in east x 0.55	2867
22	infinite linear aquifer	40 km aquifer	Permeability in east x 0.55	2874
26	infinite linear aquifer	50 km aquifer	Permeability in east x 0.55	2951
27	No additional aquifer	40 km aquifer	Permeability in east x 0.55 and Blake to Cromarty x 2	2920
33	infinite radial aquifer	40 km aquifer	Permeability in east x 0.55	2905
34	infinite radial aquifer	50 km aquifer	Permeability in east x 0.55	2987
39	No additional aquifer	40 km aquifer	Permeability in east x 0.55	2379

11.14. CO_2 Injection

The aquifer model has been used to simulate CO_2 injection using the same strategy as in the FFM 10 million tonnes of CO_2 were injected over the 10 year period from 2019 to 2029 using two wells (GYA02 and GYA05). To improve the representation of the movement of CO_2, the grid in the Goldeneye area was refined in the top two layers of the D sand both laterally (in –x and –y direction by a factor 2) and vertically (by a factor 2)This brought the areal grid size in line with the FFM in the top D sand and also gave a higher vertical resolution at the top of this layer to better model CO_2 migration. Due to the refinement being carried out in MoReS after the up-scaling of the geological model, the FFM still has a better representation of the reservoir heterogeneity and should give a more accurate representation of fluid movement.

Figure 11-15, Figure 11-16, and Figure 11-17 illustrate the CO_2 distribution at the top of the D sand in the FFM, the aquifer model with no Local Grid Refinement (LGR) and the aquifer model with LGR after injecting 10 million tonne of CO_2. The aquifer model in this situation is Case 34 (in Table 11-6) with the strongest eastern and western aquifers to obtain similar pressures to the FFM. The CO_2 distribution within the refined aquifer model is closer to that of the FFM than the distribution within the unrefined aquifer model. However, the tongue of CO_2 at the southern flank of the field is more prominent in the FFM than in the aquifer models. The less detailed property resolution of the Goldeneye area in the aquifer model means that the predicted configuration of the CO_2 plume in the aquifer model should be treated with some caution as it may be partly an effect of the coarse grid and/or the use of LGR. Due to the poorer resolution of the aquifer model it has mainly been used for pressure predictions rather than calculations of storage capacity. It has, however, also been used to model migration beyond the spill point as this is not possible in the FFM due to its limited area.

The main reason for the difference in CO_2 plume configuration in the aquifer model is the different aquifer fluxes in the FFM and aquifer model. **Figure 11-18** and **Figure 11-19** compare the flow rates from the aquifers in the FFM with the equivalent flows in the aquifer model (with LGR). Although larger volumes have flowed from the eastern aquifer in the aquifer model during the history match, when CO_2 injection starts the aquifer influx from the east rapidly drops and reverses. However, in the FFM the aquifer flow does not reverse. This is a consequence of the finite eastern aquifer in the aquifer model.

These results suggest that the injected CO_2 may not extend as far to the west as the FFM indicates making the retention of the CO_2 in the reservoir more likely and implying the FFM storage capacity estimates are conservative.

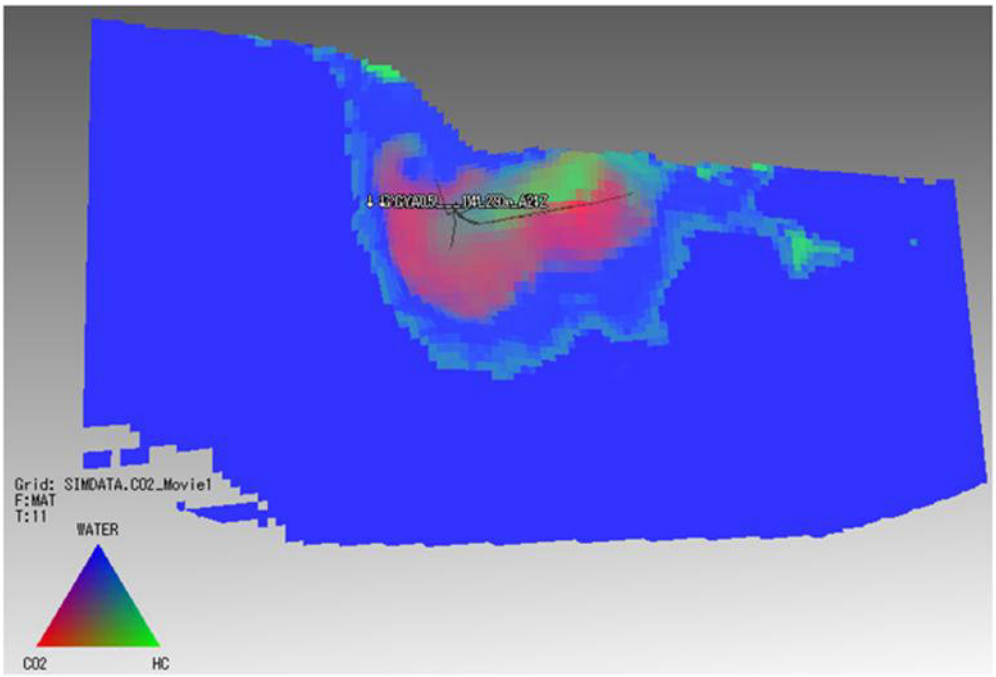

Figure 11-17. CO_2 distribution at top D in 2029 for FFM 3.1.

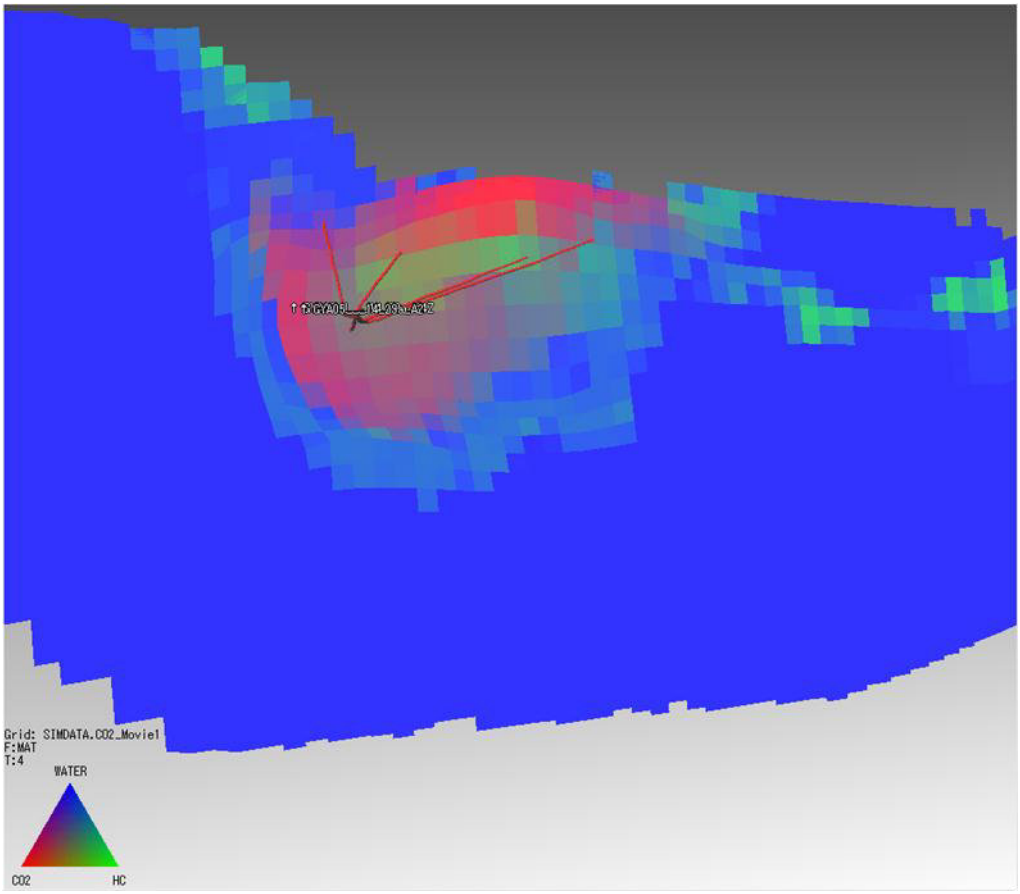

Figure 11-18. CO_2 distribution at top D in 2029 for aquifer model 34 with no LGR.

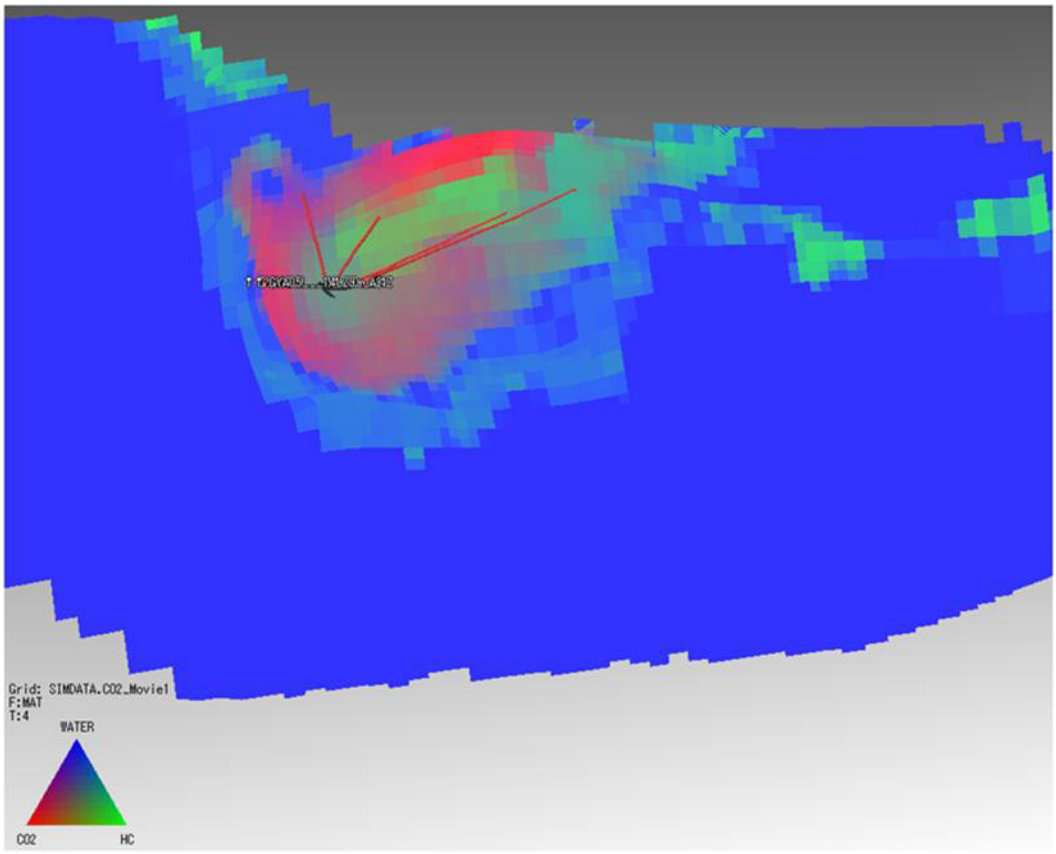

Figure 11-19. CO_2 distribution at top D in 2029 for aquifer model 34 with LGR.

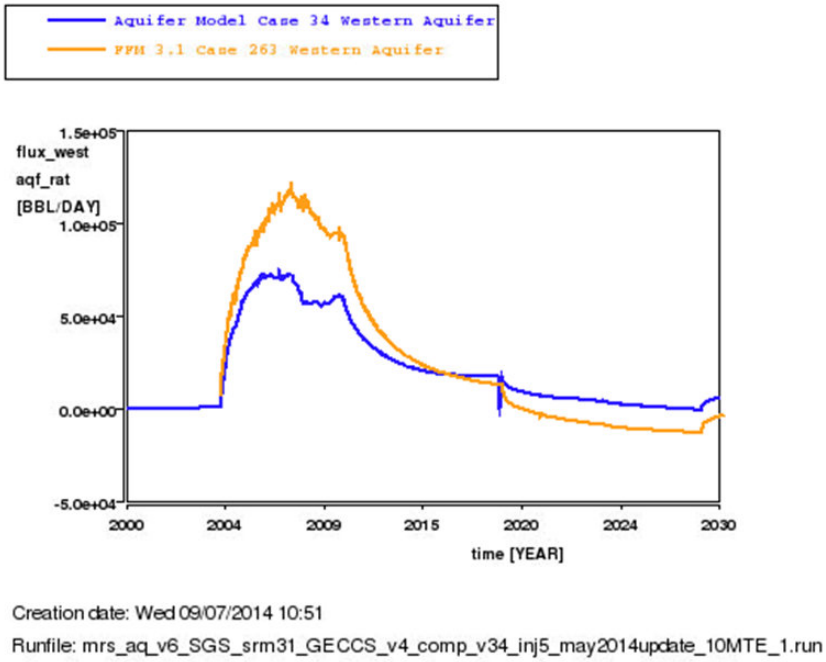

Figure 11-20. Comparison of western aquifer fluxes between FFM and aquifer model.

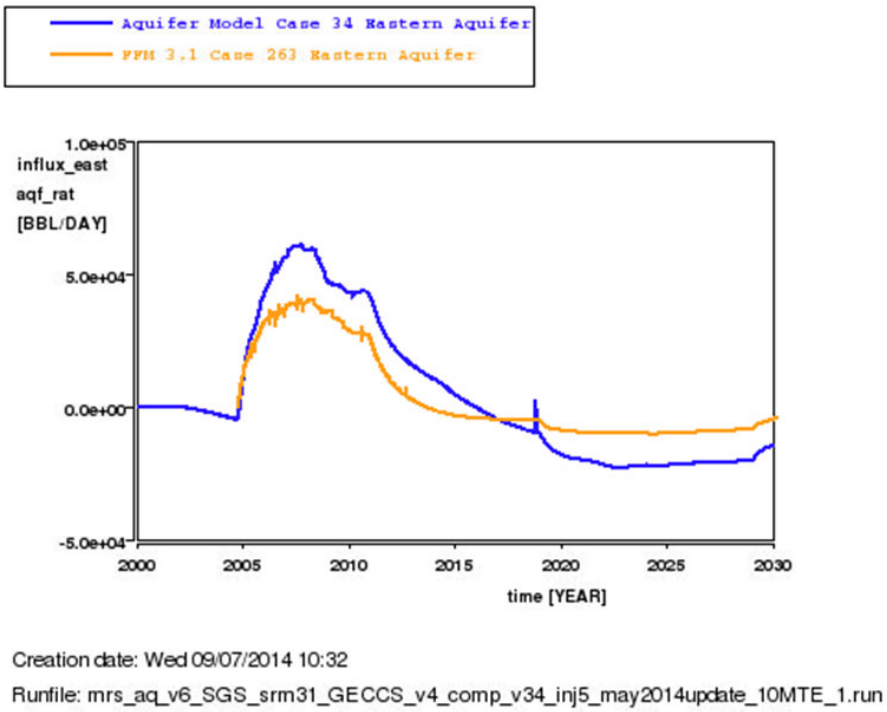

Figure 11-21. Comparison of eastern aquifer fluxes between FFM and aquifer model.

11.15. Pressure Change Post Injection

A number of history matched cases were run for up to 1000 years after the end of CO_2 injection in 2029, after having injected 10 Mt of CO_2. The results are illustrated in Figure 11-20 and Figure 11-21. The number of cases is limited as the models took over five days to run on multiple CPUs.

Immediately after the end of injection the pressure starts to decline as pressure starts to equalise across the model. This is then followed by a slow rise in pressure. Even with an infinite linear aquifer in the west this rise in pressure is slow. However, an infinite radial aquifer provides a much more rapid response and the reservoir is nearly back to initial pressure after approximately 200 years. Although the infinite radial aquifer responds much more rapidly in re-pressurising the reservoir, the difference over the 15 year period from the end of production to the end of injection is modest. The peak reservoir pressure at the end of injection is 89 psi higher with the infinite radial aquifer than with the infinite linear aquifer. In the cases using only an additional 40 km eastern aquifer the reservoir pressure does not return to its original value as there is no infinite western aquifer to continue to recharge the reservoir. The pressure at the end of injection in 2029 for the different cases is given in Table 11-7.

Figure 11-20 and Figure 11-21 include a case with Rochelle production as described in Section 11.13. The impact of Rochelle production is much more obvious after injection starts as the depletion from the reservoir starts to have an effect on Goldeneye pressure. A scenario without Rochelle production is shown for the infinite aquifer radial western aquifer case represented by dotted lines for comparison with the reference case which accounts for Rochelle production (solid line). The plot indicates that the Goldeneye pressures are being influenced by Rochelle production from 2016 onwards.

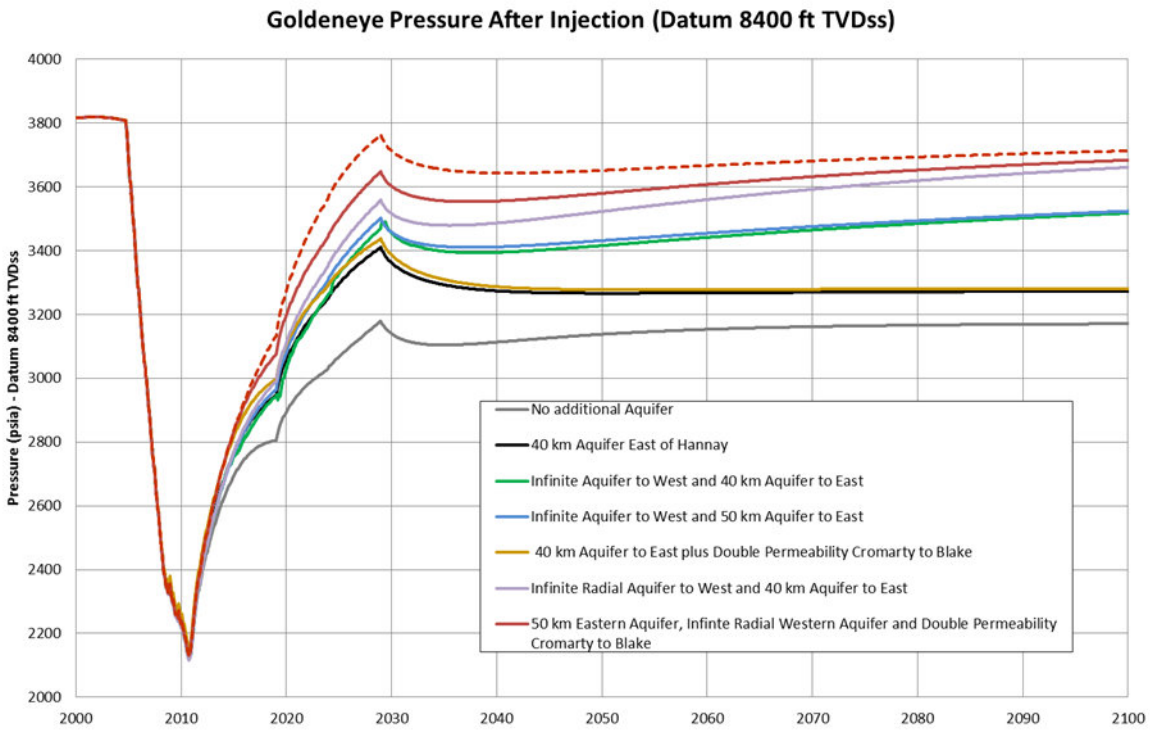

Figure 11-22. Pressure change over 75 year period after end of CO_2 injection.

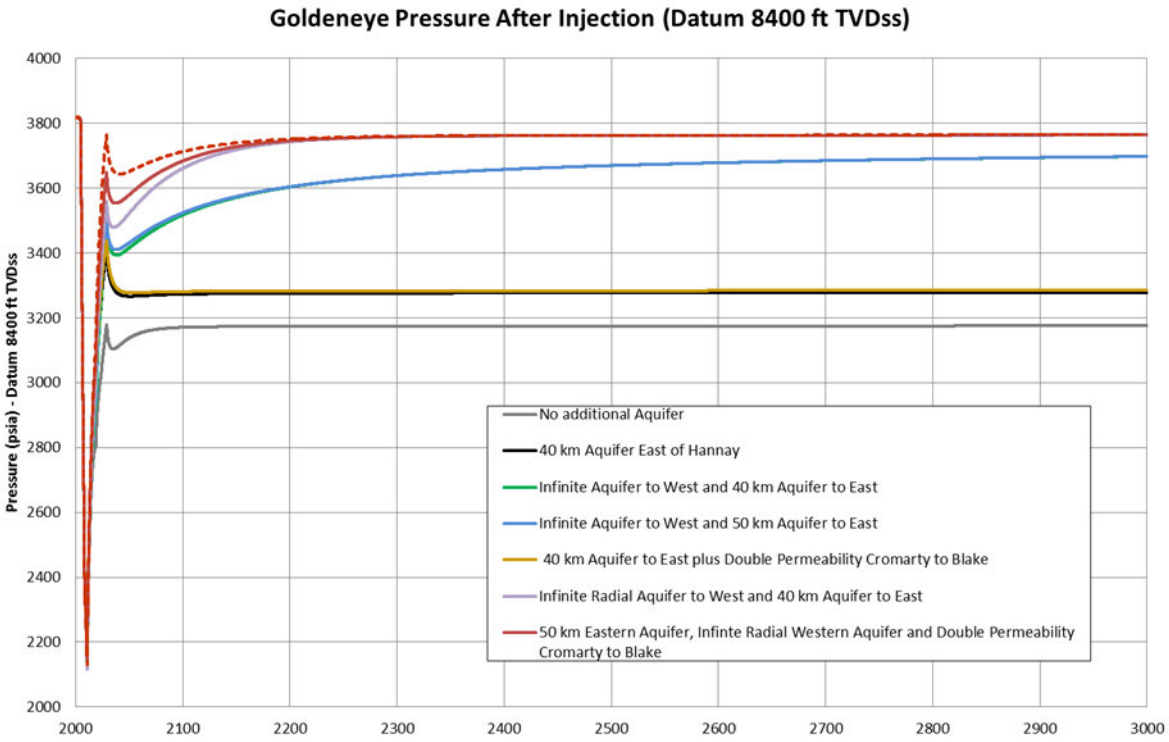

Figure 11-23. Pressure change over 1000 year period after end of CO_2 injection. Again, dotted line represents case without Rochelle production.

Table 11-7. Pressure in 2029 at end of CO_2 injection – 10 million tonnes

Case	Western Aquifer	Eastern Aquifer	Permeability Changes	D Sand Pressure 1/1/2029 (psia)
9	No additional aquifer	No additional aquifer	None	3177
15	No additional aquifer	40 km aquifer	Permeability in east x 0.55	3422
22	infinite linear aquifer	40 km aquifer	Permeability in east x 0.55	3485
26	infinite linear aquifer	50 km aquifer	Permeability in east x 0.55	3502
27	No additional aquifer	40 km aquifer	Permeability in east and Blake to Cromarty x 0.55	3438
33	infinite radial aquifer	40 km aquifer	Permeability in east x 0.55	3559
34	No additional aquifer	50 km aquifer	Permeability in east x 0.55, Rochelle production included	3648 (3770)

Figure 11-24 illustrates a traverse pressure profile across the regional aquifer model as a function of time for aquifer model 34. The pressure sink is caused by Goldeneye production. After cessation of production in December 2010 the pressure rises due to the regional aquifer encroachment. When

CO_2 injection starts in 2019 pressure starts to build-up around Goldeneye alongside the continuing aquifer encroachment. Pressures on the eastern side of the aquifer model remains low due to Rochelle production which takes place between 2014 and 2020. After Rochelle ceases production in 2020 pressures start to rise also in this part of the Captain fairway due to aquifer encroachment and continued CO_2 injection in Goldeneye. When Goldeneye ceases CO_2 injection in 2029, regional aquifer encroachment takes over and a slow rise in pressures begin. Even with the infinite radial aquifer model in the west this rise in pressure is very slow and only after 1000 years it may have just reached initial conditions of the Goldeneye field as shown in Figure 11-24.

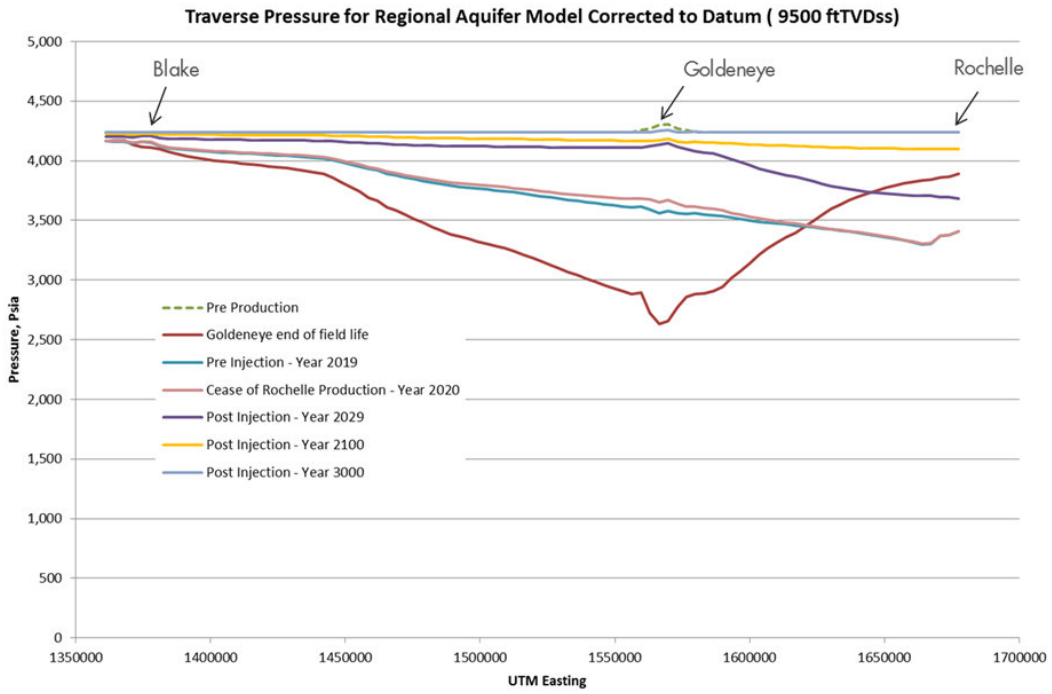

Figure 11-24: Traverse Pressure Plot for Aquifer Model 34.

A set of history matched cases were also run for the 20 Mt CO_2 injection cases until 2100 after the end of injection in 2039. The results are illustrated in Figure 11-25 and Table 11-8.

These give a range of pressures in year 2039 from 3404 psia to 3831 psia [23.47Mpa to 26.41Mpa]. Only the strongest aquifer, the infinite radial western aquifer recharges pressure to above initial hydrostatic pressure by some 17 psia.

A scenario without Rochelle production is shown for the infinite aquifer radial western aquifer case represented by dotted lines for comparison with the reference case which accounts for Rochelle.

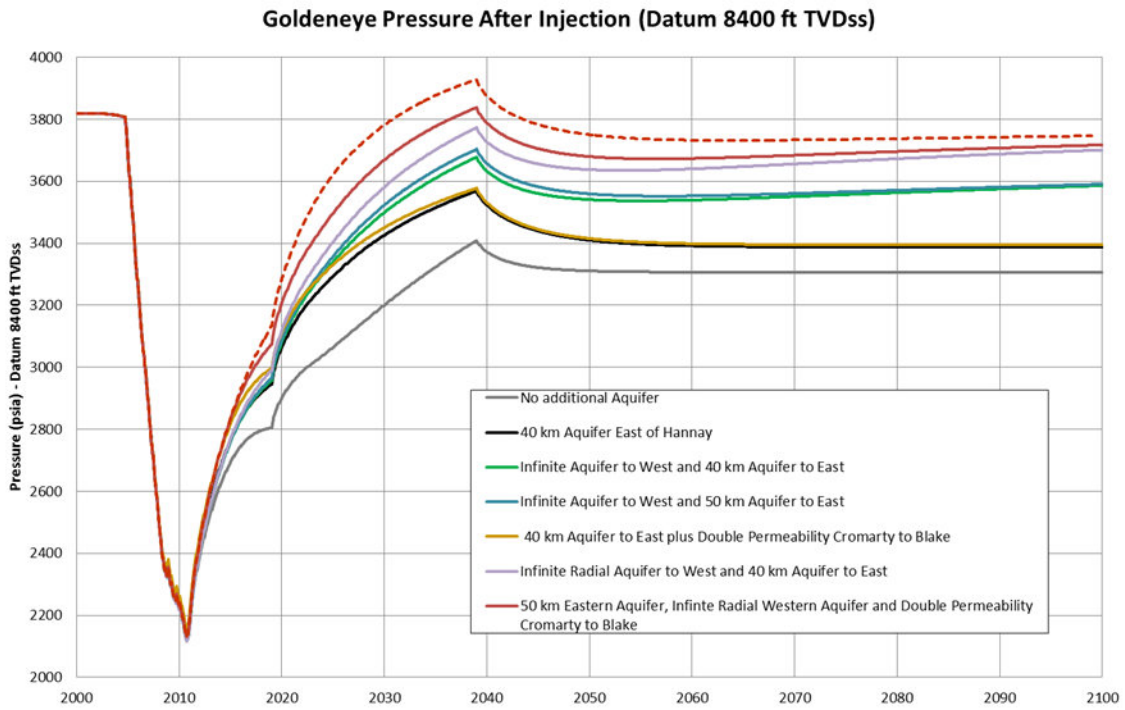

Figure 11-25: The pressure at end of injection in 2039 – 20 million tonnes of CO_2

Table 11-8: Pressure in 2039 at end of CO_2 injection after injecting 20 Mt of CO_2

Case	Western Aquifer	Eastern Aquifer	Permeability Changes	D Sand Pressure 1/1/2039 (psia)
9	No additional aquifer	No additional aquifer	None	3404
15	No additional aquifer	40 km aquifer	Permeability in east x 0.55	3562
22	infinite linear aquifer	40 km aquifer	Permeability in east x 0.55	3686
26	infinite linear aquifer	50 km aquifer	Permeability in east x 0.55	3702
27	No additional aquifer	40 km aquifer	Permeability in east and Blake to Cromarty x 0.55	3573
33	infinite radial aquifer	40 km aquifer	Permeability in east x 0.55	3765
34	No additional aquifer	50 km aquifer	Permeability in east x 0.55, Rochelle production included	3831 (3919)

11.16. Effect of CO_2 Dissolution

Most cases have been run without CO_2 dissolution as including this process significantly increases the model run time. However, a number of cases have been run with this option in order to determine the effect. Figure 11-26 illustrates the change in the mass of CO_2 dissolved in water for a case with

10 years injection followed by the field being shut in for 1000 years. By the end of CO_2 injection 0.9 Mt of CO_2 have dissolved in water and all of this is within the original gas cap. This is just below 5% of the injected CO_2. During the following 1000 years the amount of CO_2 dissolved in water slowly increases and it moves outside the original gas cap area. After 1000 years 1.55 Mt of CO_2 have dissolved in water with 0.6 Mt of this outside the original gas cap. As explained in Section 10.6 the amount of CO_2 dissolved in water in the model is overestimated, primarily due to the large grid block size. More details are available in Section 4.3 of the Geochemical Reactivity Report (4), which shows that about 5% of the CO_2 is dissolved.

Figure 11-27 is a cross section through the reservoir 1000 years after the end of injection showing the distribution of CO_2 in the water phase. The movement of CO_2 downdip and below the original contact is clearly seen.

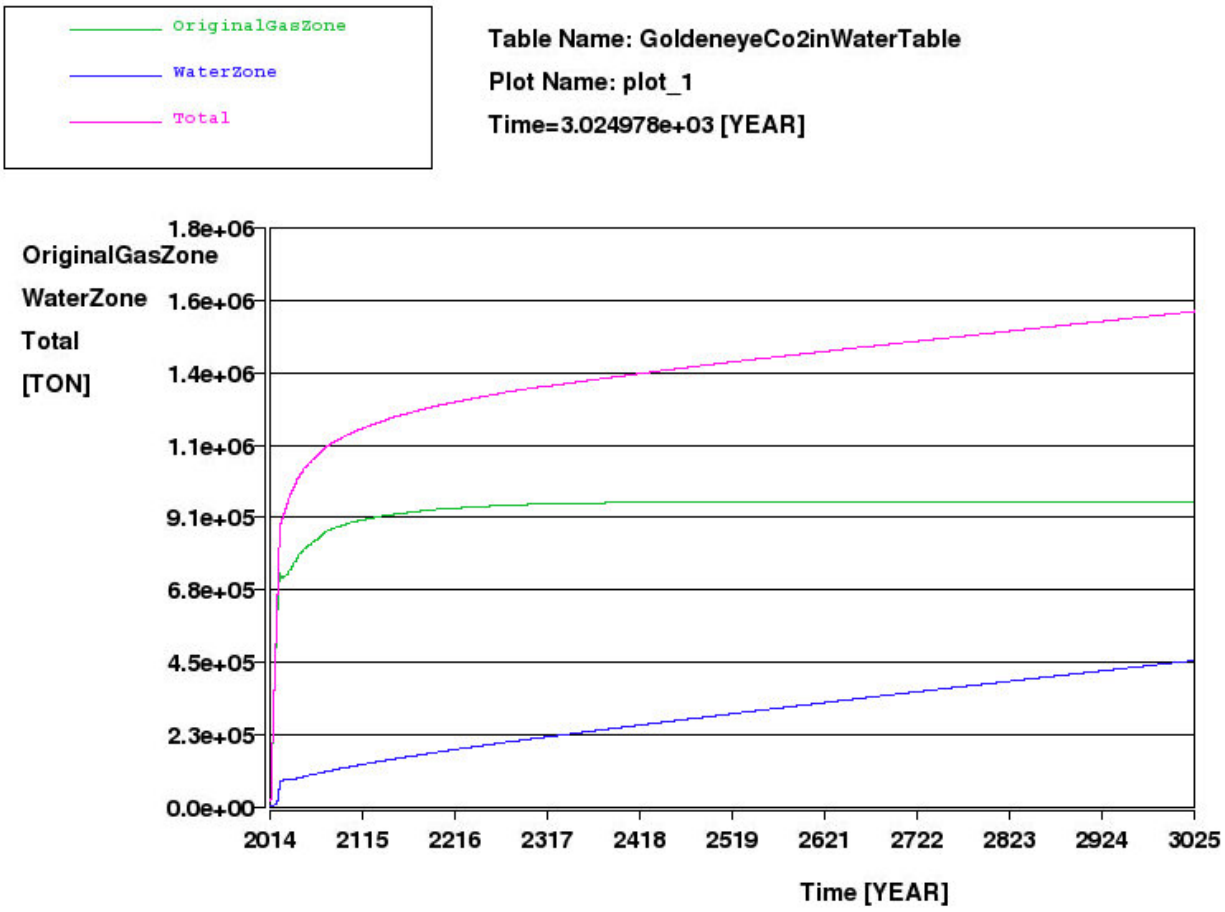

Figure 11-26. Mass of CO_2 dissolved in water for case 27 with 10 years injection followed by 1000 years shut in.

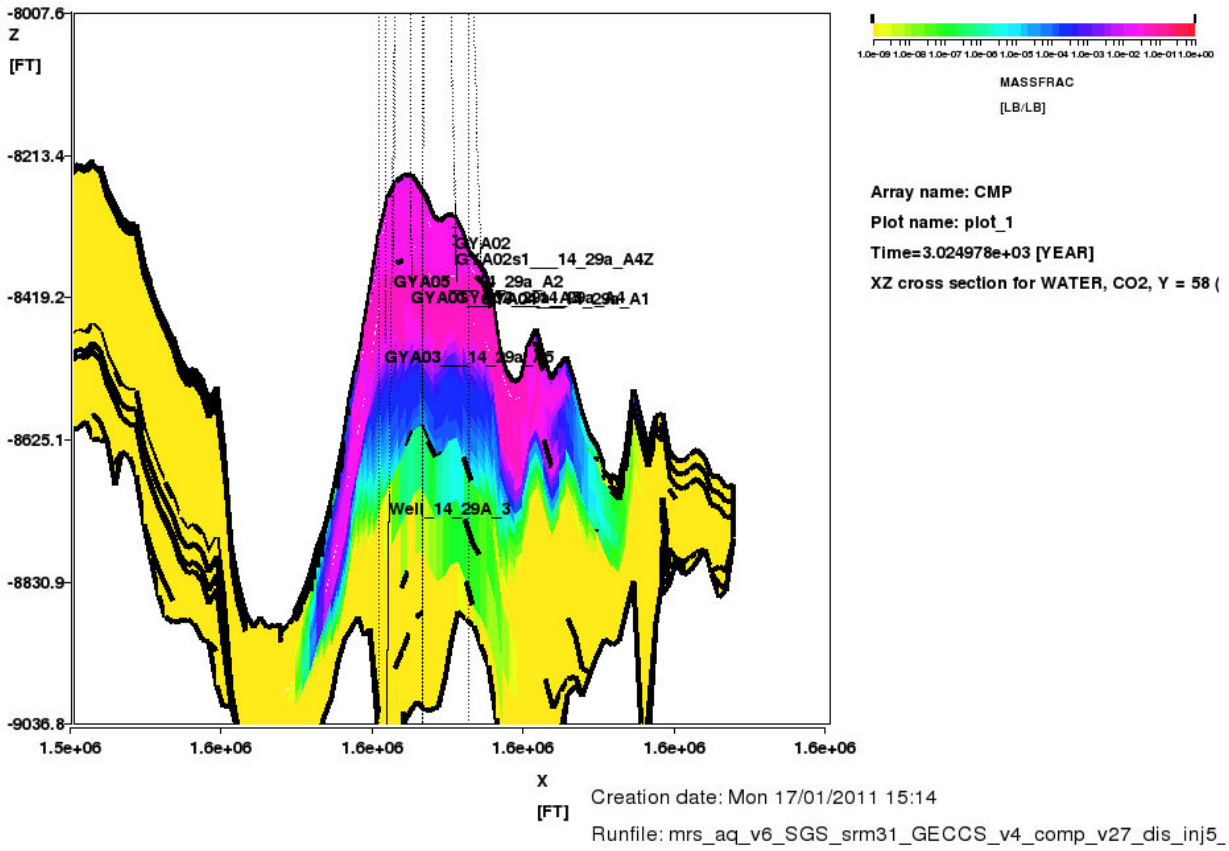

Figure 11-27. East west cross-section showing distribution of CO_2 in water 1000 years after end of injection (logarithmic scale). This CO_2 is dissolution trapped.

11.17. Migration of CO_2 beyond the Spill Point

As illustrated above, in the aquifer model the CO_2 does not migrate beyond the reservoir when only 20 million tonnes of CO_2 are injected. For this reason, during the Longannet study, two hypothetical cases were run where varying amounts of CO_2 were injected directly at the spill point to the west of Goldeneye. These cases included CO_2 dissolution, as this mechanism slows the migration of CO_2 from the reservoir. The cases involved the injection of 1 million and 5 million tonnes of CO_2.

Figure 11-28 and Figure 11-29 illustrate the 1 million tonne case after 28 years. Figure 11-28 is a 3D view of the top of the E sand. The CO_2 migrates updip away from the injection point. Figure 11-29 is a west-east cross-section through the model at the position of the spill point injection well. Most of the dense phase CO_2 migrates from the D sand where it was originally injected up into the lower permeability E sand, where it is able to migrate updip a distance of 2 km. A small amount remains behind trapped in the D sand as residual gas. Figure 11-30 illustrates the distribution of CO_2 after 100 years. The CO_2 has moved approximately 200 metres farther west. The model has been run on to 1000 years after the end of injection but there is very little further change in CO_2 distribution.

Figure 11-31 illustrates the 5 million tonne case after 28 years. The CO_2 spreads farther away from the well in this case. Some of the CO_2 still rises into the E sand leaving behind an area of trapped gas in the D sand but it migrates a longer distance of 4 km in the D sand and is still moving. After 100 years the CO_2 has moved less than 6 km up dip as illustrated in Figure 11-32 which is an aerial plot of the top of the D sand. The figure also illustrates the two closest abandoned exploration wells to the

west. Neither of these wells is near the plume. In the E sand the CO_2 has still only moved about 1.5 km due to the low permeability. Figure 11-33 shows that after 1000 years there is little further movement of CO_2 in the D sand. The total distance the CO_2 has moved remains about 6km but the saturations have reduced. This is due to CO_2 dissolving in water rather than migrating upwards to the E sand. Figure 11-34 shows the distribution of CO_2 in the top of the E sand after 1000 years. The spilled CO_2 is trapped along the northern edge of the model as in the D sand but has migrated only about 1.5 km due to the poorer reservoir properties.

Figure 11-35 illustrates the vertical distribution of CO_2 dissolved in water for the case with 5 million tonnes of CO_2 50 years after the end of injection. The CO_2 has migrated approximately 7 km and spread throughout the whole thickness of the reservoir. Figure 11-36 is the distribution of dissolved CO_2 at the top of the D sand illustrating the movement of the CO_2 away from the spill point to the west. CO_2 has migrated about 7 km to the west. Figure 11-37 illustrates the dissolved CO_2 in the E sand at the top of the reservoir; here the CO_2 has only migrated about 1.5 km.

In all cases the CO_2 plume does not reach the abandoned exploration wells to the west of Goldeneye as these wells are downdip of the plume.

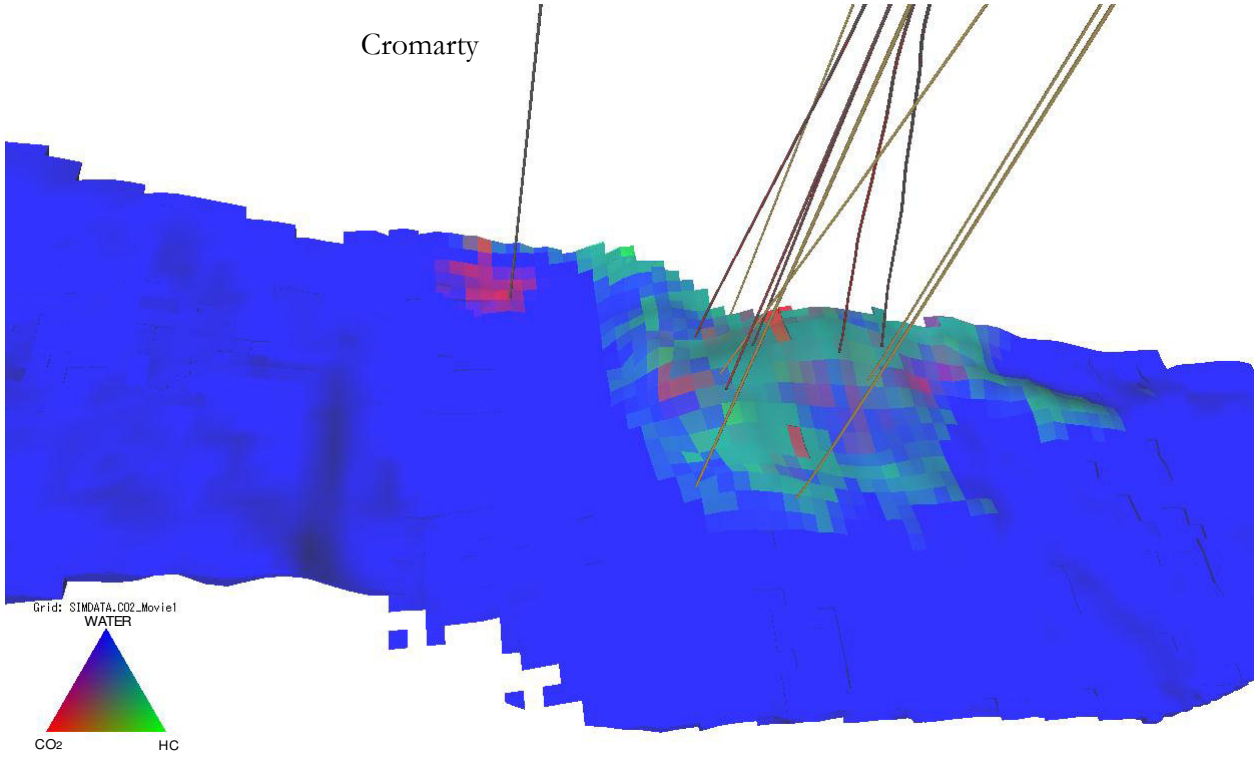

Figure 11-28. Distribution of CO_2 28 years after injection of 1 million tonnes at spill point in Case 22 model (top E)

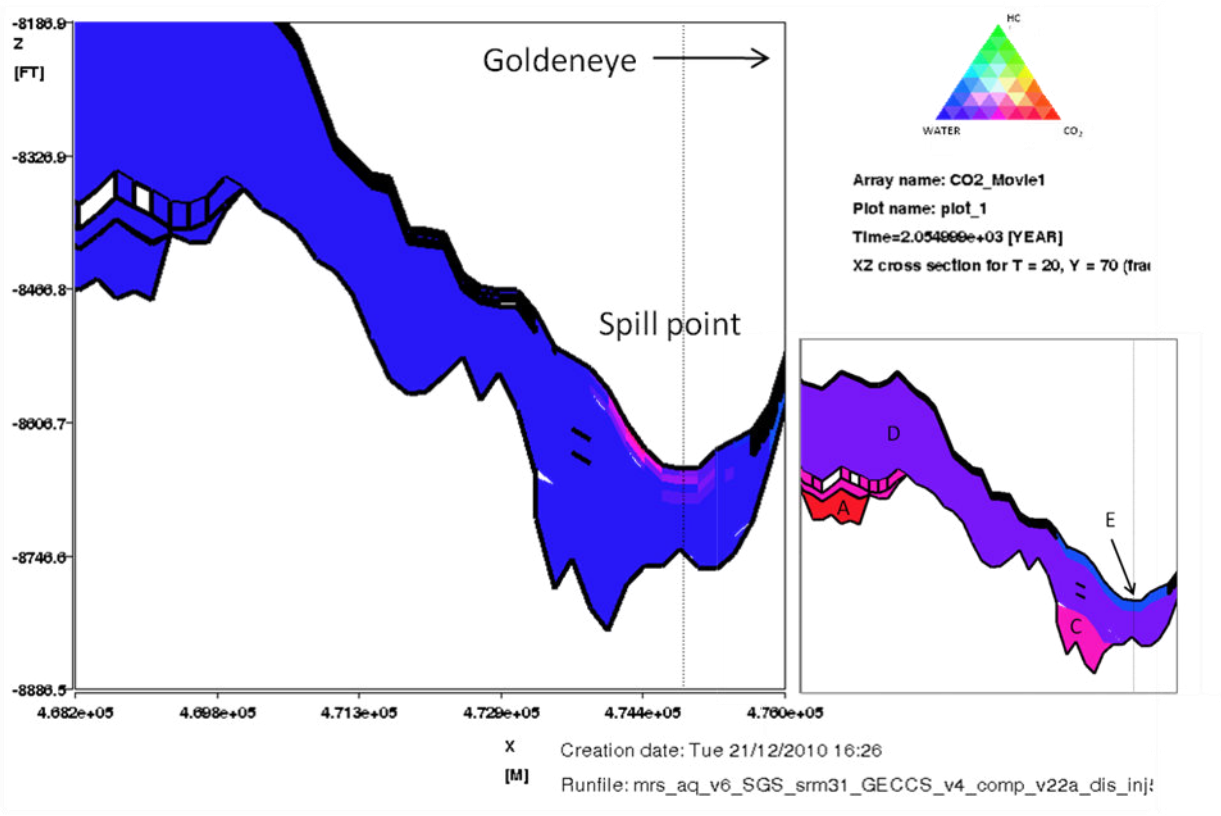

Figure 11-29. Distribution of CO_2 28 years after injection of 1 million tonnes at spill point in Case 22 model (west – east cross-section at Y=70).

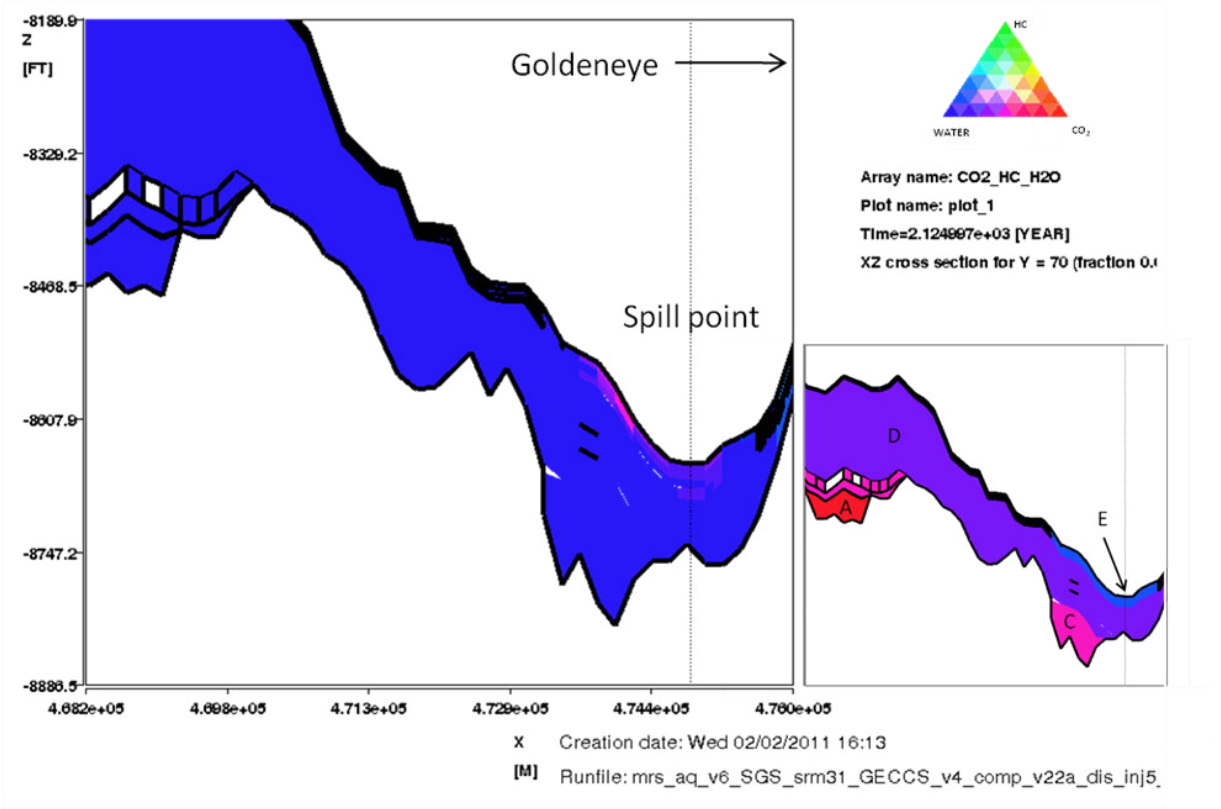

Figure 11-30. Distribution of CO_2 100 years after injection of 1 million tonnes at spill point in Case 22 model (west – east cross-section at Y=70).

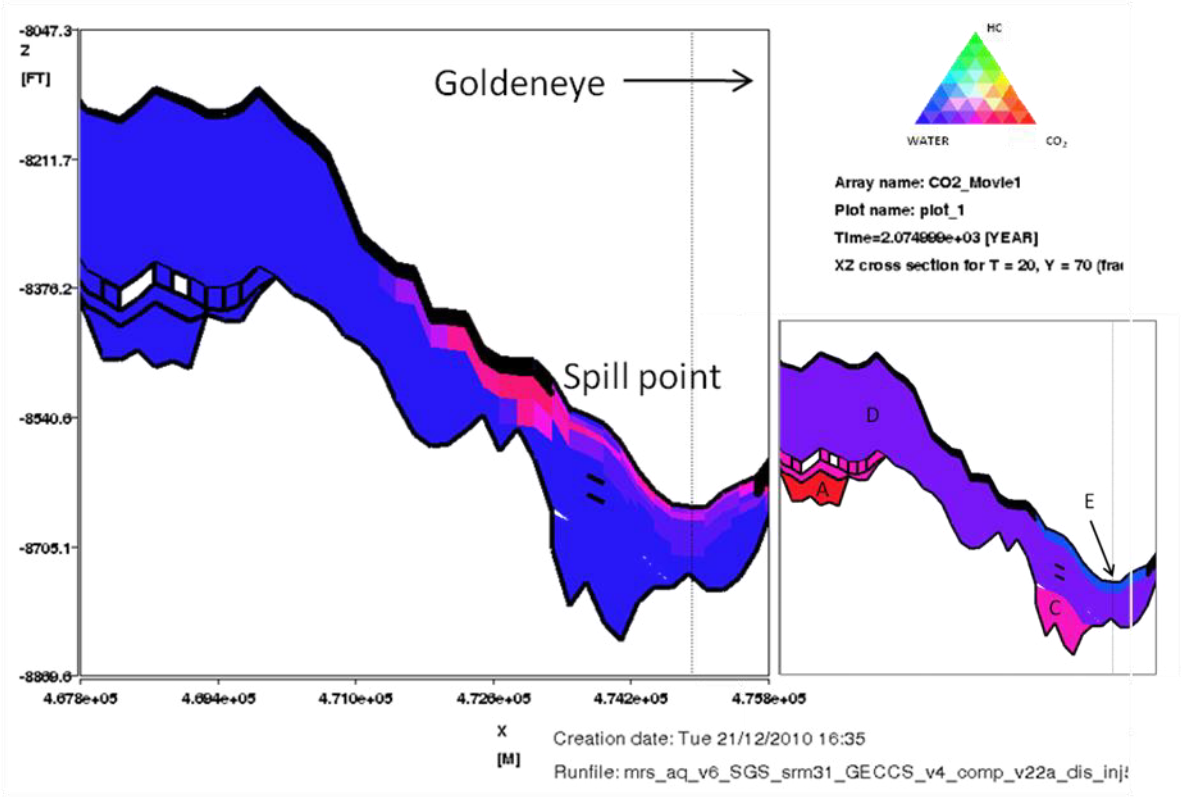

Figure 11-31. Distribution of CO_2 28 years after injection of 5 million tonnes at spill point in Case 22 model (west – east cross-section at Y=70).

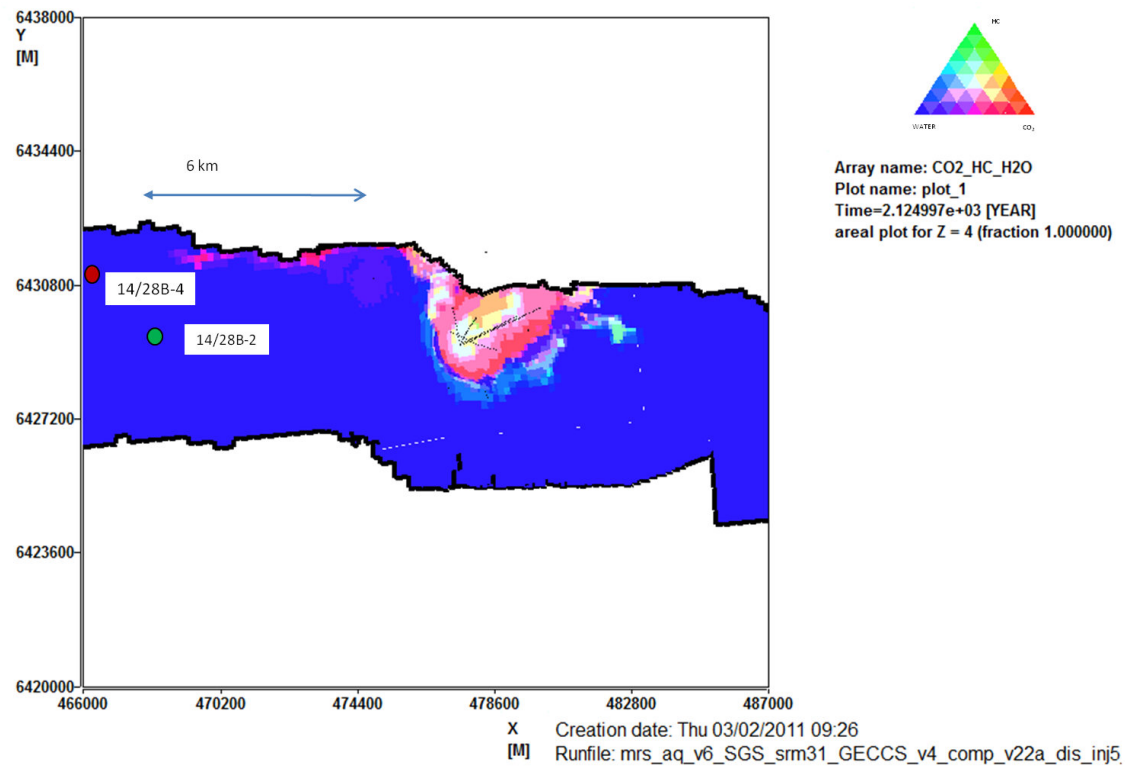

Figure 11-32. Distribution of CO_2 100 years after injection of 5 million tonnes at spill point in Case 22 model (top D, showing abandoned wells to west).

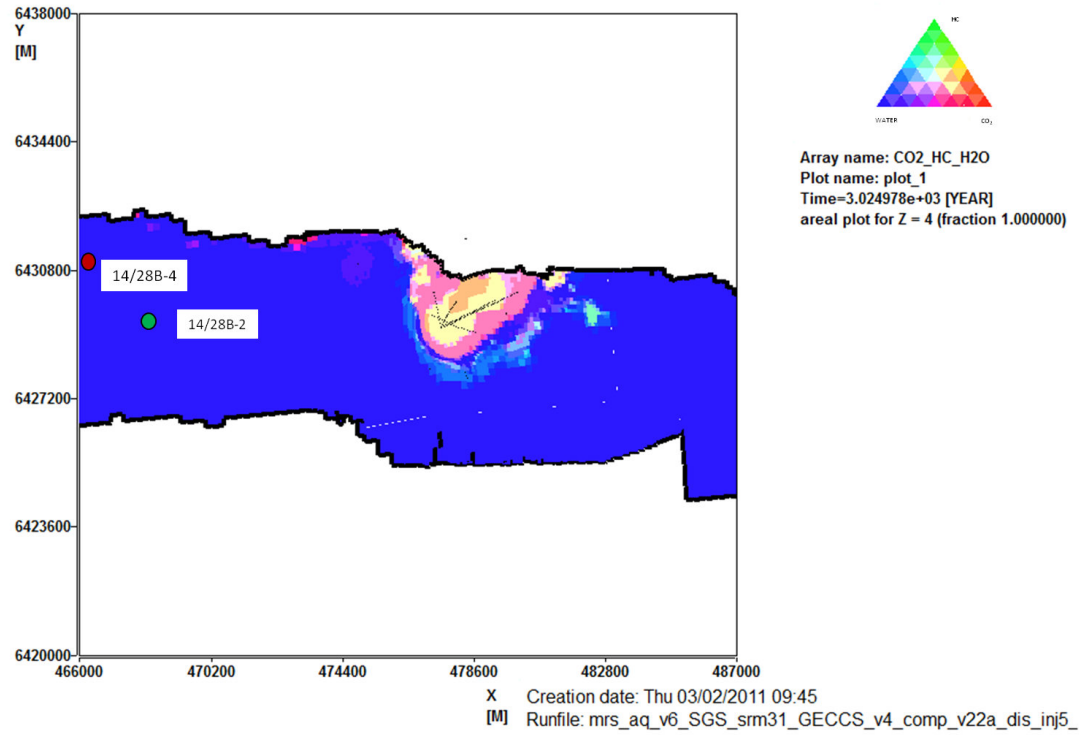

Figure 11-33. Distribution of CO_2 1000 years after injection of 5 million tonnes at spill point in Case 22 model (top D, showing abandoned wells to west).

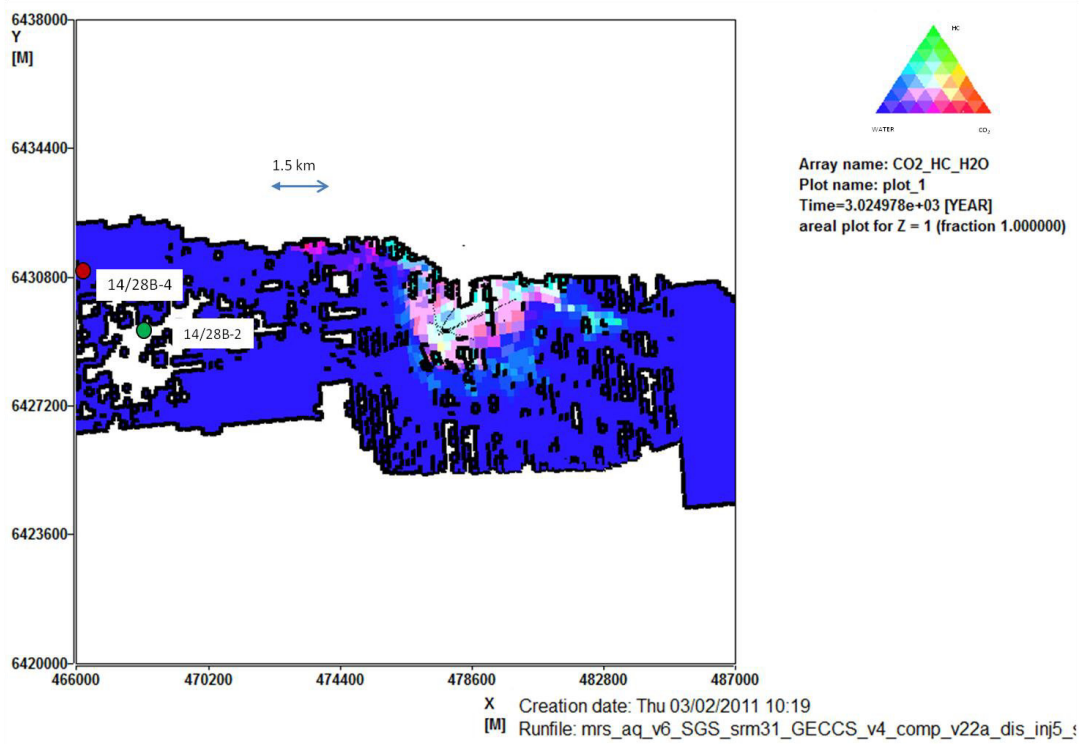

Figure 11-34. Distribution of CO_2 1000 years after injection of 5 million tonnes at spill point in Case 22 model (top E, showing abandoned wells to west).

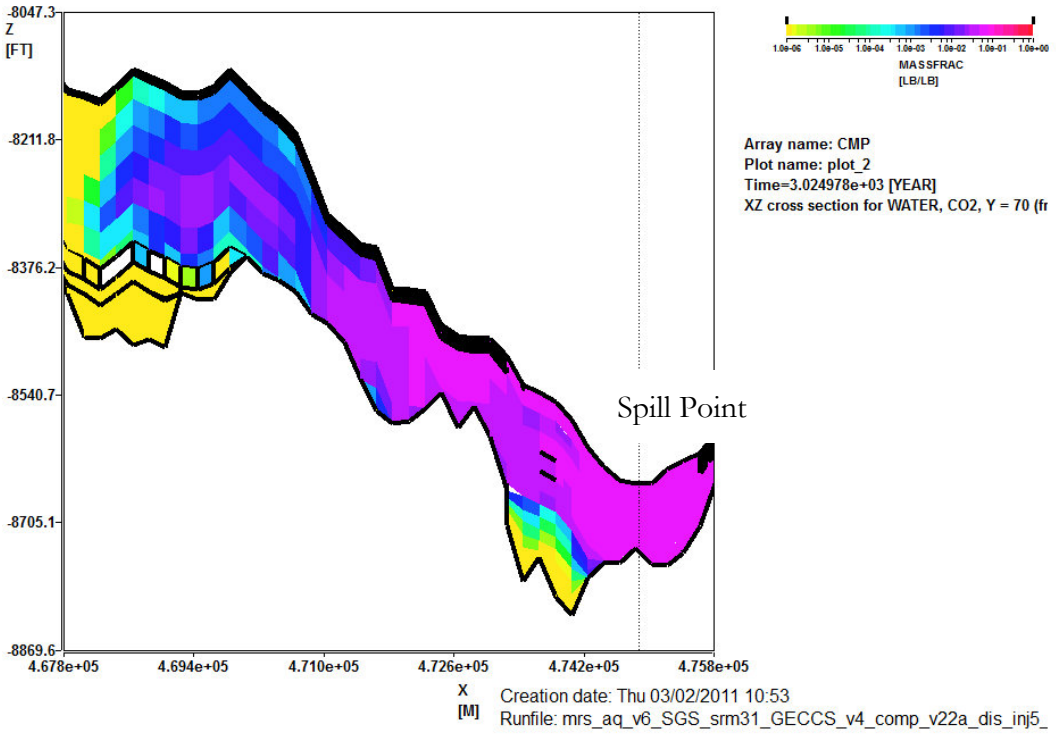

Figure 11-35. Distribution of CO_2 in water (dissolution trapping) 1000 years after injection of 5 million tonnes at spill point in Case 22 model (Y=70, logarithmic scale).

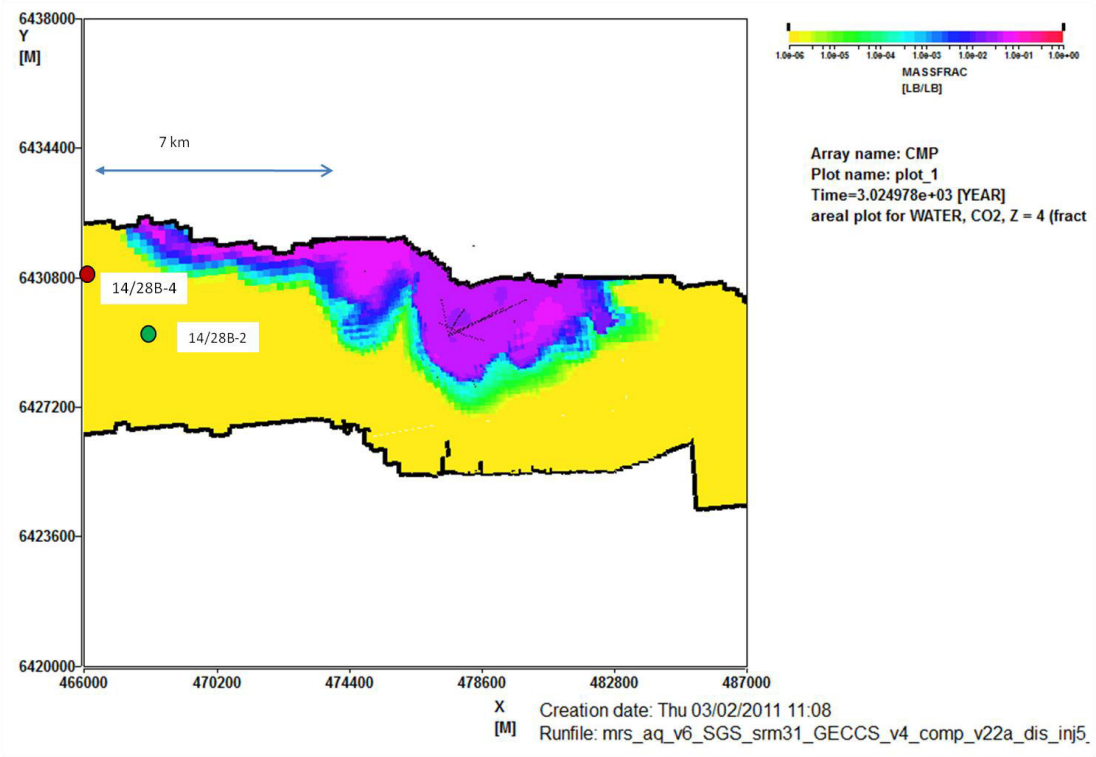

Figure 11-36. Distribution of CO_2 in water 1000 years after injection of 5 million tonnes at spill point in Case 22 model (top D, showing abandoned wells to west, logarithmic scale).

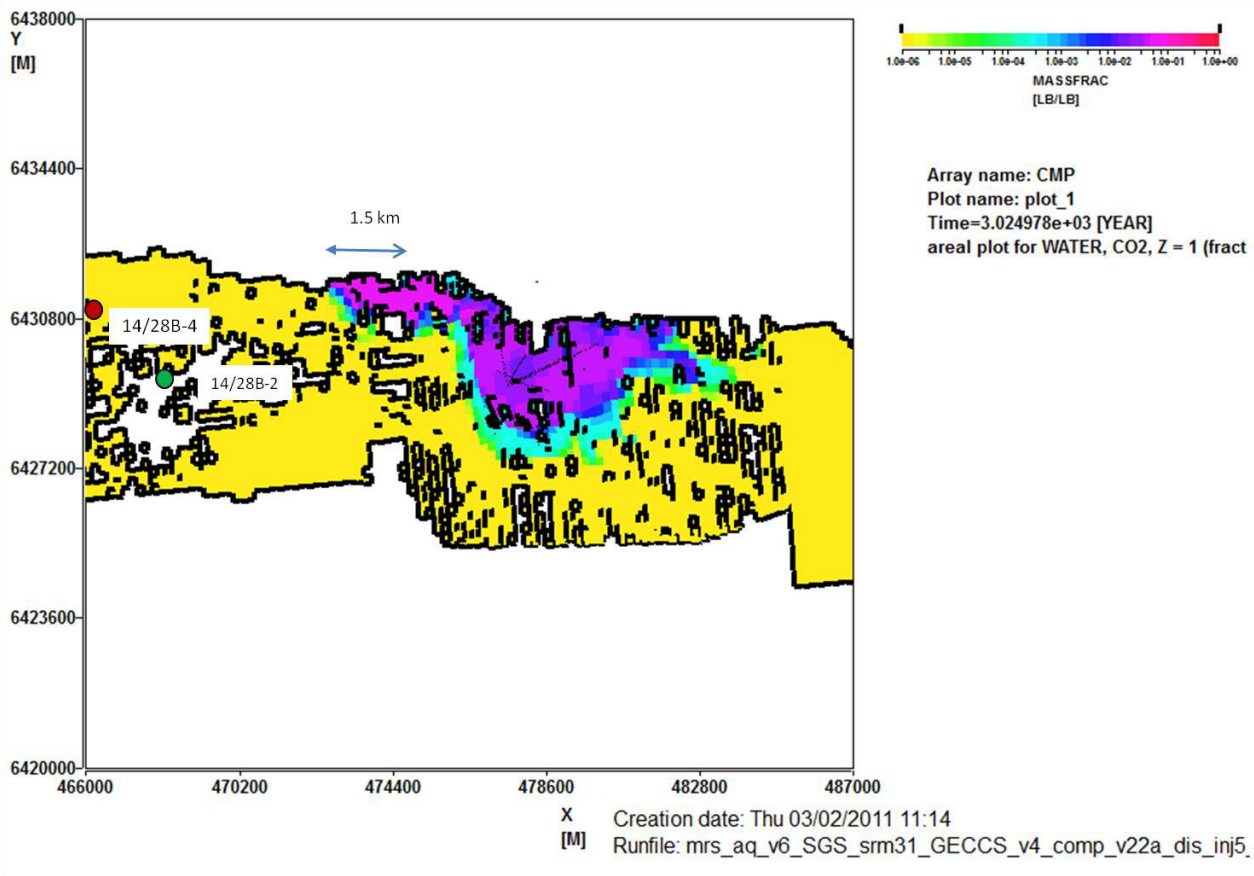

Figure 11-37. Distribution of CO_2 in water 1000 years after injection of 5 million tonnes at spill point in Case 22 model (top E, showing abandoned wells to west, logarithmic scale).

11.18. Effect of CO_2 Injection on Neighbouring Field Pressure

The three nearest fields to Goldeneye (Hannay, Atlantic and Cromarty) have all ceased production. The pressures in these fields have fallen, even after the end of production due to continuing production from Goldeneye. Now that Goldeneye is shut in the pressures in these fields have started to rise and this rise will accelerate once injection starts. The rise in pressure in Hannay, Atlantic and Cromarty is illustrated in Figure 11-38, Figure 11-39 and Figure 11-40. The pressure in Hannay rises rapidly up to about 300-500 psi over the period to 2029 if the impact of Rochelle is accounted for. When Rochelle production not accounted for the pressure is about 200 psi higher although the exact impact is uncertain. The pressure in Atlantic rises by 200 psi – 500 psi over the period to 2029 and is less affected by Rochelle. The predicted pressure rise in Cromarty is similar to Atlantic but is very uncertain as it is close to Blake which is still in production and subject to water injection. The rise in pressure in Rochelle West is illustrated in Figure 11-41. After Rochelle East/West ceases to produce, around the year 2020, the pressure rises rapidly by about 400 psi over the period to 2029.

It should be noted that activities in other fields will also affect the pressures in these fields and not all of these activities have been modelled (e.g water injection in Blake has not been modelled and modelling of Rochelle production is very rudimentary (combines Rochelle West and East into one field).

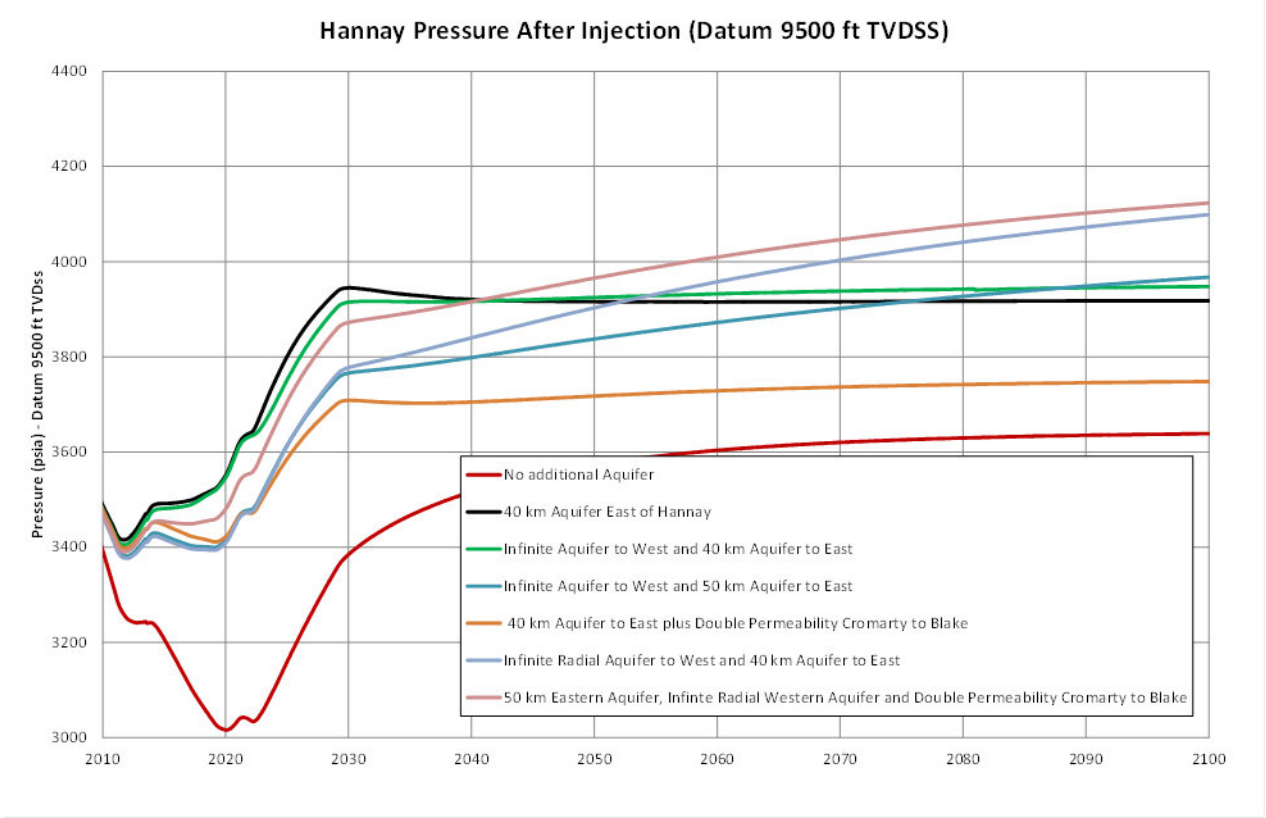

Figure 11-38. Rise in Hannay pressure after end of Goldeneye production.

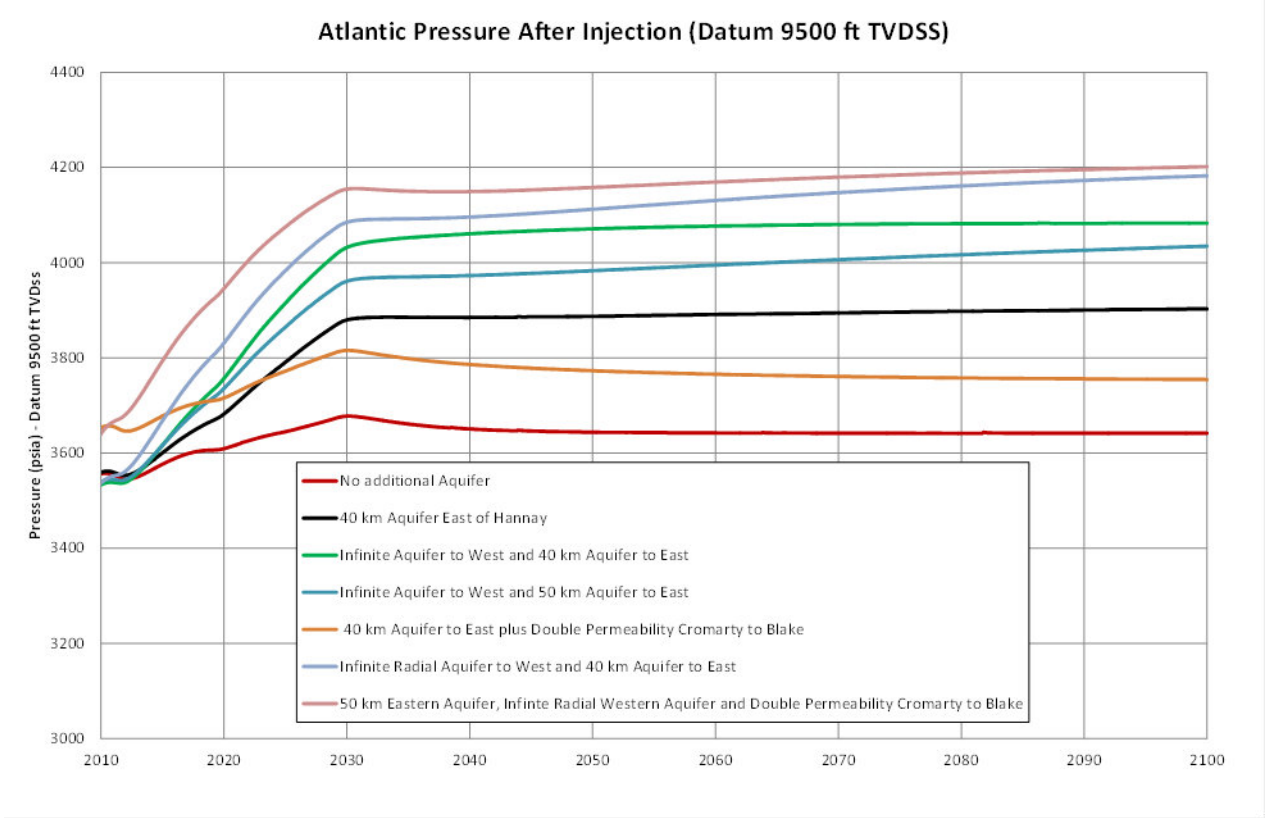

Figure 11-39. Rise in Atlantic pressure after end of Goldeneye production.

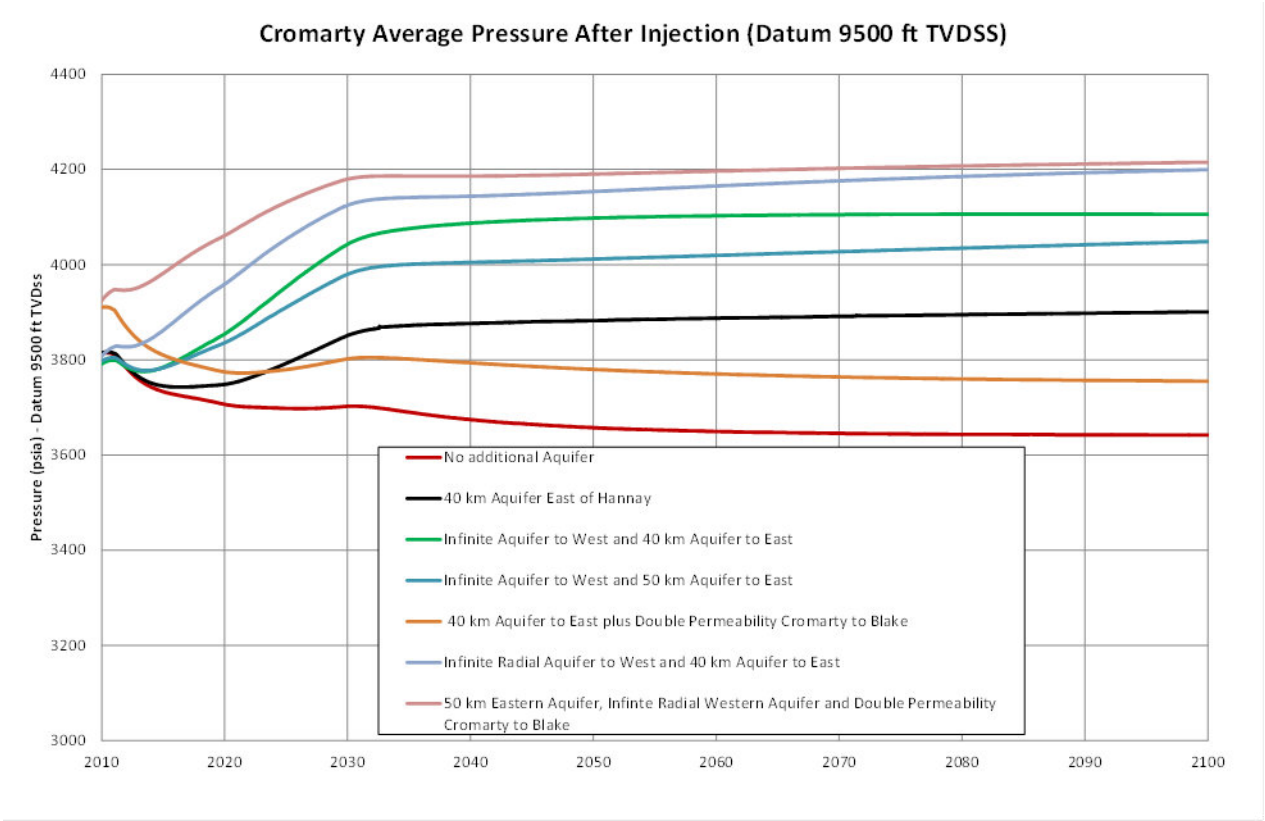

Figure 11-40. Rise in Cromarty pressure after end of Goldeneye production.

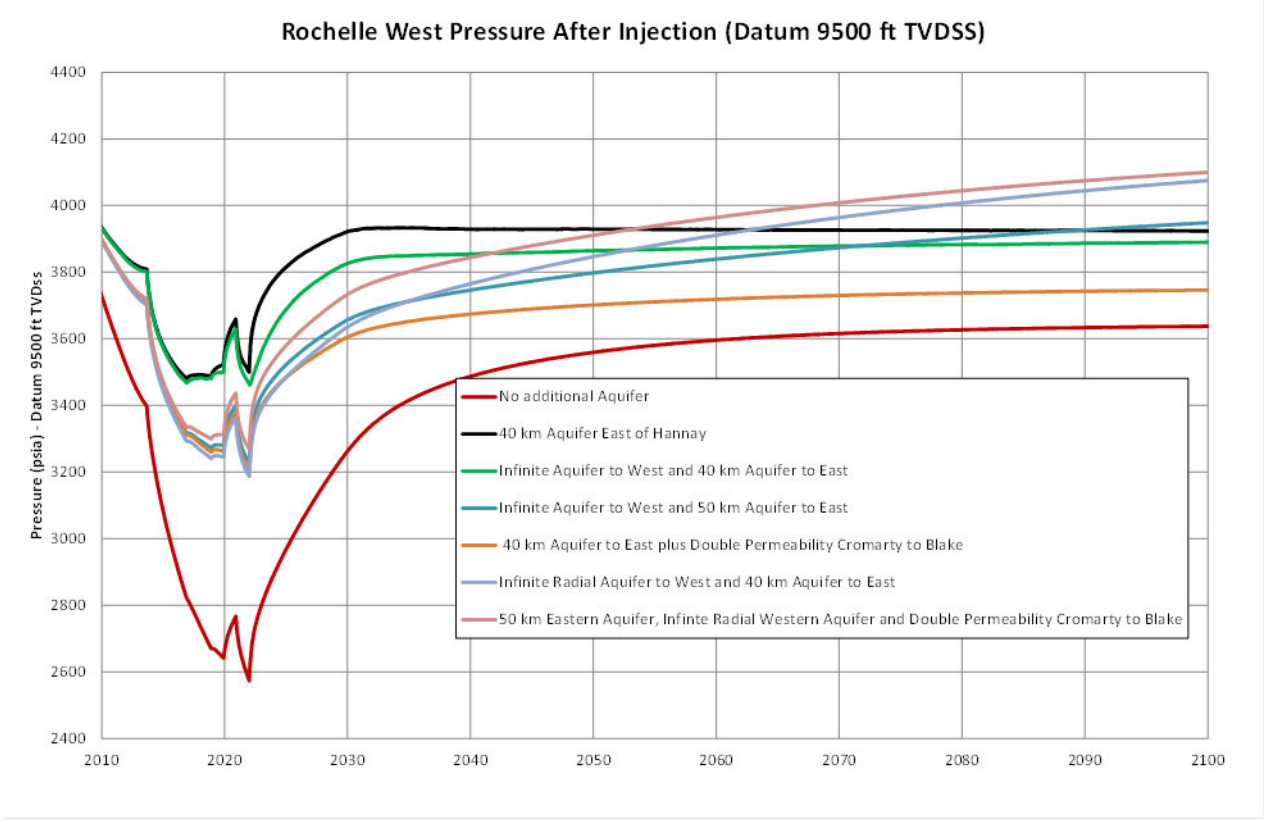

Figure 11-41: Rise in Rochelle West pressure after end of Goldeneye production.

11.19. Summary of Results

A dynamic model of approximately 100 km of the Captain sandstone has been created which contains Goldeneye and four other fields. A range of history match cases have been run but a unique match to the available data is not possible. An additional aquifer is required to the east of Rochelle in order to provide pressure support for Hannay and Rochelle. A 40-50 km aquifer in the east is sufficient to match the long term pressure decline in Hannay as well as in Rochelle prior to start of production in Rochelle in 2013. The western aquifer needs to extend beyond the Grampian Arch but exactly how far to the west the aquifer extends is not clear. The western aquifer could be effectively infinite as the formation is thought to outcrop at the sea bed west of Blake.

A range of models has been used to predict future pressures in Goldeneye. These give a range of pressures in year 2019 from 2703 psia to 2987 psia [186.4 bar to 206.0 bar].

Limited data is available for the Rochelle reservoir but the impact of its production from 2013 until 2015 seems to be limited but it could have a significant impact after this. The lower reservoir pressure would allow more CO_2 to be stored in Goldeneye and the surrounding Captain aquifer.

In all cases the 10 and 20 million tonnes of injected CO_2 does not reach the spill point. The model is more optimistic than the FFM in terms of the extent of the CO_2 plume due to the different distribution of aquifer influx and the inclusion of production from Hannay. This gives high confidence that the storage capacity estimate from the FFM is achievable.

CO_2 dissolution traps approximately 5% of the injected CO_2 but this is thought to be optimistic due to factors such as the large grid size.

Injecting CO_2 directly at the spill point allows the evaluation of CO_2 migrating updip. This is a slow process due to the varying dip of the formation. After 1000 years 5 million tonnes of CO_2 has migrated 6-7 km and is dissolving in the aquifer water. The CO_2 does not reach the two nearest abandoned wells to the west of Goldeneye as these are downdip from the plume or too far to the west.

The pressure in Hannay is most affected by Goldeneye and the pressure in this field will rise most rapidly now that Goldeneye is shut in. However, it is also the field most likely to be affected by Rochelle production which starts in 2012 and so its pressure is most uncertain. The rise in pressure to 2029 is probably in the range 300 - 500 psi [20.7 – 34.5 bar]. Atlantic and Cromarty pressures will also rise by 200 - 500 psi [13.8 – 34.5 bar] over the period to 2029 but this is also uncertain as they are more sensitive to the size of the western aquifer and the impact of continuing production and injection at Blake. After cessation of production in Rochelle West and East around 2020 the pressures rise rapidly by about 400 psi [27 bar] over the period to 2029.

12. Secondary containment/migration modelling

In the unlikely event of vertical migration from the storage site, CO_2 could pass from the Captain Reservoir and accumulate or migrate through permeable lithologies above the Goldeneye field. An overburden assessment has been conducted to identify possible secondary containment. If CO_2 passes the storage seal – *e.g.*, through well bores or faults – it is expected to migrate into shallower, permeable formations beneath the complex seal of the Lista and Dornoch mudstones. These include the low permeability Chalk Group and the interbedded sandstones and mudstones of the Montrose Group (including the Balmoral and Mey Sandstone Members of the Lista Formation) and the lower part of the Moray Group (Lower Dornoch sandstone).

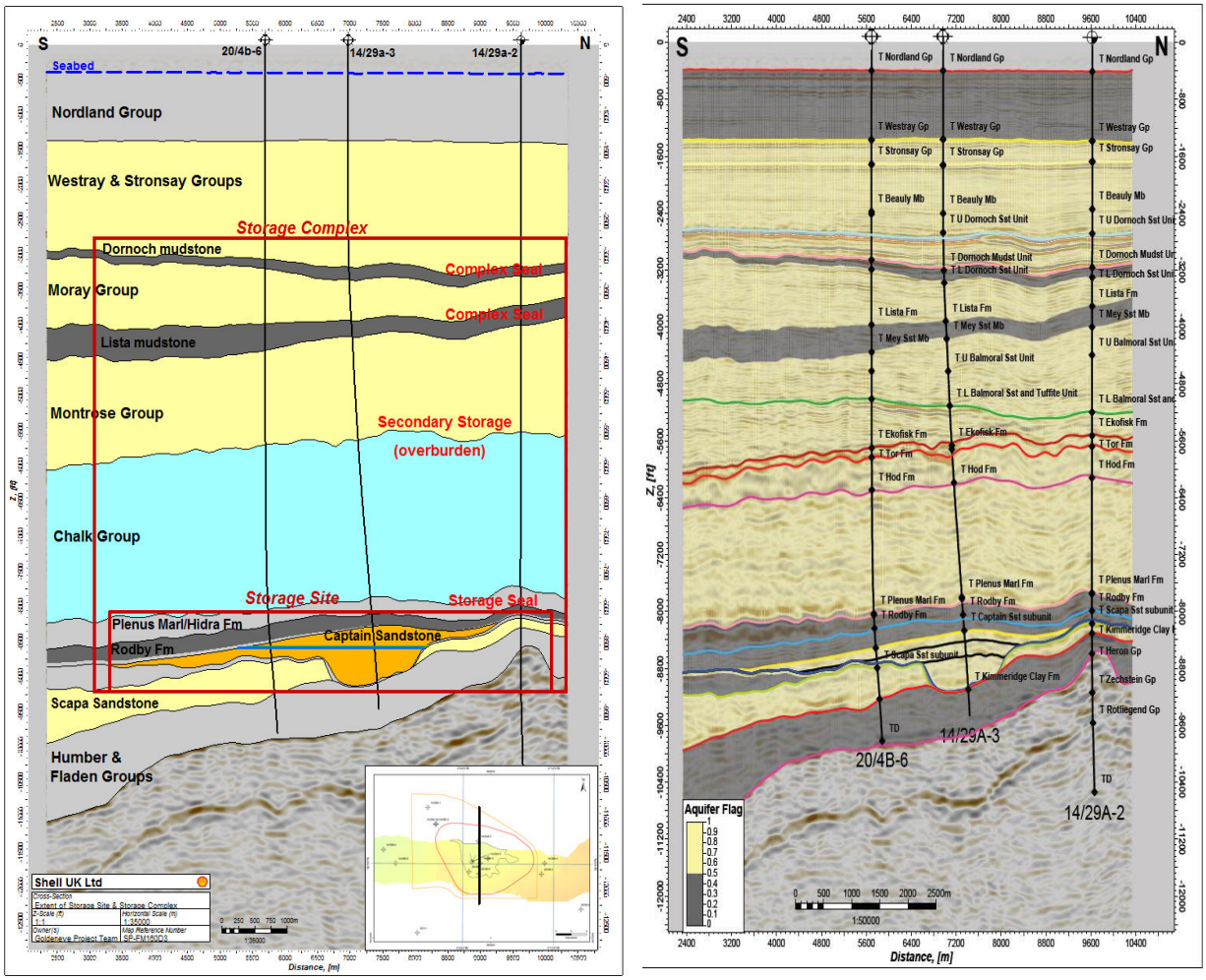

Figure 12-1. Seismic Cross section showing the field, storage site, storage seal, storage complex and secondary storage i.e. Lista, Mey, Upper Balmorals Sandstone and Lower Balmoral sandstone and Tuffite Unit.

The leak paths considered in the study include existing wells. Existing faults have been mapped and fractures have been analysed and none have been identified to be pervasive throughout the seal systems (37) and as a consequence, are not included in this study.

For a comprehensive understanding of the containment risks, which include the critical parameters affecting leakage, a summary of risks and contingency plans in case of leakage, refer to the Peterhead CCS Storage Development Plan (38).

12.1. Geology of the secondary storage

Any migration of CO_2 vertically out of the Captain reservoir could be contained above the Goldeneye Field within a number of overlying aquifers bound by the Lista mudstone which sits at the Top of the Lista Formation. There are, however, no secondary structural closures identified in the overburden above the Goldeneye Field.

Any CO_2 reaching the base of the Lista mudstone is expected to migrate largely in the direction of the regional dip. Migration occurs until it is trapped by a local structure, capillary, dissolution or chemical trapping. The questions to be answered by this modelling exercise therefore are, how much CO_2 and, over what period, will CO_2 be contained in the Mey? And, will it be in the proximity of the

storage complex? The Lista Formation is proposed as a secondary store and seal for sequestered CO_2 in the Goldeneye Field. The Lista Formation is interpreted to outcrop at the seabed over 150km to the west of Goldeneye, within the Inner Moray Firth. The formation includes the Lista mudstone which is a non-calcareous, bioturbated, non-carbonaceous and non-pyritic mudstone. The Lista mudstone is a proven hydrocarbon seal in the central North Sea.

The Lista mudstone facies is widely present in the Halibut Trough area (60 out of 72 wells) and is present throughout the storage site and closest offset wells. It is 60-120m thick in the Goldeneye area, and appears to thin slightly to the west.

The Lista mudstone facies overlies approximately 1200m of stratigraphy believed to be of aquifer quality i.e. Mey Sandstone Member, Upper and Lower Balmoral Units, Marueen, Ekofisk, Tor, Hod and Herring Formations. These stratigraphies, together with the Lista Formation as its seal, offer the main possibility for secondary containment of CO_2 above the Goldeneye Field.

There are several Paleocene fields in the central North Sea that have Andrew or Mey sandstone reservoirs capped by a Lista Formation seal. The closest to the Goldeneye Field is the Rubie Field (40km) and the MacCulloch cluster fields (50km: MacCulloch, Donan, Nicol, Lochranza, Blenheim, Blair, Beauly, Burghley and Andrew Fields).

The Mey is equivalent to the Andrew Formation outside of the Goldeneye area. The Mey Sandstone Member itself is subdivided into an Upper Balmoral Sandstone Unit and a Lower Balmoral Sandstone Unit based on the presence of a mid tuffaceous sand (the Balmoral Tuffite Unit). It consists of variable sandstones, mostly ranging from fine to medium grain and displaying more pervasive cementation than the Balmoral Sandstones. Its upper boundary marks the start of stacked sequences of interbedded massive sands and shales. Its lower boundary corresponds to a sharp downward change from sandstone to green-grey mudstone. It is present in all overburden model wells and closest offset wells but is not widely distributed elsewhere in the Halibut Trough area. Tilting during mid-Palaeocene led to repeated build-out of shelf-slope foresets. Goldeneye sits under the thickest section of these shelf-slope foresets. The Mey sandstone is likely to be a channelised deposit.

The Upper Balmoral Sandstone Unit consists of sandstones, mostly ranging from fine to medium grained and displaying variable cementation. Its upper boundary is typically defined by a downward change from green grey to grey green mudstone. In the Goldeneye area, the base of the Upper Balmoral Sandstone Unit coincides with the Balmoral Tuffite unit. It is present in all overburden model wells and closest offset wells, but is not elsewhere in the Halibut Trough area.

12.2. Static modelling

Objectives of the Mey Sandstone Model

A geologically realistic structure and property model of the Mey sandstone was required as input to the dynamic simulation so that the path of CO_2 migration through the overburden could be simulated and containment within the storage complex over an acceptable period of time, i.e. 1000 years, could be assured.

In the Overburden model the Lista Formation and Mey Sandstone stratigraphic horizons were isopached down from the Lower Dornoch Mudstone seismic pick. This was done because these Formations cannot be identified on seismic. It was noted however that, in places, the isochored surfaces did not correctly follow the approximate seismic dip. This problem is exacerbated by the existing depth conversion methodology which is not focussed on the shallow horizons. The depth conversion used treats the whole interval surface to Top Chalk in one step and subsequently adds a wedge of higher velocity sediments over the west flank area of the field. This high velocity wedge is

then imprinted in the shallower horizons giving an appearance of westward closure which does not match with regional or well data.

Unfortunately, it is not easy to directly interpret the top Lista on 3D seismic due to the lack of contrast (acoustic transparency) in the thick sequence of Montrose Groups sands and shales. The large thickness of lignites above generates considerable multiples and absorption losses. In addition because of the build out foreset stratigraphy of the Mey, the Top Lista is hard to correlate regionally.

Given the dip of the Mey which causes a north-westerly direction of flow the AOI of the overburden model was also found to not extend sufficiently far north and west to model CO_2 movement for 1000 years. Thus it was decided to build a more detailed Mey model which would cover a revised more northerly AOI than the existing overburden model and if possible, include improved top Mey/Lista depth surfaces.

Picking top Lista in the new model

Well tops from adjacent fields were used to identify a candidate 'Top Lista Mst' reflector, then 2D lines were used to extend the seismic interpretation over a wider area. The AOI of the new model is 13 x 24.5 km.

Fourteen 2D seismic lines were interpreted.

Workflow:

- Grid TWT surface (with well tops)
- Calculate well velocities and produce a velocity map
- Combine gridded velocity with gridded TWT to produce Z map (tied to wells)
- Smooth result to remove data input artefact
    - (dense data along track of 2D lines – no data elsewhere)
- Cut resulting surface to AOI
    - (this means, if we extend it, do not change geometry within AOI when regrid)
- Repeat for Top Chalk (base of model)

The new Mey and Lista depth surfaces honour the seismic data and wells, and are therefore considered more suitable for the overburden simulation work than in the previous overburden model. As these depth maps were generated using sparse 2D seismic lines there are however gaps in interpretation and as such some fine scale detail is possibly missing. There are also limitations resulting from the simple velocity model applied i.e. well based depth conversion but this was the best that could be achieved with the data.

A simple overburden model was constructed without faults (there are no major faults in the Mey) using a 50 x 50 grid. The Top and Base of the model are the Top Lista & Top Chalk, respectively. Internally the model is split into 4 broad zones and 27 layers.

- Top Lista-Top Mey (1 layer)
- Top 100 feet of Mey (5 foot layers)
- Rest of Mey (Base=Top Balmoral) (20 foot layers)
- Balmoral-Chalk (1 layer)

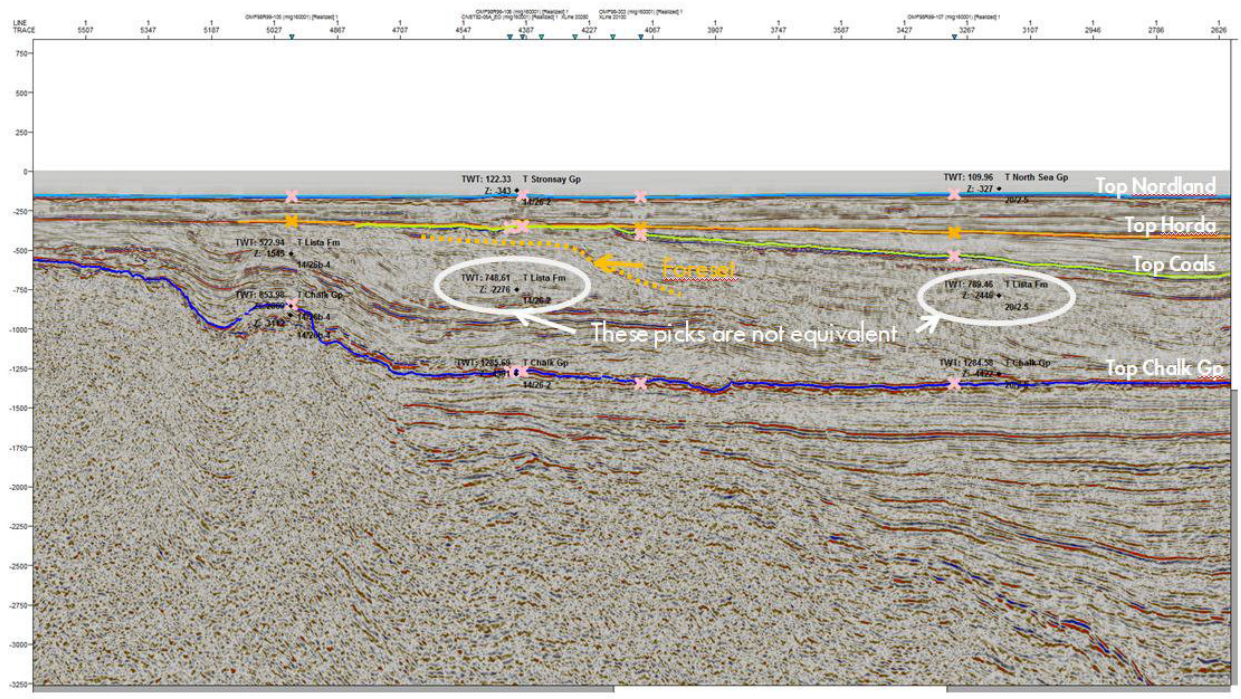

Figure 12-2. **Figure shows the difficulty in picking a Top Lista on seismic, pick in wells does not conform to an easily identifiable, consistent seismic horizon. Foreset geometries can be seen.**

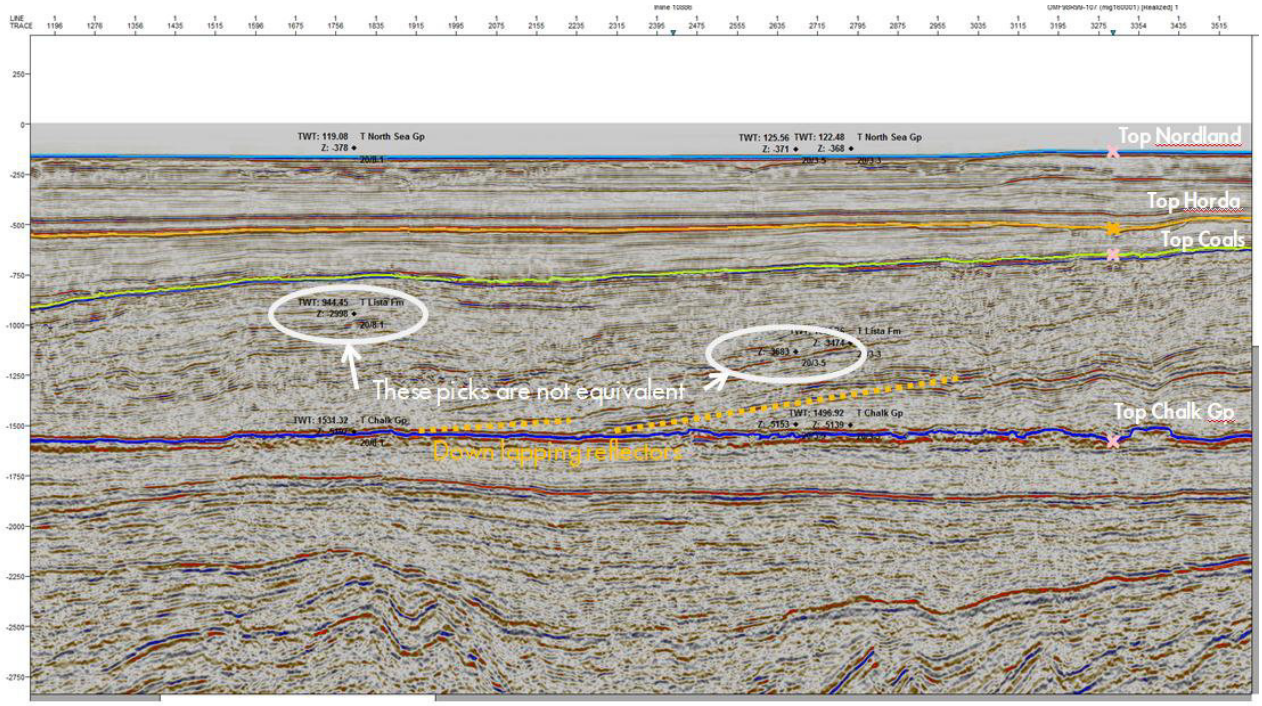

Figure 12-3. **Figure shows the difficulty in picking a Top Lista on seismic, pick in wells does not conform to an easily identifiable, consistent seismic horizon.**

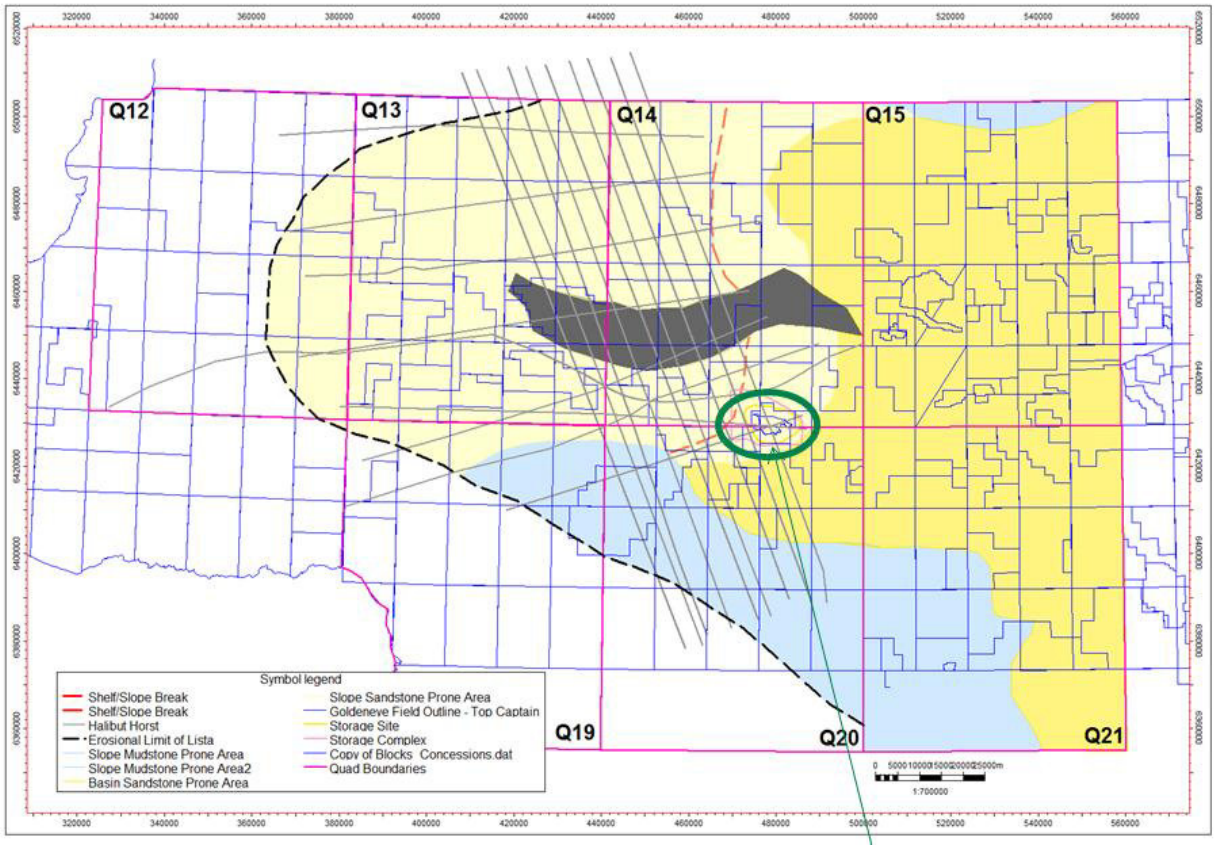

Figure 12-4. 2D data coverage (Millennium Atlas palaeogeography as backdrop) field highlighted by green oval.

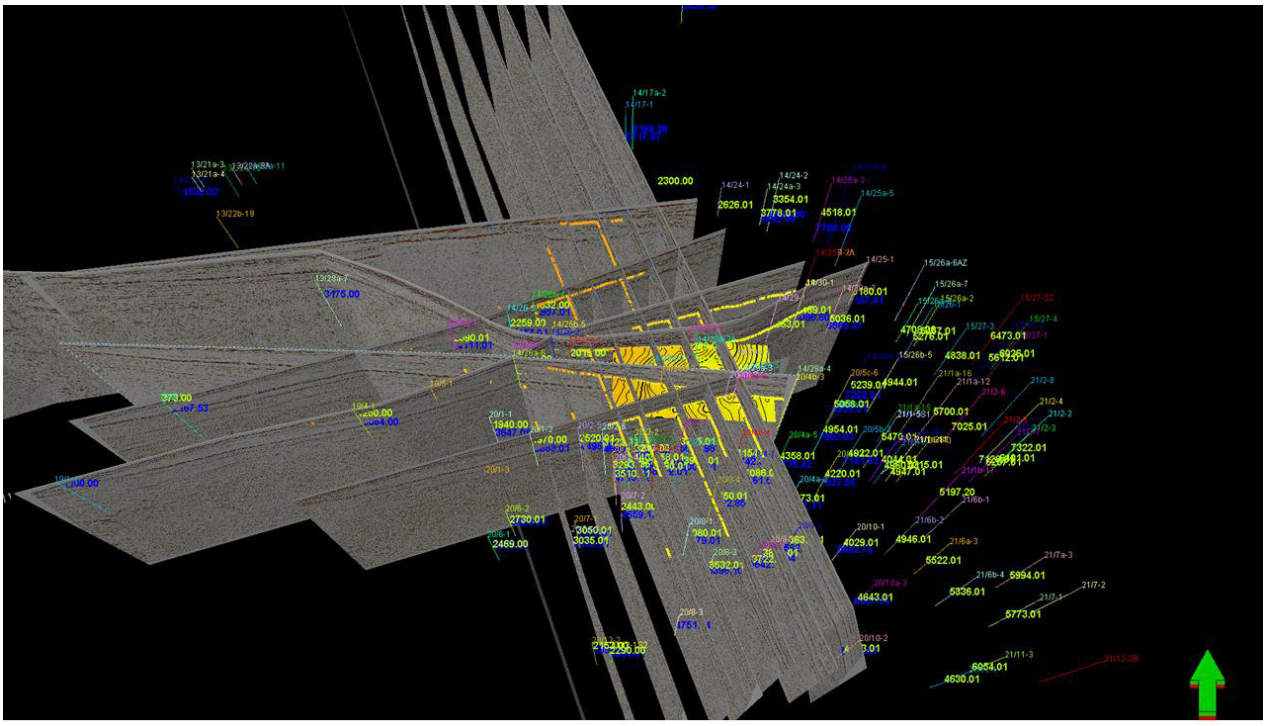

Figure 12-5. 3D view of 2D line data set with the 14 seismic lines and all wells. Field area shown by solid surface.

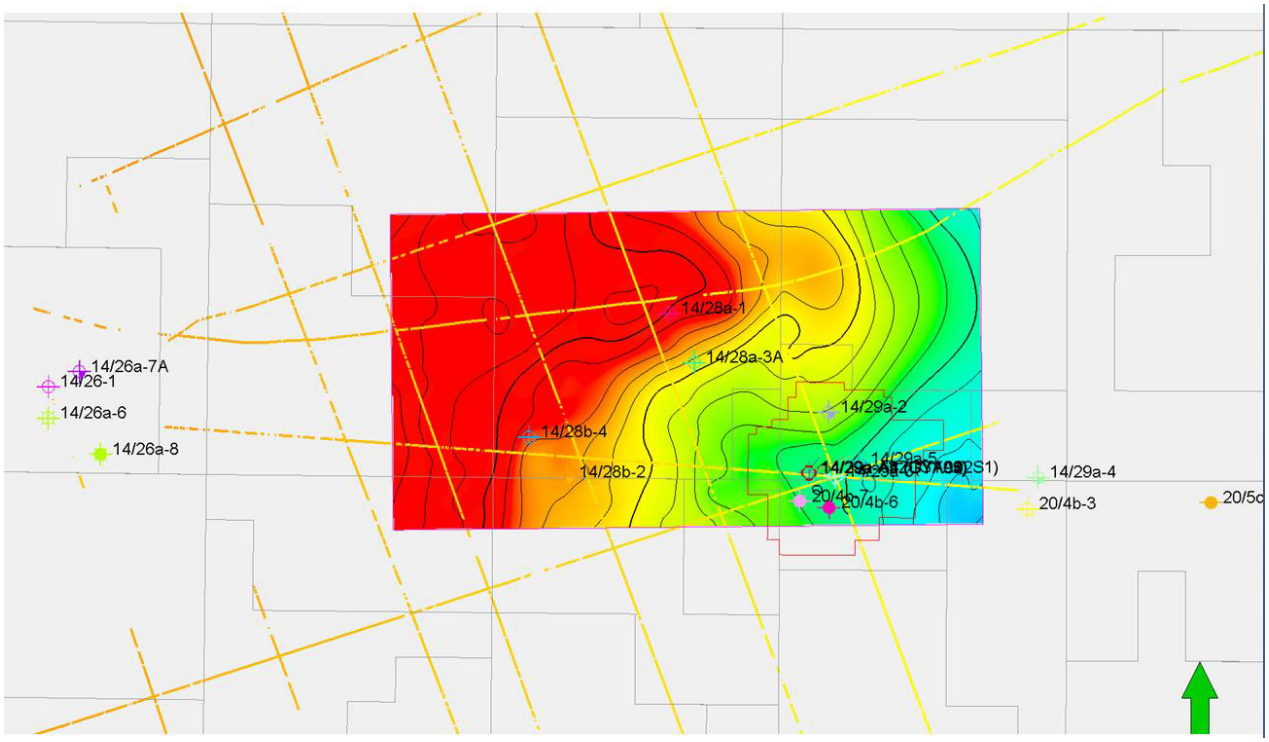

Figure 12-6. New Top Lista map which ties to wells and available seismic lines.

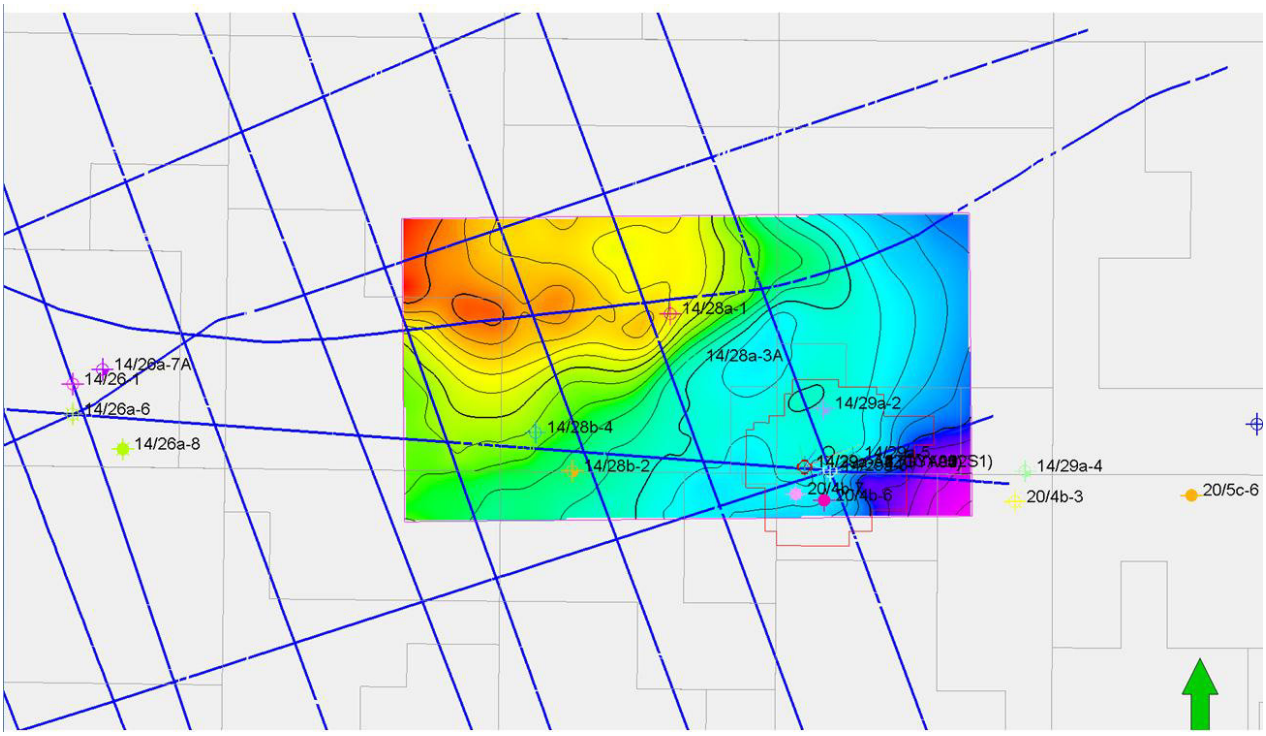

Figure 12-7. New Top Chalk map which ties to wells and available seismic lines.

Property Modelling

Two property models were generated which are considered to reflect end member scenarios with respect to the possible geology of the Mey Sandstone and expected behaviour of CO_2 within the Mey sandstone.

In one realisation homogenous properties were modelled for the Mey, essentially treating it as a tank of sand. This enabled a realisation where the CO_2 plume can move unrestricted as a diffuse plume. In this scenario it is likely that the topography of the Top Lista will be the primary control on the CO_2 pathway.

Workflow: Homogenous properties simulated using values: Mey Sst Por: 0.34, K: 210 mD

In a second realisation a more channelized Mey sandstone was modelled using a facies model which evoked a north-west, south-east lineament to the channel body orientation. There is no specific evidence to indicate this channel orientation (seismic derived attributes which appeared to show strong channel features in the Mey are in fact artefacts of glacial channels in the shallow overburden). However, a channelized Mey is possible and a north-west south-east orientation would be the most challenging to containment as it could enhance or dominate the flow of CO_2 to the northwest which is the natural direction of flow due to the dip at Top Lista.

Workflow: Properties were modelled using the moving average algorithm applied to up-scaled well logs and the facies model as a trend.

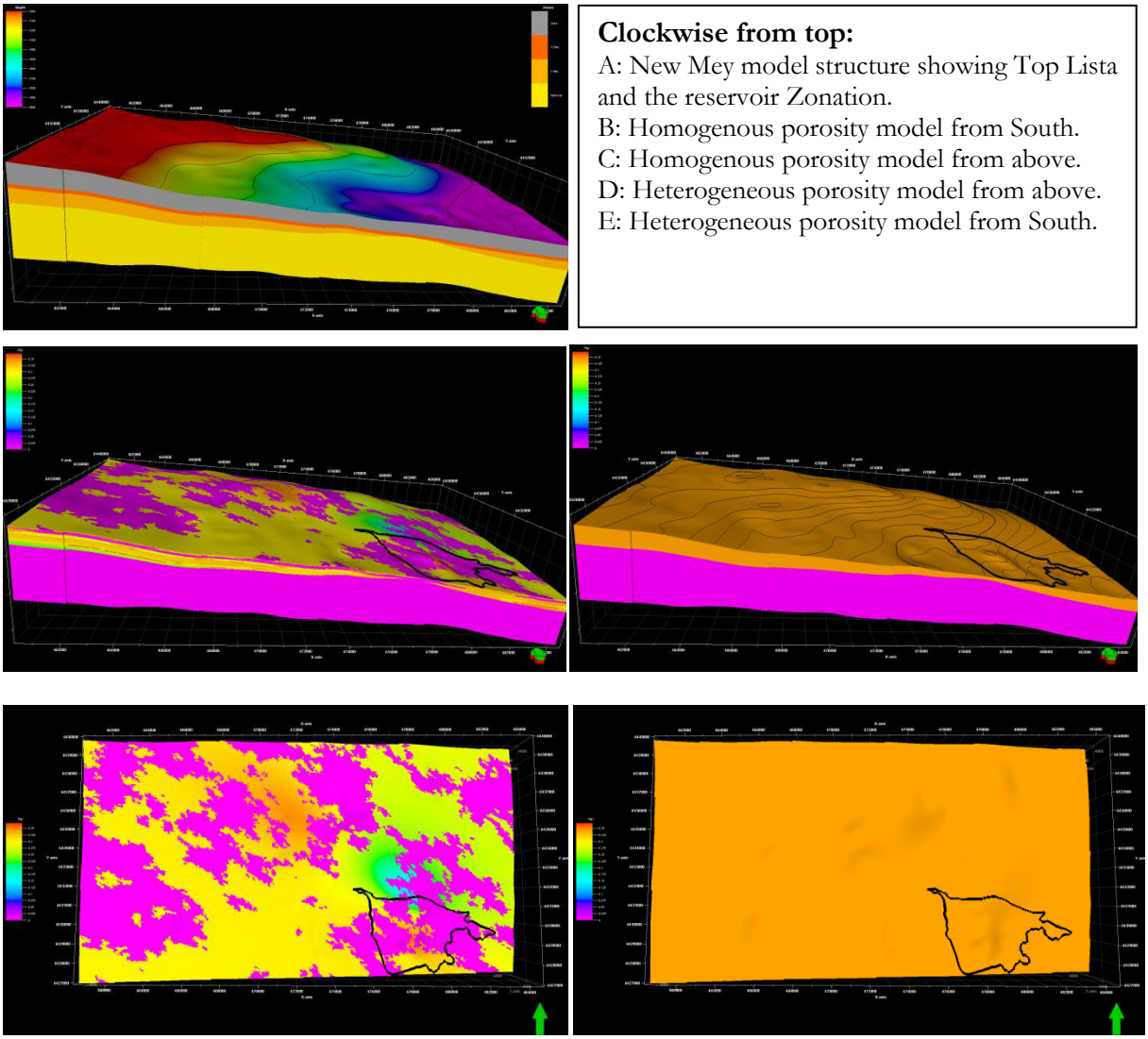

Clockwise from top:
A: New Mey model structure showing Top Lista and the reservoir Zonation.
B: Homogenous porosity model from South.
C: Homogenous porosity model from above.
D: Heterogeneous porosity model from above.
E: Heterogeneous porosity model from South.

Figure 12-8. Clockwise from top

12.3. Features of overburden dynamic models

To evaluate the possible migration through these formations a set of 3D models of the Mey sandstone were constructed. Most of this work was carried out during the 2011 Longannet to Goldeneye CCS project, and consequently many sensitivities are based on a target of 20 Mt CO_2 being injected into the Goldeneye store at a rate of 2 Mt p.a. As there have been no substantial changes to the dynamic models, these may be considered as high case leak scenarios in the context of the Peterhead CCS injection rate of 1 Mt p.a.

The initial model comprises a simple rectangular box with a constant dip of 1.5°, the average dip of the Lista formation which forms the seal to the Mey sandstone. The grid is 200 x 60 x 20 with total dimensions of 60,000 ft x 25,500 ft x 400 ft [18,288 m x 7,773 m x 122 m]. The horizontal grid block size is 300 ft x 300 ft [91 m x 91 m] except for the first and last 5 blocks in the y direction. These blocks increase in size in the y direction to a maximum of 2,400 ft [732 m]. The model has a depth of 4,100 ft [1,250 m] at x=1 which decreases to 2,529 ft [771 m] at x=200. The top layer has a thickness of 1 ft [0.305 m] which increases by a factor of 1.4 to a maximum of 33 ft [10 m] to give a total thickness of 400 ft [122 m]. The thickness of 400 ft is the approximate thickness of the Mey

sandstone near Goldeneye. To ensure constant pressure boundaries the volumes of the first and last rows of blocks in the x direction were multiplied by 10,000. It has constant properties and has been used to evaluate the distance CO_2 will migrate and the timescales involved.

A more detailed model was created based on the 3D geological model of Mey sandstone. The grid is 110 x 66 x 40 with total dimensions of 80,380.57 ft x 42,650.9 ft x ~400 ft [24,500 m x 13,000 m x ~122 m]. The horizontal grid block size is 200 ft x 200 ft [60 m x 60 m] except for the first and last 5 blocks in the x direction. These blocks increase in size in the x direction to a maximum of 2,400 ft [732 m]. The top 20 layers have a thickness of 5 ft [0.305 m] in order to properly solve the CO_2 plume. The following 20 layers are each 20ft in thickness to give a total thickness of 500 ft [152 m]. In the more heterogeneous version of the detailed model, channelized property model was also simulated. The sensitivity of the results to variations in reservoir properties was used to evaluate the uncertainty in the predictions.

The estimated average properties for the Mey sandstone are permeability of 210 mD, porosity of 34% and net to gross of 46%. The Kv/Kh in the model was initially set to 0.1. The alternative heterogeneous property model varies the properties honouring the log data**.**

Only two components are used in the PVT description, CO_2 and water, in all three models. A temperature gradient of 10 °C/1000 ft [32.8 °C/1000 m] is imposed with a temperature of 83 °C at 8,400 ft [2,560 m]. The properties of CO_2 are strongly dependent on temperature and pressure. The critical temperature of 31.1 °C occurs in the model at a depth of 3260 ft [99 m], below this depth the CO_2 is supercritical. The simulator allows CO_2 to dissolve in water. The initial pressure in the model is 1,890 psia [130 bara] at a depth of 4,200 ft [1,280 m] which is in line with the hydrostatic gradient.

Water/gas relatives permeability curves with hysteresis are used with similar parameters to the Goldeneye reservoir model. These are listed in the following table.

Table 12-1. Relative permeability parameters.

Relative Permeability data for dynamic model	
S_{wc}	0.15
S_{gc}	0.05
S_{gr}	0.25
n_w	5
n_g	2.5

A single capillary pressure curve is included from the Goldeneye model corresponding to permeability values greater than 100 mD. No hysteresis is included for capillary pressure.

12.4. Volume at risk

One of the key parameters to be assessed in this secondary containment modelling study is how much CO_2 could be at risk of an egression from the Goldeneye reservoir into the Mey sandstone , in order to use it as a constraint for the leaking wells. This can be estimated by quantifying how much mobile CO_2 will be below a certain depth like the top Captain sandstone at each well at risk.

Figure 12-9 shows the volume at risk below each well within the Goldeneye field after the system has reached gravity equilibrium (for realisation FFM 3.15) 25 years after injection of 20Mt had ceased. The chart separates CO_2 into mobile and immobile CO_2. The immobile CO_2 is the mass of CO_2 in a grid block where the saturation is below the critical gas saturation.

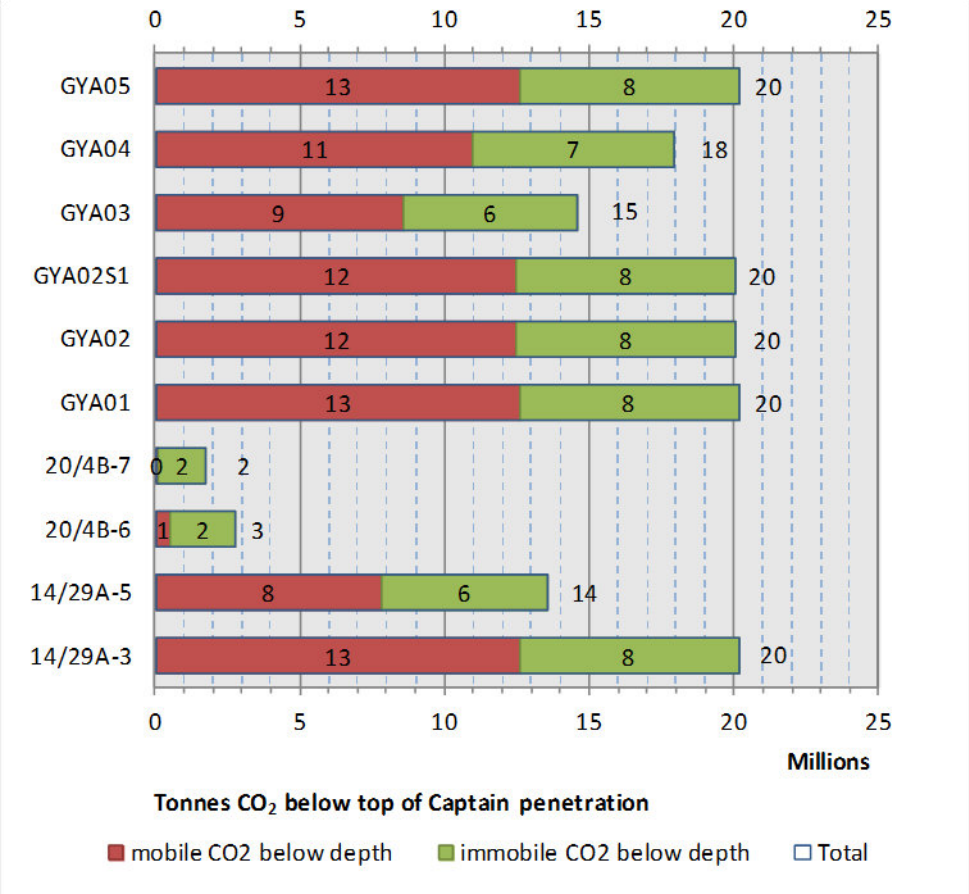

Figure 12-9. CO_2 below the top Captain penetrations of wells within Goldeneye, 25 years after cessation of injection (20 Mt), FFM3.15.

The chart shows that wells 20/4B-7 and 20/4B-6 have no and very little mobile CO_2 (1 Mt) at risk respectively. Even if an integrity issue occurred in these wells then the volume at risk would be minimal. Other wells have larger volumes at risk with the largest mobile volume being 13 Mt for the most crestal wells. These numbers will be used as maximum leak volumes in the egression cases.

12.5. Well constraints and rates

In the initial reference case in the simulacrum box model, a vertical injection well is positioned 6,000 ft. from the downdip edge of the model and is used as a source of CO_2 escaping from Goldeneye and migrating up to the Mey sandstone. Initially there are 200 ft [61 m] of perforations in the middle of the reservoir.

In the detailed model based on the 3D geological model of the Mey sandstone, the initial reference case used well 14-29a-3 as a source of CO_2 escaping from Goldeneye and migrating up to the Mey sandstone. Initially there are 200 ft [61 ft] of perforations in the top of the reservoir.

The maximum pressure in the Goldeneye reservoir after injection of 20 Mt of CO_2 was taken to be between 3,470 psia and 3,720 psia [239.3 bara to 225.5 bara] at a datum depth of 8,400 ft [2,560 m].

Assuming a pressure of 3,600 psia [248.3 bara] in the Goldeneye reservoir at a depth of 8,400 ft the difference in hydrostatic pressure between a well with a full column of CO_2 and the hydrostatic at the model depth of 4,200 ft is around 400 psi [27.6 bar], which was chosen as the maximum pressure difference for the injection well.

For a case where 20 million tonnes of CO_2 are intended to be stored in the Goldeneye reservoir, it has been estimated that 7 million tonnes are trapped leaving 13 million tonnes which could potentially escape from the reservoir. An initial limit of 10 million tonnes was placed on the injection volume with sensitivities run to higher and lower values.

The maximum rate used in the simulations was set at 1500 tonnes/day (~29 MMScfd) of CO_2. To put this in context, a single well in both the Longannet and Peterhead projects will be injecting at a rate of approximately 1370 tonnes/day. Calculations of hypothetical leak rates from the Goldeneye reservoir depend mainly on the assumed downhole geometry. A well performance simulator which considers the variable PVT properties of the CO_2 has been used. Different scenarios of micro-annulus, simulated as concentric pipe flow, were assessed (see Figure 12-10). From the analysis, there is a huge range of hypothetical leak rates for different leak geometries. The geometry of the leak path, which in turn determines the leak rate, is a substantial uncertainty.

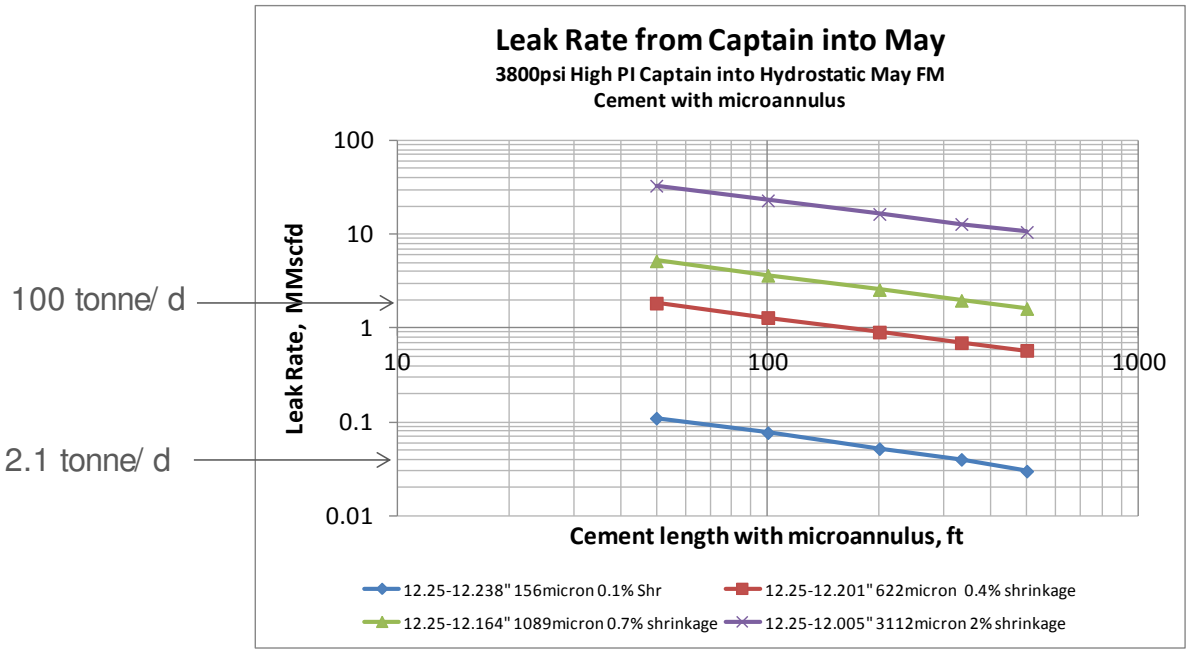

Figure 12-10. Estimated micro-annulus leak rates from Goldeneye reservoir into Mey

Test from cement formulations equivalent to Goldeneye 9 5/8" casing slurry design indicated negligible shrinkage or expansion of the cement. As such, during the setting process of the cement, micro-annulus formation is not expected. The absence of shrinkage of the cement in combination with the cement column and plugs used in the different abandonments make a leak from the well difficult to conceive.

A hypothetical leak scenario was generated by running an injection rate of 100 tonnes/day (1.9 MMscfd) which corresponds to a continuous micro-annulus in 300 ft of cement with an external shrinkage factor of about 0.7%.

Another scenario involved a rate of 2.1 tonnes/d (0.04 MMscfd) which corresponds to an external shrinkage factor of the cement of 0.1%.

12.6. Overburden Model Forecast (Box Model)

The CO_2 distribution at the top of the model after 45 years is illustrated in Figure 12-11 for the reference case. CO_2 leakage has ceased at this point and the gas has spread out into a circle surrounding the well. The situation after 1,000 years is illustrated in Figure 12-12 and Figure 12-13. The areal distribution in Figure 12-12 shows that the CO_2 has migrated up dip leaving an oval shaped area of trapped residual gas behind the CO_2 front. The cross section in Figure 12-13 shows that the CO_2 forms an inverted cone around the leakage well where it is trapped as residual gas. Being less dense than water the mobile CO_2 migrates to the top of the formation where it slowly moves up dip in a thin layer.

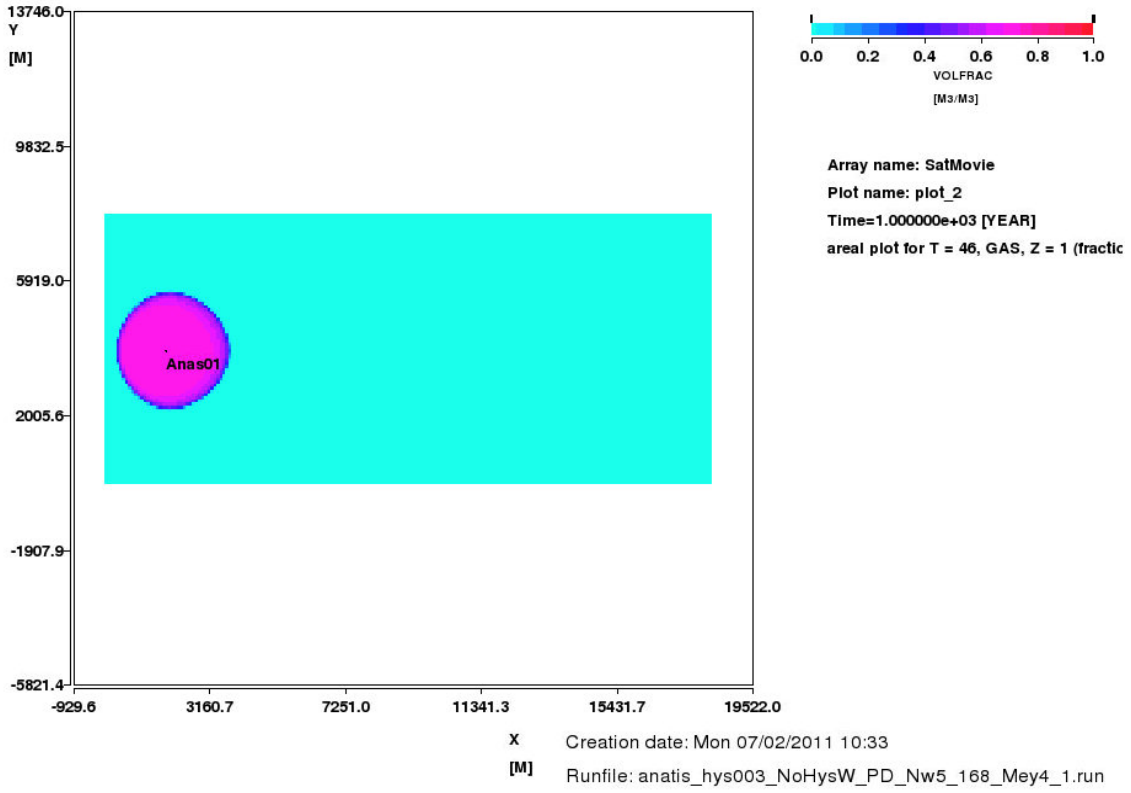

Figure 12-11. Distribution of CO_2 in top layer of model after 45 years for reference case.

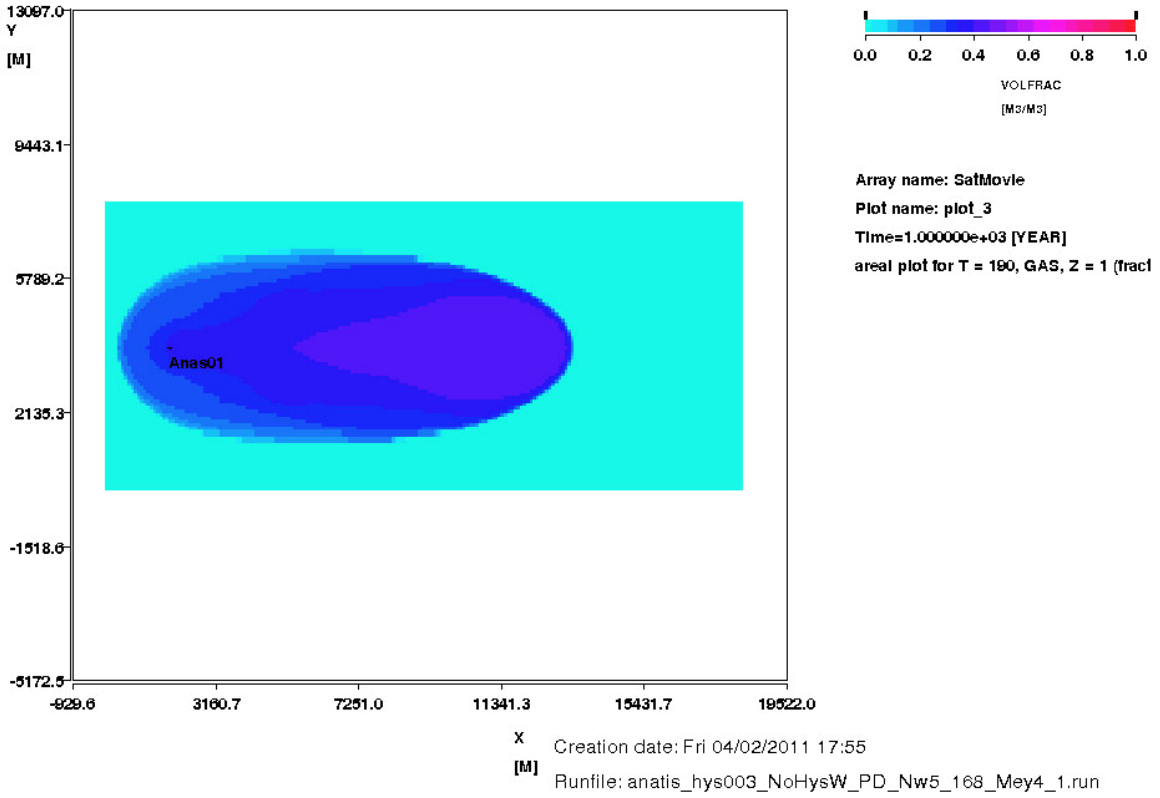

Figure 12-12. Distribution of CO_2 in top layer of model after 1,000 years for reference case.

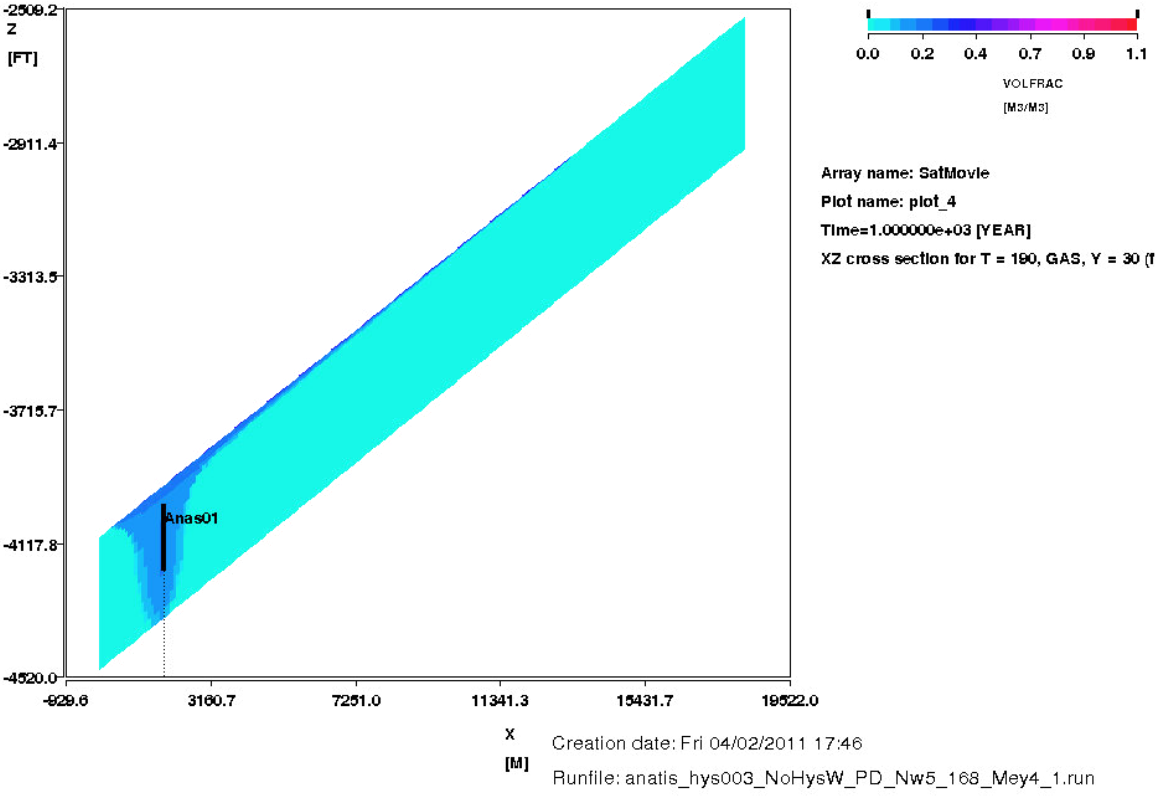

Figure 12-13. Distribution of CO_2 in cross section through well after 1,000 years for reference case.

Figure 12-14 illustrates the distribution of dissolved CO_2 in water after 1,000 years. The dissolved CO_2 has spread away from the well and covers a radius of about 1 km away from the well. The total mass of CO_2 dissolved in water as a function of time is shown in

Figure 12-15. After 1000 years 0.81 Mt of CO_2 have dissolved in water outside the gas zone (i.e the water zone) and 2.67 Mt of CO_2 have dissolved in water inside the gas tongue (the gas zone) to give a total of 3.48 Mt of CO_2 dissolved in water. The high proportion (35%) of CO_2 dissolved in water is due to the large contact area between the CO_2 and water provided by the long CO_2 tongue.

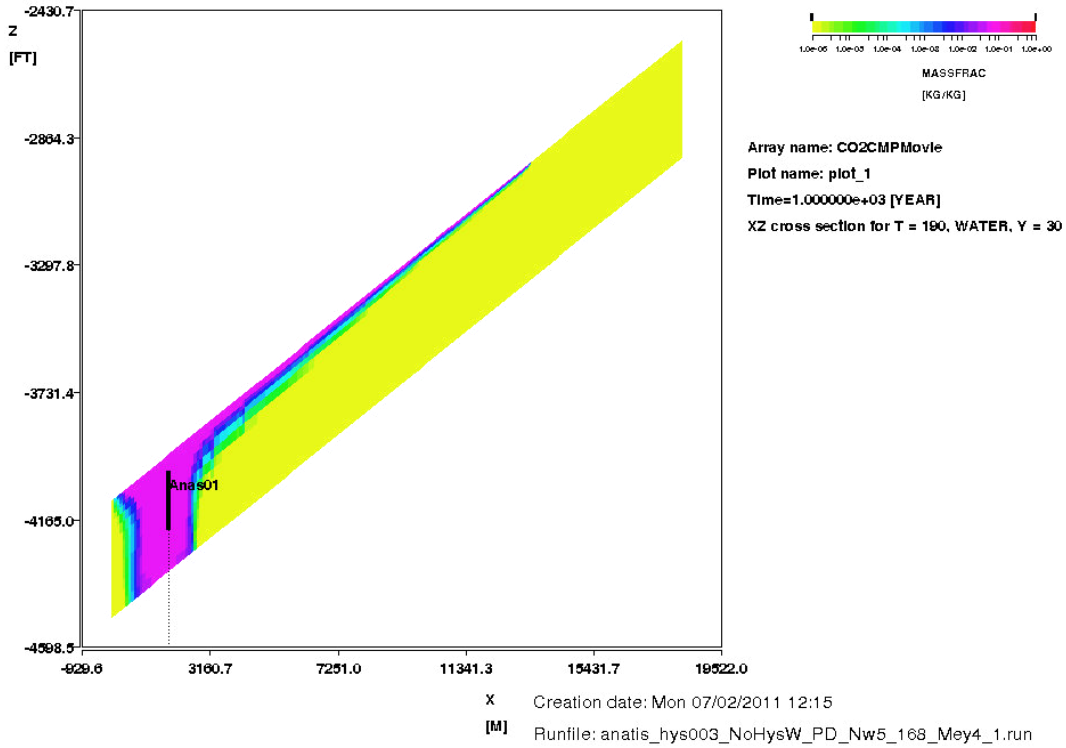

Figure 12-14. Cross section through well showing concentration of CO_2 dissolved in water for reference case after 1,000 years (logarithmic scale).

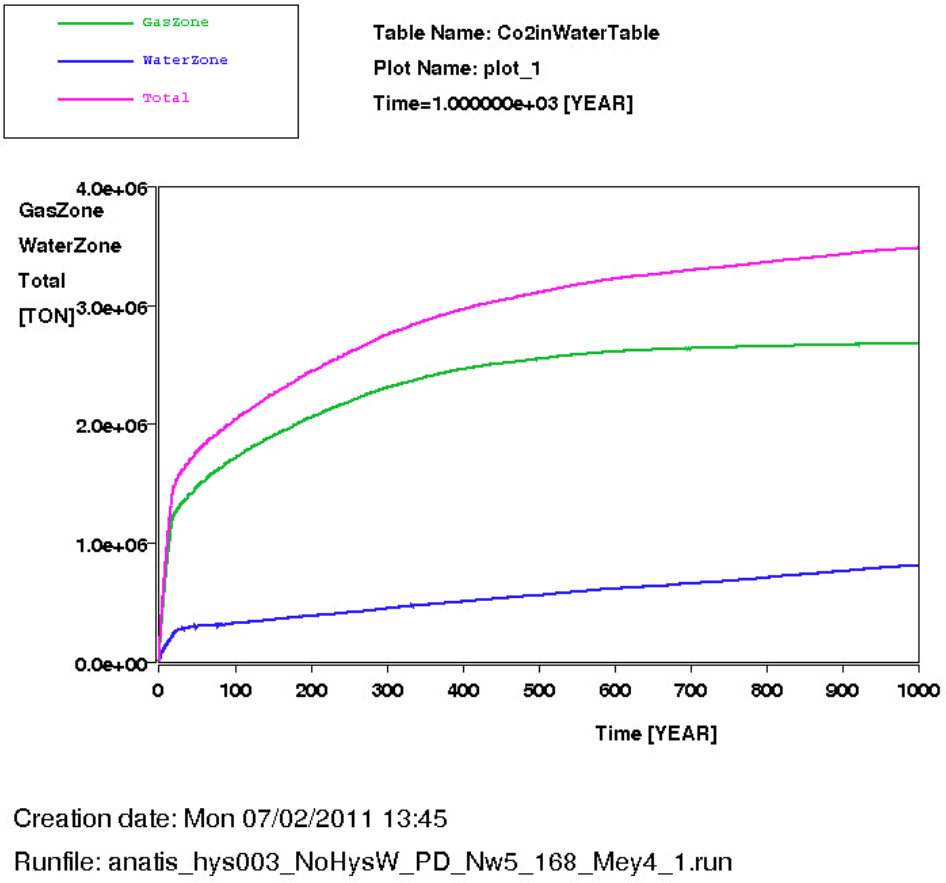

Figure 12-15. Mass of CO_2 dissolved in water for reference case.

Figure 12-16 shows the distance CO_2 has migrated from the well against time. Although the plume of CO_2 migrates a large distance along the top of the reservoir, this is mostly in a very thin layer a few feet in thickness and so the majority of the CO_2 has migrated a much shorter distance. This can be seen more clearly in Figure 12-17 which illustrates the mass of CO_2 per unit area after 1000 years for the reference case. Most of the CO_2 is still within a few kilometres of the well.

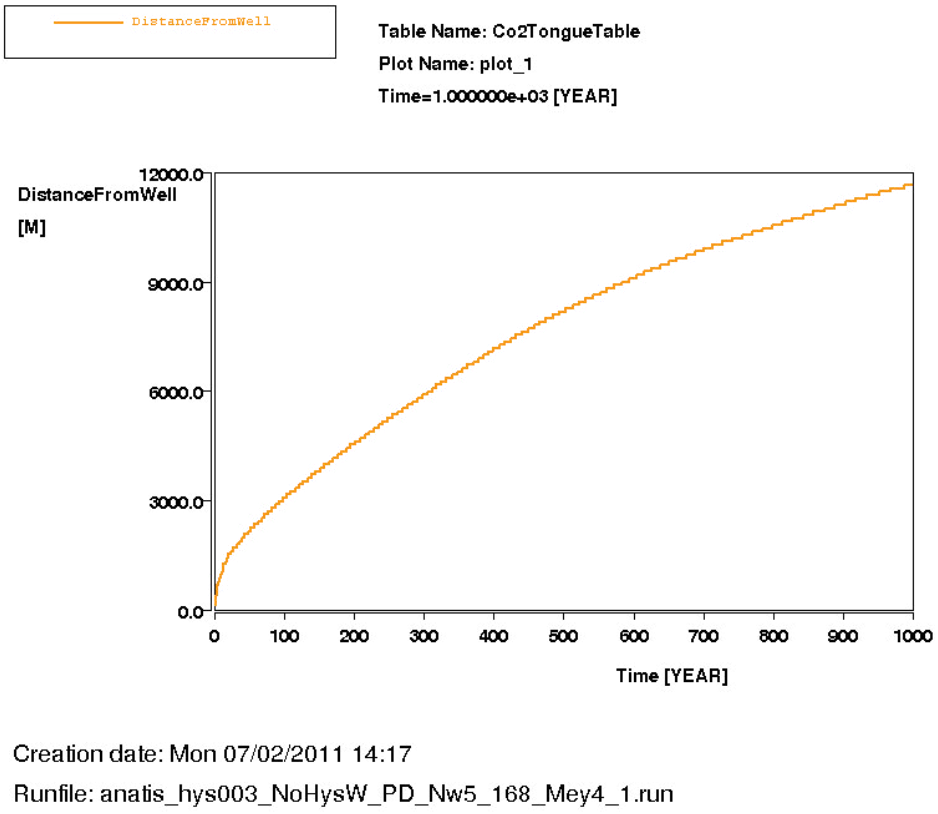

Figure 12-16. Distance of edge of CO_2 plume from well vs time.

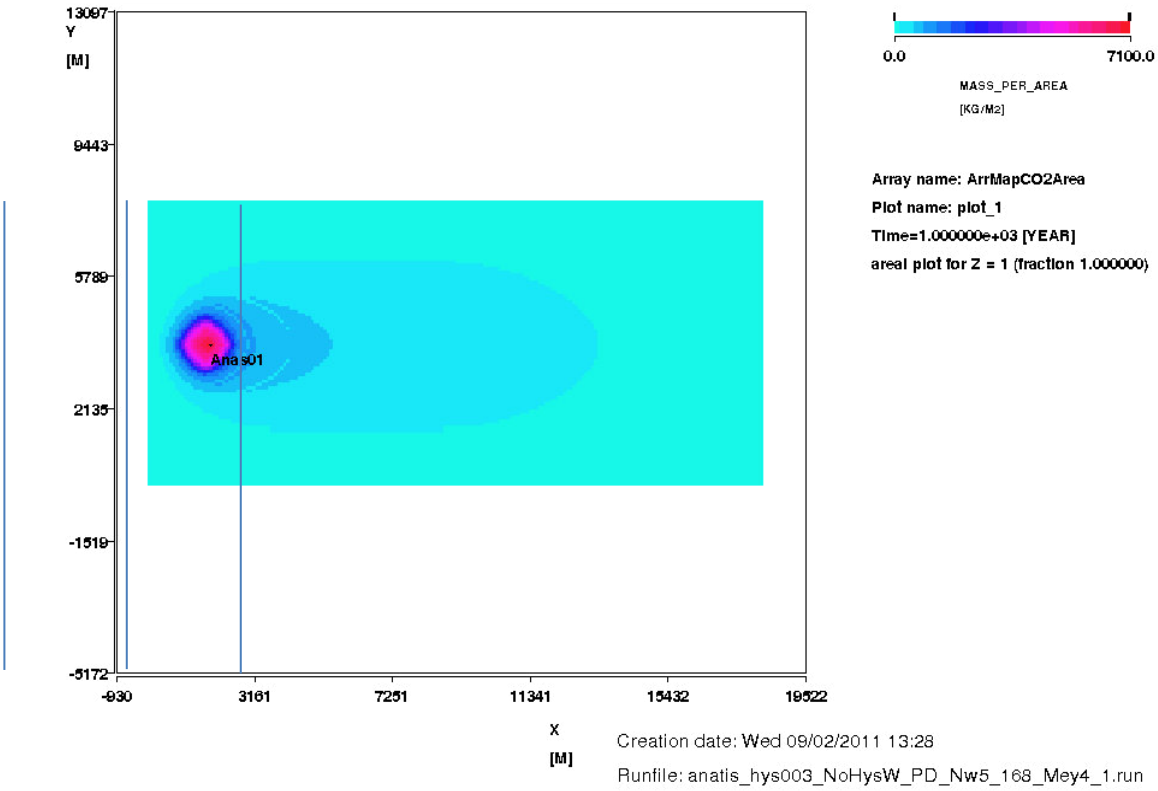

Figure 12-17. Mass of CO_2 per unit area after 1000 years for reference case (10 million tonnes leaked). Lines indicate mass of CO_2 migrated beyond that point.

Another way of illustrating this is to look at the mass of CO_2 that has migrated beyond a certain distance from the well at any given time. This is done in Figure 12-18. This shows that of 10 million tonnes leaked in the reference case, 5 million tonnes has migrated more than 1 km after 127 years but after a thousand years this has only increased to 5.5 million tonnes due to trapping of the gas. Taking a distance of 5 km, only 2 million tonnes has migrated more than this distance after 1,000 years. Slightly more than 1 million tonnes has migrated more than 7 km. This contrasts with the total distance reached by the plume of 11.7 km. It takes 25 years for more than 100 tonnes to travel more than 2 km from the well and 68 years for it to travel more than 3 km from the well. It is 47 years before any CO_2 has migrated more than 3 km from the well. After 1000 years approximately 0.5 million tonnes has migrated more than 9 km from the well.

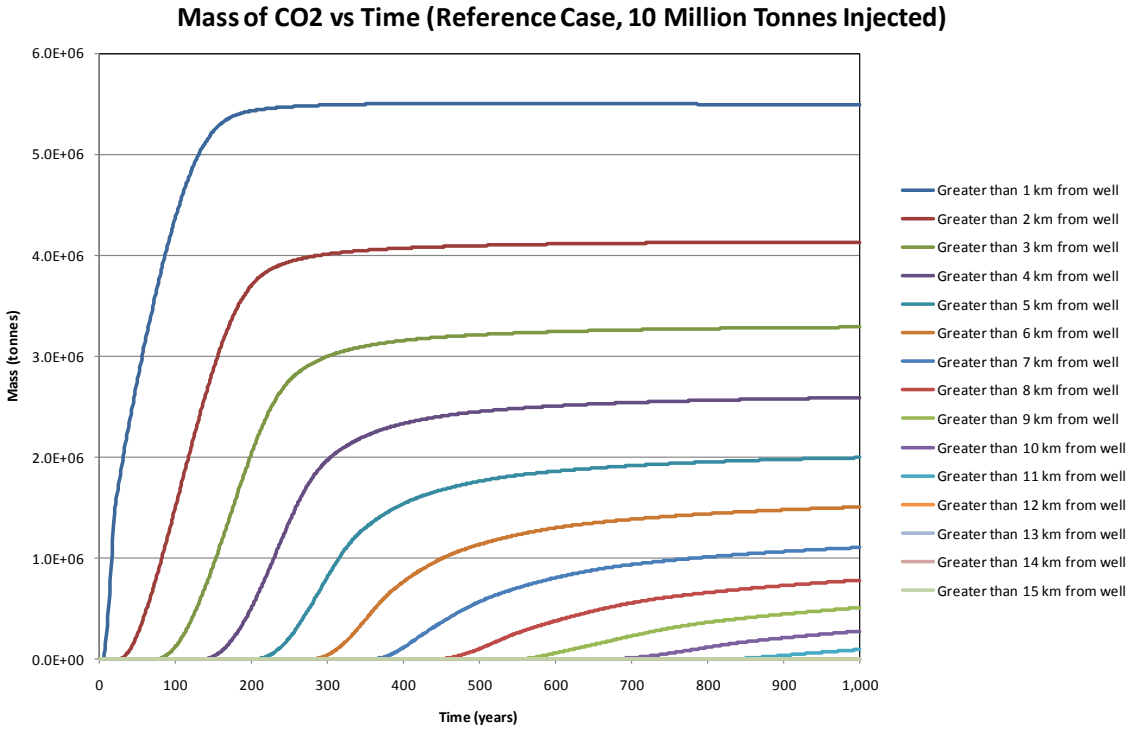

Figure 12-18. Mass of CO_2 migrating greater than given distance against time for reference case with 10 million tonnes leaked.

As an initial assessment of the sensitivity of the migration distance to the model parameters the model was run for 1,000 years with the parameter sensitivities given in Table 12-2.

Table 12-2. Initial parameter sensitivities (high/low values represent distance CO_2 migrates, not size of parameter value).

Sensitivity	Low value	Reference Value	High Value
Perforation position	Base	Mid	High
Delta P (psi)	600	400	100
Perforation length (ft)	400	200	5
Max rate (tonnes/day)	2000	1500	100
nw	7	5	3

Sensitivity	Low value	Reference Value	High Value
$S_g$trap	0.3	0.25	0.2
Kv/Kh	0.01	0.1	1
Mass CO_2 (tonnes)	5,000,000	10,000,000	15,000,000
Permeability (mD)	105	210	420

The results of the simple box model study are summarized as follows:

1. The results from a simple box model with constant properties show that the main reservoir parameters governing the migration of CO_2 are the horizontal and vertical permeability and the trapped gas saturation.
2. The plume migration distance is sensitive to the CO_2 leakage rate, lower rates result in longer migration distances due to less gas being trapped near the well.
3. In the reference case considered here, of 10 million tonnes leaked into the Mey sandstone 5 million tonnes has migrated more than 1 km after 127 years but after a thousand years this has only increased to 5.5 million tonnes due to trapping of the gas. Slightly more than 1 million tonnes has migrated more than 7 km after a thousand years. This contrasts with the total distance reached by the plume of 11.7 km. After a thousand years approximately 0.5 million tonnes has migrated more than 9 km from the well.
4. The constant dip of the current model does not account for the trapping of CO_2 in local highs. The structure needs to be mapped in 3D for this to be modelled.
5. These results do not take account of variations in the top structure of the Mey sandstone which will results in local trapping of CO_2 and a shorter plume migration distance.
6. Heterogeneity. The lack of heterogeneity results in too smooth a migration front.

Based on the above results the more detailed 3D geological model of the Mey sandstone was simulated and is discussed in the following section.

12.7. Overburden Model Forecast (3D Homogeneous Model)

In order to expand the outcome of the simulation results from the simple box model, a more detailed version was built using the 3D geological models of the Mey sandstone (described above).

The reference case uses 14/29-a3 as a hypothetical leaking well. The well, completed at top 200ft is modelled with a rate set at 1500 tonnes CO_2 per day (28.3 MMscfd), roughly equivalent to the rate of one Goldeneye injection well. The total CO_2 leaked is set at 10 Mt. This represents a total failure of all barriers and will test what is known as a Finite Release: how a predefined mass of ascending CO_2 would migrate in the subsurface out with the storage formation.

The CO_2 distribution at the top of the model after 20, 100 and 1000 years is illustrated in the following three figures for the reference case. In Figure 12-19 the CO_2 leak has ceased at this point (after 20 years) and the gas has spread out into a circle surrounding the well. The areal distribution after 100 years in Figure 12-20 shows that the CO_2 has migrated up dip leaving an oval shaped area of trapped residual gas behind the CO_2 front. Finally, after 1000 years (Figure 12-21), CO_2 has migrated further updip totally controlled by the top surface of the Mey formation, following the structural

highs where the CO_2 is still in dense phase with saturation in the order of 70-75%, but also leaving behind a large tail of permanently sequestered CO_2 due to trapping mechanisms such as residual gas saturation (25-30%) and dissolution.

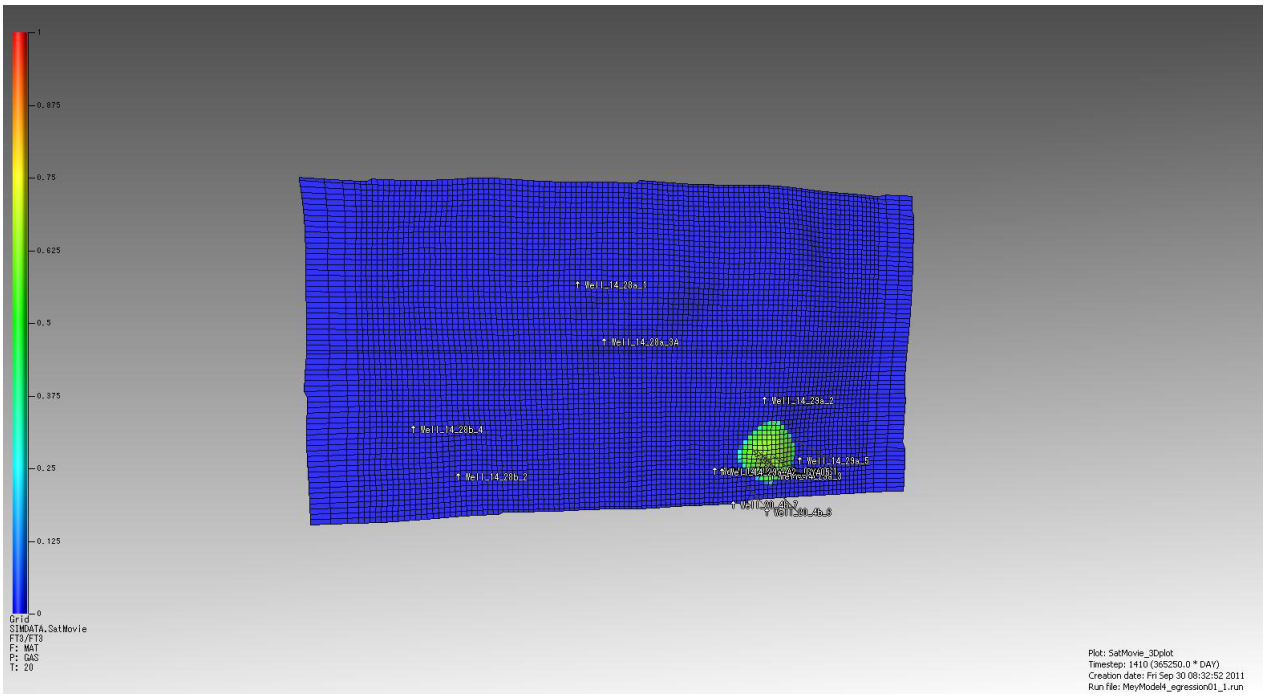

Figure 12-19. Distribution of CO_2 after 20 years in top layer of model for homogeneous case.

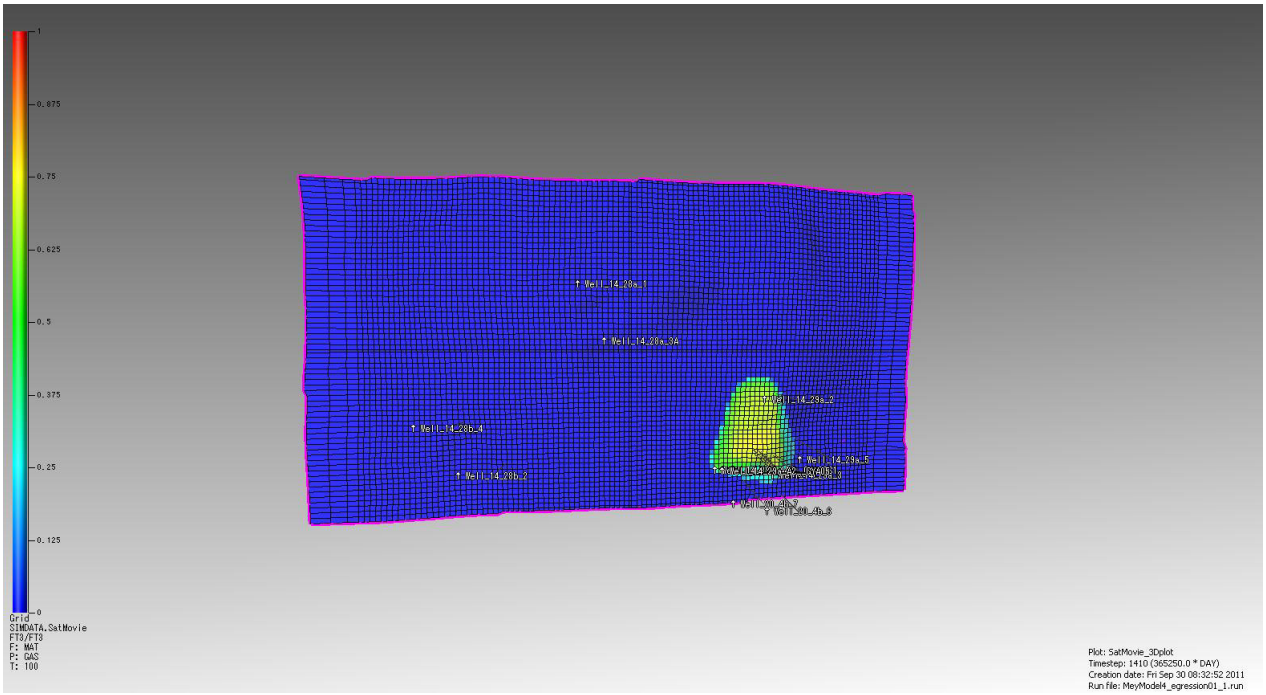

Figure 12-20. Distribution of CO_2 after 100 years in top layer of model for homogeneous case.

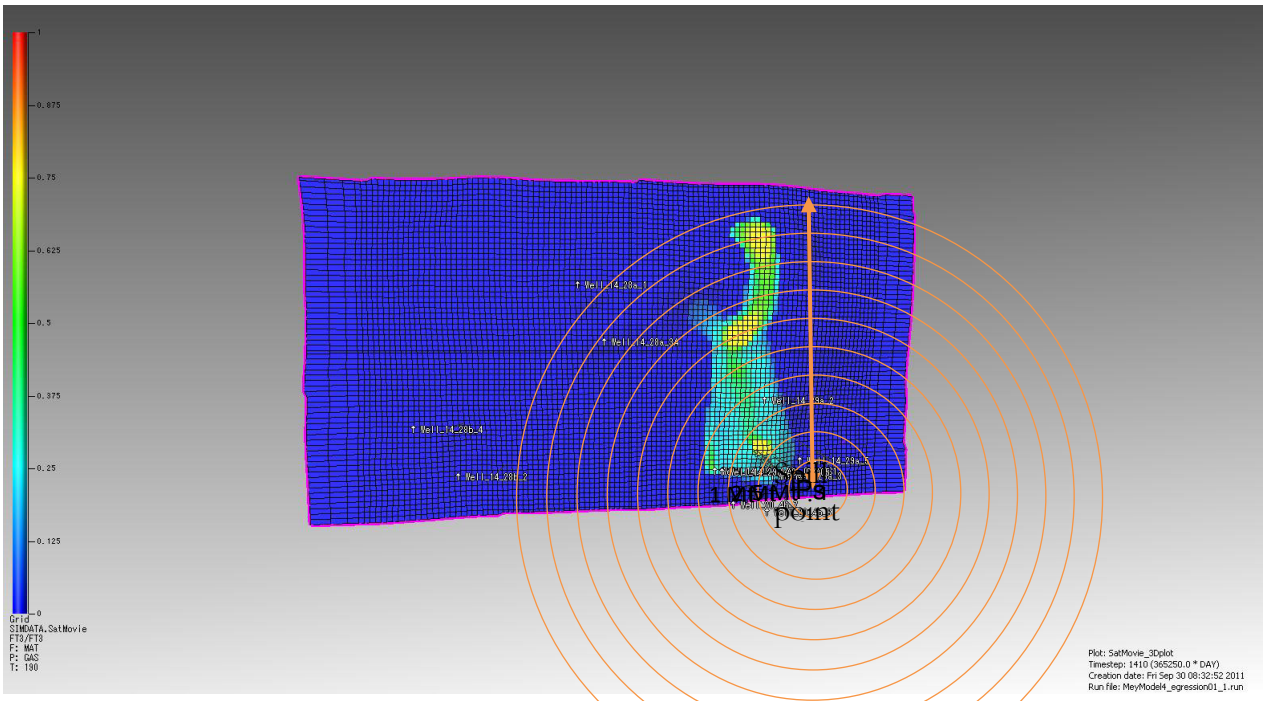

Figure 12-21. Distribution of CO_2 after 1000 years in top layer of model for homogeneous case.

Figure 12-21 also shows that after 1000 years of migration this ~10 km CO_2 plume is not near other wells that could potentially provide secondary leak paths. NW The closest wells in a north-westerly direction: 14/28a-1 and 14/28a-3A represent the highest risk because of their proximity to the leakage area and the lack of a cement plug at Lista/Dornoch level in the first one. Nevertheless, based on these results, there is no CO_2 in contact with either well. Towards the west, wells 14/28b-4 and 14/28b-2 which are between 8 and 10 km away will not be in contact with CO_2 either. The same applies to southern wells (downdip): 20/4b-6, 20/4b-7 and south eastern wells (downdip): 14/29a-4, 20/4b-3 and 20/5c-6. However, it must be considered that this is represents the results of a single top structure realization due to the limited information available for the Mey sandstone and therefore the predictions of CO_2 migration path have a high uncertainty.

The cross section in Figure 12-22 shows that the CO_2 forms an inverted cone around the leak well where it is trapped as residual gas. Being less dense than water the mobile CO_2 migrates to the top of the formation where it slowly moves up dip in a thin layer. It is important to notice that, even though the tip of the CO_2 plume has travelled a considerable distance (approximately 10 km) most of it is concentrated in the area surrounding the well and just a small proportion (thin top layer – 10 ft) moves away from the leak point.

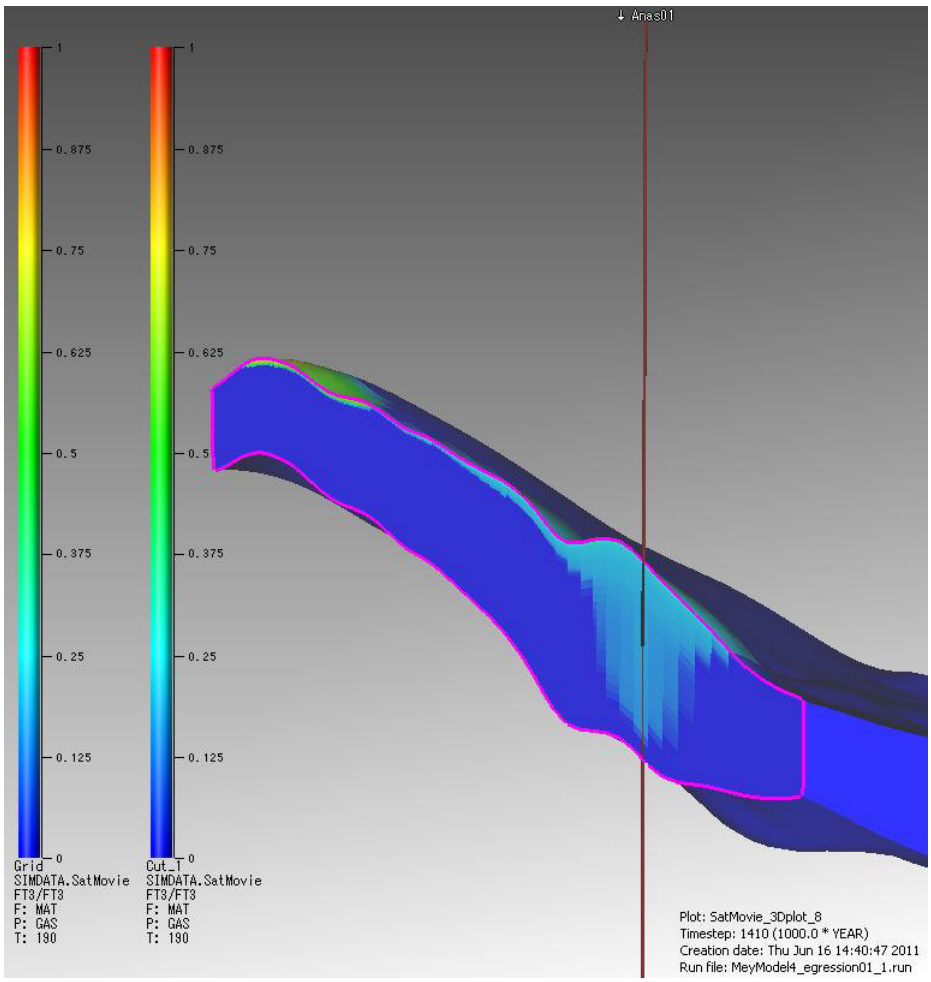

Figure 12-22. Distribution of CO_2 in cross section through well after 1,000 years for homogeneous case.

Figure 12-23 illustrates the distribution of dissolved CO_2 in water after 1,000 years. The dissolved CO_2 has spread away from the well and covers a wide area. The scale is logarithmic and highlights the small amount of CO_2 dissolved in brine.

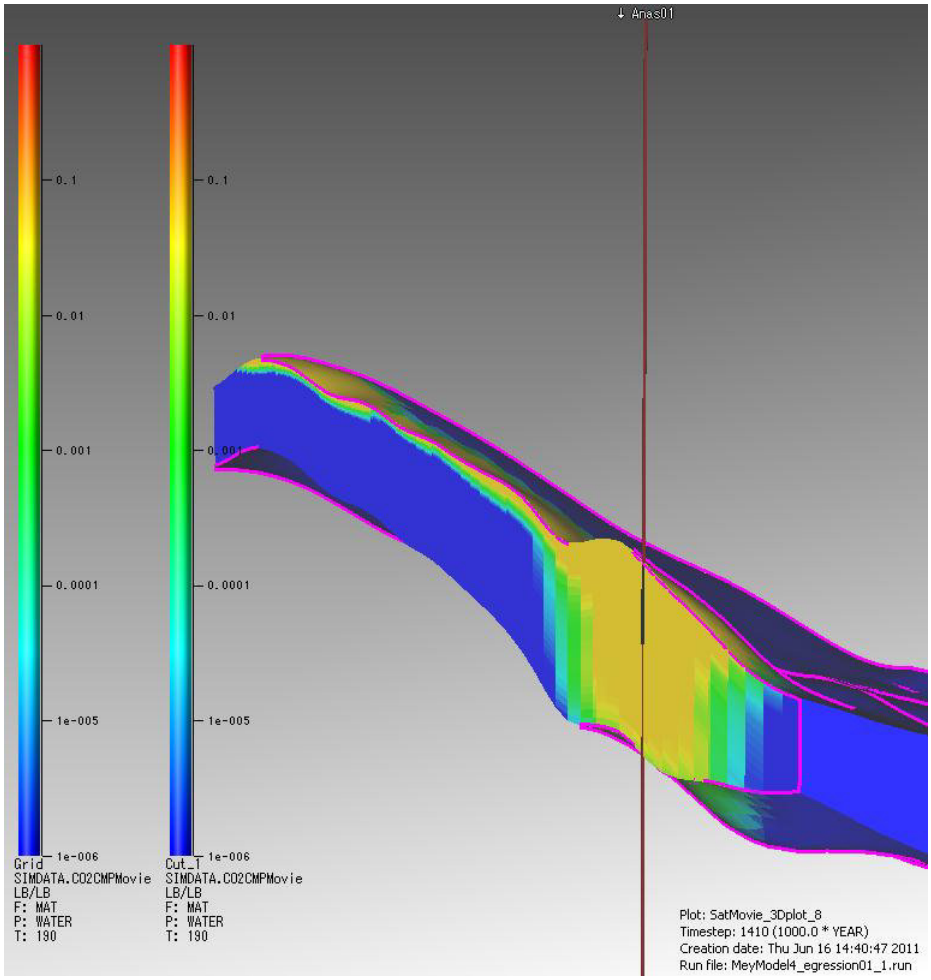

Figure 12-23. CO_2 dissolved in brine @ 1000 years homogeneous model.

Figure 12-24 shows the inventory of mass (left) and percentage (right) of CO_2 trapped, dissolved and still in dense phase as a function of time. After 1000 years, $3.1x10^6$ tonnes of CO_2 have dissolved in water. The high proportion (31%) of CO_2 dissolved in water is due to the large contact area between the CO_2 and water provided by the long CO_2 tongue.

The volume of CO_2 dissolved in water is overestimated in the simulation mainly due to the fact that all the CO_2 in a block is assumed to be in contact with the water and the CO_2 saturation of the water immediately increases to the maximum amount allowed by the mass of CO_2. In reality, the CO_2 will not be in immediate contact with the water. In addition, the grid block size will also play a role in the amount of CO_2 dissolved in water in the model, overestimating it due to the large grid block size, mainly at the bottom.

The CO_2 Inventory shows that after 1000 years, about 60% of CO_2 has been sequestered via dissolution and capillary trapping mechanisms, leaving just 40% still as CO_2 in dense phase capable of still migrating updip. However, this split depends on many factors and one critical one is the residual gas saturation. The reference case scenario uses 25% for this parameter, but as will be seen on the uncertainty analysis in Section 12.7.1, a higher S_{gr} will reduce the mobile CO_2 by as much as 10%.

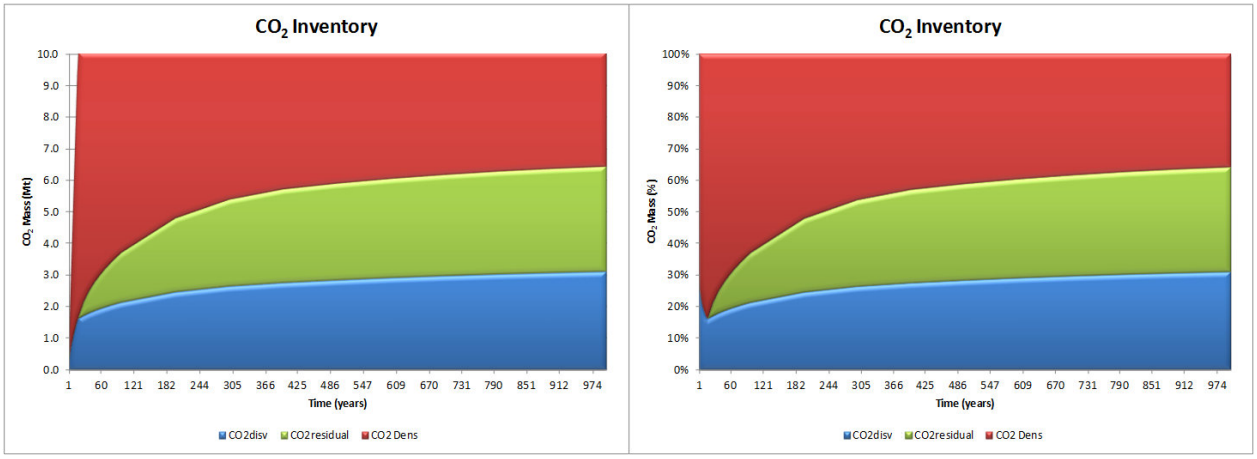

Figure 12-24. CO_2 Mass inventory as a function of time (left). CO_2 percentage inventory as a function of time (right) – homogenous model.

Figure 12-25 shows the distance CO_2 has migrated from the well against time. Although the tip of the CO_2 plume migrates a large distance along the top of the reservoir, this is mostly in a very thin layer a few feet in thickness and so the bulk of the CO_2 has migrated a much shorter distance. This can be seen more clearly in Figure 12-27 which illustrates the mass of CO_2 per unit area after 1000 years for the reference case. Most of the CO_2 is still within a few kilometres of the well.

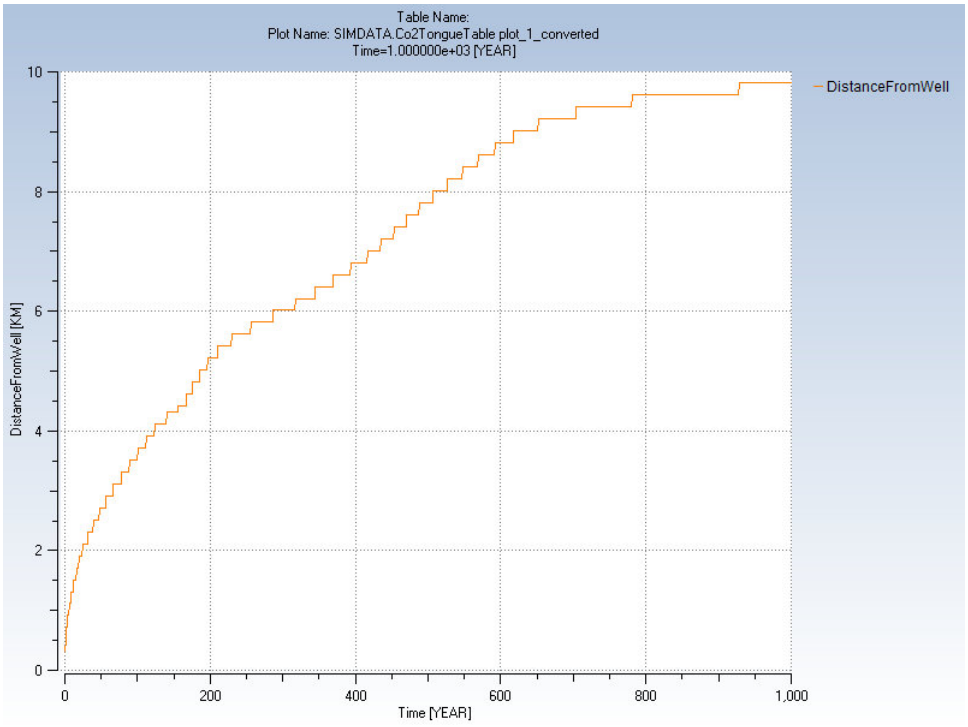

Figure 12-25. Distance of edge of CO_2 plume from well vs time, homogeneous model.

It can also be observed that it has travelled a shorter distance in this more detailed 3D model than in the simple simulacrum model where the top structure was just a tilted flat box (9.81 km vs 11.65 km – 18% shorter). This piece of evidence, exemplifies the importance of properly modelling the container architecture. It also highlights that a homogeneous flat top structure would represent an end member or worst case scenario.

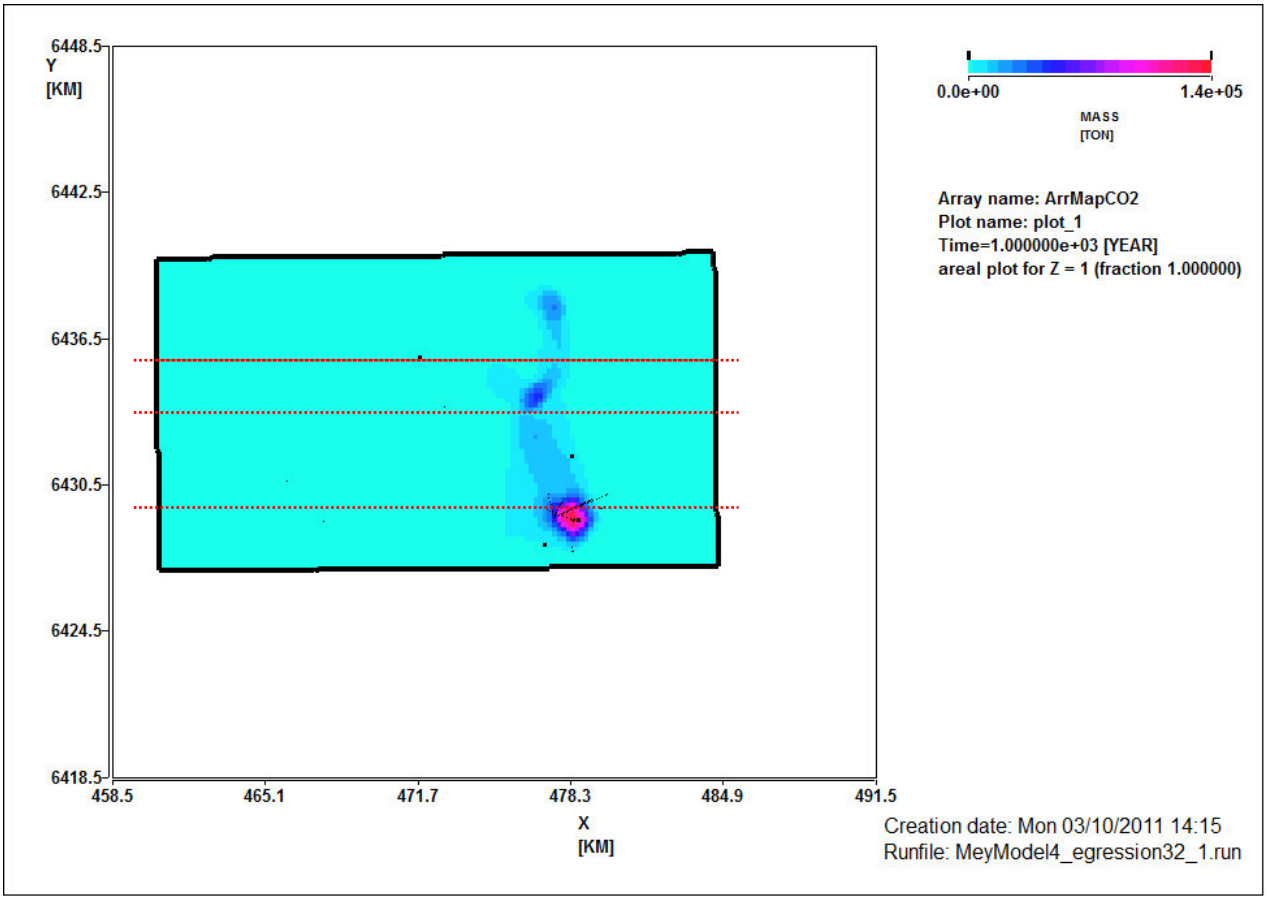

Figure 12-26. Mass of CO_2 after 1000 years for reference case, homogeneous model (10 million tonnes leaked). Lines indicate mass of CO_2 migrated beyond that point.

As in Section 12.6, another way of illustrating this is to look at the mass of CO_2 that has migrated beyond a certain distance from the well at any given time. This is done in Figure 12-27. This shows that of 10 million tonnes leaked in the reference case 6 million tonnes has migrated more than 1 km after 150 years but after a thousand years this has only increased to 6.5 million tonnes due to trapping of the gas. Taking a distance of 5 km, only 2.2 million tonnes has migrated more than this distance after 1,000 years. Slightly less than 1 million tonnes has migrated more than 7 km. This contrasts with the total distance reached by the plume of 9.8 km. It takes 12 years for more than 100 tonnes to travel more than 2 km from the well and 44 years for it to travel more than 3 km from the well. It is 36 years before any CO_2 has migrated more than 3 km from the well. After 1000 years approximately 0.5 million tonnes has migrated more than 9 km from the well. CO_2 dissolution and capillary trapping mechanism constrain the migration and sequester a large proportion of it (approx. 60% illustrated in Figure 12-24)

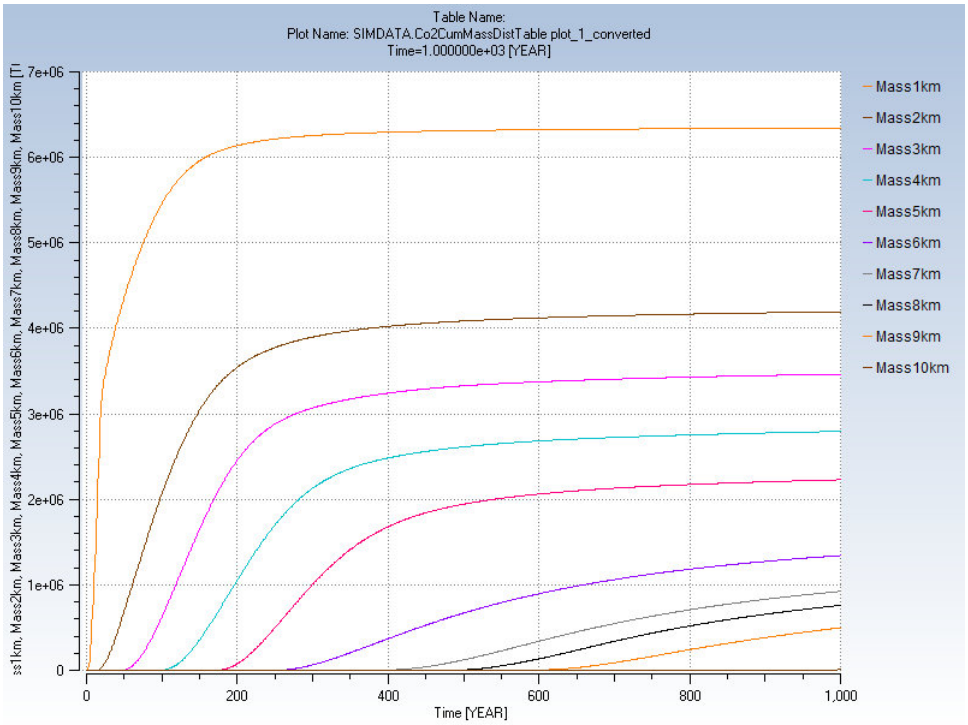

Figure 12-27. Mass of CO_2 migrating greater than given distance against time for reference case with 10 million tonnes leaked, homogeneous model.

12.7.1. Uncertainty Analysis

Using as a reference the sensitivities analysed in the simple box model (Table 12-2) a set of runs were prepared in order to enhance the understanding of the CO_2 migration path in the more realistic 3D geological model. Parameters were defined as follow.

Table 12-3. Parameter sensitivities (high/low values represent distance CO_2 migrates, not size of parameter value).

Sensitivity	Low value	Reference Value	High Value
Perforation position	Base	Mid	High
Delta P (psi)	700	500	100
Perforation length (ft)	400	200	10
Max rate (tonnes/day)	2000	1500	100
Nw	7	5	3
Sgtrap	0.35	0.25	0.2
Kv/Kh	0.01	0.1	1
Mass CO_2 (tonnes)	1000000	10000000	13000000
Permeability (mD)	105	210	420

The results of these sensitivities are shown in the Tornado diagram in Figure 12-28. The labelling of high and low for the various parameters is based on the distance the plume travels rather than the absolute value of the parameters which makes reading the chart clearer. For instance, a high flow rate results in a smaller migration distance as described below. The solid colours bars represent results from the mode detailed 3D Mey model, while the transparent bars are results from the simulacrum box model. As can be seen, in some cases having a simple tilted but flat top structure can cause CO_2 to travel larger distance and would represent an unlikely worst scenario, e.g. permeability.

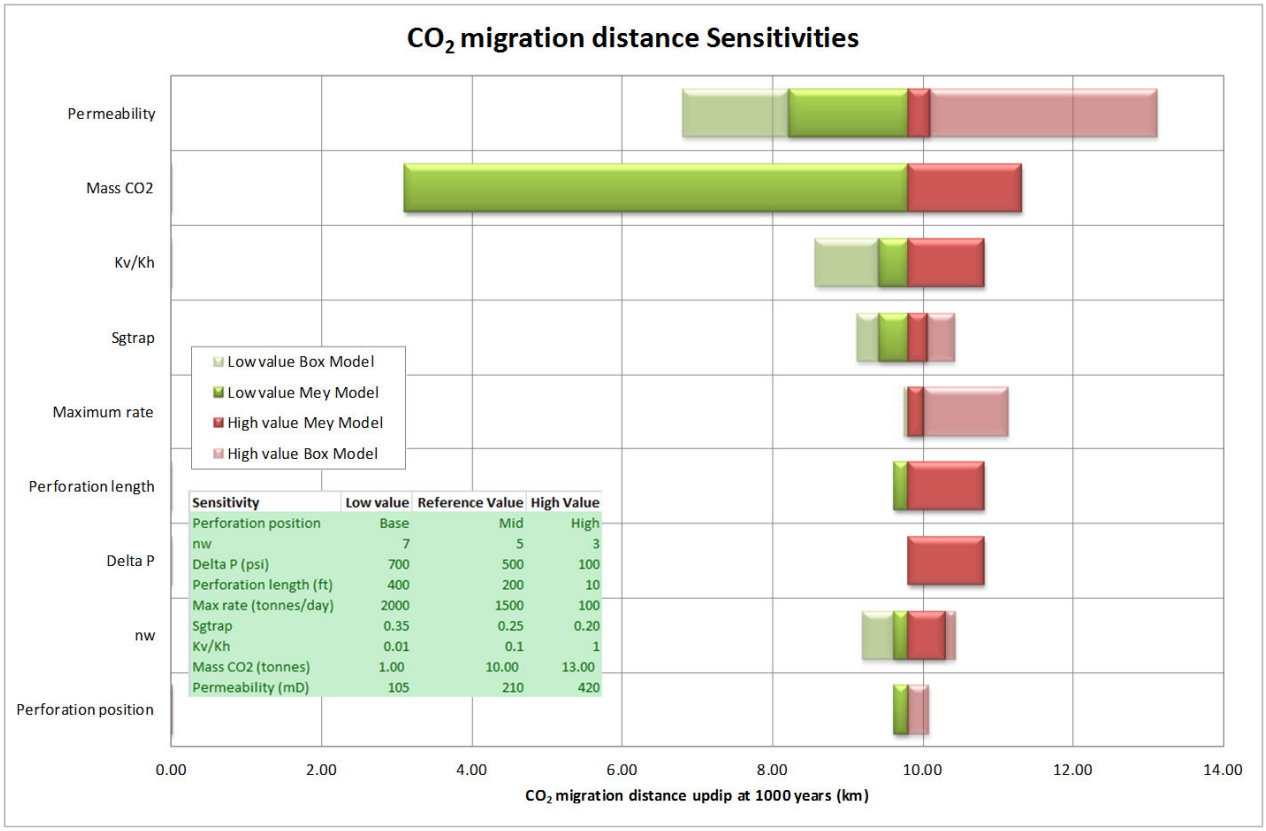

Sensitivity	Low value	Reference Value	High Value
Perforation position	Base	Mid	High
nw	7	5	3
Delta P (psi)	700	500	100
Perforation length (ft)	400	200	10
Max rate (tonnes/day)	2000	1500	100
Sgtrap	0.35	0.25	0.20
Kv/Kh	0.01	0.1	1
Mass CO2 (tonnes)	1.00	10.00	13.00
Permeability (mD)	105	210	420

Figure 12-28. Tornado diagram for migration sensitivities.

From the figure it can be seen that the most important parameters affecting the migration distance are the permeability, mass of CO_2 leaked and the vertical to horizontal permeability ratio k_v/k_h. The perforation length and position are less important in this chart. The reference case injection rate is relatively high, being set at the rate of a typical Goldeneye well. In reality, a leak from the Goldeneye reservoir will probably be at a much lower rate, and it can be seen from the figure that while migration distance is insensitive to increases in the leak rate, there is a significant increase in migration distance as the rate decreases to 100 tonnes/day. The CO_2 distribution for this case is shown in Figure 12-29 where it can be seen that the inverted cone of trapped CO_2 around the well is much smaller due to the lower leak rate allowing buoyancy forces to become more important in the movement of CO_2 away from the well. This resulted in less gas being trapped near the well and more being available to migrate up dip. The same mechanism explains the sensitivity of the migration distance to permeability and pressure difference. Higher vertical permeability (Figure 12-30) or lower pressure difference enhance the importance of the buoyancy force creating a smaller cone around the well and leaving less trapped gas behind.

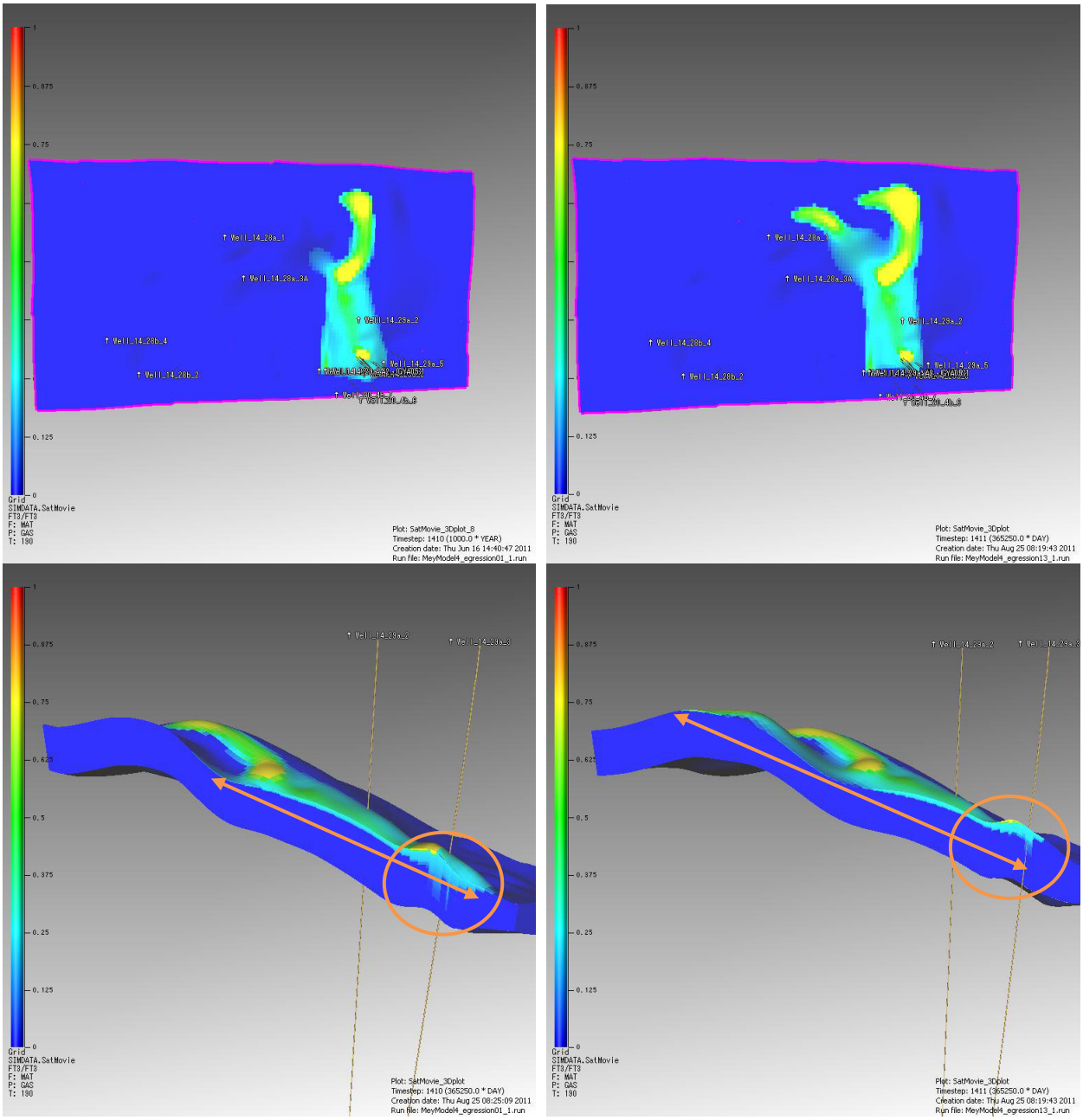

Figure 12-29. Distribution of CO_2 in XY and XZ sections through well after 1,000 years for 1500 tonnes/d (left) and 100 tonnes/day (right) leak rate case – homogeneous model.

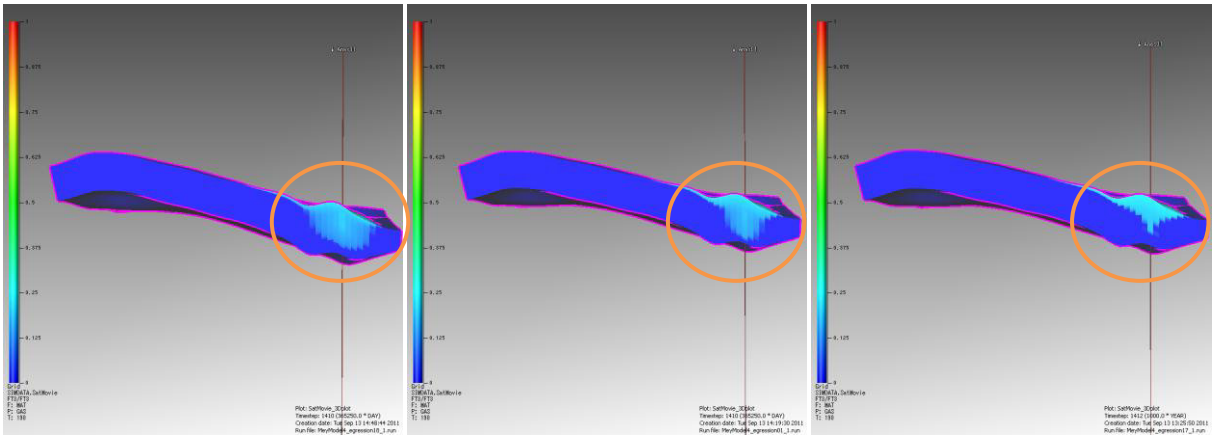

Figure 12-30. Distribution of CO_2 in XZ sections through well after 1,000 years for k_v/k_h = 0.01 (left); 0.1 (middle:- Base Case); 1.0 (right) – homogeneous model.

Over relatively short periods of time, altering the residual gas saturation does not cause a substantial change in how far the plume travels. However, after 500 years the S_{gr} effect becomes more evident, with a difference of a few hundreds of meters (0.4 – 1.0 km) (5% – 12%).

Table 12-4 – Residual gas saturation sensitivity results

S_{gr}	Time	Distance from well	Diff
	YEAR	*KM*	*KM*
0.20	508	8.21	-0.2
0.25	508	8.01	
0.30	508	7.61	0.4
0.35	508	7.01	1.0

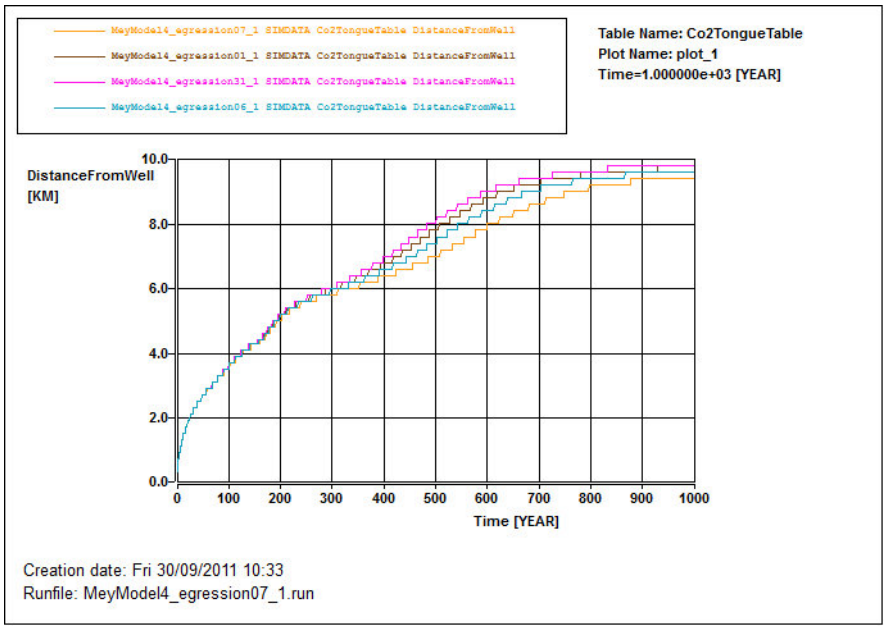

Figure 12-31. Residual gas saturation sensitivity, homogenous model. Sgr = 0.20, 0.25, 0.30, 0.35.

The residual gas saturation also has an effect on the CO_2 dissolution in brine. A higher residual gas saturation case (ochre line) constrains the CO_2 plume migration length because it is trapping more CO_2 as it travels. This means that less water is contacted and hence, less CO_2 is dissolved (Table 12-5). The direct impact on dissolution could be -10% to +7.5%.

Table 12-5. Impact of Sgr on CO_2 dissolution in brine.

S_{gr}	CO_2 Dissolved	Diff
	Mt	Mt
0.20	3.2877	0.2308
0.25	3.0569	
0.30	2.894	-0.1629
0.35	2.7491	-0.3078

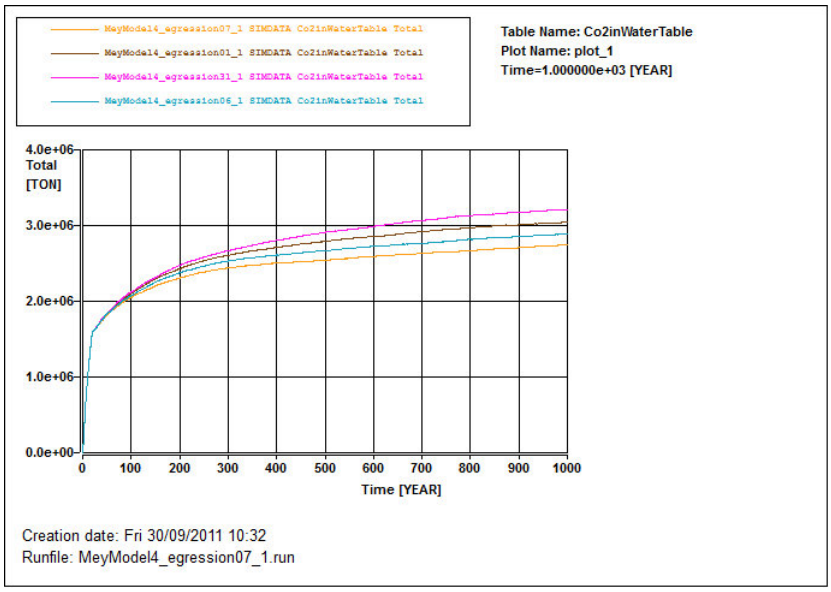

Figure 12-32. Impact of Sgr on CO_2 dissolution in brine.

There is no direct measurement of trapped gas saturation in Mey cores unlike for Goldeneye core plugs. Residual gas saturation for Goldeneye was estimated to be between 0.25 -0.35 based on the ambient conditions SCAL test[47]. The reservoir condition CO_2 specific flooding test produced a wider range (0.16 – 0.38) depending on the pre - conditioning of the samples (18).
The uncertainty ranges used for Mey egression model encompass the SCAL data available and the impact on CO_2 plume length and dissolution is approximately 10%, which is small in comparison with the range of uncertainty of other parameters such as the top reservoir structure.

The topography (top structure of Mey sands) is not explicitly included as an uncertainty even though, it will dominate the geometry/direction that the CO_2 plume will develop. Nonetheless, it is believed that the top structure uncertainty is covered by the simple tilted box model as an extreme case, because this represents the worst case scenario in terms of plume migration. Any topography element will generally constrain the CO_2 closer to the leak point, representing a lower risk.

12.7.2. Alternative source points

There are four abandoned exploration and appraisal wells within the Captain formation, with another one just to the north of the field (14/29a-2) which did not encounter Captain reservoir but instead the Scapa formation, which is not in communication with the Captain reservoir. Of the five production wells, GYA02 was sidetracked at reservoir level. The current Goldeneye wells have no barrier over the Lista/Dornoch until these wells are abandoned.

Simulation results presented so far show an egression from Goldeneye into the Mey sandstone via E&A well 14/29-a3 which has one of the highest volumes at risk (13Mt). From the detailed leak path analysis some of the wells can be ruled out because based on simulation results they will have 0 Mt of mobile CO_2 to get in contact with (14/28a-1, 14/28a-3a, 20/4b-7, 14/29a-2). Nevertheless, well 14/29-a5 and 20/4B-6, with some 8Mt and 1Mt volume at risk respectively (Figure 12-33), are worth simulating to assess their probable CO_2 migration path.

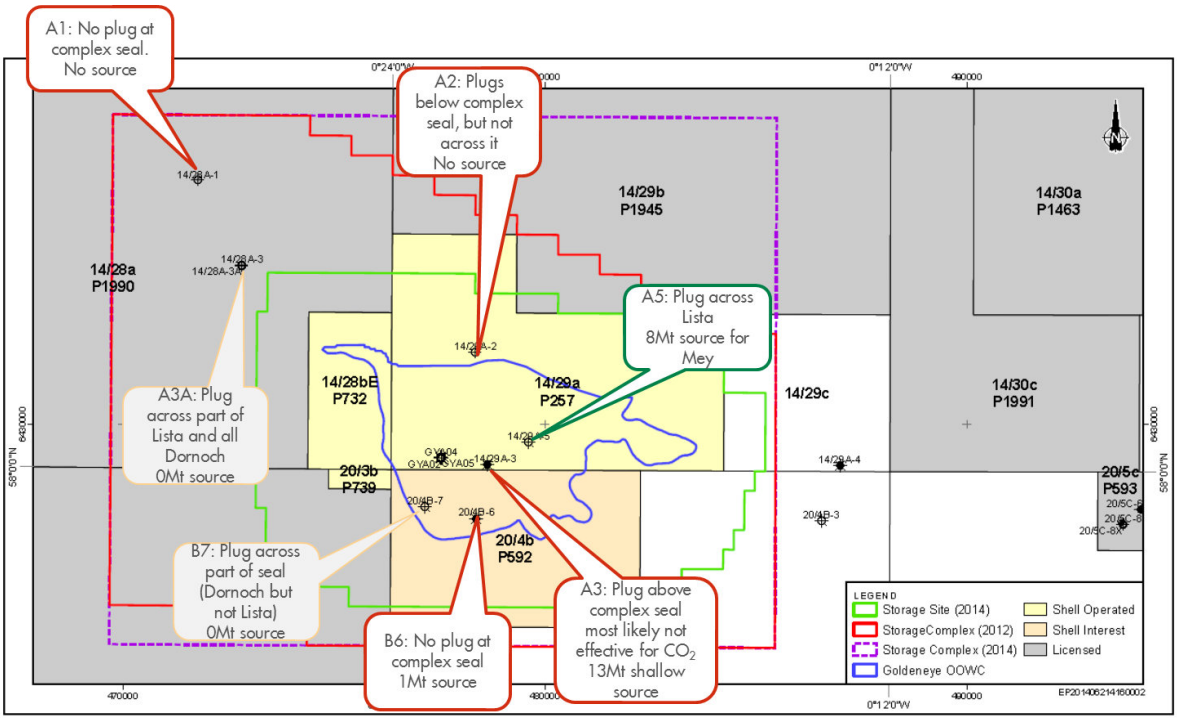

Figure 12-33. Well Risk map of the complex seal.

The following results show a hypothetic leaking well based on 14/29-a5,completed at top 200ft with a leak rate set as 1500 tonnes of CO_2 per day (28.3 MMscfd), roughly equivalent to one Goldeneye injection well, as in the box model case (section 12.5). The total CO_2 leaked is 10 Mt. Again, as in the box model case, this represents a total failure of all barriers and will represent a finite release.

The CO_2 migration path is very similar to the scenario where 14/29-a3 is used as a leaking well. However, well 14/29-a5 offers an interesting alternative as leak point, as its down dip position in the structure means that CO_2 is spread through a wider area and benefits from trapping mechanisms such as capillarity and dissolution. This makes the plume travel a slightly shorter distance (10% shorter) as illustrated in

Figure 12-36.

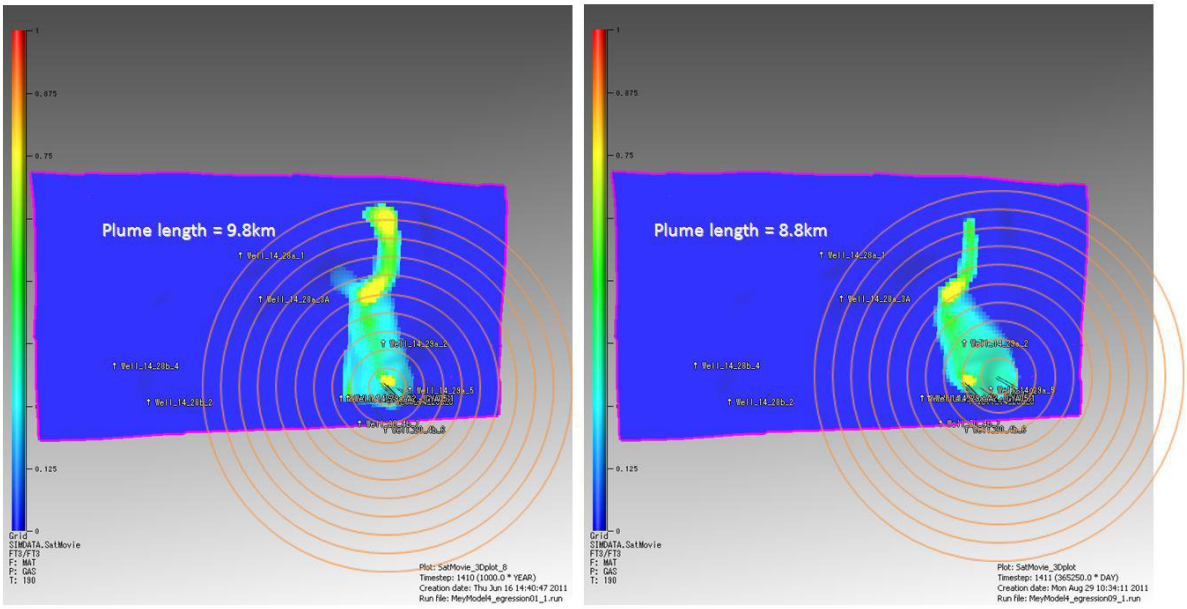

Figure 12-36. Distribution of CO_2 in XY sections through well 14/29-a3 (left) and 14/29-a5 (right) after 1,000 years. Each concentric line represent 1 km. Both homogeneous models.

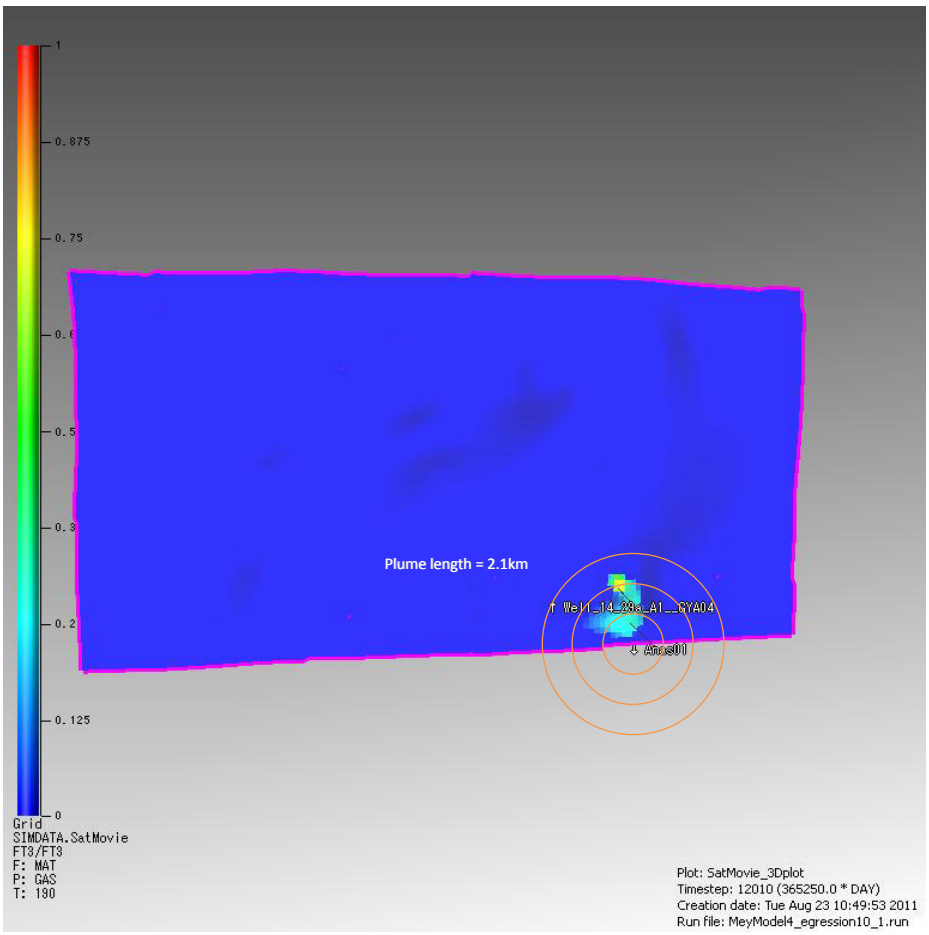

Figure 12-37: Distribution of CO_2 in XY section of well 20/4b-6 after 100 years. homogenous model

Another possible scenario involving well 20/4b-6 would involve only 1 Mt volume at risk (Figure 12-9). Again, the well is assumed to be completed at the top 200ft, with the maximum leak rate set as 1500 Tonnes per day. To release all of the 1 Mt at risk would take 1.8 years.

This small leak volume of CO_2 will travel approximately 2.1 km away from the well in 1000 years.

A sensitivity was also done in this case with a leak rate set as 100 tonnes per day (1.9 MMscfd) that represents a probable leak through a micro annulus in a cement plug, assuming shrinkage of 0.7%. It will require almost 28 years to release 1 Mt at 100 tonnes per day. This scenario would be a steady state CO_2 egression. Results showed that CO_2 travels further in the lower leak rate scenario. As before, this is because the inverted cone of trapped CO_2 around the well is much smaller due to the lower leak rate allowing buoyancy forces to become more important in the movement of CO_2 away from the well. This results in less gas being trapped near the well and more being available to migrate up dip.

12.7.3. Combined leak scenarios

In the unlikely scenario of a primary leak from the Goldeneye reservoir into the secondary storage (the Mey Formation), via one of the E&A wells (e.g. 14/29-a5), a secondary leak to seabed could in principle occur via neighbouring wells such as 14/29-a3.

The injection of CO_2 into the Mey at 400 psi overpressure increases the local Mey pressure approximately from 2050 psi to 2150 psi during 20 years of the hypothetical leak. It is during this "active injection" period when CO_2 could have the greatest potential (higher pressure) to find its way out to leak through other wells to a higher level in the overburden.

The following table considers the four abandoned exploration and appraisal wells within the Captain formation and their possible combination of leaking into each other.

Table 12-6. Combined leak scenarios.

Primary Leak Well	Vol @risk Mt	Secondary Leak Well			
20/4B-6	1	14/29a3 (30 years)	20/4B7 (50 years)	Any GYA (100 years)	
20/4B-7	0				
14/29a-3	13	GYA04 (20 years)		Any GYA (30 years)	14/29a2 (120 years)
14/29a-5	8	14/29a3 (20 years)	GYA04 (30 years)	Any GYA (40 years)	14/29a2 (60 years)

If a leak happens in well 14/29-a5, the first well to be in contact with the CO_2 footprint would be 14/29-a3. CO_2 will take approximately 20 years to arrive (Figure 12-38). The volume at risk for 14/29-a5 is 8Mt, the sensitivity was done with 10Mt.

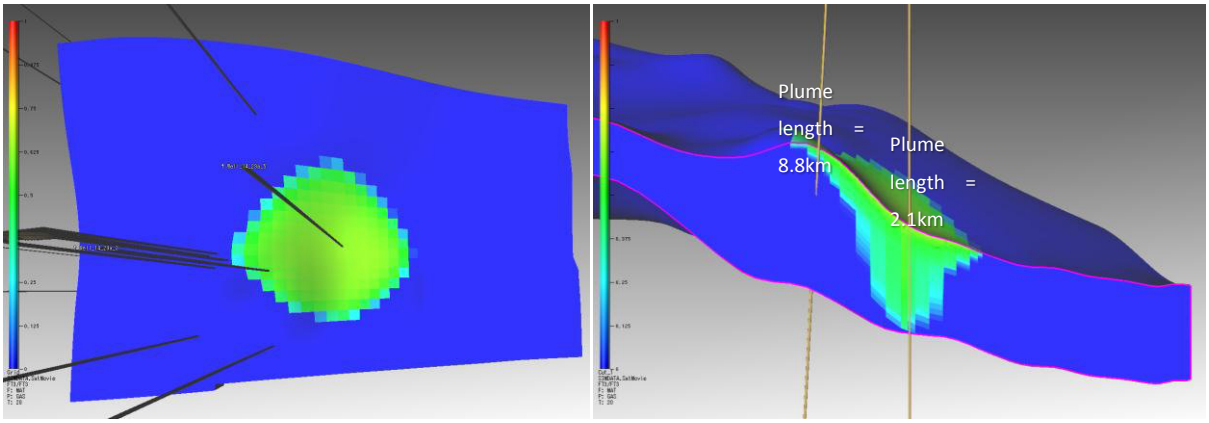

Figure 12-38. Distribution of CO_2 in XY and XZ sections through wells 14/29-a3 and 14/29-a5 after 20 years.

Once the connection between the primary leak well (14/29-a5) and the secondary leak well (14/29-a3) has been made, there would be a direct migration path (Figure 12-39) and most of the CO_2 coming from Goldeneye will be produced by 14/29-a3.

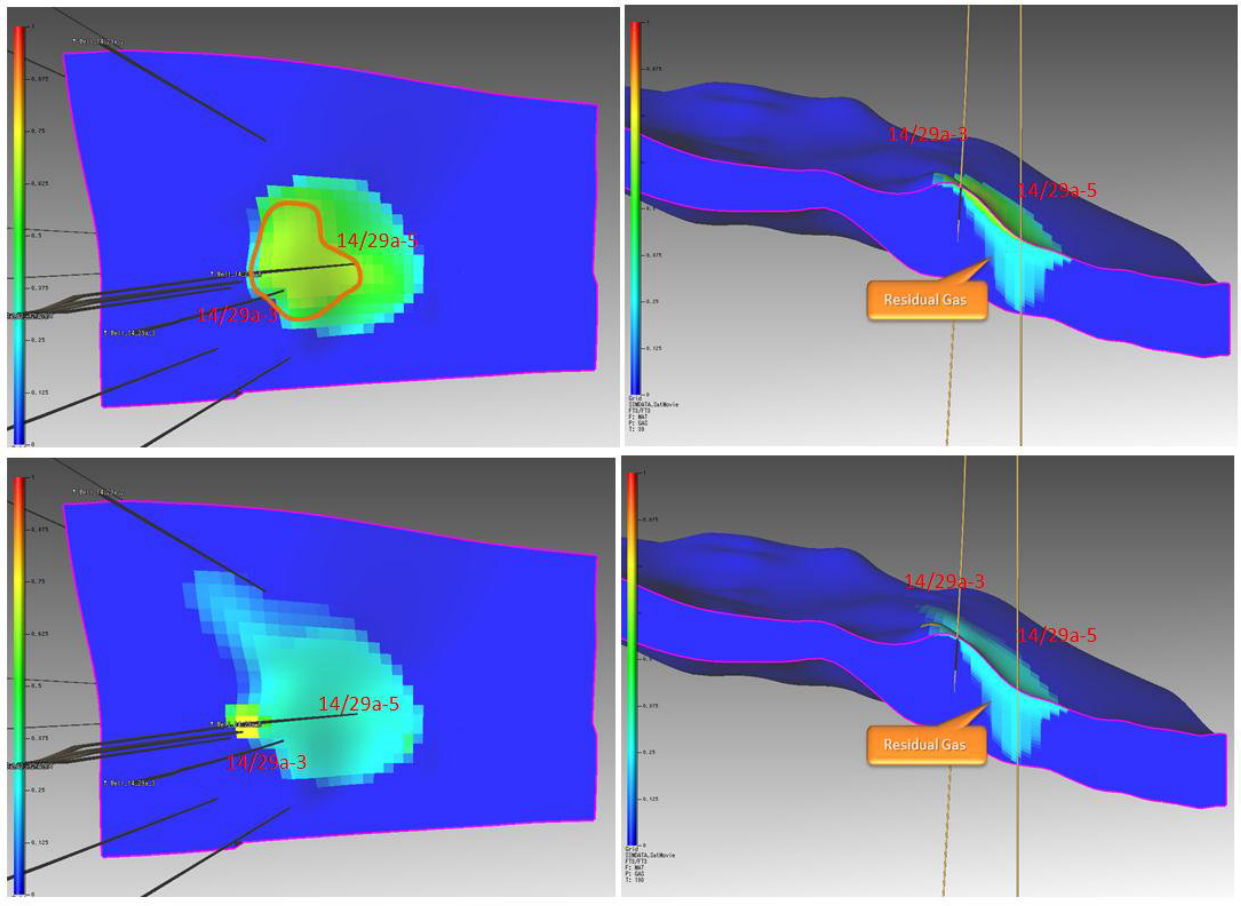

Figure 12-39. Distribution of CO_2 in XY and XZ sections through wells 14/29-a3 and 14/29-a5 after 40 years (top) and 1000 years (bottom).

The secondary leak through well 14/29-a3 would have the following characteristics:

- CO_2 acts as a natural gas lift mechanism for the well.
- Small amount of CO_2 in the well will empower the well to flow to seabed.
- Big pressure drop from seabed also helps the well to flow.

The direct migration path created between the source well (14/29-a5) and the sink well (14/29-a3) would change completely the CO_2 footprint in the Mey sandstone. CO_2 will not travel a large distance from the primary leak well, it would mainly spread until it reaches the secondary leak well.

From the model results, we can see that a good proportion of the total CO_2 would probably be sequestered by capillary trapping and dissolution (47%). The reverse CO_2 cone is then produced leaving behind trapped gas. In addition, there is only a finite volume at risk (8 – 13 Mt) which constrains the CO_2 source and allows the aquifer to act and trap CO_2. In the unlikely event that there is a massive leak in well 14/29-a3, which would represent a total failure of all barriers, some 4.1 Mt of CO_2 (41% of the injected 10 Mt) could escape to seabed. 1000 years later, some 1.2 Mt would still be in dense phase in the Mey sandstone, so not all the mobile CO_2 will travel to seabed (Figure 12-40).

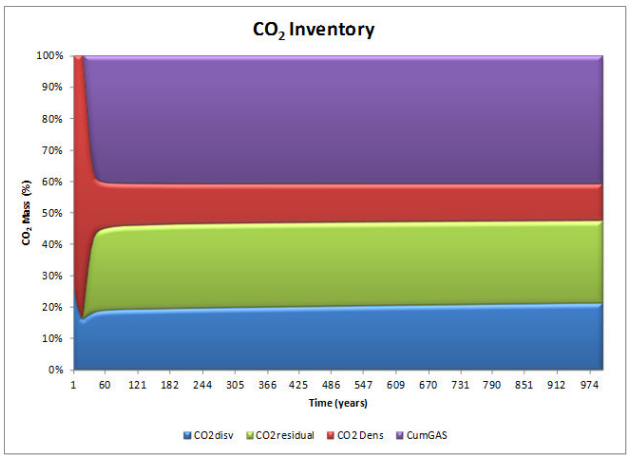

Figure 12-40. CO_2 mass inventory as a function of time (top). CO_2 percentage inventory as a function of time (bottom). Combined leak scenario, homogeneous model.

Combined numerical and analytical estimations show that, if a CO_2 plume reaches well 14/29-a3 with CO_2 saturation of about 45-52%, Land's correlation would suggest $20\% < S_{gr} < 25\%$ (other correlations will push the S_{gr} range to be 19%-27% with an average of 23%) . Numerical results say that 84% of CO_2 will still be in dense phase and some 16% probably dissolved (optimistic because of numerical dispersion, could be 92% in dense phase and only 8% dissolved). With these ranges of uncertainty the trapped CO_2 could be between 48% and 52%.

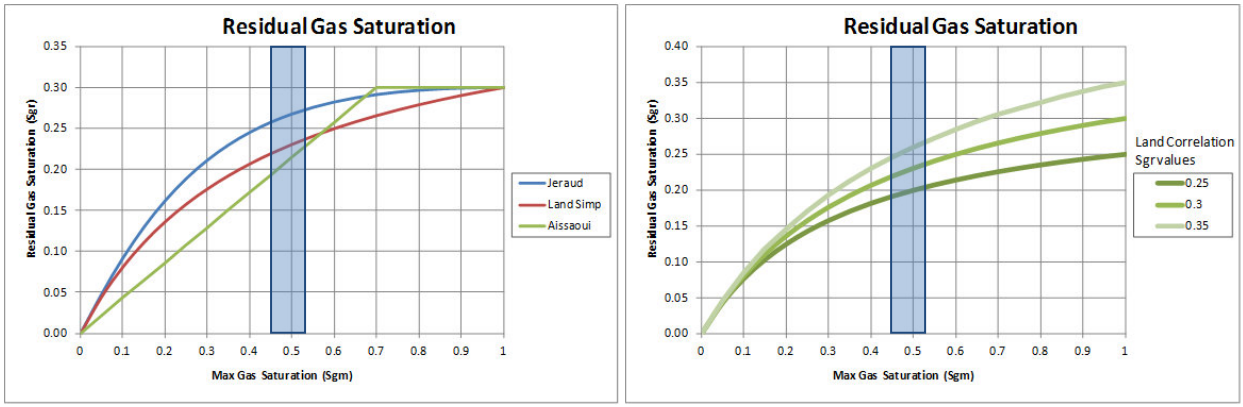

Figure 12-41. Different residual gas saturation correlations (left). Lands correlation sensitivity (right)

A combined leak scenario was also modelled between wells 20/4b-6 as primary leak well and 14/29-a3 as secondary leak well. The volume at risk would be smaller (1Mt) but results showed similar proportions of dissolve, capillary trapped, dense phase and escaped volume.

The following table summarizes the interaction of the four abandoned exploration and appraisal wells among themselves. Principal diagonal numbers are the volume at risk estimated for each well. Intersection between 14/29-a5 and 14/29-a3, and 20/4b-6 and 14/29-a3 gives the volume of CO_2 that could reach seabed in case a combined leak occurs. In addition, the table also depicts which wells could be involved (interact) if a leak occurs at the Mey sandstone. The assessment didn't consider the five production wells (GYA01 to GYA05), however, it shows when those wells could be impacted if there is a leak through one of the E&A wells.

Table 12-7. Traffic light combined leak scenarios.

		Secondary Leak Wells					
		20/4B-6	20/4B-7	14/29a-3	14/29a-5	14/29a-2	GYA
Primary Leak Wells	20/4B-6	**1 Mt**		**0.327 Mt**			
	20/4B-7		**0Mt**				
	14/29a-3			**13 Mt**			
	14/29a-5			**4.1 Mt**	**8 Mt**		
	14/29a-2					**0 Mt**	
	GYA				**?**	**?**	**13 Mt**

12.8. Overburden Model Forecast (3D Heterogeneous Model)

A heterogeneous version of the 3D geological model for the Mey sandstone was also constructed, to mimic a channelized distribution of reservoir properties.

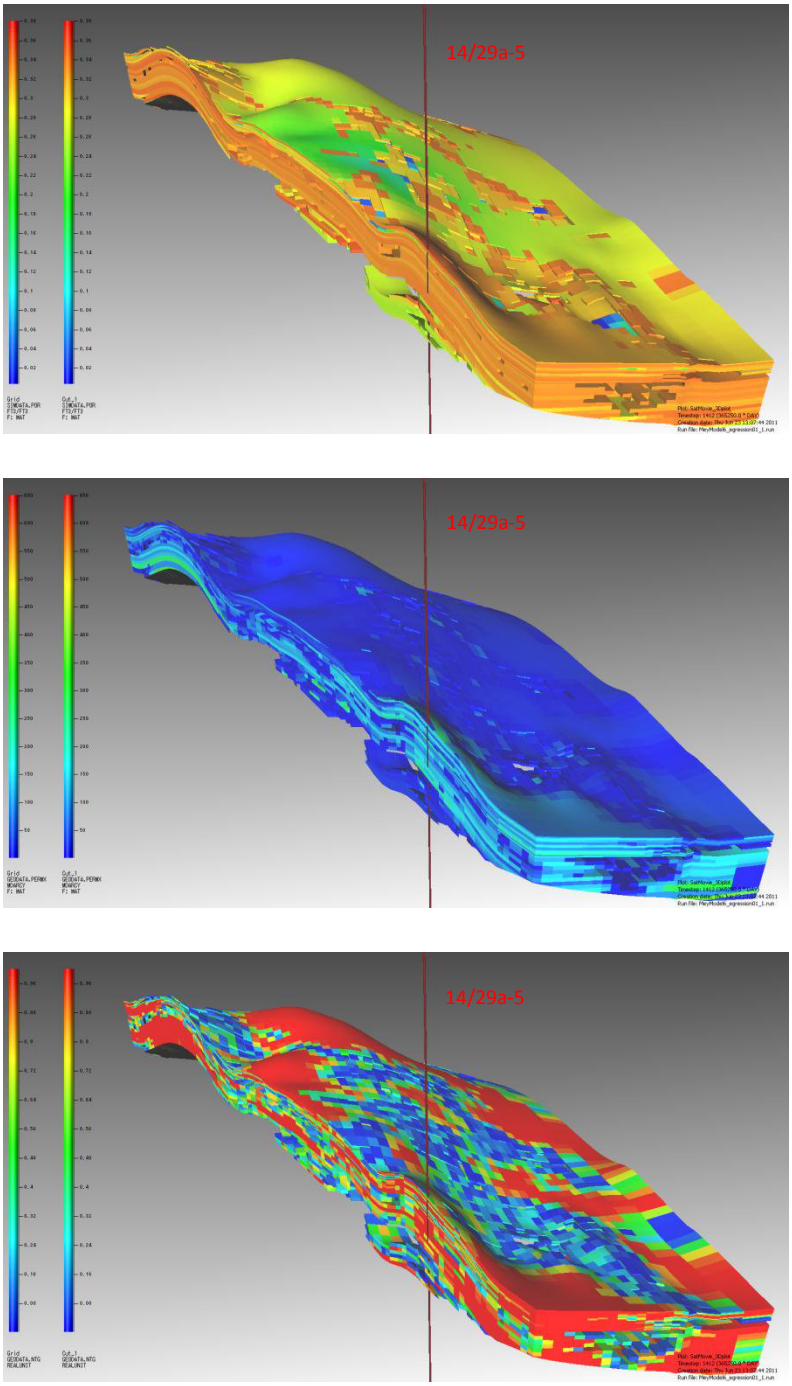

Figure 12-42. Heterogeneous version of Mey Geological Model. Porosity distribution (top); Permeability distribution (middle); Net to Gross distribution (bottom).

The reference case leakage scenario was rerun using this alternative realisation, in order to assess the impact of heterogeneities on the CO_2 migration path. The results can be seen in the following figure.

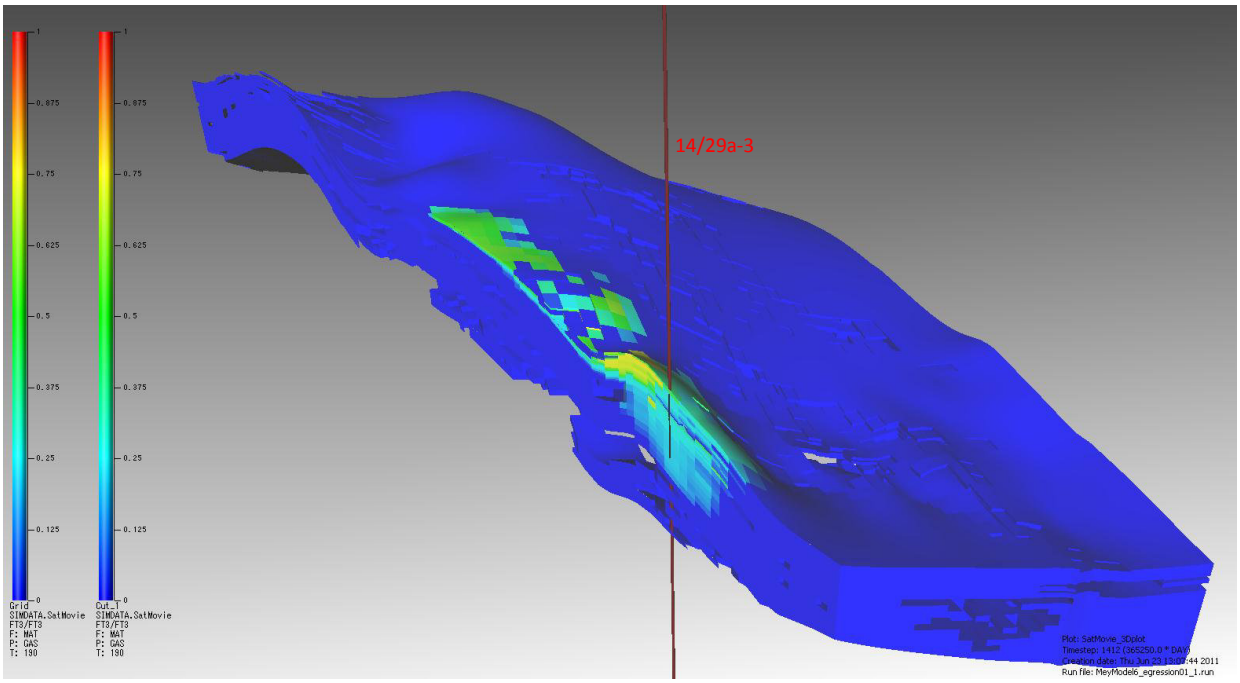

Figure 12-43. Distribution of CO_2 in a 3D cross section at well 14/29-a3 after 1000 years. Heterogeneous model.

The results showed that the lack of connectivity in this version of the model produces a distorted migration path for the CO_2. As a consequence, the distance travelled is shorter (+/- 4.5 km from the well) as the CO_2 gets widely distributed in the vertical sense generating different CO_2 footprints per layer. Once some CO_2 finally finds a connection to the top of the formation, the top structure then dominates the migration path. This is similar to the behaviour seen in the Sleipner CO_2 storage project. The following sequence of 3D panel views at 100, 500 and 1000 years, show the vertical distribution of CO_2 concentrated mainly near the leaking well.

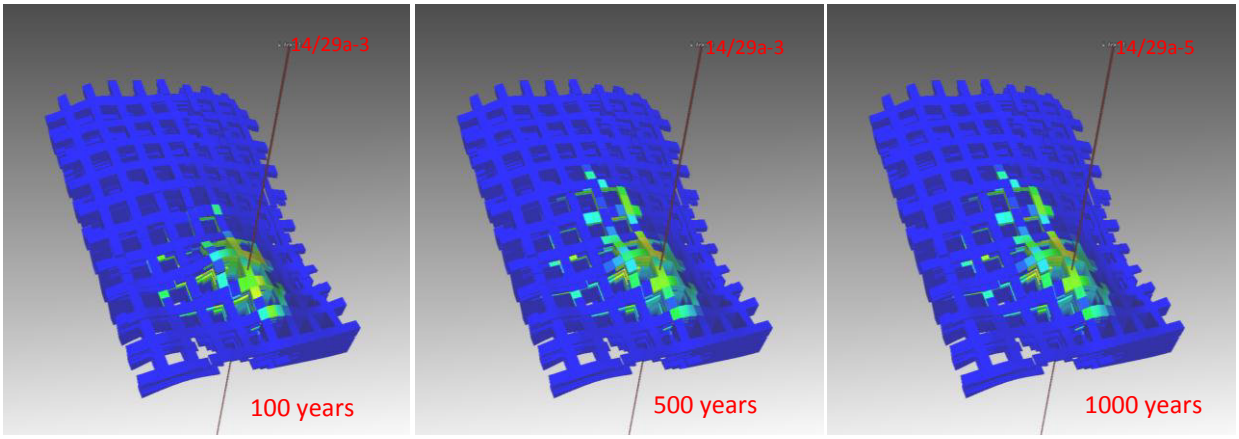

Figure 12-44. CO_2 distribution in 3D panel view at 100, 500 and 1000 years. Heterogeneous model.

The heterogeneous version of the Mey sandstone model is probably the most realistic of the realisations simulated in this study however a large uncertainty exists on the actual distribution of the

reservoir properties. The results show that incorporating heterogeneities into the model actually reduces the chances of CO_2 migrating very far and potentially leaking out of the storage complex. The reservoir heterogeneity creates a tortuous migration path which constrains the CO_2 footprint.

12.9. Seismic detection of CO_2

A number of seismic surveys will be conducted during and after injection The use of 4D seismic will allow leaks from the reservoir to be detected but only if the gas plume is above a certain size. The detection limit in the Mey sandstone is estimated to be 300 – 3000 tonnes of CO_2, depending on the quality of the seismic. For a leak via a micro annulus with a cement shrinkage factor of 0.1%, 2.1 tonnes/day of CO_2 might leak into the Mey sandstone. This implies it would take 5 months to 4 years before a large enough plume of CO_2 had formed. The time for detection might well be longer if the plume was not of the optimum shape for detection.

To investigate the plume shape, both the homogeneous and heterogeneous geological models of the Mey sandstone have been exported to Xstream for study. For details see the MMV technology screening report. The key results are summarized below:

Monitoring a CO_2 plume at the Mey sandstone level caused by a well leak or through faults/fracture is feasible. Based on the assumptions above, seismic amplitude or seismic acoustic impedance changes will detect (gross) CO_2 columns of 30 ft or even less.

On 4D seismic both RMS and time-shift changes should be able to clearly detect and delineate the CO_2 plume from by well leaks or fracture/fault leakage.

The detection limits in this study show some improvement over the detection limited predicted in earlier estimates. Assuming good quality seismic, leaked volumes of less than 300 tons should be detectable in the best case and less than 3,000 tons in the worst case.

The 3D seismic forward model in this study includes the effect of shale layering in the Mey sandstone and shows that the shale layers do not adversely affect the ability to detect a CO_2 plume related to a leaking well or leak path. This gives good confidence that 4D seismic can be applied to detect and delineate CO_2 plumes in the overburden.

12.10. Key results from the secondary containment study

- **Leakage mechanism/paths investigated**. The leak paths considered in the study include existing wells. Existing faults have been mapped and fractures have been analysed and none have been identified to be pervasive throughout the seal systems. As a consequence, they are not included in this study. For a comprehensive understanding of the containment risk, which include the critical parameters affecting leakage, a summary of risks and contingency plans in case of leakage, refer to the Storage Development Plan (38).
- **Key assumptions of input**. The initial model comprises a simple rectangular box with a constant dip of 1.5°; average permeability of 210 mD; porosity of 34%; net to gross of 46% and Kv/Kh set to 0.1. A more detailed model was created based on the 3D geological model of the Mey sandstone from limited data available.
- **Leak rates**. In the case of a CO_2 leak via a micro annulus in the well due to cement shrinkage as a consequence of thermal effects, the leak rate from a cement shrinkage of 0.1% could be 2.1 tonnes/d (0.04 MMscf/d). The cement shrinkage could be as much as 0.7% producing a leak rate of 100 tonnes/d (1.9 MMscf/d). These scenarios represent a steady state CO_2 egression. A total absence of barriers (i.e. no cement plugs) will investigate a finite release of a volume at risk. These scenarios have been modelled with a leak rate of 1500 tonnes/d (28.3 MMscf/d) equivalent to

expected CO_2 injection rate into Goldeneye from one injection well and represent the reference extreme case.

- **Volumes at risk**. The CO_2 volume at risk below each well within the Goldeneye field after the system has reached gravity equilibrium after injection of 20Mt varies between 1 and 13 Mt.
- **Trapping mechanism**. Any CO_2 reaching the base of the Lista mudstone is expected to migrate in the general direction of the regional dip, steered by local heterogeneities. (Migration occurs until it is trapped by a local structure; or capillary, dissolution or chemical trapping. For a explanation of the physics of the trapping see Section 7 of this report).
- **Typical migration plume expected in Mey** for a total failure of barriers and a leakage volume of 10Mt is ~10km. Analysis of the uncertainty in the migration distance yields a range between 3 km and 13 km. This range covers the impacts of permeability variation both horizontal and vertical; mass of CO_2; trapped gas saturation; relative permeability parameters; leakage rate; leakage point (perforation) length and position and the pressure difference between the source (Goldeneye field) and the sink (Mey sandstone).
- **Uncertainty in migration and key uncertainties – impact on extent of plume.** The results show that the main reservoir parameters governing the migration of CO_2 are the horizontal and vertical permeability and the trapped gas saturation, besides the topography of the container.
- **Is a ~10 km plume a problem?** Analyses show that after 1000 years of migration this ~10 km CO_2 plume is not near other wells that could potentially work as secondary leak paths. The closest wells to the NW: 14/28a-1 and 14/28a-3Arepresent the highest risk because of their proximity to the leakage area and the lack of a cement plug at Lista/Dornoch level in 14/28a-1. Nevertheless, based on these results, there is no CO_2 in contact with either well. Other wells are located too far away or downdip where CO_2 is not expected to migrate due to buoyancy forces. However, it must be considered that this finding represents the results of a single top structure realization. Due to the limited information available of the Mey sandstone the predictions of CO_2 migration paths have a high uncertainty.
- **Can a leak be detected / and what would be done?** Yes, it can be detected. Seismic detection of leaking CO_2 appears possible as the initial distribution of CO_2 around the well forms a fairly compact volume which should be capable of being detected by 4D seismic. The detection limit in the Mey sandstone is estimated to be 300 – 3,000 tonnes of CO_2 depending on the quality of the seismic. A comprehensive Corrective Measures Plan[63] (Doc. No. SP-FM160D3A-RT 063) is available.

13. Conclusions

Geologic carbon storage capacity has been calculated for the Goldeneye reservoir, resulting in 47 million tonnes of CO_2 equivalent available for storage as maximum theoretical boundary from voidage.

This maximum storage volume initially estimated was modified by storage efficiency factors which account for the fact that CO_2 will not be able to completely refill this volume.

The major static elements that could impact the storage capacity of Goldeneye are: (a) extension of the stratigraphic pinch-out; (b) structural dip on the western flank of the field; and (c) internal Captain Sand stratigraphy (thickness) and (d) injection pattern. Dynamic elements have also been considered and are mainly related to the displacement mechanism and the unfavourable mobility ratio

[63] Corrective Measures Plan, PCCS-05-PT-ZP-9025-00001, Shell 2014.

of the process. These elements are summarized in: (a) relative permeability end points (both water and gas/CO_2), and (b) residual gas saturation (S_{gr}).

The conjunction of these static and dynamic uncertainties depicts the framework which is necessary for understanding the storage efficiency factors that discount the total theoretical capacity.

A three-dimensional, three-phase, full field Goldeneye numerical simulation model corroborated the initial storage estimations and evaluated different injection scenarios to map out the range of capacity available for CO_2 storage.

The complete suite of static reservoir models created to investigate CO_2 injection performance in the field demonstrated that Goldeneye has sufficient storage capacity to hold 10 million tonnes of CO_2, as well as the possible extension to 20 million tonnes of CO_2. All of the uncertainty scenarios currently evaluated showed that the field can safely sequester the intended volume.

None of the injected CO_2 would move outside the original OWC when injecting 10 million tonnes of CO_2. In the 20 Mt injection case, the model indicated that only 3 % of the total injected CO_2 would lie outside the original OWC at the end of injection. However, after cessation of injection all of the CO_2 is either recovered back into the geological store or is otherwise sequestered (by means of dissolution or capillary trapping).

A range of models has been used to predict future pressures in Goldeneye. These give a range of pressures in year 2019 (before CO_2 injection) from 2703 psia to 2987 psia [186.4 bar to 206 bar].

CO_2 is not expected to egress from the reservoir. However, this scenario was tested by injecting CO_2 directly at the spill point which allows the CO_2 to migrate updip. This is a slow process due to the varying dip of the formation. After 1000 years 5 million tonnes of CO_2 has migrated 6-7 km to the west and is dissolving in the aquifer water. It does not reach the Atlantic and Cromarty fields or any of the nearby abandoned exploration wells to the west.

The rise in pressure in the neighbouring Hannay field to 2029 is expected to fall in the range 300 - 500 psi [20.7 – 34.5 bar]. The rise in pressure will be affected by production from the West Rochelle field which started production in October 2013 and East Rochelle which started in January 2014. (Atlantic and Cromarty pressures will also rise by 200 - 500 psi [13.8 – 34.5 bar] over the period to 2029 but this is also uncertain as they are more sensitive to the size of the western aquifer and the impact of continuing production and injection at Blake. After cessation of production in Rochelle West and East, around 2020, the pressure rises rapidly by about 400 psi over the period to 2029.

In order to determine the maximum geologic carbon storage capacity for the Goldeneye reservoir, a theoretical continuous CO_2 injection revealed that over 29 million tonnes of CO_2 had to be injected to reach the spill point and create an egression. This considers a combined Goldeneye hydrocarbon reservoir in addition to the storage capacity of the aquifer beneath the field. This situation will represent a significant storage capacity margin for both 10 Mt or 20 Mt of CO_2.

14. Bibliography

1. **Shell.** *Report on Results of Lab Experiments (Geo-Mechanical Investigation).* 2014. PCCS-05-PT-ZP-9018-00001, Key Knowledge Deliverable 11.112.

2. —. *Geochemical Reactivity Report.* 2014. PCCS-05-PT-ZR-3323-00001, Key Knowledge Deliverable 11.116.

3. **Edinburgh, University of.** *Progressing Scotland's CO2 storage opportunities, .* March 2011. ISBN: 978-0-85272-684-6.

4. **Shell.** *Geochemical Reactivity Report.* 2014. PCCS-05-PT-ZR-3323-00001, Key Knowledge Deliverable 11.116.

5. **Peneloux, A., E. Rauzy., and R. Freze.** *A Consistent Correction for Redlich-Kwong-Soave Volumes. Fluid Phase Eq. 8, 7-27.* 1982.

6. **Robinson, D.B. and D.Y. Peng.** *The characterization of the heptanes and heavier fractions for the GPA Peng-Robinson programs. (Booklet only sold by the Gas Processors Association, GPA), RR-28 Research Report.* s.l. : Gas processors association, 1978.

7. **Shell.** *Goldeneye Static Model (Field).* 2014. PCCS-05-PT-ZG-0580-00004, Key Knowledge Deliverable 11.108.

8. **Peneloux, A., E. Rauzy., and R. Freze.** *A Consistent Correction for Redlich-Kwong-Soave Volumes. Fluid Phase Eq. 8, 7-27.* 1982.

9. **al., Whitson C.H. et.** *Gas Condensate PVT – What's really important and why?, IBC Conference "Optimization of Gas Condensate Fields".* London (U.K.) : s.n., 1999.

10. **Technology, National Institute of Standards and.** *http://webbook.nist.gov/chemistry/fluid.*

11. **Shell.** *PVT Modelling Report for CO2 in Goldeneye Project.* 2014. PCCS-05-PT-ZR-0580-00001, Key Knowledge Deliverable 11.118.

12. **Leverett, M.C.** *"Capillary behaviour in porous solids". Transactions of the AIME (142): 159–172.* 1941.

13. **Archie, G.E.** *The Electrical Resistivity Log as an Aid in Determining Some Reservoir Characteristics, Dallas Meeting.* October 1941.

14. **Shell.** *Petrophysical Modelling Report.* 2014. PCCS-00-PT-ZP-9032-00001, Key Knowledge Deliverable 11.111.

15. —. *Initially In-Place (IIP) Volumes report for Goldeneye project.* 2014. PCCS-05-PT-ZG-0580-00001, Key Knowledge Deliverable 11.119.

16. —. *Static reservoir modelling (field) report for CO2 in Goldeneye project.* 2014. PCCS-05-PT-ZG-0580-00004, Key Knowledge Deliverable 11.108.

17. —. *Goldeneye Seismic Interpretation Report.* PCCS-05-PT-ZG-0580-00002, Key Knowledge Deliverable 11.106.

18. —. *Special Core Analysis (SCAL) Report.* 2014. PCCS-05-PT-ZP-9034-00001, Key Knowledge Deliverable 11.112.

19. **Dake, L.P.** *Fundamentals of Reservoir Engineering.* s.l. : Elsevier , 1978.

20. **J.M. Schembre-McCabe (SPE), J. Kamath (Chevron Energy Technology Company), R. Gurton (Chevron Australia).** *Mechanistic Studies of CO2 Sequestration.* 2007. IPTC 11391.

21. **B Bennion, S Bachu.** *Relative permeability characteristic for supercritical CO2 displacing water in a variety of potential sequestration zones in the Western Canada sedimentary basin.* 2005. SPE95547.

22. **Bachu, B. Bennion and S.** *Drainage and imbibition relative permeability relationships for supercritical CO2/brine and H2S/brine systems in intergranular sandstone, carbonate, shale, and anhydrite rocks.* 2008. SPE 99326:1–13.

23. **Horne, Roland N.** *Physical Modelling of CO2 sequestration.* s.l. : Stanford University. Department of Energy Resources Engineering. , 2008. CEC-500-2007-113.

24. **Shell.** *Conceptual Well Completion Design Proposal.* 2014. PCCS-05-PT-ZW-7180-00003, Key Knowledge Deliverable 11.093.

25. **Chang, Coats and Nolen.** *A Compositional Model for CO2 Floods Including CO2 Solubility in Water.* 1996 . SPE35164.

26. **Wiebe, R.** *The Binary System Carbon Dioxide-Water Under Pressure, Chemical Reviews (1941) 29, 475.*

27. **Chang, Y-B, Coats, B. K. and Nolen, J. S.** *A Compositional Model for CO2 Floods Including CO2 Solubility in Water. SPE Reservoir Evaluation and Engineering.* 1998.

28. *Endeavour West Rochelle Development Environmental Statement report.* 2011.

29. *http://www.endeavourcorp.com/_presentations/20101130%20Canaccord%20Genuity%20Conf.pdf.*

30. **Oil, Premier.** *Hoylake Licence Relinquishment report.* 2013.

31. **Shell.** *Static Model (Aquifer).* 2014. PCCS-05-PT-ZG-0580-00003, Key Knowledge Deliverable 11.108.

32. **Quinn, M.F., Callaghan, E. and Hitchen, K.** *Scottish CCTS Development Study: The mapping and characterisation of the Captain Sandstone saline aquifer, Moray Firth. British Geological Survey Commissioned Report, CR/10/114.* 2010.

33. **Killough, J. E.** *Reservoir simulation with history-dependent saturation functions.* 1976. Trans. AIME 261, 37-48..

34. *https://www.og.decc.gov.uk/pprs/pprsindex.htm.*

35. **Peggs, J.K., Duncan, B.S., Weatherstone, P.M. and Webster, C.McK.** *North Sea Hannay Field Case History: Perforating Through a Cased –Hole Gravel Pack To Significantly Increase Oil Production.* Aberdeen : s.n., 2005. Paper 95325.

36. **Du, K.E. et al.** *Optimising the Development of Blake Field under Tough Economic and Environmental Conditions. Paper SPE 64714 presented at the SPE International Oil and Gas Conference and Exhibition in China held in Beijing, China, 7–10.* 2000.

37. **Shell.** *Static Model Overburden Report.* 2014. PCCS-05-PT-ZG-0580-00005, Key Knowledge Deliverable 11.108.

38. —. *Storage Development Plan (FDP).* 2014. PCCS-00-PT-AA-5726-00001, Key Knowledge Deliverable 11.128.

15. Glossary of terms

BHP	Bottom Hole Pressure
BIP	Binary Interaction Parameters
Bscf	Billion Standard Cubic Feet
CCS	Carbon Capture & Storage
CCS	Carbon Capture & Storage
CME	Constant Mass Expansion
CO_2	Carbon Dioxide
CO_2	Carbon Dioxide
CoP	Cessation of Production
CoP	Cessation of Production
CVD	Constant Volume Depletion
DST	Drill Stem Test
EGR	Enhanced Gas Recovery
EOFL	End of Field Life
EOS	Equation of State
EOS	Equation of State
EUR	Estimated Ultimate Recovery
EUR	Estimated Ultimate Recovery
FEED	Front End Engineering Design
FEED	Front End Engineering Design
FFM	Full Field Model
FFM	Full Field Model
FOL	Free Oil Level
FWL	Free Water Level
GIIP	Gas Initially In-Place
GIIP	Gas Initially In-Place
GOC	Gas Oil Contact
GWC	Gas Water Contact
HAFWL	Height Above Free Water Level
HAFWL	Height Above Free Water Level
HCPV	Hydrocarbon Pore Volume
IFT	Interfacial Tension
IFT	Interfacial Tension
IIP	Initially In-Place (volumes)
IIP	Initially In-Place (volumes)
LGR	Local Grid Refinement
LGR	Local Grid Refinement
Mcf	Thousand cubic feet at reservoir conditions
Mcf	Thousand cubic feet at reservoir conditions
MDT	Modular formation Dynamic Tester
Mscf	Thousand cubic feet at standard conditions
Mscf	Thousand cubic feet at standard conditions
Mt	Thousand Tonnes
Mtpa	Thousand tonnes per annum
NIST	National Institute of Standards and Technology
NTG	Net to Gross

OOWC Original Oil-Water Contact
OWC Oil-Water Contact
PDHG Permanent Downhole Pressure Gauge
Psia Pounds per square inch (relative to atmospheric conditions).
PTA Pressure Transient Analysis
PTA Pressure Transient Analysis
PVT Pressure, Volume, Temperature
PVT Pressure, Volume, Temperature
RFT Repeat Formation Tester
rm^3 Reservoir Volume of a Gas
SBHP Shut-in Bottom Hole Pressure
SBHP Shut-in Bottom Hole Pressure
SCADA Supervisory Control And Data Acquisition
SCADA Supervisory Control And Data Acquisition
SCAL Special Core Analysis Special Core Analysis
SCAL Special Core Analysis Special Core Analysis
Scf Standard Cubic Feet
Scm Standard Cubic Metres
SGS Sequential Gaussian Simulation
sm^3 Surface Volume of a Gas
SRM Static Reservoir Model
SRM Static Reservoir Model
STB Stock Tank Barrel
STOIIP Stock Tank Oil Initially In-Place
TVDSS True Vertical Depth Sub Sea

In the text names have been abbreviated to their operational form. The full names are given in Table 15-1.

Table 15-1. Name abbreviations

Full name	Abbreviated name
DTI 14/29a-A3	GYA01
DTI 14/29a-A4Z	GYA02S1
DTI 14/29a-A4	GYA02
DTI 14/29a-A5	GYA03
DTI 14/29a-A1	GYA04
DTI 14/29a-A2	GYA05

For the provision of the SI metric conversion factor as applicable to all imperial units in the Key Knowledge Deliverable.

Table 15-2: Unit Conversion Table

Function	Unit - Imperial to Metric conversion Factor
Length	1 Foot = 0.3048 metres 1 Inch = 25.4 millimetres
Pressure	1 Psia = 0.0689 Bara
Volume	1 scf = 0.028317 scm 1 stb (bbl) = 0.1589 m^3 scf/stb = 0.18 m^3/m^3
Temperature	°F=(1.8)(°C)+32 °R=(1.8)(K) (absolute scale)
Weight	1 Pound = 0.454 Kilogram

All volumes in this report quoted at 'standard conditions' assume temperature of 60°F [15.5°C] and pressure of 14.7 psia [101.35 KPa or 1.0135bar]. A conversion factors of 1m = 3.28048 ft and 1 scf = 0.028317 m^3 have been assumed.